THE UNIVERSITY
of EDINBURGH

This thesis has been submitted in fulfilment of the requirements for a postgraduate degree (e.g. PhD, MPhil, DClinPsychol) at the University of Edinburgh. Please note the following terms and conditions of use:

Imaging extracellular vesicles arising from apoptotic tumour cells for cancer diagnosis and monitoring

Maria Panagopoulou

Doctor of Philosophy with Integrated Study
Optical Medical Imaging with Healthcare Innovation
and Entrepreneurship

The University of Edinburgh and The University of
Strathclyde
2020

Declaration of authorship

I confirm the following statements are true for this thesis presented for the degree of Doctor of Philosophy with Integrated Study:

(a) this thesis has been composed entirely by myself.

(b) it is the result of my own work unless explicitly stated otherwise in the text.

(c) this work has not been submitted for any other degree or professional qualification.

Signed:

Maria Panagopoulou

August 30 2020

Acknowledgements

I would like to demonstrate my warmest appreciation to my supervisor Prof Chris Gregory and co-supervisors Prof David Birch, Dr Fabio Nudelman and Dr Alastair Wark for their guidance and sharing of their scientific insight throughout my studies.

Also, I would like to thank everyone in the Gregory group, and especially Maggie Paterson, Lynsey Melville and Pam Holland for sharing their knowledge and experience, and for making life in the lab so smooth with their assistance and kindness.

Special thanks to OPTIMA CDT for the administrative and financial support all these 4 years.

Finally, this journey would not have been as exciting without the continuous support from my family and friends.

To them, I dedicate this thesis.

Abstract

As a large part of all health-related research is focused on cancer, and with several diagnostic and therapeutic procedures continuously emerging, the fact that this disease remains mostly uncured often seems overwhelming. Cancer is a disease with extremely heterogenous causes and biologic backgrounds, and multiple mechanisms have been identified as cancer-promoting, acting on several stages of the tumour progression. Among numerous other networks, cancer cells use their own death in order to signal an urgency for survival to their neighbouring cells. It has been observed that while a cancer cell is undergoing apoptosis, it can release signals which upon receipt by surrounding cells can promote the growth of tumour. Apoptosis is a form of programmed cell death with diverse roles in the tumour microenvironment and emerging data indicate that, besides its role in tumour suppression, it can also promote oncogenic proliferation. Highly aggressive tumours such as Burkitt Lymphoma (BL) show high levels of apoptosis, which has a diagnostic and prognostic value for classifying and staging the disease. The network of regeneration and tissue repair mechanisms driven by cell-death has been named as the "onco-regenerative niche" by our group, and it is hypothesized that amongst other elements, extracellular vesicles (EVs) are key mediators of apoptotic cell-derived tumour microenvironment signals.

EVs are membrane delimited structures secreted by cells, containing multiple types of bioactive material, including markers of the tissue they originate from. They are released by almost all cells and during several phases of the cell life cycle. EVs show numerous applications in diagnostics, and there is an increasing interest in their biological functions. However, mainly because of their small size and heterogeneity, there are challenges associated with their analysis, and although EVs are gaining popularity in clinical diagnostic practice, the guidelines for analytic procedures have not been established to date. Because the vesicles are much smaller than cells and fall in the category of nanoparticles, the methods which can be applied for their analysis are dedicated to smaller entities or are special adaptations of other methods routinely used for larger particles such as cells. Here, we report on EVs released by apoptotic BL cells (Apo-EVs) in relation to their potential use as cancer biomarkers in lymphoma.

The hypothesis of this project examines the Apo-EVs as to their distinct structural and biochemical characteristics which can be used in the context of disease diagnosis and monitoring. As Apo-EVs can reach the main blood circulation, the analysis of Apo-EVs in

patients can provide with information about the stages and the progression of the disease. The two main axes this work move around on are firstly, the structural and biochemical analysis of the Apo-EVs in order to examine their special molecular characteristics which render those different from other EVs which are not related to apoptosis and secondly, the study of how Apo-EVs interact with cells present in the blood and whether their cargo can be transferred to the second. Those two sets of studies can provide a better understanding of Apo-EVs and their roles, aiming at contributing towards the development of a disease monitoring platform.

This project is focused on analytical platforms and techniques which can be applied to the nano-scale for imaging EVs in pre-clinical research and with the potential for application on patient samples. In particular, EVs released *in vitro* by Burkitt Lymphoma cells undergoing apoptosis upon UV irradiation are used throughout this study. Basic physical properties of Apo-EVs such as structure, size distribution, surface charge and membrane fluidity are discussed using Cryo Electron Microscopy (EM) and tomography, Nanoparticle Tracking Analysis, Dynamic Light Scattering and fluorescence anisotropy respectively. For phenotypic analysis we apply immunocapture and flow cytometry, immunogold labelling on transmission EM, fluorescence microscopy and quantitative PCR.

The second part of the analysis consists of a study of the interaction of Apo-EVs with blood components such as platelets, leukocytes and red cells, in order to understand their effects in the circulation and therefore their potential for analysis in blood samples. For this purpose, cells and platelets from human blood were co-incubated with Apo-EVs in order to examine the uptake and the possibility of Apo-EV cargo delivery intracellularly.

Looking at the differences between Apo- and non-Apo-EVs, the Apo-EVs have a larger diameter, while structurally, the two populations are not different. However, we have identified distinct Apo-EV markers such as active caspase 3 and histone-3, or DNA and small non-coding RNA-Y. There is also a strong interaction of EVs with platelets and leukocytes but not with red cells, indicating potential mechanisms of transfer of EV cargo in the circulation. It was also found that this interaction does not only concern the surface of the cells, but EVs can enter the platelets or cells, which supports the hypothesis that their special biochemical cargo can be transferred inside those cells.

It is concluded that for the characterization of the heterogenous Apo-EV populations, comparison of results from of each method is essential for choosing the appropriate combination of analytical tools. Finally, we consider that the monitoring free circulating Apo-EV or blood cells with which they have interacted is a promising approach to improve cancer diagnosis, prognosis and evaluation of therapeutic response.

Lay Summary

Although researchers have studied cancer biology and anti-tumour therapies for a long time, it is in many cases observed that this disease remains uncured. One of the reasons why cancer is still prevalent is that the building blocks of the tumour, the cells, have developed mechanisms and networks via which they promote their growth and escape destruction. Among other factors, cancer cell death can drive tumour growth. This 'paradox' happens because while cells begin to die (with a process called apoptosis), they are able to release tumour-promoting signals which eventually reach neighboring cells and cause them to grow, sustaining the cancer. It is also true that for some types of cancer, large numbers of dying cells are related to high aggressiveness, therefore apoptosis can be an indication of how the disease progresses in a patient. One channel the dying cells use to deliver survival messages to their fellow cancer cells is via apoptotic cell-derived extracellular vesicles (Apo-EVs). The EVs are small membrane particles which are released by almost all cells in the body, and are loaded with messages from the parental cell which are eventually delivered to the recipient cells. The EVs which are obtained as a cell is undergoing apoptosis are therefore, the Apo-EVs.

The aim of this work is to enrich our knowledge on the Apo-EVs with the ultimate goal to use Apo-EVs found in blood as a cancer indicator. Therefore, two different paths have been followed: in the first, we examine what unique characteristics the Apo-EVs have which can be potentially used as biomarkers, and the second is to study how these EVs interact with the blood cells once they escape the site of the tumour and reach the main blood circulation. The results showed that there are three main biomolecules which were highlighted as unique for the Apo-EVs compared to other EVs, and in addition, it was indicated that the vesicles can fuse with platelets and white blood cells in the blood, which can imply that their cargo is transferred to them. Those results can be useful for future studies in which the Apo-EVs can be applied on a number of tumours which show high levels of cell death, as those levels can reflect the severity of the disease.

List of Abbreviations

3-D, 2-D	Three-, two-dimensional
AF (AF488, AF568 etc.)	Alexa fluor®
Apo-EVs	Apoptotic (tumour) cell -derived Extracellular vesicles
AUC	Area under the curve
AxV	Annexin V
BL	Burkitt lymphoma
BSA	Bovine serum albumin
CCD (camera)	Charge-coupled device camera
CEA	Carcinoembryonic antigen
Chol	Cholesterol
cMOS	complementary metal oxide semiconductor
CryoEM	Cryogenic electron microscopy
CryoET	Cryogenic electron tomography
DLS	Dynamic light scattering
DMF	Dimethyl formamide
DMPC	Dimyristoyl-phosphatidyl-choline
DMSO	Dimethyl sulfoxide
DNA, cDNA	Deoxyribonucleic acid, complementary DNA
DPBS	Dulbecco's phosphate-buffered saline
DPH	Diphenyl-hexatriene
DPPC	Dipalmitoyl-phosphatidyl-choline
dSTORM	direct Stochastic optical reconstruction microscopy
EBV	Epstein-Barr virus
EDC	1-ethyl-3-(3-dimethylaminopropyl)-carbodiimide
EDTA	Ethylenediaminetetra-acetic acid
ESCRT	Endosomal sorting complex required for transport
EVs	Extracellular vesicles
FISH	Fluorescence in situ hybridization
FITC	Fluorescein
HBSS	Hank's balanced salt solution

HEP	refers to HEPES in the buffer
HEPES	4-(2-Hyrdroxyethyl)piperazine-1-ethanesulfonic acid
HLA	Human leukocyte antigen
HUVEC	Human umbilical vein endothelial cells
hY4 RNA	human Y4 RNA
MCS	Multichannel analyser
MES	2-(N-morpholino)ethanesulfonic acid
MHC class I and II	Major histocompatibility complex
microNMR	microNuclear magnetic resonance
MRD	Minimal residual disease
MVBs	Multivesicular bodies
NHL	Non-Hodgkin lymphoma
NHS	N-Hydroxysuccinimide
NK	Natural killer cell
NTA	Nanoparticle tracking analysis
PBMCs	Peripheral blood mononuclear cells
PBS	Phosphate-buffered saline
PC	Phosphatidylcholine
PDI	Polydispersity index
PEG	Polyethyleneglycol
PET	Positron emission tomography
PGE1	Prostaglandin E1
PMNs	Polymorphonuclear cells
PRP	Platelet rich plasma
PS	Phosphatidyl serine
PVDF	Polyvinylidene difluoride
qPCR	quantitative Polymerase chain reaction
RNA, miRNA, mRNA, rRNA	Ribonucleic acid, micro, messenger, ribosomal
RT	Reverse transcription
RT	Room temperature
SAXS	small-angle X-ray scattering
SEC	Size exclusion chromatography

SEM	Scanning electron microscopy
SPC	Single photon counting
SUVs	Single unilamellar vesicles
T	rotational correlation time
TAC	Time-to-amplitude converter
TCSPC	Time-correlated single photon counting
TEM	Transmission electron microscopy
TEPs	Tumour-educated platelets
THF	Tetrahydrofurane
Tm	phase transition temperature
TMA-DPH	4-Trimethylammoniumphenyl DPH
UC	Ultracentrifugation
UV	Ultraviolet

Table of Contents

1. Introduction

1.1. Extracellular vesicles

The presence of sub-cellular functional factors in the blood was first reported in 1946, when pellets from ultracentrifuged blood plasma exhibited coagulation properties. Although the authors referred to the material responsible for this effect as 'particulate fraction containing breakdown material of blood components', this was the first time extracellular vesicles (EVs) were introduced in the literature (Chargaff and West, 1946). Two decades later, pellets from plasma centrifugation were shown to contain vesicular structures referred to as 'platelet dust' (Wolf, 1967). The interest in the vesicles has since been constantly increasing, and the field of vesicle research currently includes a large number of researchers worldwide.

EVs are membrane particles released from cells, in which cellular material is encapsulated within a lipid bilayer. While it remains unknown whether all cell lineages have the ability to release EVs, various cell types have been found to be capable of doing so, with a few examples being the mast cells, neurons, dendritic cells, platelets, endothelial and epithelial cells and B-lymphocytes, among others (Théry, Zitvogel and Amigorena, 2002). Although there is a number of questions related to their functions and the purposes the EVs serve, the process of EV release appears to be conserved in evolution, leading to the assumption that the EVs contribute significantly to homeostasis and disease (Colombo, Raposo and Théry, 2014). The diameter of the vesicles ranges from a few nanometers (nm) up to microns, depending on the subtype, and they have been isolated from the majority of human body fluids such as blood, urine, breastmilk or ascites in disease. Based on the observation that they are physiologically secreted from cells at constitutive levels, the initial explanation for their presence was that cells use EVs to eliminate unwanted proteins and side-products of the metabolic process from their interior to the extracellular space. Nowadays, it is believed that EVs also mediate communication signals among cells both in physiological and pathological situations (tumours, neurodegenerative diseases) (Hannafon and Ding, 2013).

The biochemical composition of the EVs is relatively complex, as their structure incorporates material from the parental cell such as proteins, lipids and nucleic acids (Figure 1-1). Some proteins are commonly found in the majority of EVs, such as kinases, heat-shock proteins or actin, while others vary in levels of expression or are only present in specific tissues or disease as for instance the MHC class II from antigen-presenting cells (Théry, Zitvogel and Amigorena,

2002) or CEA (carcinoembryonic antigen) and HER-2 from colon and breast tumours respectively (Dai *et al.*, 2005; Barok *et al.*, 2018). A second component is the lipids which form the EV membrane, mainly structured with phospholipids such as phosphatidylcholine (PC), saturated fatty acids, sphingomyelin and various levels of cholesterol. Interestingly, the EV membranes show a distinct difference from the cell membranes in the localization of the phospholipid phosphatidylserine (PS). In healthy cells, this lipid is normally found in the inner monolayer via an active PS asymmetry maintenance system (see below) and is exposed on the outer surface upon initiation of apoptosis, platelet activation or other processes (Nagata *et al.*, 2016), (Shlomovitz, Speir and Gerlic, 2019); however, EVs seem to have exposed PS under normal conditions and there are two main theories explaining this observation. The first comes from the perspective of the thermodynamics of the lipid arrangement on the membrane and this is because the EV membranes have a higher degree of curvature compared to plasma cell membranes, which leads to mechanically induced 'lipid-packing defects' in which hydrophobic lipid heads such as the negatively charged PS can be found in the outer leaflet (Kastelowitz and Yin, 2014). The second possible explanation is attributed to the lack of flippase and active scramblase in EVs, enzymes which maintain asymmetry in the composition of lipids on the cell membrane by actively transferring lipids to the relevant side of the bilayer (Hugel *et al.*, 2005), (Barclay *et al.*, 1997). Therefore, with the majority of EVs exposing PS, Annexin V, a protein capable of binding on aminophospholipids with high affinity can act as a detection or capture probe, as indicated by the capturing of EV on beads coated with Annexin V (Dachary-Prigent *et al.*, 1993; Shih *et al.*, 2016). Apart from proteins and lipids, EVs are also nucleic acid-bearing entities with the most prevalent acids being RNA and especially small molecules such as miRNA, mRNA or rRNA. DNA is detected in some cases, often in EVs deriving from apoptotic cells but also in other smaller vesicles (Ehnfors *et al.*, 2009; Cai *et al.*, 2015). With the above evidence, it is implied that the transfer of genetic material from EV releasing cells to recipient cells via EVs can have potential effects in the intercellular communication and progression of several diseases. In conclusion, there is a basic biochemical pattern which most EVs have in common, however, this composition can be altered significantly under special conditions such as inflammation or tumour, which offers researchers a powerful tool for diagnostic analyses. In other words, detecting changes in the expression levels of proteins, lipids or nucleic acids of EVs can indicate potential

pathology which may not be detectable by other clinical means (Colombo, Raposo and Théry, 2014).
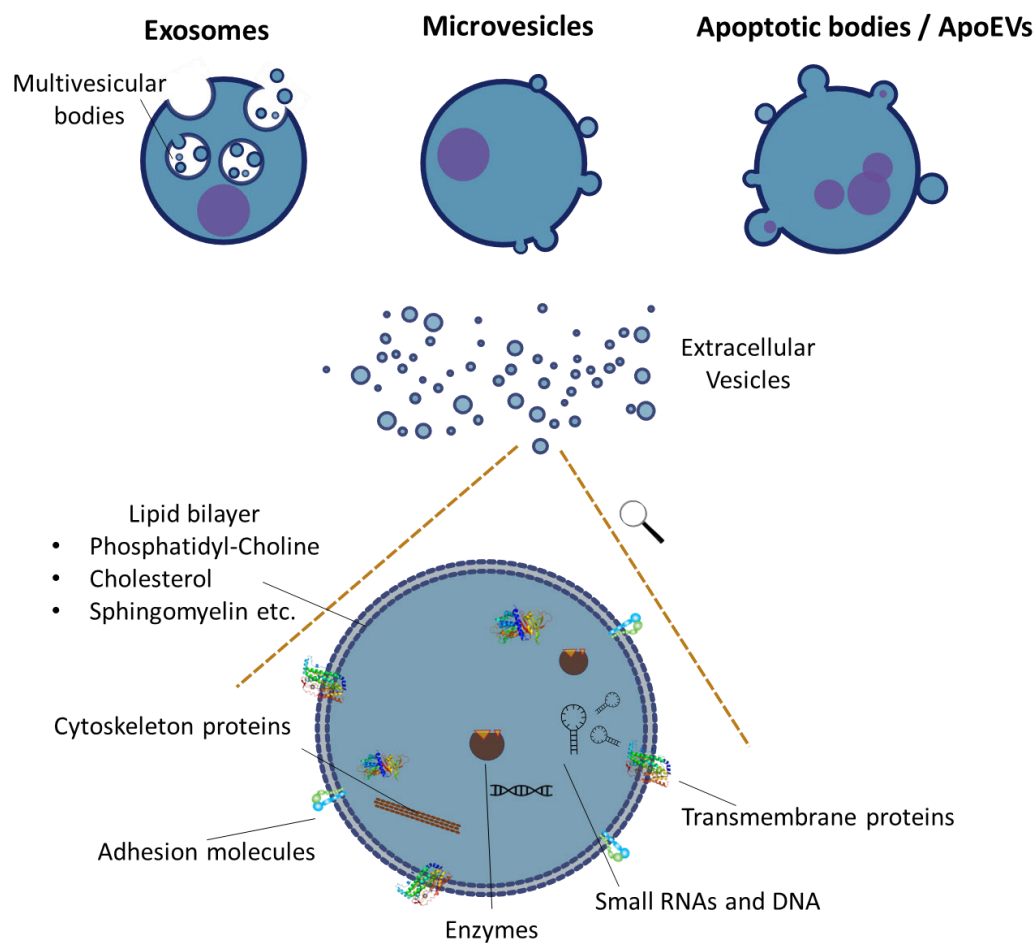
Figure 1-1. Schematic representation of the categories of EVs and biochemical composition. The EVs are a sum of membrane particles released by cells through different mechanisms (exosomes, microvesicles or Apo-EVs). The common characteristics of all types of vesicles is the general structure, i.e. the lipid bilayer, the membrane and intravesicular proteins and the genetic material.

The generally recognised intracellular pathway for EV formation and secretion involves a process initiating in endosomal compartments where cellular components accumulate as part of a recycling/degradation process. Early vesicles (multivesicular bodies, MVBs) are formed by the inward budding of the endosomal membrane, enclosing part of the cytosol including proteins and also lipids. Some of these early MVBs finally fuse with the endosomal membrane in order to undergo degradation, while others are distinctively labelled for fusion with the plasma membrane and release of their load (smaller vesicles) to the extracellular

space (Théry, Zitvogel and Amigorena, 2002) (Denzer *et al.*, 2000). In more detail, it is believed that the triggering signal towards vesicles formation is dependent on a protein complex, named as the endosomal sorting complex required for transport (ESCRT). This machinery enables the budding of the lysosomal membrane to the formation of the early multivesicular bodies inside the lumen of the organelle, as well as the scission of the membrane so that the MVBs are released into it. Besides ESCRT, there is an alternative EV production route which is independent of the sorting complex machinery and involves the lipid ceramide that acts as a signalling molecule in the processes of vesicle formation, membrane fusion and vesicle trafficking (Bobrie *et al.*, 2011) (Colombo, Raposo and Théry, 2014).

The finally formed vesicles are secreted to the extracellular matrix by the process of exocytosis, where the MVBs fuse with the interior lumen of the cytoplasmic membrane and release their cargo (EVs) out of the cellular space. A complex set of signals are involved in the mechanics of secretion and the regulation of the vesicle concentration levels and kinetics/frequency of release. The main molecules necessary for the final release are the SNARE complex, actin microtubules, and Rab GTPases. The regulation of secretion is influenced by multiple biological, chemical and even mechanical stimuli, dependent on local factors. In some cases, there is an interesting correlation between diseases and the increased levels of signalling molecules which promote vesicle secretion (Hannafon and Ding, 2013). This trend is observed especially in various cancer types (Grizzle and Zhang, 2013). Monitoring the patterns of secretion or performing more advanced analysis on the content of the vesicles could give some evidence about the presence of underlying diseases.

Next, these vesicles often transfer information to recipient cells, which is achieved by three main processes. The first is described as a direct interaction of the transmembrane vesicular proteins with signalling receptors on the surface of the recipient cells. The second is the fusion of their membrane with the plasma membrane of the recipient, thus, delivering their encapsulated material directly and non-selectively into the cytosol and thirdly, whole EVs can be taken up in the cell (by endocytosis and/or macropinocytosis), where two possible routes can be followed. The internalized vesicles can fuse with lysosomes and undergo degradation, or merge with endosomes, move across the cytosol and finally be released out again, targeting a new recipient cell. This process is known as transcytosis (Zhang *et al.*, 2015).

As to the functions EVs have, they can be often characterized as "multi-purpose carriers" due to their varied cargo profiles. Briefly, their roles are related to cell-to-cell communication (transport of secondary messengers to recipient cells), exchange of genetic information (e.g. by sharing mRNA and microRNAs) and protection (cells eliminate dangerous substances and unwanted metabolites such as chemotherapeutics, caspase 3, oxidized lipids) (Nieuwland and Sturk, 2010). However, it is observed that the signals mediated by EVs have multiple patterns depending on the cell type, the different tissues and most importantly, on the local microenvironment.

Because of the highly specific cargo, EVs can be considered as disease biomarkers and because of their structure, they have some advantages compared to bulk blood biomarker samples commonly used. Firstly, using a sample of EVs can be less complex to analyse compared to blood or serum sample. This is because separation steps can result in pure vesicle samples where no other blood components are present. Consequently, using a sample which exclusively contains vesicles without the interference of other components, can reduce the noise and set the detection threshold lower. However, the complexity of the vesicles' contents (either encapsulated or on the surface) are still a challenging area and one of the main interests for the present project. The stability of the EVs has also been investigated and there is evidence that they can be stored without significant loss of their properties for a certain period of time (Fendl *et al.*, 2016). However, as described in the next paragraphs, a common guideline should be established on storage conditions, as there are no common procedures and practices in the community regarding this issue yet. In addition to this, in cases where the proteins serving as biomarkers are enclosed by the vesicular membrane, they are protected from distortion and proteolytic enzymes, providing a highly reliable source of disease marker (Boukouris and Mathivanan, 2015).

The number of molecules loaded on vesicles can be used as specific cancer biomarkers. The largest known family of markers consists of various versions of small RNA (Canella *et al.*, 2016; Nakamura *et al.*, 2016; Valentino *et al.*, 2017; Salehi and Sharifi, 2018) and there are other markers which vary significantly depending on the type of disease or tissue, such as glycosylated molecules on the membrane surface (Costa, 2017) and expression of certain receptors, oncoproteins and even circulating tumour DNA (Westphal and Lamszus, 2015).

Apart from their use as biomarkers, EVs have been investigated as to their clinical functions such as therapeutic activity and potential use as vaccines. For instance, administering mesenchymal stem cell EVs to cardiac tissue has shown to assist recovery from injury and also EVs with pro-inflammatory properties have been effective in triggering immune response (György *et al.*, 2015).

1.2. Tumour and extracellular vesicles from apoptotic tumour cells (Apo-EVs)

Apoptosis is a form of programmed cell death which is thought to have multiple roles in physiological processes such as organised removal of cells and tissue regeneration, as well as in pathological conditions such as tumour progression, which is of interest in this project. Morphologically, it is characterized by cell shrinkage, nuclear fragmentation and plasma membrane blebbing, among others. It should not be confused with necrosis where the cell dies either accidentally or via a complex signalling pathway and is manifested by swelling of the plasma membrane, rupture and release of the cellular contents (Kroemer *et al.*, 2009). In cancer, apoptosis is best known as a tumour suppressive process, however, our research is focused on other tumour-related effects of apoptosis besides its ability to reduce the tumour volume. It is known that apoptotic cells in tumours communicate with the neighbouring cancer cells by various signal mediators including soluble factors and microparticles or other membrane-associated forms (Gregory and Pound, 2010). The roles of apoptosis are not fully understood, but there is increasing evidence that it plays a significant role in mediating communication signals within the tumour microenvironment. More specifically, it is observed that apoptosis can either induce further apoptosis in the neighbouring cells or promote compensatory proliferation in others, depending on the signals the apoptotic cells mediate (Gregory, Ford and Voss, 2016). Therefore, understanding the impact of apoptosis within the tumour microenvironment can provide useful information which could enable researchers to address potential therapeutic approaches against cancer. EVs are likely to be important, yet not fully studied mediators of the interactions between apoptotic and the nearby cells. It should be here pointed out that apoptotic cells also secrete other types of vesicles which can be both apoptosis-related or physiological EVs, although the distinction between the two is not well defined (Gregory and Pound, 2011). Apoptotic bodies are defined as the largest type of vesicles (1 to 5 μm) resulting from the cellular

disassembly process while EVs are smaller in size and usually result from the ESCRT machinery, as mentioned earlier (Atkin-Smith *et al.*, 2016). Among the range of vesicles involved in tumour progression, this work elaborates on the investigation of the apoptotic cancer cell derived EVs (Apo-EVs), as there is early evidence that Apo-EVs could be important regulators of the tumour microenvironment (Lynch, Panagopoulou and Gregory, 2017).

The nomenclature for the different types of particles released from apoptotic cells is a matter of discussion, as a standardized terminology has not been defined to date (Gould and Raposo, 2013). The general classification of vesicles, although the size ranges suggested by different researchers varies, includes exosomes ranging between 30 to 100nm, microvesicles/ectosomes that directly bud from the plasma membrane covering the size range of 50-2000nm, and apoptotic bodies (50–5,000 nm) (Figure 1-1). Apoptotic bodies can be discriminated from other types of vesicles because they are actively released during the process of apoptosis (Akers *et al.*, 2013), (Atkin-Smith *et al.*, 2016) and can also encapsulate smaller vesicles or organelles (Minciacchi, Freeman and Di Vizio, 2015). At the same time, tumour cells release larger vesicles containing tumour-promoting material with paracrine activity, often described as oncosomes (1-10μm) (Minciacchi, Freeman and Di Vizio, 2015). There is evidence of significant levels of non-constitutively produced proteins loaded on EVs prior to the complete dissociation of the plasma membrane due to necrosis and these special signals have been associated with the process of apoptosis (Wickman *et al.*, 2013). Apoptotic bodies and microparticles can be characterized as metabolically active structures that provide the apoptotic cells with the capacity to convey molecular messages over longer distances due to their ability to encapsulate functional molecules such as proteins or even cellular organelles (Gregory, Ford and Voss, 2016). Moreover, it is shown that apoptotic bodies released from tumour cells are responsible for transferring DNA to neighbouring cells and induce tumour progression and appearance of p53-deficient fibroblasts (Bergsmedh *et al.*, 2001). With signs leading towards the conclusion that the Apo-EVs mediate signals that have an impact on tumour progression, it is essential to determine their properties and cargo, aiming at the development of therapeutic and diagnostic platforms (Lynch, Panagopoulou and Gregory, 2017).

The effects of apoptotic cell-derived vesicles have been described in a number of studies, yet the mechanisms and functions are not entirely clear (Gregory, Ford and Voss, 2016).

It has been indicated that cancer cells under stress transfer genetically active material to the nearby cells and given that the EVs are loaded with nucleic acids, they possibly play a significant role in this communication (Ehnfors *et al.*, 2009). In the case of stromal cells, there are data proving that EVs (smaller than 100nm) released from these cells upon a stress stimulus transfer signals supporting the neighbouring tumour cells in creating metastatic sites, promoting growth and inhibiting apoptosis (Vallabhaneni *et al.*, 2016). In addition, *in vitro*-induced apoptosis to cancer cells by radiotherapy has been shown to have an impact on T-cell responses against tumour and this implies the potential of combining radiation with immunomodulatory therapies in cancer (Xie *et al.*, 2009). Moreover, apoptotic bodies released from tumour cells are responsible for transferring DNA to neighbouring cells and can induce tumour and the appearance of p53-deficient fibroblasts (Bergsmedh *et al.*, 2001). It is supported that the stress chemotherapeutics cause to cancer cells triggers massive EV release directly associated with apoptosis, while in parallel, necrosis does not cause this effect to such an extent. This observation has led to the idea that "mild" therapies which are not reactive enough to induce necrosis are potentially harmful due to the tumour-promoting signals mediated by apoptotic cell EVs (Aubertin *et al.*, 2016). Other research groups have also expressed the idea that successful anticancer therapies are associated with reduction of EV release from the targeted cells, as those EVs can transfer therapy resistance genes ((Shao *et al.*, 2012)-(Mitchell *et al.*, 2009)).

1.3. Burkitt Lymphoma and apoptosis

Among the most aggressive types of lymphoma, Burkitt Lymphoma (BL) is classified as a B cell Non-Hodgkin Lymphoma (NHL), associated with the overexpression of the c-MYC transcription factor, caused by the deregulation of the MYC gene (Kalisz *et al.*, 2019). This overexpression in c-MYC drives abnormally high B-cell proliferation rates, as well as significant levels of apoptosis (O'Malley, Auerbach and Weiss, 2015). Variations of the 'single hit' MYC-related mechanism are the 'double' and 'triple hit' cases in which the Bcl-2 and Bcl-6 are additionally rearranged respectively, which leads to inhibition of apoptosis, therefore higher aggressiveness (Kalisz *et al.*, 2019). Histologically, a typical characteristic of this particular type of tumour is the starry-sky appearance of the tissue, referring to the large extent of macrophage infiltration in the cancerous mass (Berard, C., G. T. O'Conor, L. B. Thomas, 1969) (Ogden *et al.*, 2005). BL has been classified among the mature B-cell

lymphomas by the World Health Organization, according to the 2016 revision of the lymphoid neoplasm classification directive (Swerdlow *et al.*, 2016). There are three main variants of the disease which also follow a demographic pattern. The first is the endemic BL, mainly occurring in African areas, affecting children around 7 years of age and almost always associated with Epstein-Barr Virus (EBV) infection, the second is the sporadic BL which has been observed worldwide and affects children as well as adults around 30 years old. Finally, there is a Human Immunodeficiency Virus (HIV)-related BL variant observed within the endemic HIV African areas, affecting HIV patients and children/adolescents. In African regions, the disease is more prevalent in young males, while the cumulative statistics show that Eastern Africa holds the highest NHL incidence and mortality rates with 7.5 and 5.7 per 100,000 respectively (Orem *et al.*, 2007).

Diagnosis of the disease is currently based on histopathological examination, although the morphological pattern of the tissue might not always give a clear answer, therefore it is believed that a combination of histology with immunophenotyping and analysis of the genetic characteristics is considered to be a more complete approach (Wook Youn Kim, Matthew Pugh, Stefan Dojcinov, 2019). For cases in which there is an indication that specific genetic mutations are the main cause, Fluorescence In Situ Hybridization (FISH) is recommended for the detection of MYC and BCL2 genes (Sesques and Johnson, 2017). The above methods require the examination of the cancerous tissue, therefore invasive biopsies are needed. There is a clear lack of widely available methods for the evaluation of the stage of the disease as well as the success rate of the treatment as reported in the literature, and the current options include Positron Emission Tomography (PET) and minimal residual disease (MRD) technology, both of which require special and expensive equipment (Sandlund, 2012).

A key characteristic of BL which can serve as a tool for the development of prognostic and diagnostic platforms is the high levels of apoptosis, which appears contradictory to the established knowledge that apoptosis prevents tumorigenesis. Paradoxically, it has been shown that apoptotic cells in BL tumours can have oncoregenerative properties by acting on angiogenic, trophic and reparatory pathways, among others (Ford *et al.*, 2015). In addition to lymphoma, a similar pattern where increased apoptosis is correlated with aggressive progression of the disease is observed in tongue squamous carcinoma, urinary bladder and synovial tumours respectively (Naresh *et al.*, 2001a; Jalalinadoushan, M., Peivareh, H.,

Azizzadeh Delshad, 2004; Sun *et al.*, 2006) while other studies have shown that when a pro-apoptotic protein was genetically ablated from thymic T-cells, tumour formation was inhibited (Labi *et al.*, 2010; Michalak *et al.*, 2010). Therefore, since high levels of apoptosis can be an indication for poor prognosis for the patient, the use of EVs as a non-invasive biomarker is a potential tool which can be used to complement the lack of monitoring methods, as shown earlier for Burkitt Lymphoma, but can also extend to other tumours (Figure 1-2).
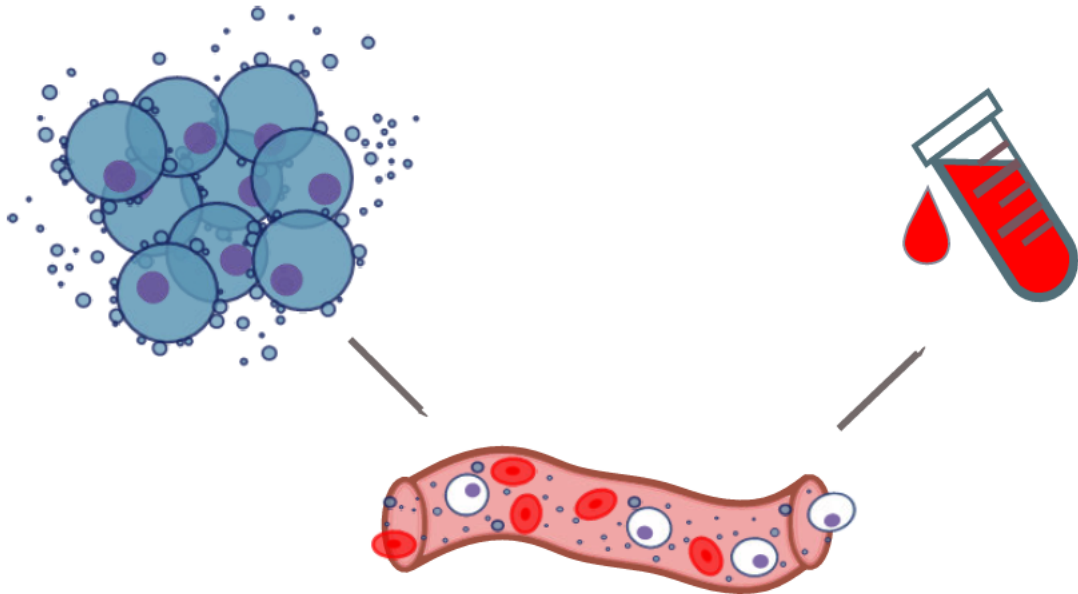

Figure 1-2. Apo-EVs from tumour enter the main circulation and can provide with a diagnostic/prognostic platform for Burkitt Lymphoma and other tumours with high levels of apoptosis.

1.4. EVs in the blood circulation

EVs are released by tumours located at various sites of the body, yet a percentage of them is eventually found in the blood circulation. This property of EVs to enter the blood enables their analysis from blood samples, which is minimally invasive and clinically preferable to biopsies. However, the kinetics, stability and general 'behaviour' of EVs regarding interactions with other cells in the blood are only understood to some extent and it is therefore relevant to present a brief review of the literature findings on the topic.

A study looking at the rates of clearance and secretion of EVs in the blood has shown that after injection of small EVs prepared from murine cells in mice, 50% of the initial injected EV amount was cleared within 7min. Although the absolute quantification of fresh EVs entering

the circulation remains a challenge, it is suggested that this dynamic process happens at high rates. Interestingly, when liver macrophages were depleted in the animal models, the EVs were retained in the circulation for a significantly longer period and therefore the EV concentration in the blood was higher (Matsumoto *et al.*, 2020). These results agree with a previous study reporting that the clearance of circulating EVs was mainly performed by liver and spleen macrophages (Imai *et al.*, 2015). The concentration of EVs in the blood is also another matter of discussion, for which there is not a definite answer due to technical limitations and differences in the systems under measurement. In an effort to collect the relevant literature and compare findings from various studies, Johnsen *et al.* report high variability in the results obtained after several isolation techniques were applied, however the authors extracted a mean of 10^{10} particles/ml (Johnsen *et al.*, 2019).

The following examples indicate that the cells/platelets found in the blood are releasing EVs and that the circulating EVs from various origins interact with those blood cells. To begin with, there is evidence that red blood cells release EVs not only physiologically, but also upon storage, which is of great significance in blood units intended for transfusion (Almizraq, Holovati and Acker, 2018). Leukocyte, platelet and red cell-derived larger vesicles (over 1μm) are also a part of the total blood EV population, additionally to the smaller EVs which had already been reported to derive from the above cells/platelets (Nanou, Zeune and Terstappen, 2019). Interestingly, EVs from various glial neuronal cells have also been found in plasma, as they can cross the blood-brain barrier (Saeedi *et al.*, 2019).

Other studies have provided evidence that red blood cell-derived EVs can interact with other blood cells with significant levels of uptake both *in vivo* and *in vitro;* in the first case, EVs labelled with a radioisotope were injected in mice, subsequently labelling white blood cells (Son *et al.*, 2020), while in the second, red cell EVs were co-incubated with isolated monocytes, inducing cytokine release and subsequent increase in T-cell response (Danesh *et al.*, 2014). EVs from Natural Killer (NK) cells are also interacting with other blood cells, and the highest uptake levels were measured for the same cells (NK) and cell lines of T cells and macrophages, upon comparison with tumour cell lines (Huyan *et al.*, 2018).

Tumour-derived EVs and platelets

A significant proportion of blood consists of platelets, which are cell fragments responsible for the regulation of blood clotting (thrombosis) and hemostasis. They are released by megacaryocytes which reside in the bone marrow and regarding their numbers in the blood, after red blood cells which are the most abundant type of cells, platelets come next followed by white cells (Seyoum, Enawgaw and Melku, 2018). Interestingly, platelets have been shown to have functions beyond their well-established hemostatic role, as studies have revealed that they can be conditioned by tumour cells. In more detail, tumour-specific RNA has been found in platelets isolated from prostate and glioma patients, and it was also shown that among a number of mechanisms of RNA transfer, the most prevalent is the uptake of RNA-containing tumour EVs by the platelets (Nilsson *et al.*, 2011). The term tumour-educated platelets (TEPs) has been given to describe the changes in biochemical composition the platelets undergo upon interaction with cancer cells which is often manifested by elevation of tumour-related levels of RNA. Although the whole range of the mechanisms involved in this process are not fully understood, it has been clearly shown that TEPs occur in patients bearing a variety of tumours (Best, Wesseling and Wurdinger, 2018). Sequencing of the platelet RNA isolated from the blood of breast cancer patients of patients in various stages has indicated sequences which can have a prognostic or diagnostic value (Lips *et al.*, 2018), while the monitoring of another RNA component in lung cancer patients is a possible predictor of resistance to therapy (Nilsson *et al.*, 2016). Further evidence that platelets can interact with EVs has been given by Rossaint *et al.*, in a study where platelets and neutrophils are reciprocally activated via the release of neutrophil-derived EVs which are subsequently internalized in platelets (Rossaint *et al.*, 2016). Those observations, and in combination with their high concentration in the blood suggest that in order to analyze the levels of biomarkers, instead of isolating the relevant cells -or EVs-, platelets could be a possible minimally invasive alternative.

1.5. Analytical technologies applied on the nanoscale for the study of EVs

In order to answer basic questions about the nature and functions of EVs, it is important to apply the appropriate methods of analysis and taking into consideration that EVs are nano/microparticles, the range of available techniques is different from the classic approaches often used in the field of medical research. In this section, a review on the

methods used in this work is given, with emphasis on the specific applications on EV analysis and the limitations or strengths of the measurement outcomes of each (Figure 1-3).
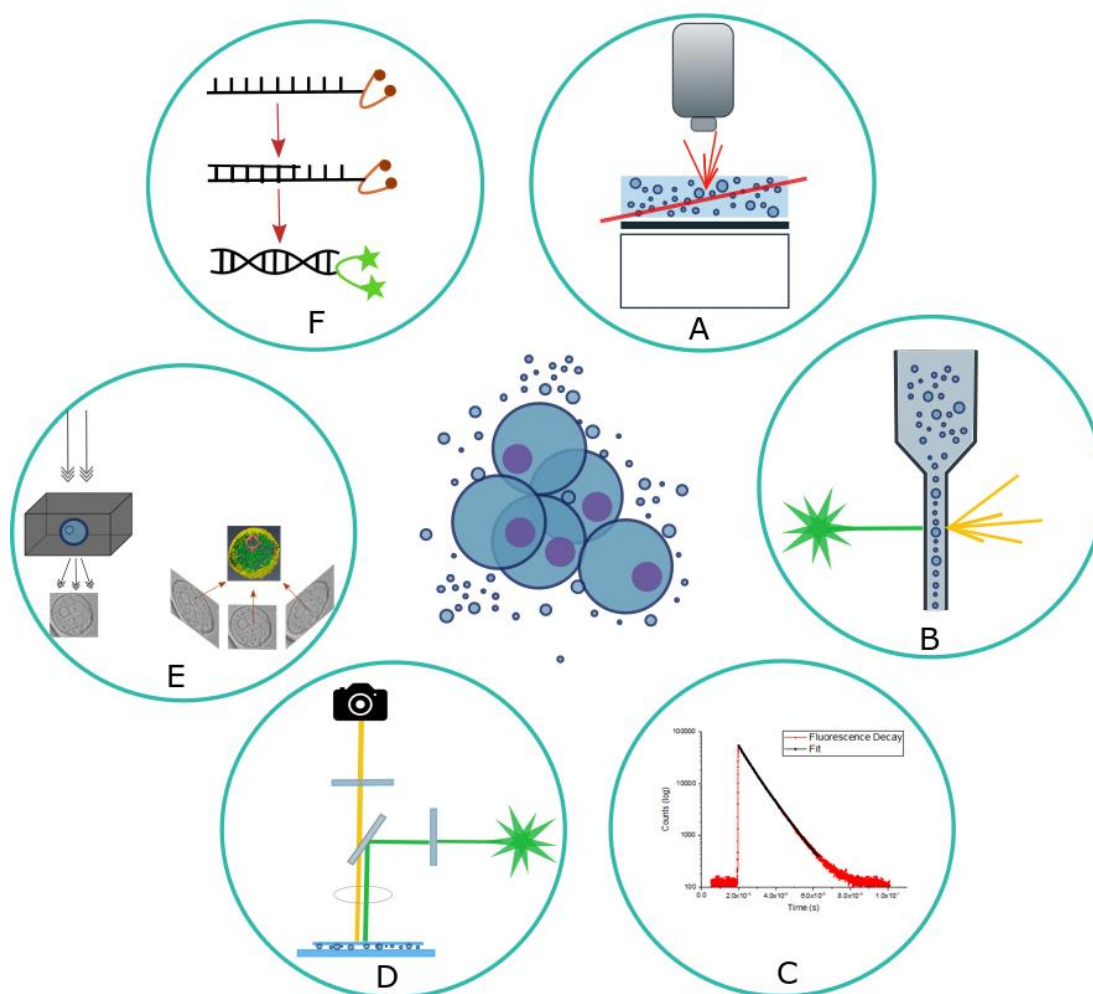

Figure 1-3. Methods of analysis for EVs: A: nanoparticle tracking analysis, B: flow cytometry, C: fluorescence anisotropy, D: fluorescence microscopy, E: cryoEM and tomography and F: quantitative PCR (adapted with permission from (Panagopoulou *et al.*, 2020))*.*

CryoEM

A technique to directly image EVs is Electron Microscopy, which offers high resolution images for structures sized in the range of a few nanometres. Electron microscopy has been successfully used for biomedical purposes such as imaging of tissues, cells and even subcellular organelles (Mielanczyk *et al.*, 2014). The basic difference from optical microscopy is that for optical observation, the source of illumination is visible light (or fluorescence) photons passing through the specimen which are viewed directly across the sample, while in electron microscopy the source of radiation is electrons. This is of great significance because

as the resolution limit is determined by the radiation wavelength, the shorter the wavelength, the higher the resolution which in case of visible light is between 4000 to 7000 Å, while the electron beam has a wavelength of approximately 0.02 Å (for an electron beam operating at 300kV). The electrons are produced by an electron gun usually containing a lanthanum or tungsten source and are accelerated under vacuum in a voltage of 80-300kV towards the fixed, sputter coated or vitrified specimen (depending on the variation of EM, see below). Their interaction with the second is detected in two ways, dividing electron microscopy techniques in two main subgroups: transmission electron microscopy (TEM) and scanning electron microscopy (SEM) (Williams and Carter, 2009). In SEM, the electrons are scattered away from the surface of a specially stained specimen and collected from detectors which produce a 3-dimensional image of the surface of the specimen, based on the orientations of the scattered electrons. In TEM, the electrons are transmitted through the ultra-thin fixed specimen and are captured at the other side, producing a thumbprint of the sample. The direct interaction of the electrons with the biologic sample results in extensive damage due to the creation of free radicals and breaking of chemical bonds, while at the same time the more intense the beam is, the higher the quality of the image obtained. One approach used to tackle this issue is to stain the specimen with a material that enhances contrast so that the intensity of the electron beam can be reduced, without affecting the resolution.

Another approach followed to avoid staining, to minimize the damage from the electron beam and to preserve the vesicles as close to their native state as possible during imaging is cryogenic TEM. This technique differs from conventional TEM in terms of the sample preparation and the temperature of the system during measurement. The thin specimen, or nanoparticle suspension in the case of EVs, is instantly frozen in order to create amorphous vitrified ice (glass-like) and non-crystalline hexagonal ice. To achieve vitrification, various procedures can be followed (jet freezing, slam freezing, high pressure cooling), yet, in this work plunge-freezing is used, which is also one of the most commonly used methods of freezing, as described in the literature (Table 1.1). The specimens are applied on a grid, usually made of gold or silver, which is a 1 μm mesh, and in case of liquid suspensions (EVs), surface tension serves as a force creating a thin film of material on the grid whereas in solid materials, sections of the appropriate thickness must be taken (Dubochet *et al.*, 2016). The grid is plunged into liquid ethane (-88.5 °C) cooled by liquid N_2 (-196°C) and upon vitrification

it is preserved in liquid N$_2$. While under the electron beam, cryogenic conditions must be preserved so that the specimen is not damaged from heating and the ice does not melt (Figure 1-4).

An advanced variation of cryoEM is cryogenic Electron Tomography, where 3D reconstructions of the specimen can be obtained. From one single particle, multiple images can be taken in different spatial orientations and are then projected on a 3-dimensional model yielding the structure of the particle with high resolution (Figure 1-4) (Nudelman, de With and Sommerdijk, 2011).
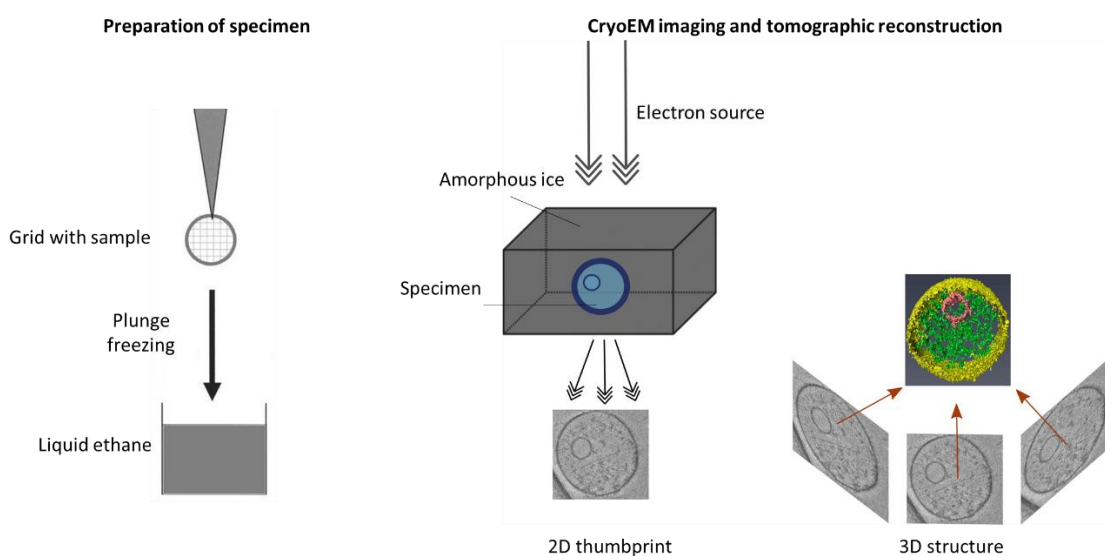

Figure 1-4. Cryo electron microscopy workflow: Preparation of sample by plunge-freezing in liquid ethane (left): a grid on which the sample has been deposited is instantly dipped in liquid ethane and vitrification of the specimen is achieved by the formation of amorphous ice. Imaging configuration for 2-D and 3-D structures (right): a 2-D image of the specimen is generated by the transmission of electrons through the sample when the grid is at 0º tilt on the axis of the transmitted electrons; a 3-D image of the specimen can be reconstructed by recording a series of images of the sample when the grid is tilted.

CryoEM has been successfully applied to the study of EVs derived from various human fluids as well as animal, plant tissues, microbes and viruses (Turpin, Kruglik and Curie, 2012) (Zeev-Ben-Mordehai *et al.*, 2014) (Renelli *et al.*, 2004). A brief overview of the most interesting studies where cryoEM has been used on human and mouse EVs is presented in Table 1.1.

Table 1.1. Cryo Electron Microscopy studies on EVs.

Sample	Method for EV preparation	Freezing technique	Reference
Platelet free plasma	Labelling with protein-conjugated gold nanoparticles	Plunge freezing in ethane	(Arraud *et al.*, 2014) (Gámez-Valero *et al.*, 2016)
	Pure unprocessed plasma		
▪ **Platelet rich plasma** ▪ **Platelet free plasma**	Citrate-EDTA anticoagulation		(Yuana *et al.*, 2013)
▪ **Platelet poor plasma** ▪ **THP1 (leukaemia) cell line**	Fresh vesicles		(Issman *et al.*, 2013)
	-80°C freezing and thawing		
▪ **MDA321 (breast cancer)** ▪ **HVT (villous trophoblasts) cell lines**	Fresh vesicles		
LIM (colon carcinoma) cell line	Fresh vesicles		(Xu *et al.*, 2015)
Human semen	Unprocessed material		(Ho and Lo, 2015)
Human pleural fluid	-80°C freezing until use		(Roca *et al.*, 2016)
▪ **Madin-Darby canine kidney (MDCK) cells** ▪ **Oncogenic H-Ras-transformed MDCK derivative 21D1 cells**	Freshly isolated vesicles		(Tauro *et al.*, 2013)
Mouse urinary sample	Fresh unprocessed vesicles		(Conde-Vancells *et al.*, 2010)
	Fresh negatively stained vesicles with uranyl acetate		

Flow Cytometry

Flow cytometry is a versatile method of analysis for biological entities such as particles or cells regarding their light scattering properties and the presence of a fluorescent reporter. The basic configuration of the measurement is the streaming of the cells through a path, in which they are excited by a laser beam. The instrumentation consists of three main parts; the fluidic compartment, optics and detection electronics. The cells or particles form a stream either by hydrodynamic focusing (high volumetric sheath flow that confines the suspension in a stream), or acoustic focusing (acoustic radiation resonance device uses a capillary coupled to a piezoelectric transducer to bring particles in a tight line (Ward *et al.*, 2009)). The light source can be either a laser beam to excite the fluorophores and discriminate based on colour, or a light beam to measure the scattering profile of the particles. As the cells interfere with the laser beam, the light is scattered and two detectors

collect the scattered photons from a forward and side position, reflecting the size and granularity of the particle, respectively. Finally, the signal from the scattered light is converted into a digital signal by the electronics system, which can be then illustrated by a variety of plots of several parameters on a computer (Macey, 2007) (Wilkerson, 2012).

As flow cytometry has been long considered a technique mainly applicable to large entities such as cells, its use on EVs is a controversial topic. Although the light scattering method has been reported for EVs only following a polystyrene bead calibration step (Lacroix *et al.*, 2010), this technique has been criticized for its validity (Nolan, 2015). The scattering method introduces limitations concerning the refractive index and the dependence of the scattered intensity on the r^{-6} of the particles, while fluorescent sensing is independent of these parameters (Nolan, 2015). For conventional instrument setups, EV detection and phenotyping using fluorescent markers for flow cytometry has been reported for vesicles with a diameter below 600nm (Menck *et al.*, 2017) (Vagida *et al.*, 2017) as well as larger apoptotic bodies (Atkin-Smith *et al.*, 2017).

To overcome the sensitivity issues with conventional instruments, a commonly used approach for EV characterization involves the selective binding of the vesicles on large magnetic particles, forming a larger complex which can be detected within the conventional detection limits of cytometers (Vagida *et al.*, 2017), (Wiklander *et al.*, 2018). The principle behind immunomagnetic bead-based isolation is to use magnetic beads whose surface has been functionalized with vesicle-specific probes (antibodies) to capture vesicles with high selectivity (Figure 1-5). Efficient capturing of EV on the surface of the magnetic particles is essential to ensure the total population can be analysed and some of the most common EV markers used for this purpose are CD9, CD63 and CD81 (Théry, Zitvogel and Amigorena, 2002). Staining all particles with non-specific membrane dye can discriminate between the magnetic particles carrying vesicles and the unconjugated particles which only appear on the scatter plots. Further labelling of the compartments of interest can bring up the positive populations.
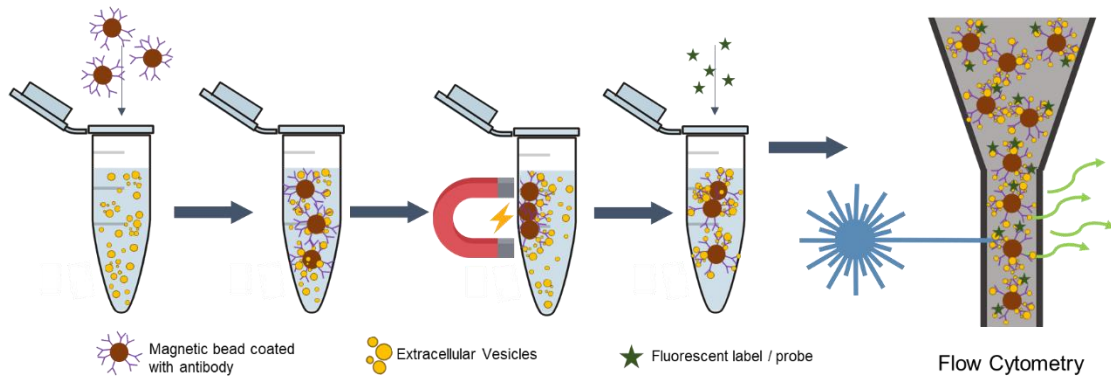
Figure 1-5. Schematic overview of immunomagnetic bead-based EV isolation and phenotyping by fluorescent labelling and flow cytometry. Magnetic beads coated with antibody against an EV surface molecule are incubated with EVs and the excessive unbound EVs are finally removed by the collection of the beads on a permanent magnet and washing off the EV-containing supernatant. Labelling of EVs with fluorescent or other probes can be performed on the bead-bound EVs and washing can be achieved again by the use of a magnet. The labelled bead-bound EVs can be measured by flow cytometry.

Examples of magnetic beads being used to isolate EVs and investigate their phenotype by flow cytometry can be found in various studies. Anti-MHC class II antibody coated magnetic beads (dynabeads) were used to isolate EVs from breast milk (Admyre *et al.*, 2007) and antigen-presenting cells (Clayton *et al.*, 2001), secondary antibody-coated beads (dynabeads) are also used for reticulocyte EV coupling, after conjugation with the appropriate antibody (Rabesandratana *et al.*, 1998). Streptavidin beads have been the vehicles to carry melanoma-derived EVs after being coated accordingly (Sharma *et al.*, 2018) and protein G beads were coated with Herceptin (anti HER-2 antibody used in cancer immunotherapy) to capture HER-2 positive vesicles (Koga *et al.*, 2005).

Although this method cannot provide data about the diameter or number of EVs, staining with fluorescent antibodies or other dyes enables EV phenotyping and is used for a large variety of molecules of interest (Oksvold, Neurauter and Pedersen, 2015), (Tauro *et al.*, 2012), (Koliha *et al.*, 2016). Another consideration about this method is that the results do not provide information about individual vesicles, but only an average of the population (Admyre *et al.*, 2003), (Morales-Kastresana and Jones, 2017).

Acknowledging the limitations of the bead-based cytometry and coming back to the cytometric analysis of free EVs in suspension, significant efforts have been made towards the development of flow cytometers specifically designed for smaller particles (Stoner *et al.*, 2016), (Pospichalova *et al.*, 2015), (van der Vlist *et al.*, 2012). In the case of direct EV

measurement, the quality of EV staining is crucial, as dye aggregates are a major cause of noise and artefacts. More recent advances enable the detection of particles with a diameter of 100 nm (Kormelink *et al.*, 2016), while variations of the conventional method such as imaging and high-resolution flow cytometry have introduced new potentials in EV measurements (Lannigan and Erdbruegger, 2017), (Erdbrügger *et al.*, 2014) and (Maas *et al.*, 2015).

Flow cytometry measurements are fast and offer the ability for analysis of multiple markers simultaneously. Despite the advantages, however, its use on EVs raises issues related to sensitivity for the smaller particles. In a comparison between flow cytometry and nanoparticle tracking analysis (NTA), it is a fact that NTA is by definition designed for particles smaller than 1 micron, therefore ensures higher sensitivity (Dragovic *et al.*, 2011), as there are parts of the total EV population which are not readable by flow cytometry due to the scattering signal from EVs being of intensity comparable to noise (Akers *et al.*, 2016). Although some custom-built instruments can bring the resolution down to approximately 100nm, for the phenotyping of even smaller vesicles, other techniques can be considered (Erdbrügger and Lannigan, 2016).

Dynamic Light Scattering (DLS)

Dynamic Light Scattering (DLS), also known as photon correlation spectroscopy, is a commonly used technique to characterize micro- and nano-particles and since the resolution range of the technique is 1 nm to 6 μm, it is particularly useful for different biologic samples which usually show a variety of size profiles. The results obtained with DLS are the mean hydrodynamic radius of the particles, polydispersity index and size distribution curves. The physical principles behind the method are the Brownian motion (particles moving in a fluid on random trajectories due to interaction with other particles) and the Tyndall effect (scattering of light by particles in colloidal suspension) (Dejan Arzenšek, 2010). When monochromatic light (laser beam, for example 633nm He-Ne laser (Lawrie *et al.*, 2009)) passes through a cuvette containing suspended particles, it interacts with them and is scattered to different directions. Because the particles are also moving due to Brownian motion at the same time, collection of the scattered beams from various angles can show significant intensity fluctuations. Larger particles diffuse more slowly in the solvent

compared to smaller ones and this is measured, which is reflected in the intensity curve of the detected signal (Bhattacharjee, 2016).

More practically, EVs derived from airway epithelial cells as well as from blood plasma have successfully been studied with DLS in two different studies. The results showed a mean hydrodynamic radius of approximately 300nm, with medium polydispersity index values (0.400) (Kesimer and Gupta, 2015). There have also been references to a highly sensitive method of determining the sample concentration when combining DLS with Bradford protein assay, achieving detection levels such as 0.01 mg/ml (Palmieri *et al.*, 2014) (Lawrie *et al.*, 2009).

DLS is one of the methods of choice for monodisperse colloids, however in the case of EVs where a broad size distribution is observed, this technique is facing a serious limitation. This is due to the fact that the intensity of the scattered light is dependent on the sixth power of the radius of the particles, meaning that a small population of large particles in the suspension contributes massively to the intensity readout, reducing the resolution for the smaller particles (Bhattacharjee, 2016).

Nanoparticle tracking analysis (NTA)

NTA is a recently developed (2006) technique, commercially known as NanoSight (Malvern Panalytical Ltd., United Kingdom) with many applications on nanoparticles ranging from 30nm to 1μm and especially on EVs (Filipe, Hawe and Jiskoot, 2010) .

The instrumentation and working principle of the measurement are as follows: the sample is a colloid enclosed between an optical prism and a glass window. A laser beam is focused through the prism into the solution and particles in the beam path scatter light. The illuminated particles are visualized directly by an optical microscope, and a CCD camera captures videos over a period of time (usually 30-60s with 30 frames per second) defined by the user. Particle movement is recorded in real time and the video can be furtherly analysed by the software in order to yield concentration and size distribution of the particles in suspension. The velocity of each particle is measured throughout the recorded frames, as the software can track an individual event over the recorded time. Next, the two-dimensional Stokes-Einstein equation (Equation 1) is solved for diameter, given the measured velocity and all other parameters related to the conditions of the measurement.

$$<x,y>^2 = \frac{K_B T_{ts}}{3\pi\eta d_h}$$
Equation 1

Where $<x,y>^2$ stands for mean square displacement, K_B for the Boltzmann's constant, T for temperature of the system (Kelvin), t_s for sampling time, η viscosity and d_h for the hydrodynamic diameter (Dragovic *et al.*, 2011).

In the biomedical field, NTA has been successfully used in the characterization of drug delivery systems with pharmaceutical interest (liposomes), protein aggregates and most importantly for this project, EVs (Filipe, Hawe and Jiskoot, 2010) with some of the most representative studies being described below. The number, size distribution and phenotype have been determined using a monochromatic laser beam at 405 nm in vesicles secreted from ovarian cancer cells isolated from blood by multiple centrifugation steps and chromatographic purification (Gercel-Taylor *et al.*, 2012). Another study proves the application of the technique on vesicles derived from immune cells isolated from T cell line cultures by sequential centrifugation and suggests that NTA is more accurate when particle concentration ranges between $2*10^8$ and $20*10^8$ particles per ml (Soo *et al.*, 2012).

The NTA method can also be used in fluorescence mode, where the particles are labelled with a fluorescent dye and the laser beam used is appropriate for the excitation of the fluorophore. In this case, the selection of the fluorophore plays an important role in the stability of the fluorescence signal, as the long exposure to the laser beam can cause bleaching. Quantum dots are considered to be among the most suitable probes, as they offer photostability and sensitivity for particles under 1 micron (Table 1.2) (Dragovic *et al.*, 2011). An example of how the NTA can be also used for analysis of a surface marker, but without fluorescent labelling has been reported for EVs from Jurkat cells which were captured on magnetic beads coated with anti-CD45 antibody and the levels of the CD45 positive EVs were determined by subtracting the EV number of the post-capture measurement from the pre-capture concentration (Soo *et al.*, 2012). The following table (Table 1.2) summarises a selection of studies measuring the levels of EV surface markers by NTA.

$$<x,y>^2 = \frac{K_B T_{ts}}{3\pi\eta d_h}$$

Table 1.2. Examples of NTA studies on the phenotype of EVs.

Origin of EVs	Surface marker under examination	Fluorescent probe	Reference
Placenta	NDOG2	Quantum dots	(Dragovic *et al.*, 2011)
Urine	CD24		(Oosthuyzen *et al.*, 2013)
Ovarian cancer	CD63 and EpCAM		(Gercel-Taylor *et al.*, 2012)
Maternal blood	CD63 and placental alkaline phosphatase		(Elfeky *et al.*, 2017) and (Miranda *et al.*, 2018)
Human ovarian cancer cells	Total EV population	PKH67	(Pasalic *et al.*, 2016)

NTA measurement is rapid (a complete set of 3 or 5 runs per sample can be performed in 4-6 min), provides real time tracking of the particles and additionally, the option for phenotypic analysis with the use of the appropriate fluorescent probe. Acknowledging that the EV samples are a heterogenous sum of particles, the Nanosight is especially sensitive for smaller particles but less reliable when larger particles such as solvent impurities are present. As described in the DLS section as well, this is due to the high intensity of light scattered from the larger EVs which 'hides' the light from the smaller particles on the detector (i.e. camera) and therefore it is essential to avoid impure media or dust in the measurement (Filipe, Hawe and Jiskoot, 2010). In addition, because the Rayleigh scattering depends on the refractive index of the particles, the angle of detection plays a crucial role in the quality of measurement and it is suggested that heterogenous samples are recorded multiple times with different focus positions, to ensure all particles have been imaged (Erdbrügger and Lannigan, 2016). Moreover, data acquisition requires a minimum level of user skills, since accurate measurements should be obtained by a) searching throughout the surface of the specimen to locate regions with a representative collection of different size populations, b) focusing the microscope and adjusting camera settings so that all populations are as clear as possible and c) adjusting processing parameters according to the specific nature of each sample (Filipe, Hawe and Jiskoot, 2010). The data obtained are large video files, which require large storage capacity and results processing need sophisticated manipulations with multiple variables to be adjusted, thus operator skills are necessary. More advanced instruments are starting to overcome limitations related to fluorescence imaging and automation, with the development of configurations using two fluorescence detection channels and the addition of autosamplers (van der Pol *et al.*, 2013a).

Fluorescence – The basics of lifetime

A physical phenomenon that has numerous applications in analytical techniques is fluorescence, the mechanism of which is illustrated in Figure 1-6 on the simplified Jablonski's diagram.
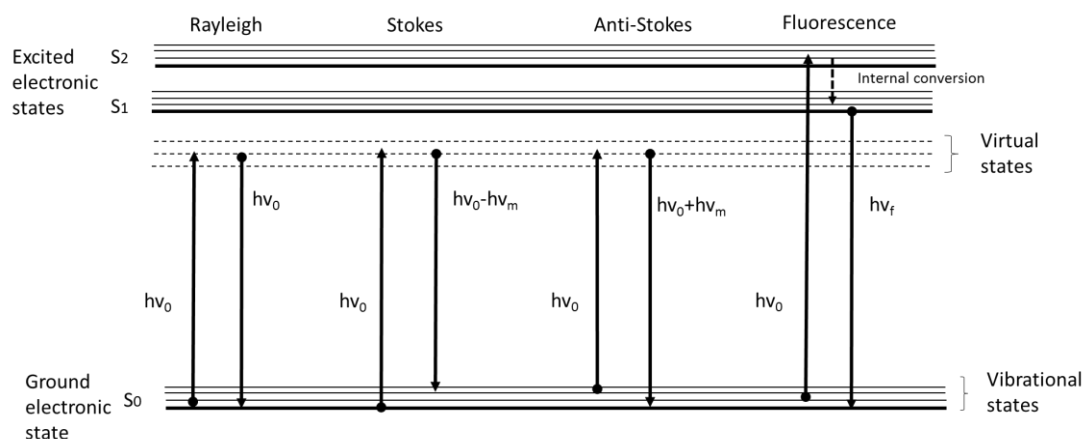

Figure 1-6. Simplified Jablonski diagram. S0, S1 and S2 represent the electronic states of the atoms in the ground (S0) and excited states (S1 and S2). The thin lines on every electronic state depict the vibrational levels and the dotted lines are the virtual energy states. When photons are absorbed by electrons found on S0, they cause their deformation to higher energy levels. Depending on the amount of the energy initially absorbed by the electron, and the energy released as the electron is returning to one of the ground states, several types of light emission can be defined: Rayleigh, Stokes and anti-Stokes and fluorescence. Each type of energy conversion mechanism is used in different analytical methods, for example Rayleigh scattering for NTA, Stokes for Raman and fluorescence for a variety of other techniques discussed in this thesis.

In this illustration, the electronic states of the atoms are depicted as S_0 for ground state and S_1, S_2 for excited states. Within the electronic states, thinner lines represent various vibrational states. There are also virtual energy levels (virtual states) which play an important role in the processes described below. Photons from the beam are transferred to the molecules of the sample, deforming them to higher vibrational levels.

When photons are absorbed, the atom is excited to a higher electronic state S_1 or S_2 and the excitation is followed by a rapid relaxation to the lowest vibrational level of S_1 which is a process named internal conversion. Fluorescence is the radiation emitted when returning to a vibrational state of the ground electronic state. The recording of fluorescence can be performed in two manners, which categorize the analytical methods in two large groups: the steady state and time-resolved mode. In the steady state measurement, the intensity of the emitted light is recorded upon excitation of the fluorophore with a continuous light source,

averaging the emission intensities from the total time period required for the phenomenon to be completed. In contrast, the time resolved mode uses a pulsed light beam and the emission from each pulse is recorded separately over time, resulting in a decay curve (Birch, Chen and Rolinski, 2015).

In lifetime measurements, depending on the approach followed, there are two main sides that can be explored. As for the time domain, the technique is named pulse fluorometry and in the frequency domain there is phase-modulation fluorometry. Although these two approaches are equivalent in theory, the experimental set up and data analysis reveals some differences. In pulse fluorometry a sharp excitation beam is interacting with the sample and the decay is recorded, while in phase-modulation method, the excitation light is modulated as to its phase or cropped as to the wavelength and is compared to the wavelength shift or level of modulation in the emitted light. The most common lifetime recording technique in the time domain is the Time-Correlated Single Photon Counting (TCSPC) in which the fluorophore of interest is excited by a pulsed laser beam (short pulses in the range of picoseconds or femtoseconds). The delay between the excitation and detection of fluorescent photons is measured, resulting in a decay curve of the dye, which illustrates the fluorescence intensity over time. Experimentally, in the TCSPC setup a pulsed laser provides a short excitation beam to the sample while a signal synchronized with the light pulse is used to trigger a timing system such as a time-to-amplitude converter (TAC). The TAC records an analogue signal proportional to the time difference between the reference pulse and the fluorescent photon detected and converts it to voltage, which is then stored as an event in a multichannel analyser (MCA). The decay photons are filtered and captured by a fast detector such as a photomultiplier tube able to detect single photons, after which the technique Single Photon Counting (SPC) is named. The completion of multiple circles as described above yields the decay curve. The initially simplex form TCSPC systems which allows recording of the fluorescent decay of one wavelength at a time can also be developed in multiplex systems enabling the recording of multiple dyes in the same sample and has facilitated microscopy and lifetime imaging (Gerritsen *et al.*, 2009).

Time-resolved Fluorescence Anisotropy (Depolarization)
Fluorescence anisotropy is a term that describes the diffusion of a fluorophore due to rotation and the migration of energy to other components of the microenvironment and is

measurable thanks to the ability of the fluorescent light to be polarized. The basics of this process involve the use of polarized light to excite the fluorophore (i.e. from all possible planes the excitation light can oscillate on, only one is allowed, excluding all others) which only excites the fluorescent molecules found parallel to the same plane at that moment. As the excited molecules rotate back to randomized positions due to Brownian motion or other energy transfer phenomena in the suspension, the emitted photons are recorded in a time-resolved mode, generating a depolarization curve. This curve illustrates the rotational behaviour of the fluorophore and gives information about the degrees of freedom of the molecule in the particular microenvironment (Birch, Chen and Rolinski, 2015).

Steady state and time resolved anisotropy can be determined by the same basic configuration of geometric planes of the polarized light and the molecular orientations. For time resolved depolarization measurements, the lifetime instrumentation is used (as described in the previous section 'Fluorescence – The basics of lifetime'), with the only addition of polarizers on the excitation and emission arm. Recording a series of decay curves and applying Equation 2 gives a time resolved correlation between anisotropy (r) and the measured parameters.

$$r(t) = \frac{I_{VV}(t) - G I_{VH}(t)}{I_{VV}(t) + 2 G I_{VH}(t)} \qquad \text{Equation 2}$$

where $I_{VV}(t)$ and $I_{VH}(t)$ are the fluorescence decay curves recorded vertically (V) and horizontally (H) after having excited the sample with a vertically (V) polarized source. G ($G = \frac{I_{HV}(t)}{I_{HH}(t)}$) is a factor used to correct the difference in the transmissions of fluorescent signal between the vertical and horizontal positions that result from the parts of the instrumentation (Birch, Chen and Rolinski, 2015).

By further calculations, Equation 3 arises, where r_0 stands for the initial anisotropy at t=0 and τ_c for the rotational correlation time, which is the rate of depolarization due to isotropic rotation. The maximum value for r_0 is 0.4 from the literature (Birch, Chen and Rolinski, 2015), (Lakowicz and Knutson, 1980), (Bisby and Birch, 1989).

$$r(t) = r0 \, exp \left(-\frac{t}{\tau_c} \right) \qquad \text{Equation 3}$$

Equation 3 can be altered into binomial (Equation 4) when the fluorophore is present in two or more different environments, for example the molecules incorporated within the lipid

bilayer of the membrane and the free dye molecules. Both species have different rotational correlation time values which reflect their freedom to rotate within the microenvironment.

A useful value that should be defined at this point is the membrane order parameter (S) which describes how strictly the membrane components are ordered. Membrane order is a function of the initial anisotropy, r_0 and the residual anisotropy in infinite time, r_∞.

$$S = \sqrt{\frac{r_\infty}{r_0}}$$

Equation 4

Anisotropy has been long used to study the fluidity properties of biological membranes in their physiological state or after changes of pH, temperature, mechanical stress or other physical parameters. Model membranes such as liposomes with known lipid composition have been initially used (Birch, Holmes and Imhof, 1988) to prove that fluorescence depolarization can detect even subtle changes of the fluorophore's rotational behaviour under a variety of stimuli (Bisby and Birch, 1989), (Holmes *et al.*, 1991), (Holmes *et al.*, 1997).

This method has been extensively applied on cell membranes for the examination of lipid rafts, with the first references dating back to the 70's (Shinitzky and Inbar, 1976a; Schachter and Shinitzky, 1977), continuing up to recently (Troup *et al.*, 2006; Ben-Dov and Korenstein, 2013). The membrane of EVs is a topic studied to a smaller extent because of the challenges associated with their heterogenous size, however, fluorescence anisotropy is a method sensitive enough to detect changes in nanovesicles and give information about the membrane integrity, a critical factor when it comes to cargo transfer and exchange of biological materials. EVs isolated from dendritic and mast cells were stained with DPH (diphenyl-hexatriene) and the steady state anisotropy was determined for a range of pH and temperature values. The results showed that the membrane fluidity rises for pH 5-7, indicating that the membrane is potentially rearranged as the EVs migrate from the acidic multivesicular bodies to the neutral environment of the extracellular matrix (Laulagnier *et al.*, 2004). DPH with steady state measurement was applied on a similar setting for the study of epididymosomes, EVs found in the epididymal fluid, showing that there are changes in the levels of sphingomyelin and increased microviscosity as the EVs are transferred to the final compartments of the organ (Rejraji *et al.*, 2006). One more application of the above setup has been described for EVs from ovarian cancer, showing that the phase transition point of those membranes is found around 37°C (Shenoy *et al.*, 2018). The examples reviewed here

use steady state anisotropy measurement systems, and it is observed that there is a lack of studies on depolarization using time-resolved instrumentation (TCSPC) and therefore, one of the goals of this thesis is to analyse the EVs in the time domain.

Fluorescence microscopy and super resolution microscopy

Visualizing EVs directly in tissues or organisms is a topic on which a lot of attention has been drawn, as live imaging can answer basic and remaining questions about the biogenesis, trafficking, interactions and clearance of EVs. Several groups have reported the imaging of EVs by fluorescence microscopy, either by conventional confocal setup or super resolution methods, extracting information from a resolution which depends on the limits of each imaging modality. As EVs range from a few nm up to microns in diameter, it is acknowledged that detailed brightfield imaging is not possible for the smaller fractions of EV, as the resolution of a conventional microscope is limited by light diffraction to approximately 200-300nm. However, by attaching a fluorophore on EVs and using a configuration which eliminates out-of-focus light and 'sharpens' the emitted signal such as a confocal, EVs and their interactions with live biological systems can be studied. As confocal microscopy offers the option of live imaging, there are several examples of its use in localizing the EVs in cells. To name a few, EVs with a dimeter around 50 to 80 nm were imaged within the Golgi complex (Nakano, 2002), or inside cellular compartments upon uptake (Lai *et al.*, 2015; Lerner, Avissar and Beit-Yannai, 2017). The mechanism of uptake of EVs by cancer cells was also investigated (Koga *et al.*, 2005), while CD63-labelled EVs have been tracked in zebrafish live (Verweij *et al.*, 2019). In addition, individual EVs attached on a solid surface can be directly imaged for the purpose of phenotyping by appropriate staining (Hisada *et al.*, 2017), while a number of articles refer to the use of multiphoton microscopy for direct imaging in live tissue (see (Panagopoulou *et al.*, 2020) for a review of applications).

Given the small size of the EVs, confocal microscopy has by definition limitations in imaging the whole range of sizes and therefore, super resolution microscopy is considered the most suitable approach, as it breaks the diffraction limit. This general category of microscopy techniques includes, among others, the direct Stochastic Optical Reconstruction Microscopy (dSTORM), which is based on the chemical induction of 'blinking' of a fluorophore so that not all molecules emit simultaneously, allowing precise localization of each isolated emitter. By taking a series of frames in which different molecules blink randomly at different locations,

the final reconstruction gives a detailed representation of the image with a resolution at even 20 nm (Rust, Bates and Zhuang, 2006; Van De Linde *et al.*, 2011). Examples of the application of STORM on EVs is the imaging of CD9-labelled particles inside dendrites of cells from Alzheimer's animal tissue (Polanco *et al.*, 2018), or the study of interactions of CD63-labelled EVs from breast cancer with other cell types (Chen *et al.*, 2016). In this work, confocal microscopy has been mainly applied on EV live tracking and phenotyping, and STORM has been used to a smaller extent, for the structural imaging of the particles.

Both microscopy strategies have strengths and limitations which are inherent to the working principle, thus the selection of the appropriate setup depending on the scientific question of the experiment is crucial. For confocal microscopy live imaging is possible, while a wide range of fluorophores is available for EVs and other tissues. On the contrary, STORM is mainly performed on fixed samples and the list of suitable dyes is significantly shorter, as they need to be chemically suitable for 'blinking' (Godin, Lounis and Cognet, 2014). Recent advances in the field promise super resolution tracking of EVs intracellularly, as well as simultaneous size profiling, as alternative to NTA (ONI, 2019).

qPCR for RNA

Most of the methods discussed earlier in this chapter refer mainly to the detection of specific protein cargo on the vesicles, especially by fluorescent or immunogold labelling. However, as mentioned earlier in the Introduction, some very distinct EV biomarkers are nucleic acids and especially various types of RNA. There is a large number of studies in which mRNA, miRNAs or other small RNA sequences have been shown to give EVs special functional or phenotypic properties and the method of choice for analysis of these macromolecules is quantitative Polymerase Chain Reaction (qPCR) after reverse transcription of the RNA in DNA (RT-qPCR) (Liu and Lu, 2015), (Sun *et al.*, 2018). Apart from RNA, DNA has been also reported in EVs, especially from vesicles secreted from apoptotic cells (unpublished data, Gregory lab) or other EV types (Momen-Heravi, Getting and Moschos, 2018; Wang *et al.*, 2018). The working principle of this technique is the use of a fluorescent probe which only fluoresces upon hybridization with the product of each cycle of the polymerase reaction, therefore, the kinetics of the fluorescence intensity indicate the levels of the existing sequence of interest. As the fluorescence intensity gives only relative levels of expression, but does not reflect the absolute quantity of the initial sample, it is essential to apply endogenous controls of stable

expression of an RNA, in order to normalize the values of each run, as well as controls on the sequence of interest so that the final result is expressed in -fold increase or decrease in the levels of the sequence of interest compared to the control (Jo Vandesompele *et al.*, 2002; Bustin *et al.*, 2009; IRIC, 2017). Practical considerations in the performance of qPCR for the EV samples are discussed in the relevant chapter (Chapter 4).

Fluorescent labelling technologies

As the majority of methods discussed and used in this thesis use fluorescence, it is important to give a brief overview of the range of labelling probes for EV components. Also, given the small EV diameter, taking into consideration the size of the fluorescent probes is in some cases essential, to avoid mis-match between the labelling probe and the imaging method (Figure 1-7).
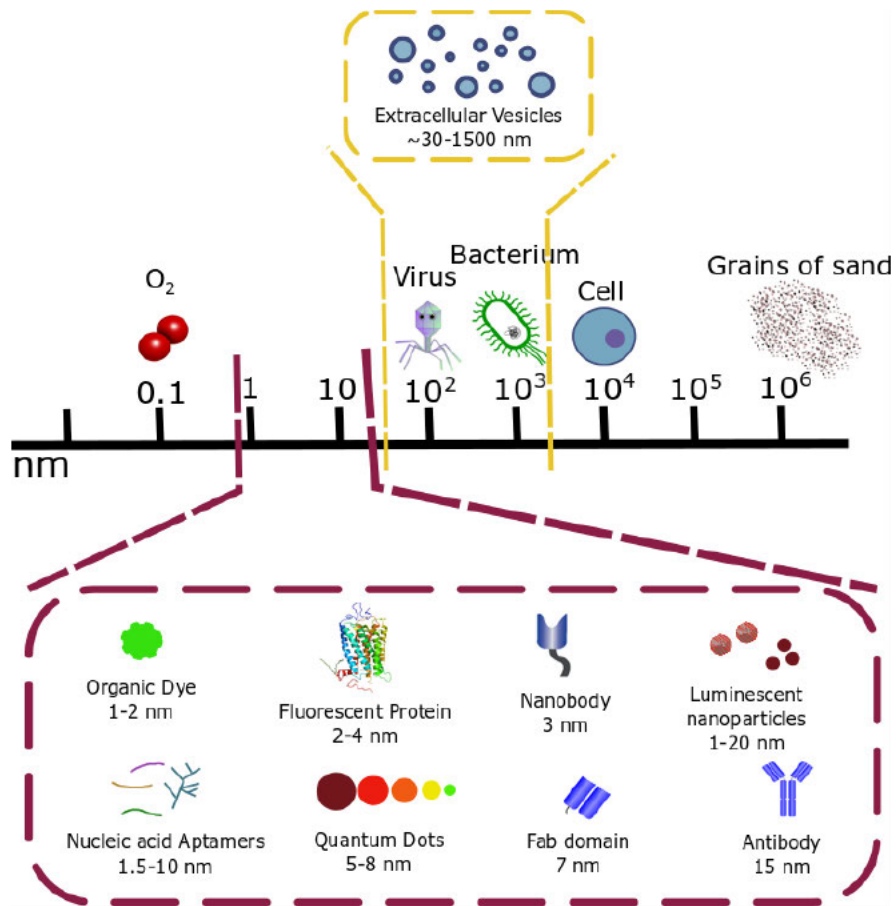
Figure 1-7. Size scale for EV diameter and size of labelling probes. The EVs are smaller than cells and bacteria; the box illustrates a variety of fluorescent dyes and probes which can be used for the labelling of EVs, with respect to the size of each molecule/probe (re-printed with permission from (Panagopoulou *et al.*, 2020)).

There are three main strategies for labelling and examples of each of these are given in the following table (Table 1.3).

Table 1.3. Examples of dyes and affinity probes used on EVs or with potential for EV use, categorized by mechanism of labelling. Content extracted and adapted from (Panagopoulou *et al.*, 2020).

Labelling mechanism	Examples of dyes/probes	Application	Reference
Hydrophobic interactions or genetically	Calcein AM	Flow cytometric study of membrane integrity	(Gray, Mitchell and Searles, 2015)

encoding fluorescent proteins	BODIPY-PC, DiI, Dio, DiC	Flow cytometry and microscopy	(Nicola, Frases and Casadevall, 2009)
	PKH26, PKH67	High resolution flow cytometry, confocal and fluorescence lifetime microscopy	(Dabrowska *et al.*, 2018), (Macklin *et al.*, 2016)
	PY3304, PY3174 and PY3184	Imaging membrane order (artificial vesicles)	(Kwiatek *et al.*, 2013)
	di-4-ANEPPDHQ		(Jin *et al.*, 2006)
Covalent chemical bond of a fluorescent agent with an affinity probe	AlexaFluor and Atto range	Super resolution microscopy (STORM)	(Van De Linde *et al.*, 2011)
	Red-NIR dyes such as azadioxatriangulenium (ADOTA)	Fluorescence lifetime spectroscopy and anisotropy	(Sorensen *et al.*, 2013)
	Luminescent nanoparticles: quantum dots	Nanoparticle tracking analysis	(Carnell-Morris *et al.*, 2017)
	Luminescent nanoparticles: upconversion nanoparticles, nanodiamonds and gold nanoparticles	Microscopy and spectroscopy	(Sreenivasan, Zvyagin and Goldys, 2013)
Affinity probes for labelling	Antibodies	Microscopy, flow cytometry, immunogold EM, NTA	Widespread first-line use
	Nanobodies	Microscopy and super resolution microscopy	(Ries *et al.*, 2012)
	Nucleic acid aptamers	Signal amplification by dendrimers; imaging by microscopy	(Tian *et al.*, 2018)

Other methods of analysis

The methods discussed in the previous paragraphs are some of the most well-established approaches for overcoming the challenges of analysing EVs and are applied to this doctoral project on different levels. However, it is essential to acknowledge that there is a long list of other technologies, most of which are currently under development and promise to simplify EV procedures and bridge the distance between laboratory research and clinical use. A characteristic example of platforms for isolation and analysis of EVs in one device is the microfluidics chips and microarrays, which miniaturize laboratory procedures on a cartridge with several functional compartments. For example, serum can be processed on a chip and the EVs have been analysed for a pancreatic mRNA biomarker using a nucleic acid hybridization and signal amplification reaction (Hu *et al.*, 2017). A more simple setup involves the immobilization of EVs on a CD63 binding surface and after staining with the fluorescent probes of interest, the signal can be read by other instruments such as a plate reader or a confocal microscope (Kanwar *et al.*, 2014).

Research is also moving towards the improvement of the currently used methods, for example by the addition of an autosampler for automation of Nanosight measurements (van der Pol *et al.*, 2013b). Novel commercial platforms are also being developed for the purpose of phenotyping using fluorescent tags on microfluidics compartments (Bachurski *et al.*, 2019), (Lee *et al.*, 2018). Finally, there is a variety of spectroscopic methods which have been applied on EVs or similar systems including mass spectroscopy for lipid, protein and nucleic acid sequencing, Raman spectroscopy, micronuclear magnetic resonance (microNMR) and small-angle X-ray scattering (SAXS), however are not discussed in more detail for the purpose of this thesis.

1.6. Extracellular vesicle isolation, purification and storage

The International Society for Extracellular Vesicles (ISEV) has identified the lack of standardized isolation workflow and are making efforts towards the establishment of protocols for isolation and enrichment of EV samples (Gardiner *et al.*, 2016; Clayton *et al.*, 2019), so that EVs can be used more widely and reliably in both research and clinical settings (Ramirez *et al.*, 2018).

Among the most common isolation methods are gel permeation chromatography, immunoaffinity capture or polymer-facilitated precipitation or ultracentrifugation among others (Lane *et al.*, 2018). The different isolation strategies are taking advantage of distinct EV properties such as size, surface charge, density, affinity for biological targets and hydrophilic interactions with solvents (Konoshenko *et al.*, 2018). More recent approaches based on microfluidics promise both capture and analysis of EVs on the same device as mentioned earlier. Some of the most popular isolation methods are presented in Figure 1-8. Due to the heterogenous nature of EV populations, combinations of methods are often used in order to overcome the limitations of each strategy. Moreover, each method yields slightly different EV populations or with different levels of enrichment in proteins or nucleic acids etc, therefore a common point authors often make when comparing different techniques is that the isolation protocol needs to be carefully selected, taking into account the purpose the EVs will be used for (Tauro *et al.*, 2012; Patel *et al.*, 2019). For example, EVs from spin column chromatography are preferred for RNA analysis over other methods (Mussack, Wittmann and Pfaffl, 2019).
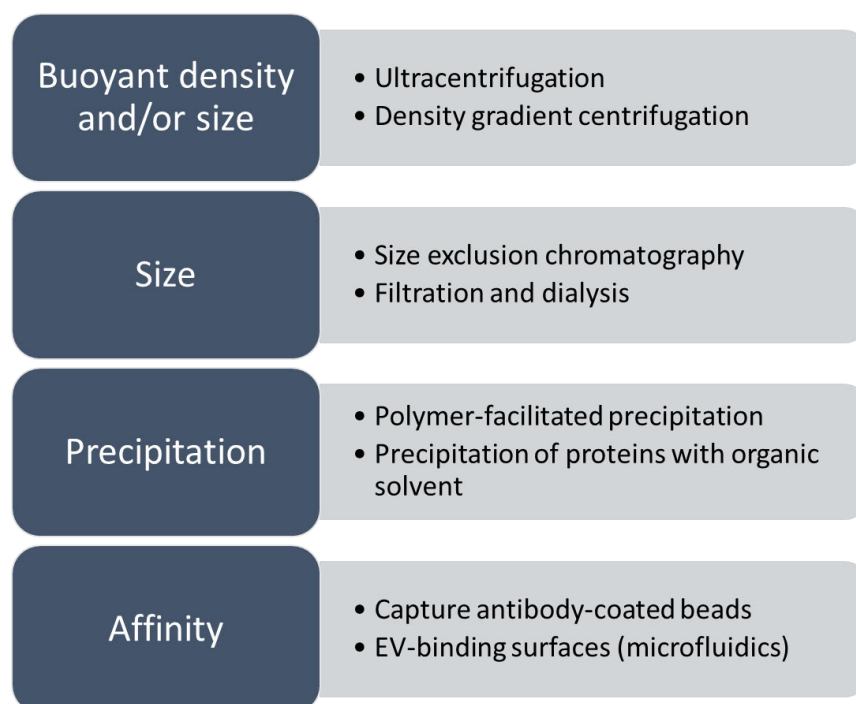

Figure 1-8. List of most commonly used methods in EV isolation (extracted from literature search, see main text for a description).

One of the historically first and very classical ways of preparing an EV suspension from cell culture supernatants or biological fluids is ultracentrifugation (UC). This approach separates EVs using their density and was established in 2006 in a protocol where the EV suspension is centrifuged at 100,000g for 70min (Théry *et al.*, 2006). UC has been a popular method for a number of research groups (Willms *et al.*, 2018), while a survey is showing over 80% of the EV researchers are routinely using it (Bu *et al.*, 2019). However, there is a theoretical background in the optimal centrifugation conditions for maximum EV recovery and while it is essential that the centrifugation conditions are calculated and adjusted to each rotor type, this step is often overlooked by researchers, resulting in variations in the EV preparations among the different studies (Cvjetkovic, Lötvall and Lässer, 2014; Livshts *et al.*, 2015; Zhang, Yeo and Lim, 2019). As ultracentrifugation can lead to other types of particles being pelleted with the EVs, a variation of classical UC is the density gradient UC, in which the EVs are ultracentrifuged in a density cushion, resulting in the EVs being retained in the appropriate layer, while other particles of different densities such as mitochondria are found in other levels (Webber and Clayton, 2013; Campoy *et al.*, 2016).

However, this technique has not been the method of choice in this thesis, as there are concerns about the quality of the EV preparation and enrichment in proteins of interest. In a comparison among ultracentrifugation, immunomagnetic bead isolation and density gradient centrifugation, the Transmission Electron Microscopy images of the EVs showed vesicle aggregation and structural distortion, while the EV protein recovery after ultracentrifugation was lower than the other two methods (Tauro *et al.*, 2012). In another study in which ultracentrifuged EVs were compared with EVs isolated from commercial immunocapture or density gradient kits, the EV specific proteins and RNA levels were significantly lower for the UC EVs than other kits (Patel *et al.*, 2019).

Another series of isolation methods involves different versions of filtration of EV. There are several types of 'filters' through which the EVs are separated by size such as through a membrane filter, a dialysis compartment or gel chromatography. In more detail, filtration through a membrane with small pores has been used as a stand-alone method or in combination with other steps such as UC or gel chromatography. Typical pore sizes range from 0.8 μm to 0.1 μm and the EVs can be fractionated as per size by the application of

multiple filters sequentially (Konoshenko *et al.*, 2018). A very promising filtration approach which recovers the majority of EV is based on the use of 100kDa centrifugal filters, where the separation is assisted by centrifugation at 3,000g (Cheruvanky *et al.*, 2007). It is expected that this method also has limitations in the EV yield and quality, because for large pore sizes the smaller EVs are filtered through, while for small pores such as the 100kDa, some contaminating proteins might be retained in the EV fraction. The latter was shown in a comparative study between UC and 100kDa filtration, where the EV contained lower levels of EV-related proteins and higher contaminant levels (Rood *et al.*, 2010). An additional drawback is that EVs tend to bind and aggregate on the surface of most membranes (even on the low-protein-binding membranes) and in order to reduce the EV loss, more centrifugation or vacuum steps are often followed, the impact of which on the structural integrity of EVs is yet to be investigated (Taylor and Shah, 2015).

Within the filtration category, a similar principle separates EVs from particles of different sizes by dialysis driven by hydrostatic pressure, called hydrostatic filtration dialysis. The EV suspension is retained into a 1000kDa membrane and all soluble components are dialysed to the buffer outside the membrane. This is a method that allows large volumes of dilute EV samples such as urine to be cleared from proteins, although one of the disadvantages is that some small vesicles can be dialyzed off the EV preparation (Tataruch-Weinert *et al.*, 2016).

Size exclusion, or gel filtration chromatography (SEC) is a filtration-type separation technique, although the EVs are passing through a gel rather than a porous membrane. In this method, a chromatography column is stacked with filling material which is often sepharose. This material consists of microscopic beads which have grooves and interdigitations that trap the smaller particles of the suspension. The impure EV sample is allowed to run through the column and the particles of smaller diameter or proteins and soluble factors are interacting with the filling material, delaying their elution. On the contrary, the larger entities such as the EVs exit the column first and therefore, by collecting sequential fractions during elution, the separation of EVs from soluble components can be achieved. Analysis of the EV and protein content of each fraction has shown that for a column of the appropriate dimensions, the EV-containing fractions do not overlap with the protein-containing fractions (Böing *et al.*, 2014; Welton *et al.*, 2015). More recent efforts to optimize the performance of SEC have been made in order to determine the most efficient filling material and elute. The EVs obtained from comparing various parameters were analysed for

their protein content by a sensitive technique based on mass spectroscopy and it was concluded that Sepharose CL-4B in combination with PBS ensures the highest resolution in EV-protein separation (Lane *et al.*, 2019).

One disadvantage of this technique is that chylomicrons or large lipoproteins from plasma samples might be eluted together with the EVs (Taylor and Shah, 2015) , and besides, the EV suspension is diluted after elution which often means that a concentration step is needed.

The next range of isolation methods includes several techniques based on the change of solubility or precipitation. Separation between the soluble materials and organic particles such as EVs takes place by the addition of a hydrophilic polymer (often polyethylenoglycol, PEG) in the aqueous EV suspension. The molecules of the suspension medium (i.e. water) are used to solubilize the polymer and therefore, they become less available to the EVs, leading to the reduction of their affinity for the solvent. As a result, the EVs can be removed from the suspension by a centrifugation step at relatively low speed, often 1500 g. The basic idea of this method has been described since 1970, when it was used to isolate viruses (Yamamoto *et al.*, 1970). However, it has been successfully applied in the EV field and is currently in use, especially after the commercialization of relevant kits dedicated for EVs and although EVs have been isolated in high yields (Antounians *et al.*, 2019), the working principle reveals one significant drawback of this method. This is the co-precipitation of large particles such as albumin aggregates or other (eg blood) components, leading to compromised purity of preparations, especially for plasma derived EVs. In a comparative study among SEC and precipitation by a commercial kit, and precipitation coupled with a chromatographic device, it was shown that the SEC column results in the highest purity of plasma derived EVs, followed by chromatography-coupled precipitation and finally precipitation alone (Lobb *et al.*, 2015).

The methods listed above are some of the most widely used and extensively studied techniques which are based on the physical properties of EVs. However, some biological features can be also used for effective isolation and purification, such as immunoaffinity binding on surfaces or beads. Surfaces coated with antibodies specific against EV surface molecules are trending mainly in microfluidic systems, however, in this work, immunomagnetic beads have been used to perform selection and characterisation and are discussed in more detail. Besides selectivity, immunomagnetic beads are a gentle means of

handling EVs as their coupling on larger entities allows the performance of various processing steps by the use of low force magnetic attraction. Chemical modification of the bead surface with antibodies adds the property of versatility and makes this platform the method of choice for a number of applications (Ruffert, 2016).

This approach has been especially useful for plasma-EVs, as plasma comprises of a large number of components with a size similar to the vesicles of interest. This results in the contamination of the vesicle population with large protein aggregates (mostly lipoproteins), cell and platelet fragments and most interestingly, chylomicrons, a type of micelles of lipids and proteins that cannot be reliably removed by common purification methods such as centrifugation or size exclusion chromatography (Sódar *et al.*, 2016; Simonsen, 2017).

Storage

As the EV field has seen rapid expansion over the past few decades, researchers have been focusing on their properties and functions, however, the EV stability under storage conditions has been investigated to a smaller extent. Some key facts regarding storage and handling have been recently shared by Clayton *et. al.*, indicating the need for the establishment of common procedures among different research units so that results can be compared and validated (Clayton *et al.*, 2019).

Because either human or animal blood is collected usually according to specific clinical protocols or guidelines, time becomes a significant parameter in plasma handling. This means that it is often necessary to store plasma for future use or store aliquots of the same donor's plasma for further research, or until a trial is completed and samples from all timepoints have been collected. Some research has been conducted on the optimal conditions of storage and quality of plasma derived vesicles and the common storage method is freezing at -80°C after removing the platelets, which would otherwise become activated during the freezing-thawing procedure (Kriebardis *et al.*, 2016), (Witwer *et al.*, 2013). Also, depending on the components of interest in EVs, the conditions can differ; for example, it has been shown that DNA content remains generally intact after freezing and thawing cycles or after 7 days at different temperatures (Jin *et al.*, 2016). Also, the use of cryoprotectant is another variable which can have an effect on the EV properties such as increased secretion of pro-coagulant vesicles from frozen platelet preparations (Tegegn *et*

al., 2016). It is therefore important to identify the appropriate method to ensure maximum recovery of the molecules of interest.

Among the publications discussing the optimal conditions of storage for EVs in general, only a small number refer to cell culture supernatant-derived EVs, possibly due to the urgent need to study biological fluid- derived EVs (Jeyaram and Jay, 2018). From this limited number of articles, it is indicated that, similarly to blood plasma, freezing at -80°C results in the smallest reduction in EV number and RNA content compared to $+4\,^{\circ}$C or $-20\,^{\circ}$C (Witwer *et al.*, 2013; Lorincz *et al.*, 2014).

1.7. Hypothesis and Aims of the project

Based on previous studies showing the effects of apoptotic tumour cells in disease progression, and with preliminary evidence supporting the notion that Apo-EVs are involved in the oncoregenerative network, it is hypothesized that the detection of Apo-EVs in patients can serve as an indication of the stage and aggressiveness of a malignant disease. As discussed earlier in this chapter (1.2) for BL, the diagnostic and monitoring protocols can be invasive and often lacking important information, which is one reason behind unsuccessful therapeutic attempts. It is also known that the levels of apoptosis play a significant role in the patient's clinical outcome and can be used as indicators of stages of the tumour, metastatic tendency and overall survival prognosis not only for BL, but for other highly aggressive tumours such as squamous carcinoma, synovial sarcoma and bladder cancer for example (Naresh *et al.*, 2001b), (Kawauchi *et al.*, 2000), (Lara *et al.*, 1999)(Leoncini *et al.*, 1993). Therefore, the development of a minimally invasive analysis which would offer the ability for continuous monitoring and the collection of multiple samples could provide clinicians with a useful platform which could enable early detection and more efficient planning of the appropriate therapeutic strategy.

The main aim of this project is to explore the nature of apoptotic tumour cell-derived EVs and reveal their potential as blood biomarkers in BL, but also in other tumours where the apoptotic index offers prognostic value (see above).

To achieve this goal, there are two points to be addressed:

a) as the field of Apo-EVs is currently emerging, the information about these vesicles is limited, and especially in the case of lymphoma, the existing knowledge about their biochemical properties is insufficient. Therefore, in order to use Apo-EVs in analysis, it is essential to understand the molecular and structural differences of those populations in comparison to other tumour-derived, non-Apo-EVs.

b) the detection of Apo-EVs in the blood highly depends on their availability and the potential cross-talk they have with the circulating components of the blood. It is important to assess whether the Apo-signals are maintained in the EVs or are transferred to cells including platelets in the blood, as this information will drastically shape the analysis procedure.

For the first point, which is the largest part of this thesis, emphasis has been given on the methods which can be used to answer those basic questions about Apo-EVs. Acknowledging that the EVs are significantly smaller than cells, the techniques suitable for detection and analysis are lying in the area of nanometrology or can be methods used for cells which have been adapted for the detection of vesicles. Of special interest is the application of a variety of methods for Apo-EV analysis, each of which targets a specific subset of the EV spectrum and can give different sets of information. A comparison between similar methods will also be an important part of this process, in an attempt to set the bases for standardisation of future analyses. The features where differences between Apo-EVs and non-apoptotic tumour cell EVs will be sought are the physical structure, the membrane fluidity properties, size distribution and secretion patterns, protein and RNA markers. A schematic example of how the available techniques should be critically examined and how multiple methods could be used for the confirmation of results is shown in Figure 1-9.
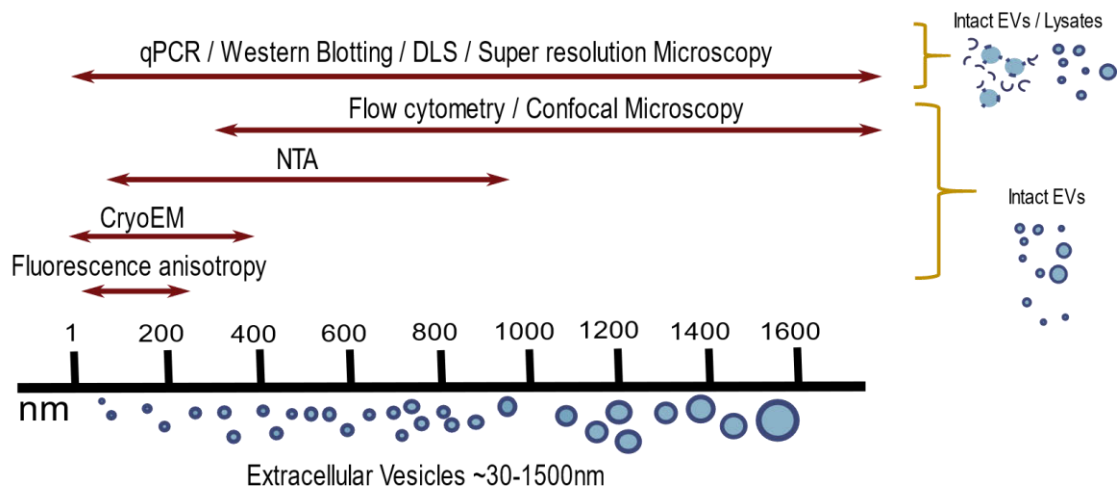
Figure 1-9. Size scale of EVs and resolution of available analysis methods. The methods of analysis can be grouped in those which can measure intact EVs, such as the NTA, cryoEM, anisotropy, DLS, microscopy and flow cytometry and the techniques in which the EVs can be lysed, such as qPCR and Western blotting. Each of the above methods can examine a specific range of EV sizes, therefore they need to be selected with respect to the research question.

For the second part where the Apo-EV are examined in blood, platelets, erythrocytes and leukocytes from the blood of healthy volunteers are treated with EVs and this interaction is measured in terms of quantity and quality. The levels of uptake are assessed and the nature of EV-cell interaction is also studied in order to determine whether the Apo-EVs are only binding on the surface of the cells or can be internalized and possibly deliver their cargo intracellularly. An initial examination of potential Apo-EV marker transfer in treated platelets is also performed, as platelets are less complex structures compared to the cells and those observations can assist in optimising the procedures for further studies.

Both parts of this study are performed on *in vitro* generated vesicles from Burkitt's lymphoma cell lines, and more details on the practical objectives of each section are presented in the relevant results chapters.

2. Materials and Methods

2.1. Cell culture

Two human Burkitt Lymphoma (BL) cell lines were used for EV isolation *in vitro*, the BL2 and BL2-Bcl-2. This is because in order to assess the uniqueness of the Apo-EV characteristics compared to non-apoptotic tumour cell EVs, a control physiological vesicle population is required. For this purpose, a special cell line was used, which is a BL2 apoptosis-resistant line transfected with the apoptosis-suppressing gene Bcl-2. The BL2-Bcl-2 cells are resistant to apoptosis and have been previously generated by colleagues in the Gregory group by transfecting BL2 cells with the Bcl-2 gene using an existing protocol (Wang *et al.*, 1996). All cells have been cultured in serum-free media (RPMI 1640 and X-Vivo 20) at 37°C, 100% humidity and 5% CO_2.

2.2. EV preparations *in vitro*

2.2.1. From cultured cells

BL2 and BL2-bcl-2 cells were exposed to apoptosis inducing factor (UV treatment) and next, Apo-EVs and the corresponding Bcl-2 control vesicles were isolated from the culture supernatants. The process involved UV irradiation of the cells at high concentration ($20*10^6$ cells/ml) followed by incubation in standard culture conditions while apoptosis was being monitored hourly. In more detail, apoptosis was induced on cells by UV-B irradiation using a CL-1000 Ultraviolet Crossslinker instrument and a total dose of 3,000 mJ/cm^2 as 6 doses of 500 mJ/cm^2. The conditions for the UV irradiation regarding the dose and the concentration of the cells have been established by Margaret Paterson in the Gregory group in order for the cells to undergo apoptosis but not proceed to necrosis by the end of the incubation period. Because there is a time-dependent relationship between apoptosis and subsequent secondary necrosis, both apoptosis and necrosis were measured every hour after UV treatment. Annexin V assay is a well-established method for assessing the level of apoptosis and is based on the translocation of the phospholipid phosphatidyl serine (PS) from the inner side of the cell membrane where it is physiologically found, to the outer part when the cell becomes apoptotic (van Engeland, M., Nieland, L. J. W., Ramaekers, F. C. S., Schutte, B. and Reutelingsperger, 1998). Annexin V conjugated with Alexa Fluor 488 (Table 2.2) binds selectively to PS and can be detected by flow cytometry. Necrosis was measured by the

addition of a DNA stain, Sytox Blue which is a cell impermeable dye for non-necrotic cells, but manages to stain the DNA when the membrane is permeabilized (sign of necrosis). The aim was to isolate EVs from cells being Annexin V single positive with the minimum percentage of necrotic cells possible. At the time point when the Annexin V single positive cells count for at least 80% of the population (with Sytox Blue positive and double positive cells not exceeding 5%), the cells were harvested and the EVs isolated (Figure 2-1). The process of isolation requires the collection of the culture supernatant with mild centrifugation force (25g) for 1h followed by sequential filtering through a 5µm mesh filter and finally through a 1.2µm syringe filter. The force of centrifugation was kept low (therefore the duration of centrifugation was longer) in order to avoid fracture and uncontrolled particle release from the fragile apoptotic cells, which would result in a contamination of the EV preparation. During the filtration steps no external force was applied, as this could possibly result in damaging the vesicles' structure and unlike other protocols reported that involve density gradient centrifugation and ultracentrifugation (Kalra *et al.*, 2013), gentle handling was preferred, so that the final material remains structurally intact for the series of analyses that will follow. Diluents and culture media during the isolation procedure and possible dilution steps were always 0.1µm filtered so that any impurities do not interfere with the EV studies due to similar size.
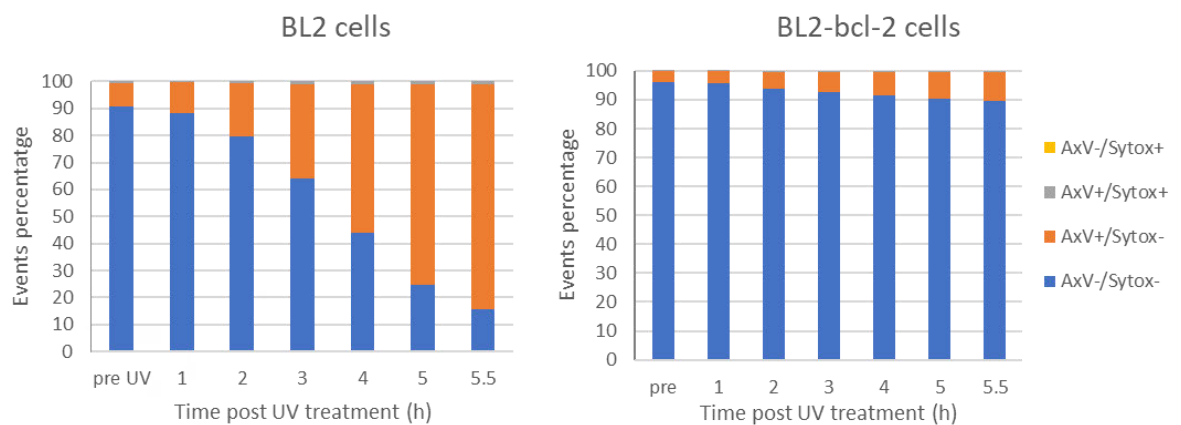

Figure 2-1. Apoptosis progression for BL2 and BL2-Bcl-2 cells after UV treatment, as measured by Annexin V/Sytox Blue staining by flow cytometry. The cells are treated with UV-B irradiation at $20*10^6$ cells/ml for a total dose of 3,000 mJ/cm^2 as 6 doses of 500 mJ/cm^2. The levels of apoptosis are measured in hourly intervals after UV treatment and the graphs represent the average of three independent experiments. The BL2 cells undergo apoptosis, whereas the apoptosis-resistant BL2-bcl-2 cells remain AxV- during this time-frame (protocol developed by Margaret Paterson).

2.2.2. From blood plasma

EV isolation from blood is a process more complex than isolation from culture supernatants and the literature offers a number of studies on blood vesicles, but what is firstly observed in all these references is the lack of common experimental procedures on plasma handling for vesicle isolation. In some cases, significant discrepancies are observed as to which fraction of plasma contains the vesicles or which method of isolation is less harmful to the final sample (Baranyai *et al.*, 2015), (Witwer *et al.*, 2013), (Yuana, Bertina and Osanto, 2011).

The first approach to examining the use of blood as a source of vesicles was to identify the differences between blood serum and plasma, so that the appropriate source could be used for all the procedures to follow. According to ISEV, serum which results from spontaneous blood clotting contains approximately 50% platelet derived vesicles, due to platelet activation during the clot formation process. Plasma, on the other hand, which is collected after the addition of anticoagulants has a lower percentage of platelets and their side-products. In this study, the material of interest was the Apo-EVs from cancer cells, thus, plasma was the most appropriate source (Witwer *et al.*, 2013). There are also studies using sera as a source when the isolation of specific type of vesicles is desired (Kim *et al.*, 2005). Because either human or animal blood can be collected only within specific guidelines and often with limited access to the donor, time becomes a significant parameter in plasma handling. This means that it is usually necessary to store plasma for future use or store aliquots of the same donor's plasma for further research, once enough knowledge is obtained from the preliminary experiments. Some research has been conducted on the optimal conditions of storage and quality of plasma derived vesicles and the common storage method is freezing at -80°C after removing the platelets (Kriebardis *et al.*, 2016), (Witwer *et al.*, 2013).

The protocol applied for blood-derived EV isolation has been designed by comparing multiple protocols described by other groups, excluding all procedures which might cause structural distortion such as ultracentrifugation, and was the following:

Blood was collected in 3.8% sodium citrate and centrifuged at 300g for 20min without brake in order to obtain plasma, followed by a second centrifugation at 2,300g for 15 min to

remove all platelet and cell debris residuals. To avoid activation of platelets with subsequent vesicle release, the temperature was maintained above 20°C and shear forces were minimized until the platelets were removed with the first centrifugation.

The supernatant from the second centrifugation could be collected fresh and analysed immediately, or rapidly frozen at -80°C and stored for future use.

The frozen plasma aliquots could be used by rapid thawing in a 37°C water-bath and centrifugation at 2,300g for 15 min at 4°C to remove all impurities resulting from vesicle or protein aggregation caused during the freeze-thaw cycle.

The above procedure applies for animal and human samples with the only difference being that the volume of mouse blood is less than 1ml, while human samples can be up to 150ml or more.

2.2.3. Chromatography columns preparation, validation and use for EV purification

For experiments where the EVs needed to be purified from proteins and other soluble factors in which they were suspended, size exclusion chromatography was used. For this method, chromatography columns were prepared in-house, using Sepharose CL-6B as a filling material, to ensure EV-sized particles are separated from proteins.

To pack the columns, empty columns were filled with Sepharose CL-6B suspended in DPBS.

In order to validate the separation and identify the fractions which contain the eluted EVs, 1ml of EV sample from cell culture was added to the columns and DPBS was added in order to collect several 1ml fractions.

All fractions were measured by Nanosight to determine the EV concentration, while protein content was measured by Bradford Protein Assay with a procedure described in detail in the Western Blotting section of this chapter.

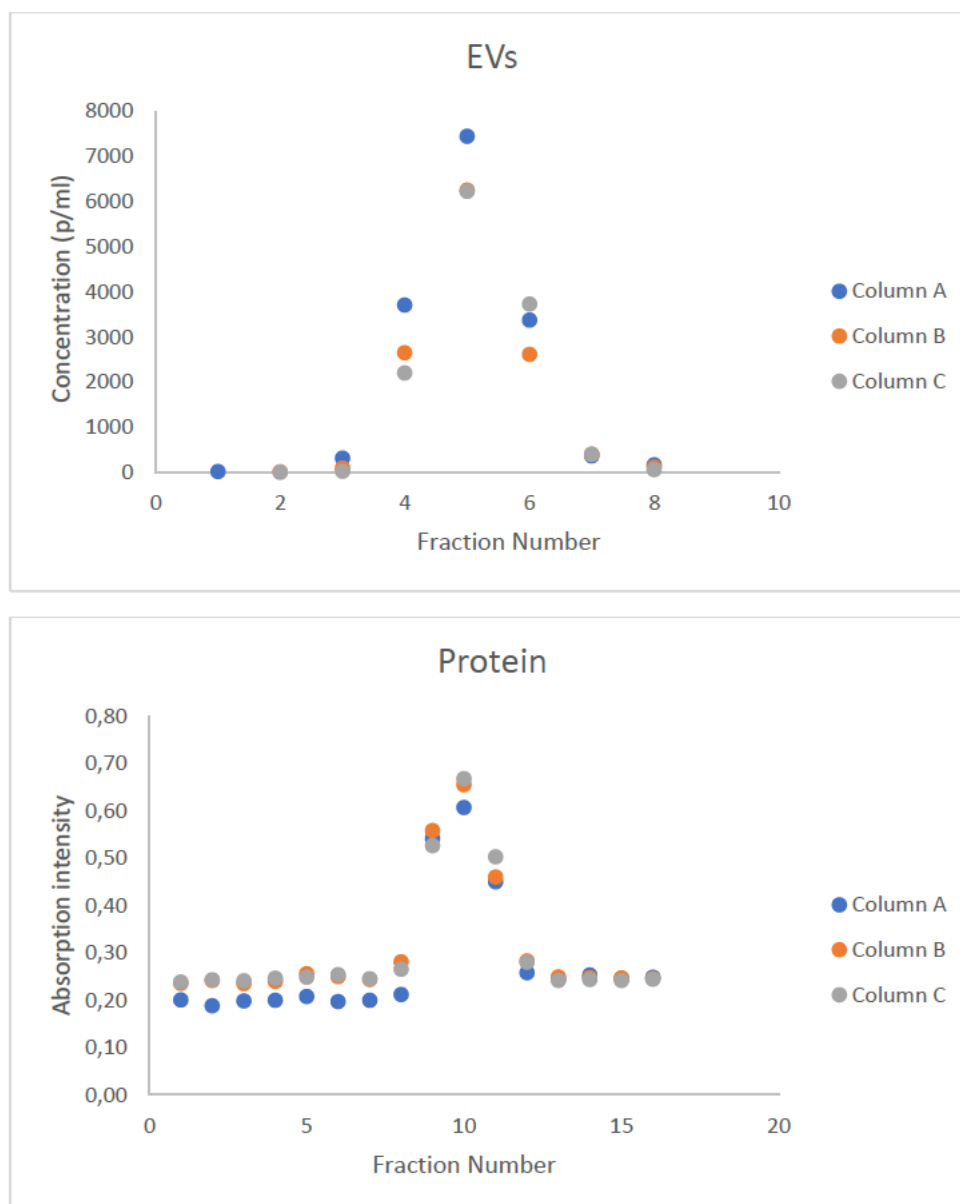The results for EVs and protein fractions are presented in Figure 2-2.

Figure 2-2. Sepharose columns validation for EVs and protein quantity per 1ml fraction. 1ml EV sample was eluted through a freshly prepared Sepharose column and the fractions collected after the addition of EVs were measured as following: EV concentration measured by Nanosight, and protein content by Bradford protein assay. The resulting curves indicate that the EVs are eluted in different fractions from the proteins, confirming successful EV purification.

From the above validation, it is shown that proteins are separated from EVs as they are eluted in different fractions, and EVs can be collected by pooling fractions 5-7. The same columns can be re-used after thorough washing of all remaining material and freshly prepared columns were always validated following the method described above.

2.3. Platelets isolation from blood plasma

The platelets used for all relevant studies have been isolated from blood of healthy volunteers within the Centre for Inflammation Research Blood Donor Register after informed consent. The blood was drawn into a 50ml centrifuge tube containing 4ml sodium citrate 3.8%, and platelet rich plasma (PRP) was prepared by centrifugation of whole blood at 350g for 20 min, according to the internal CIR protocol (Davidson, 2015). After the PRP was collected, the method followed for the isolation and washing of platelets has been described by Abcam and has been adjusted to the following procedure:

The PRP was diluted 1:1 in HEP buffer (140 mM NaCl, 2.7 mM KCl, 3.8 mM HEPES, 5 mM EGTA, pH 7.4) and 1 μM prostaglandin E1 was added to prevent platelet activation. The contaminating red and white blood cells were removed by centrifugation at 100g for 20 min at room temperature and next, the platelets were pelleted by centrifugation at 800g for 20 min at RT. The platelet pellet was washed with wash buffer (10 mM sodium citrate, 150 mM NaCl, 1 mM EDTA, 1% dextrose, pH 7.4) and the platelets were finally resuspended in Tyrode's buffer (134 mM NaCl, 12 mM NaHCO3, 2.9 mM KCl, 0.34 mM Na2HPO4, 1 mM MgCl2, 10 mM HEPES, pH 7.4) containing 5 mM glucose and 1 μM PGE1. The platelets were counted and the concentration was adjusted at $1\text{-}3*10^8$ platelets/ml in the above medium. The suspension was kept at room temperature with gentle shaking.

Phenotyping of platelets was performed using CD42b staining (Abcam #ab119496 - CM405F, and isotype BD #562438 BV421) by flow cytometry (details about all antibodies in Table 2.2).

2.4. Red and White blood cells isolation from whole human blood

Similar to platelet isolation, red and white blood cells have been isolated from blood of healthy volunteers within the Centre for Inflammation Research Blood Donor Register after informed consent. The protocol based on Percoll cell isolation was internally validated and used by the CIR ((Davidson, 2015), based on previously described methods (Dooley, Simpson and Meryman, 1982)).

Whole blood was drawn into a 50ml centrifuge tube containing 4ml sodium citrate 3.8% and platelet rich plasma (PRP) was prepared by centrifugation at 350g for 20 min. After this

centrifugation, the red cells were pelleted and the white cells formed a layer (the buffy coat) on the red cell pellet. To further purify the red cells, a quantity of the red cell pellet was removed and 9x saline volumes (0.9% NaCl) were added. The red cells were washed with 9x saline volumes 3 times by centrifugation at 300g for 5min and were stored in saline at 4°C. For leukocyte isolation, the remaining red cell pellet with the buffy coat were used after the PRP has been removed. 6% dextran solution was added to the cells at a ratio 1:4 to the initial whole blood volume, topped up with 4 volumes of saline and incubated at RT for maximum 30min. Dextran was added in order for the red cells to precipitate, allowing collection of leukocytes from the supernatant. The collected cells were pelleted by centrifugation at 350g for 6min. A Percoll gradient was prepared with three layers; the top, middle and bottom, with stock Percoll solution diluted as 81%, 70% and 55% in PBS respectively. The cell pellet was suspended in the top layer and was added on the top of a gradient formed by the bottom and middle layer. The layers were centrifuged at 720g for 20min and the PMNs (polymorphonuclear cells) were found in the bottom/middle interface, while the PBMCs (peripheral blood mononuclear cells) were isolated from the middle/top layer interface. The cell populations were washed in PBS at 230g for 6min followed by centrifugation at 300g for 5min. The cells were finally resuspended in X-Vivo 15 (Ogden *et al.*, 2001) and stored at 37°C + 5% CO_2 for a maximum of 2 days.

2.5. Immunomagnetic beads for selective EV capture – preparation

A variety of magnetic beads coated with antibodies against several EV surface molecules were used for EV studies, and each type of beads was functionalized with the appropriate surface antibody by different strategies (e.g. streptavidin-biotin interaction, formation of covalent chemical bond etc., see below). In more detail, the beads used here were prepared as follows:

- **CD9, CD63, CD81 and W6/32 beads:** Streptavidin magnetic beads and biotinylated anti- CD9, CD63 and CD81 antibodies were obtained by MBL (Exocap kit). In addition to the three antibodies, anti-MHC class I-biotin antibody was used on the beads of the same kit, for comparison. The anti-MHC class I antibody was produced in-house from hybridoma cells [ECACC (#84112003) mouse anti-human HLA A, B, C hybridoma cells, clone W6/32] and was purified from culture supernatants by affinity capturing

on Protein A chromatography column. It was biotinylated following the protocol of a commercially available biotinylation kit (Sulfo-NHS, ThermoFisher), according to the manufacturer's guidance. The attachment of the biotin-antibodies on the beads was performed according to the bead kit manufacturer/s protocol.

- **CD19 beads** (Ø4.5μm) were used without further modification.

- **CD20 beads** (Ø10μm) were prepared by conjugation of anti-CD20 antibody on Protein A beads, following the manufacturer's protocol.

- **-COOH surface activated beads:** beads of Ø1μm with surface carboxyl groups were purchased from ThermoFisher and were activated with a reagent alternative to EDC/NHS reaction, the Mix n' Go Micro without further functionalization of protein. These beads will be added to the EVs and the attachment will take place by the formation of amide bond between the activated -COOH group of the beads and the primary amines present in the EV proteins.

- **Anti-PS beads** were purchased as a kit, MagCapture (FUJIFILM Wako), and used without further processing, with the buffers and reagents contained in the kit.

After coating with the antibodies, all beads (except for -COOH activated beads and anti-PS beads) were washed and resuspended in 2mM EDTA + 0.5% BSA in PBS to minimize particle aggregation during storage. All bead handling was performed on a permanent magnet.

The assessment of the antibody coupling efficiency was conducted by flow cytometry, using a fluorescence labelled antibody specific against the coupled protein. All anti- CD9, CD19, CD20, CD63, CD81 and W6/32 mouse anti-human antibodies are of the IgG isotype, therefore a goat anti-mouse secondary immunoglobulin IgG-FITC antibody (Sigma #F0257) was used to stain the beads.

2.6. Analytical methods for the characterisation of EVs

All buffers were filtered through a 0.1μm filter.

2.6.1. Nanoparticle Tracking Analysis

EV concentration and size distribution was measured by Nanoparticle Tracking Analysis for Rayleigh scattering (Nanosight, Malvern, UK) on a Nanosight LM14 with a cMOS Hamamatsu

Orca Flash 2.8 camera and processed with NTA 2.3 software (capture settings: camera level=16, video recorded for 60s, imaging threshold=15015, T=24°C, viscosity=water and for video processing: screen gain=12, minimum expected particle size=30nm, particle detection threshold=8).

2.6.2. Dynamic light scattering

In vitro Apo-EVs from BL2 and BL2-bcl-2 cells were prepared in phenol red negative culture media (50% RPMI 1640 and 50% phenol red negative X-Vivo 15). The size and zeta potential measurement were performed on the Zetasizer (Malvern Nano ZS) and the EV suspension diluent was complete culture media, diluted with DPBS as needed. For size measurements, the instrument settings were adjusted to refractive index equal to 1.45, temperature 25°C, measurement angle at 173°, absorption 0.001, 20 runs for each measurement and 10s pause between different measurements. Similarly, liposomes were measured in PBS suspension with the same settings, with the only difference being the refractive index equal to 1.40 with 3 measurements. The zeta potential was measured on the same instrument at 25°C.

2.6.3. Cryo Electron Microscopy and Tomography

EVs isolated from BL2 and BL2-Bcl-2 cells *in vitro* have been successfully imaged with cryoTEM, following the plunge-freezing in liquid ethane method (discussed in Introduction and described in detail below). Apoptotic cell-derived vesicles were harvested from cells undergoing apoptosis after 5 to 6 hours post-UV treatment, according to the already described protocol (Section 2.2.1). A biological fluids concentrator based on blotting water away from the EV suspension while retaining larger materials in a membrane (15kDa cut-off size) was used to increase the concentration of the sample before freezing. The desired concentration of EVs needed at the point of freezing was over $2,000*10^8$ particles/ml as measured on Nanosight.

CryoEM grids (Lacey carbon films, copper) were plasma-cleaned in a vacuum glow discharger to render the carbon film on the grids hydrophilic. 4µl of the EV concentrate was loaded on the grid and the excess material was blotted away using a Vitrobot™ (FEI) under 100% moisture conditions at room temperature and immediately plunged onto liquid ethane, which was maintained in the liquid phase by the presence of liquid N_2 on the outside walls of

the freezing vessel. The frozen grids were transferred and stored in liquid N_2 while special precautions should be taken so that the vitrification of the sample was rapid and without any crystalline ice contamination which would make imaging impossible. The transfer and storage of the frozen grids must be done in liquid nitrogen, avoiding contact with the atmosphere and consequently with moisture. The grids were inserted in the microscope (F20 FEI Tecnai Cryo) on a special cryo-holder which consists of a metal rod connecting the grid edge with the opposite side of the holder, where a tank of N_2 ensures that the heat is being conducted away from the frozen specimen and the grid is maintained at low temperature. Images were acquired with SerialEM software (SerialEM, Colorado) setting the exposure times ranging from 0.2s to 2s maximum, usually at 1s, with "low dose mode" activated on the instrument, so that the electron beam causes no harm on the vitrified material, and at 200kV. Different magnifications were used during image acquisition (up to 62,000x).

To obtain a series of different angles of the same image for the 3D tomography, the grid-holding stage was tilted to certain degrees in both directions and a series of images was recorded, with the electron dose low enough so that the specimen remains intact throughout the imaging. The samples intended for tomography were mixed with gold nanoparticles (10nm, stabilized 0.1 mM PBS, reactant free, Sigma) at a 1:1 ratio before freezing. These particles do not interact with the specimen, however it is necessary that those appear in the imaging plane so that they act as reference points to align the different tilt images during the tomogram reconstruction.

Image analysis was performed with Digital Micrograph (Gatan) and Photoshop (Adobe) and tomogram reconstruction was done on eTomo (Imod) and Avizo (FEI).

2.6.4. Immunogold labelling of EV surface markers for TEM

The immunogold complexes were prepared in-house using 15nm gold nanoparticles with -COOH surface modification and antibodies against the following antigens were attached on the nanoparticles surface (details about all antibodies in Table 2.2):

- CD19 (Serotec #MCA1940EL)

- MHC class II, clone W6/32 (produced in-house from HLA A, B, C hybridoma cells [ECACC #84112003])

- MHC class II, clone HC10 (Origene #AM33035PU-N)

- Ro (TRIM21) (Thermo #pA5-22294)

- La (SSB)(Thermo #MA5-24921)

The final preparation of immunogold nanoparticles was suspended in Tris/0.1% BSA and the concentration was adjusted to $20\text{-}30*10^{10}$ particles/ml. Particle concentration was measured by optical absorption at 520nm, with known extinction coefficient $\varepsilon=3.67*10^8$ M^{-1} cm^{-1} and given that at O.D=1, the suspension contains $1.64*10^{12}$ particles/ml.

EV staining with immunogold took place on TEM grids (Formvar carbon films on Copper, Agar Scientific). Sepharose column-purified EVs were allowed to settle and adhere on the grids for 3h at RT. The excess of EVs was washed away with PBS and the grid surface was blocked with 5% BSA in PBS for 1h at RT. The immunogold suspension in Tris/0.1% BSA was added on the EVs for 30 min at RT, at a ratio determined experimentally (1:100 nanoparticle suspension of $25.6*10^{10}$ particles/ml initial suspension). The grids were washed in PBS, air-dried and imaged on a TEM microscope (F20 FEI Tecnai Cryo) operating at 200kV. Images were acquired with SerialEM software (SerialEM, Colorado). Image analysis was performed with Digital Micrograph (Gatan) and Photoshop (Adobe).

2.6.5. Fluorescence microscopy

The EVs were purified from soluble factors and proteins from the cell culture by size exclusion chromatography using in-house prepared sepharose columns. The purified EVs suspended in 0.1µm filtered PBS were stained with Alexa Fluor 568 NHS ester (AF568) with a covalent attachment of the dye on the EV proteins, according to the manufacturer's protocol. To remove unbound dye, the EVs were purified again by size exclusion chromatography through sepharose columns. The AF568 labelled and purified EVs were added on H1.0 coverslips which have been previously treated with Mix&Go™ Biosensor in order to activate the surface and increase EV binding. The EVs were allowed to adhere on the coverslips for 3h at ambient temperature. The EVs were washed with 0.2um filtered PBS and the surface was blocked using 5% BSA in PBS for 1 hour at ambient temperature. Next, the EVs were washed with 25 mM MES pH 6.0 and were stained with the antibodies in 5% goat serum for 15min at 4°C.

finally, the EVs were washed with MES buffer and mounted on a glass slide using ProLong Antifade mountant (ThermoFisher). Table 2.2 in section 2.6.7 contains all the reagents used to label EVs for confocal microscopy.

Imaging was performed on an SP8 microscope (Leica) and the quantification of EV markers was performed on Fiji/Image J software.

2.6.6. Fluorescence depolarization spectroscopy

Liposome preparation for fluorescence anisotropy measurements

The liposomes aimed for the anisotropy study were Single Unilamellar Vesicles (SUVs), which means their diameter ranges within the nanometre scale and mainly below 500nm. The method applied to achieve such populations has been described several years ago, but is an effective protocol which yields liposomal populations of relatively small sizes (Pons, Foradada and Estelrich, 1993). Ethanol injection is based on the hydrophobic properties of the lipids which spontaneously form vesicles when rapidly injected in an aqueous solution. The fluorescent probe used in the initial anisotropy measurements on liposomes was diplhenylhexatriene (DPH) (Figure 2-3), a lipophilic molecule practically non-fluorescent in aqueous environment, which emits fluorescent signal when incorporated in a lipid bilayer (Nelson *et al.*, 2012), (Troup *et al.*, 2006).

The lipid mixtures used to prepare the liposomal formulations as dictated by Table 2.1, were Dipalmitoyl-phosphatidyl-choline (DPPC) with a T_m=41 ^{o}C, Dimyristoyl-phosphatidyl-choline (DMPC), T_m= 24°C and Cholesterol.

Lipid and DPH stock solutions were prepared in methanol. For cholesterol only, a mixture of MeOH + 5% CCl_3 was used to improve solubility. Appropriate volumes of lipid and DPH solutions were mixed and rapidly injected with a syringe into PBS while the process takes place a few degrees above the transition temperature (T_m) of the lipids, where they are in "liquid" state, so that they can align and self-assemble on a bilayer. The suspension was allowed to cool down to room temperature.

The appropriate dilution of the liposomal dispersion in PBS intended for anisotropy measurements was found by trial and error, adjusting the concentration so that the absorption maximum is 0.1 (Upstone, 2006). Emission spectra and anisotropy measurements

were all taken for the same concentration, as defined by the absorption peak maximum value.

A "prompt" sample was required for every anisotropy measurement, which is a non-fluorescent scatter solution used to measure the system's response and is co-calculated by the software when the data are being fitted to exponential curves, to exclude the interference of electronics and instrumentational artefacts in the signal detection. For the liposomal samples the prompt was a liposomal preparation of DPPC without the fluorescent agent, and was used at the same dilution as the stained material.

The exact lipid composition and lipid to dye ratio for the liposomal formulations prepared are shown in Table 2.1.

Table 2.1. Composition of liposomal preparations.

Lipid composition with lipid:DPH ratio 200:1			
DPPC	DPPC:DMPC 1:1	DPPC:Chol 2:1	DMPC:Chol 2:1

Size, zeta potential and size distribution properties of the liposomal preparations were measured with Dynamic Light Scattering (Zetasizer, Malvern) and Nanoparticle Tracking Analysis (Nanosight).

EV preparation for fluorescence anisotropy measurements with DPH and TMA-DPH

DPH was dissolved in THF at a final concentration of 2mM to prepare the stock solution which was next injected in well-stirred PBS at room temperature at a final dilution of 2,000x. The solution was stirred for 2h until all THF evaporates and the solution becomes non-fluorescent (DPH in water is non-fluorescent). This working solution was mixed at a 1:1 ratio with EV suspension and incubated at room temperature for 1h (Shinitzky and Inbar, 1976b), (Schachter and Shinitzky, 1977).

TMA-DPH is a derivative of DPH which consists of the parental molecule and a polar head (Figure 2-3), allowing for more specific localization on the surface of the lipid membranes (do Canto *et al.*, 2016). For EV staining, TMA-DPH was dissolved in DMSO to a stock solution of 1mM stock and used at a 1:1000 ratio in the EV suspension (1μm final concentration in

sample). The EVs were incubated at RT for 30min prior to measuring (Sutter, Fiechter and Imanidis, 2004).

DPH
1,6-Diphenyl-1,3,5-hexatriene

TMA-DPH
N,N,N-Trimethyl-4-(6-phenyl-1,3,5-hexatrien-1-yl)
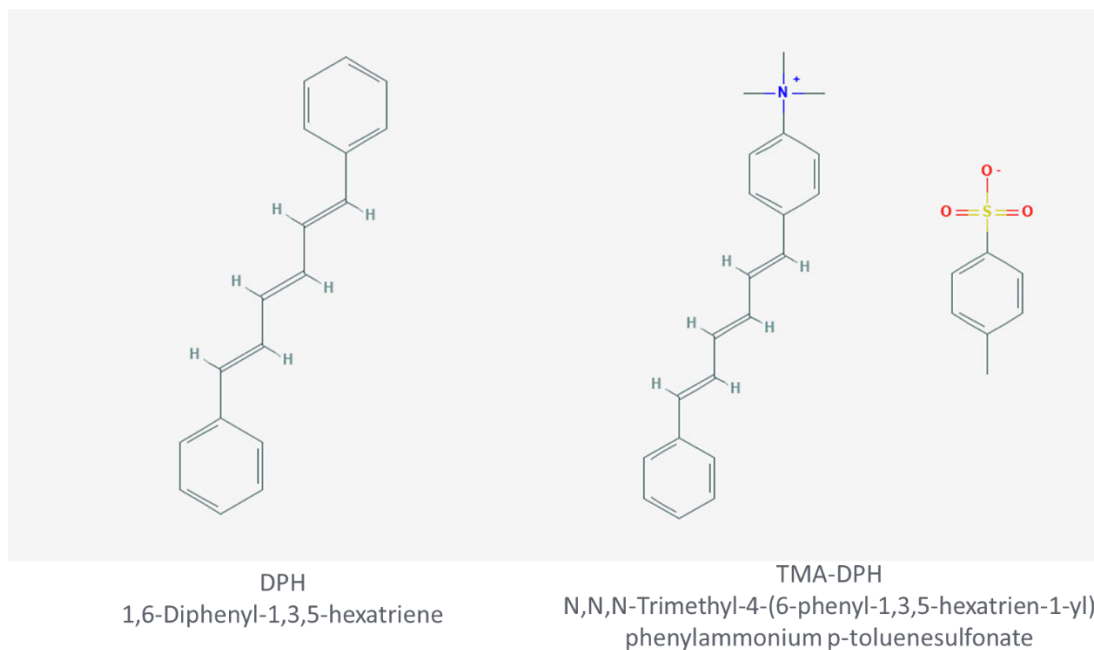phenylammonium p-toluenesulfonate

Figure 2-3. Molecular structure of DPH and TMA-DPH (PubChem).

Fluorescence depolarization was measured at room temperature, 37°C and 45°C for EVs, using Apo-EVs as scatter solution (prompt) at the same concentration as the stained working suspension. All fluorescence depolarization measurements were performed on a TCSPC lifetime kit (DeltaFlex Hybrid, Horiba) with 10,000 counts peak difference for the vertical and horizontal polarization planes and 10 cycles of measurements to determine the G factor (Equation 1 in Introduction). The sample was illuminated by a pulsed Delta Diode 374nm (Horiba) at 80MHz and the photons were collected by a detector tbx-850c 250-850nm (Horiba IBH). Data were recorded with DataStation v2.7 software (Horiba) and processed on DAS6 v6.8 by data reconvolution.

2.6.7. EV immunomagnetic capture and flow cytometry

In order to perform flow cytometry on EVs, the vesicles were attached on magnetic beads, which allows better measurement sensitivity and also easy staining, washing and isolation of EVs. Beads coated with the appropriate antibodies (commercially available or prepared in-

house; see section 2.5) were washed in washing buffer: PBS + 0.5% BSA + 2mM EDTA, using a permanent magnet. The EVs were added in the beads, diluted further in bead washing buffer if necessary, and were incubated overnight at 4°C or for up to 6h at RT with gentle rotation.

Unbound EVs were washed off the beads on a magnet, using the bead washing buffer and were resuspended in the appropriate solution for antibody staining (PBS + 5% BSA or goat serum) or AxV binding buffer for AxV staining. The appropriate concentration of staining antibodies or other dyes (Table 2.2) were added to the bead-EVs and were allowed to interact for 15 min at 4°C.

In case where EV permeabilization was needed, the Fix & Perm Cell Permeabilization Kit was used according to the manufacturer's protocol before staining.

Table 2.2. Antibodies/fluorescent probes used for flow cytometry, Western blotting, immunomagnetic bead coupling, immunogold staining and confocal microscopy on EVs and cells.

Target molecule	Fluorochrome	Vendor / Cat. N°	Species / Clone / Isotype	Isotype Control/ Secondary antibody
CD42b	CM405F	Abcam/ab119496	Mouse/IgG1/HIP1	BD/562438-BV421
CD19	none	Serotec/MCA1940EL	Mouse/IgG1/LT19	N/A
CD20	none	Serotec/MCA1710GA	Mouse/iGg2b/2H7	N/A
Histone-3	none	Abcam/ab47297	Rabbit/IgG polyclonal	Goat anti-rabbit-HRP (Sigma/A6154)
CD19	none	Bioss/BS-0079R		
Beta actin	none	Sigma/A1978	Mouse/IgG1/AC-15	Goat anti mouse-HRP (Sigma/A3673)
Thrombospondin-2	none	Millipore/ABC114	Rabbit/IgG polyclonal	Sigma/P9795 PE
Beta-2 microglobulin	none	Thermo/MA1-19141	Mouse/IgG2a/ B2M-01	Sigma/F0257 FITC
Ro (TRIM21)	none	Thermo/pA5-22294	Rabbit/IgG polyclonal	Mol Probes/A31556 AF405
La (SSB)	none	Thermo/MA5-24921	Mouse/IgG3/ OTI9D6	Sigma/F0257 FITC
Cleaved Caspase-3	AF 488	R&D/IC835G-025	Rabbit/IgG/269518	Sigma/P9795 PE

Histone-3	Pac Blue	CST/12167	Rabbit/IgG/D1H2	CST/90785
MHC class I W6/32	PE	Dako/R7000	Mouse/IgG2a/ W6/32	Dako/0950
MHC class I HC10	none	Origene/AM33035 PU-N	Mouse/IgG2a/ HC10	Sigma/F0257 FITC
MHC class II	FITC	BD/562008	Mouse/IgG2a/Tu39	
CD9	FITC	Serotec/MCA2655F	Mouse/IgG2a/Bu16	Serotec/MCA929F
CD10	FITC	Abcam/ab28096	Mouse/IgG1/MEM-78	Abcam/ab91356
CD19	AF488	Serotec/MCA1940 A488	Mouse/IgG1/LT19	Serotec/MCA928A488
CD20	AF488	Serotec/MCA1710 A488	Mouse/iGg2b/2H7	Serotec/MCA691
CD45	AF488	Serotec/MCA87A488	Mouse/IgG2a/ F10-89-4	Serotec/MCA1124
CD46	PE	BD/564252	Mouse/IgG2a/E4.3	BD/559319
CD63	Biotin	MBL/MEX002-6	Mouse/IgG2b/C047-1	Mol Probes/S32351 Streptavidin AF405
CD81	Biotin	MBL/MEX003-6	Mouse IgG2a/A103-10	
		FLUORESCENT DYES		
Annexin V	Alexa Fluor ® 488	Thermo/ A13201	N/A	N/A
	Pac Blue	Thermo/ A35122		
Sytox Blue		Thermo/S34857		
Hoechst 33342		Thermo/ H3570		
Acridine Orange		Thermo/ A1301		
AF 488 NHS Ester		Thermo/A20000		
AF 568 NHS Ester		Thermo/A20103		

2.6.8. Western Blotting

The samples intended for protein extraction and western blotting were prepared as follows:

- EVs: EVs prepared *in vitro* were centrifuged at 20,000g for 30min at 4°C and the pellets of $50*10^8$ EVs were snap frozen at -80°C.

- Cells or platelets: Platelets were incubated with 5,000 EVs/platelet for 3h at 37°C. After incubation, the platelets were washed in order to remove any unbound EVs with PBS and pelleted by centrifugation at 800g for 20min at room temperature. The pellets containing $1*10^7$ platelets each were snap frozen at -80°C. For cells, BL2 cells

were pelleted by centrifugation at 300g for 5min after washing in PBS and were similarly frozen at pellets containing $1*10^7$cells.

Lysis of platelets or cells for protein extraction: the frozen pellets of samples were thawed on ice and lysed in 150µl cell lysis buffer (10 mM HEPES, 1 mM EDTA + 1% Triton-X-100) with 10µl protease inhibitor cocktail.

Lysis of EVs: the frozen pellets of $50*10^8$ EVs were thawed on ice and lysed in 60µl cell lysis buffer with 6µl protease inhibitor cocktail.

All samples were vortexed and allowed to lyse on ice for 30min before further lysing by syringing 10x with a 23G needle and syringe. Samples were left to lyse for a further 30min on ice. The lysates resulting from this procedure were used in Western blotting.

Protein concentration measurement by Bradford protein assay: Bradford reagent was diluted 1:4 in water and was mixed with the lysates in a range of dilutions. For calibration, a standard curve using 0.5% BSA solution was plotted. The optical absorption was measured at 595nm at a Varioskan Flash plate reader (ThermoFisher) (Bradford, 1976).

Gel electrophoresis: for platelet and cell lysates, 10µg protein was made up to 10µl of final loading sample with water, NuPAGE™ Sample Reducing Agent (10X) and NuPAGE™ LDS Sample Buffer (4X). For EV lysates which are more dilute, the loading samples were made up to the maximum volume allowed per well, to maximize the protein quantity. The samples were heated at 70°C for 10' and loaded on 4-12% Bis-Tris 1.5mm thick 10-well gel, with the addition of a protein ladder (SeeBlue™ Plus2 Pre-stained Protein Standard). The gel was run in MES SDS buffer at 170V constant for approximately 1h.

Membrane transfer: the electrophoresis gel was dismantled and allowed in NuPAGE transfer buffer for 10min in order to equilibrate the gel into the new buffer. The PVDF membrane used for the transfer was treated with pure methanol for 30s and incubated for 10min in transfer buffer with 10% methanol. The transfer cassette was assembled using NuPAGE transfer buffer with 10% methanol to hydrate all parts (blotting paper, foams) and the transfer was performed at 30V for 1h 20min.

After transfer, the membrane was washed 3x in PBS+0.1% tween-20 for 10min and was blocked for 1h at RT in 5% milk/PBS+tween-20 or 5% goat serum/PBS+0.1% tween-20. The

primary antibody was added in the appropriate solution (goat serum or milk) and the membrane was incubated at 4°C overnight.

After the primary antibody incubation, the membrane was washed 3x in PBS+0.1% tween-20 for 10min. The secondary antibody was added in 5% goat serum and the membrane was incubated for 1h at RT. Finally, the membrane was washed 6x in PBS+0.1% tween-20 for 5min and the signal was developed with standard ECL prime. The signal was visualised with Amersham™ Hyperfilm™ ECL film.

Primary antibodies used in Western blots (details about all antibodies in Table 2.2):

- Histone-3: rabbit anti-human 15kDa, used 1 in 1000 in 5% milk (Abcam #ab47297)
- Beta actin: mouse anti-human 43kDa, used 1 in 5000 in 5% milk (Sigma #A1978)
- CD19: rabbit polyclonal anti-human 95kDa, used 1 in 1000 in 5% milk (Bioss #BS-0079R)

Secondary antibodies:

- Goat anti-rabbit-HRP, used 1 in 5000 in 5% goat serum (Sigma #A6154)
- Goat anti mouse-HRP, used 1 in 5000 in 5% goat serum (Sigma #A3673)

2.6.9.RT qPCR

The samples intended for RNA extraction and hY4 RNA study were prepared as follows:

- EVs: EVs prepared *in vitro* were centrifuged at 20,000g for 30min at 4°C and the pellets were snap frozen at -80°C.
- Cells: HUVEC cells were incubated with EVs $2*10^{11}$ nm^3/ml of cell media for 18h at 37°C in 75cm^2 flasks. *The volume of EVs was calculated by the following procedure: the particle diameter histogram of each EV sample was obtained by Nanosight measurement; the diameter was divided by 2, to obtain the radius and the EV volume of each radius bin was calculated assuming EVs are spheres by V=(4/3)*πr^3; the sum of the volumes from all radius bins gives the total volume of EVs in nm^3/ml.* After incubation, the cells were washed in order to remove any unbound EVs and they were detached from the container by trypsin digestion, washed with PBS and

pelleted by centrifugation at 300g for 5min at room temperature. The pellets containing $1*10^7$ cells each were snap frozen at -80°C.

RNA was extracted from the frozen EVs or cell pellets according to the manufacturer's protocol for the RNeasy RNA isolation kit. The concentration of the extracted RNA was measured by spectrophotometry (NanoDrop, ThermoFisher) and was adjusted to the appropriate dilution for the performance of reverse transcription reaction. The RT was performed with Reverse Transcriptase using a commercial kit (miScript II RT Kit), for a 10μl reaction with maximum 1μg RNA per reaction. In most cases, the concentration of RNA extracted from EVs was not as high as required for the performance of the reaction, therefore the maximum permitted RNA volume was added per reaction. The RT reaction was performed on a thermocycler (Applied Biosystems Veriti 96 well thermal cycler) for 60min at 37°C, followed by a 5min incubation at 95°C and final storage at 4°C. The cDNA generated from the RT cycle was used for the performance of quantitative PCR using SYBR Green dye and with materials and protocol provided by the miScript SYBR Green PCR Kit. The quantity of cDNA used for a 25μl reaction was a dilution of 1 in 10 for EV cDNA and 1 in 100 for cell cDNA as produced by the RT reaction.

As described in detail in section 4.5, the forward primer sequence for hY4 RNA was: 5' - GTCCGATGGTAGTGGGTTAT- 3'. The universal reverse primer from the miScript SYBR Green PCR kit was used for the hY4 RNA, while the normalization gene primers were commercially available for RNA-U6 and miR-21.

The layout of the 96 well reaction plate for all samples and genes is presented in Figure 2-4.
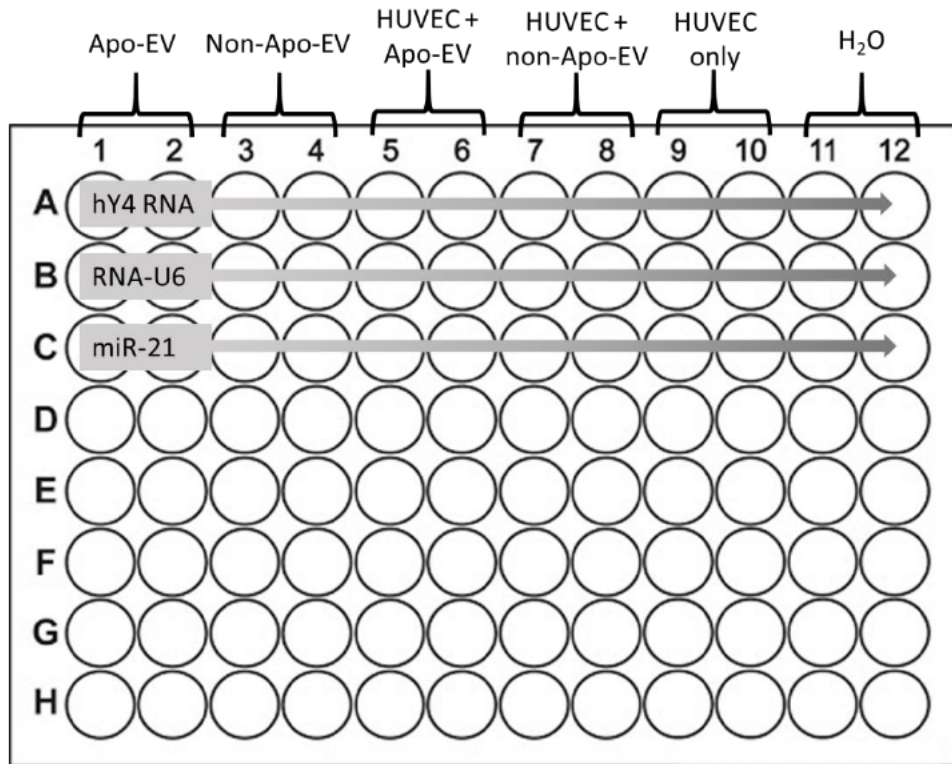
Figure 2-4. 96 well-plate template of samples for qPCR with hY4 RNA and reference genes.

The reaction and data recording took place in a Roche LC96 thermocycler using the cycles protocol according to the manufacturer of Sybr Green reagents kit. The data were obtained and analysed by LightCycler 96 software (Roche) and the expression levels of hY4 RNA were calculated on Microsoft Excel (details on the procedure in the relevant results Chapter 4).

2.7. List of materials and reagents

Table 2.3 shows a list of the materials and special reagents used in this work (a list of antibodies and fluorescent dyes has been given in Table 2.2).

Table 2.3. Materials and reagents, recorded in the order of appearance in the text.

Reagent	Supplier and Cat Nº (#)
RPMI 1640	Gibco # 31870-025
X-Vivo 20	Lonza # BE04-448Q

5µm mesh filter	Pluriselect # SKU43-50005-03
1.2µm syringe filter	Whatman # 10462260
Empty chromatography columns	GE Healthcare PD-10 # 17-0851-01
Sepharose CL-6B	Sigma # CL6B200
Prostaglandin E1 (PGE1)	Sigma # P5515
Tyrode's buffer	Sigma # T2397
Percoll solution	GE Healthcare #17089101
X-Vivo 15	Lonza # 04-418Q
Phenol red negative X-Vivo 15	Lonza # 04-744Q
Exocap Streptavidin kit	MBL # # MEX-SA
Protein A column HiTrap® Protein A	GE Healthcare # 17-0402-01
Biotinylation kit	Innova Biosciences # 371-0005
Dynabeads CD19	ThermoFisher CD19 Pan B # 11143D
Protein A magnetic beads	Merck # LSKMAGA02
Dynabeads Carboxylic Acid	ThermoFisher # 65011
Mix n' Go Micro	Sigma-Aldrich # A-LMPN100
MagCapture Exosome isolation kit with PS	FUJIFILM Wako # 299-77603
Permanent microcentrufuge tube magnet	ImmunoSolv
B15 Minicon® Concentrator	Millipore # 9031
CryoTEM grids, Lacey carbon films	Agar Scientific # AGS166
10nm gold nanoparticles, reactant free	Sigma # 752584
15nm gold nanoparticles -COOH	Cytodiagnostics # CGN5K-15-1
Mix&Go Biosensor	Merck # A-PLSC010
MES buffer	Sigma # M8250
ProLong Diamond Antifade Mountant	Thermo Fisher # P36961
Diplhenylhexatriene (DPH)	Sigma # D208000
Dipalmitoyl-phosphatidyl-choline (DPPC)	Sigma # 850355P
Dimyristoyl-phosphatidyl-choline (DMPC)	Sigma # 850355P
Cholesterol	Avanti polar # 700100P
TMA-DPH	Invitrogen # 11500766
Fix & Perm Cell Permeabilization Kit	Thermo # GAS003
Protease inhibitor cocktail	Sigma # P8340
Bradford reagent	Biorad # 500-0006

NuPAGE Sample Reducing Agent (10X)	Invitrogen # NP0009
NuPAGE LDS Sample Buffer (4X)	Invitrogen # NP0007
4-12% Bis-Tris 1.5 mm thick 10-well gel	Invitrogen # NP0335BOX
SeeBlue™ Plus2 Pre-stained Protein Standard	Invitrogen # LC5925
MES SDS buffer	Invitrogen # NP0002
NuPAGE transfer buffer	Invitrogen # NP0006
PVDF membrane for protein transfer	GE Healthcare # 10600023
Skimmed milk powder	Sigma # 1153630500
Standard ECL prime	GE Healthcare # RPN2232
Amersham™ Hyperfilm™ ECL film	GE Healthcare # 28906837
RNeasy RNA isolation kit	Qiagen # 74104
Reverse Transcriptase miScript II RT Kit	Qiagen # 218160
miScript SYBR Green PCR Kit	Qiagen # 218073
LightCycler 96 well reaction plate	Roche # 04729692001
Chloroform	Sigma # c2432
DMSO	Molecular probes # 67-68-5
THF	Sigma # 401757
Amersham Hybond blotting paper	GE Healthcare # RPN6101M
Bovine Serum Albumin (BSA) Low Endotoxin Powder	Thermo # BP9705-100
Dulbecco's Phosphate buffered saline	Gibco # 14190-094
EDTA Disodium Salt	Promega # H5031
FCS-SA	Biotech Lot 30401
Goat serum	Biosera # GO-605/500 (Lot 10075)
Hank's Balanced Salt Solution	Gibco # 14175-053
HEPES	Sigma # H4034-100G
Methanol analytical grade	Thermo # M/4000/17
N-Hydroxysuccinimide	Sigma # 130672-5G
Triton X-100	Sigma # 9002-93-1
Tween-20	Sigma # P1379-250ML

3. Study of secretion kinetics and structure of *in vitro*-derived Apo-EVs

3.1. Aims of the chapter

The model of Apo-EVs which is mainly studied in the present work is the *in vitro* prepared vesicles from BL cells. As these EVs are secreted from cells under special conditions (i.e. apoptosis), they are expected to show distinct characteristics compared to other EVs released from the same cells which are not related to apoptosis. These differences can appear in multiple levels such as the pattern of release from cells, their structural phenotype and physicochemical characteristics, as well as their biochemical phenotype and functions. In this first section, the secretion pattern and basic structural features of Apo-EVs will be discussed, using a range of techniques to examine their size distribution, surface charge, morphology and membrane fluidity properties. Biochemical and functional differences will be discussed in the next chapters.

Apo-EVs have been defined as the sum of the vesicles released from a cell throughout the process of apoptosis, however the mechanism of biogenesis or the extent to which this mechanism shares common machinery with other, non-apoptotic, EV biogenesis mechanisms is unknown. The kinetics of their release from cells can indicate the differences between the Apo-EVs and the non-apoptotic, Bcl-2-EVs and offer a starting point for further studies. For this purpose, the size and concentration of EVs as released by cells in hourly intervals after triggering of apoptosis were measured with DLS and NTA.

Once the EVs were released from the cells, direct imaging by cryoEM was performed in order to confirm the presence of vesicles and study the structural characteristics of the two populations under examination, exploring their potential differences. Conclusions can be extracted qualitatively from the images, as well as quantitatively regarding particle size and number of enclosed structures.

Finally, in order to determine the rigidity or fluidity of the EV membranes, a spectroscopic technique was applied, which can sensitively detect differences in the order of the lipid bilayer. This method was fluorescence anisotropy and although several types of vesicles have been studied using a basic configuration of steady state fluorescence, the analysis using a time-resolved system has not been reported for EVs and especially Apo-EVs. Fluorescence anisotropy was used to compare the physical properties of the vesicle membrane which can be expressed as its overall microviscosity, often corresponding to different intracellular membranous compartments. In other words, the comparison of the findings of this work on

Apo-EVs with values from the literature can suggest the origin of the membrane, for example plasma membrane or subcellular organelles (Montaudon *et al.*, 1986). Acknowledging the sensitivity of this method and the fact that statistical errors can appear due to sample heterogeneity, EVs with a narrow size distribution from blood plasma were used as a comparison to the i*n vitro* prepared EVs.

3.2. Study of kinetics of EV secretion upon stimulation of apoptosis

A fundamental property of a nanoparticle suspension is its size distribution. Especially for a diverse population such as the EVs, the range of sizes can be considerably broader compared to other artificially prepared particles such as liposomes or labelling nanoparticles. It is therefore important to know the diameter of the smallest and the largest vesicle present in the sample, as the selection of methods of further characterization depends heavily on those values. For example, very large particles are not suitable for cryoEM imaging, or very small vesicles cannot be measured with conventional flow cytometry.

The method which was most frequently used in this work to assess the quality of each EV preparation and also measure their concentration was NTA. In Figure 3-1, the size graphs of *in vitro* prepared EVs from BL2 cells are presented, while the EVs isolated from healthy human and mouse blood are shown for comparison. The *in vivo* - derived EVs are significantly smaller than the BL2-derived vesicles, possibly due to the clearance larger particles undergo by homeostasis mechanisms such as collection in the liver and spleen, or phagocytosis before or while they circulate in blood (Peinado *et al.*, 2012) (Imai *et al.*, 2015). For the purpose of this study, the properties of Apo-EVs in the cancerous tissue as well as in the blood were examined, therefore larger vesicles have not been excluded from the preparation, as these possibly contain material mediating signals leading to the alteration of the processes in the tumour microenvironment. Looking into the characteristics of Apo-EVs, the most evident difference from the control Bcl-2 EVs is that the first show a higher diameter around 300nm and there are also vesicles found in the range over 500nm, while the Bcl-2 EVs are mainly located in the peak around 170nm, which is common for both populations.

Another characteristic of suspensions consisting of lipid particles such as the EVs is the zeta potential, which is an expression of the surface charge. The value of this parameter is determined by the presence of charged moieties on the surface of the vesicles, usually polar

heads of lipids and DNA and it is an indication of the expected stability of the colloid. In other words, the zeta potential can range from negative to positive values, and the higher the absolute value, the stronger the repellent electrostatic forces between the particles, leading to smaller tendency for aggregation which subsequently offers higher stability. The surface potential of the BL2 cell-derived vesicles is presented in Figure 3-1, showing a value of approximately -10mV for both apoptotic and non-apoptotic EV samples. Some indicative charts correlating stability and voltage have been extracted from experience and suggest that those values correspond to poor stability (Kumar and Dixit, 2017).

	Zeta potential (mV)
Apo-EV	-11.44 ±0.80
Bcl-2 EV	-10.8 ±0.45

n=3
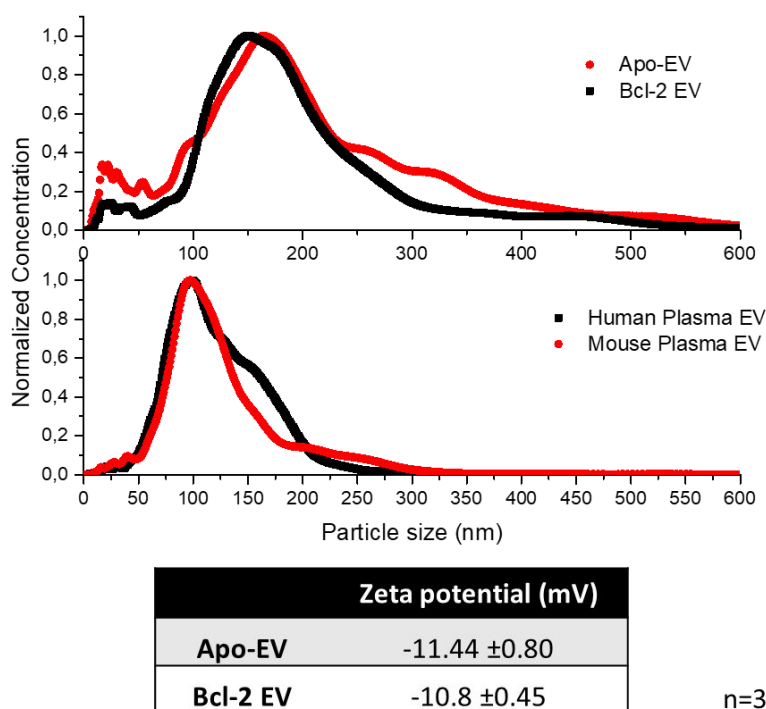
Figure 3-1. Size distribution of in vitro prepared EVs from BL2 cells (top), in vivo derived EVs from healthy human and mouse blood plasma (middle) and table of zeta potential values for in vitro prepared EVs (bottom). Size measurement performed by NTA and zeta potential recorded by DLS and the curves show the average values from 3 independent experiments.

The EV sizes shown above are referring to the final preparations after the parental cells have been incubated for 5h post apoptosis stimulus by UV, therefore the size properties measured correspond to the sum of the EVs generated in this time window. However, it is also interesting to investigate the kinetics of EV secretion in real time during the process of apoptosis and this is performed by isolating the EVs every hour after the UV treatment of

cells, in order to measure the concentration and sizes of the vesicles generated at each time point. As a reminder, the progression of apoptosis for the BL2 cells upon UV treatment has been shown in Figure 2-1. In Figure 3-2, the size and concentration for Apo- and Bcl-2 EVs are shown for every hour post UV with filtering through 1.2μm filter, as the method of analysis (NTA) is suitable for particles under 1 μm in diameter. Regarding the change in size, it is observed that a mixed population of smaller and larger particles are present in the sample in all time points, with the Apo-EVs peaks appearing in higher diameters than the control EVs. The biggest difference, however, is in the concentration, as the Apo-EVs are secreted in larger amounts and this rate is increasing over time, resulting in almost double the concentration from 3h to 5h. In contrast, the Bcl-2 EVs have a steady secretion rate up until 3h and also mark a significant increase until 5h, although the final concentration is approximately 3 times lower than the Apo-EVs, suggesting that the process of apoptosis triggers the release of a potentially different EV population. There is also a population of EVs present at t= 0h, which reflects the constitutive levels of particle expression within the few minutes of cell processing before EV isolation at t= 0h.
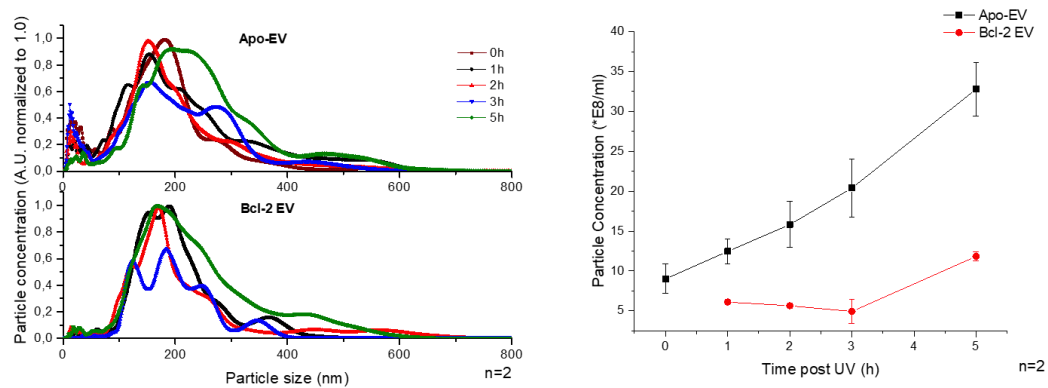
Figure 3-2. Nanosight measurement for size (left) and concentration (right) for EVs isolated hourly post UV cell treatment and filtering through 1.2um syringe filter Average values from 2 EV preparations; the error bars represent standard deviation values.

The observation of an apoptosis-related EV population secreted from apoptotic cells leads to the need for measuring the whole continuum of vesicles up to 5μm in diameter, in order to understand whether the apoptotic bodies can overlap in size with the smaller Apo-EVs. To answer this question, a method less sensitive than the Nanosight but with a broader measurement window regarding particle diameter was applied, the DLS. This technique

tends to point out the larger particles of a suspension, which is explained by its working principle (as described in the Introduction). It can therefore magnify the differences of Apo-EVs versus the control, and this is indeed shown in Figure 3-3, where EVs isolated hourly post UV treatment were filtered through 1.2μm or 5μm. In these graphs, the peaks of Apo-EVs towards the larger diameter (over 1 micron) are even more obvious than the Nanosight measurements, and it is also shown that the larger particles only appear in the period of 3-5h post apoptosis initiation, confirming the Nanosight results and indicating the presence of apoptosis-specific vesicles, which are not present in the non-apoptotic conditions. For both EV samples, the polydispersity index (PDI) value for the 5h time-point was in average 0.604±0.15 for Apo-EVs and 0.77±0.14 for Bcl-2 EVs. The PDI expresses the sharpness of the distribution curve, and values larger than 0.7 are indicative of broad size distributions (Malvern, 2011).
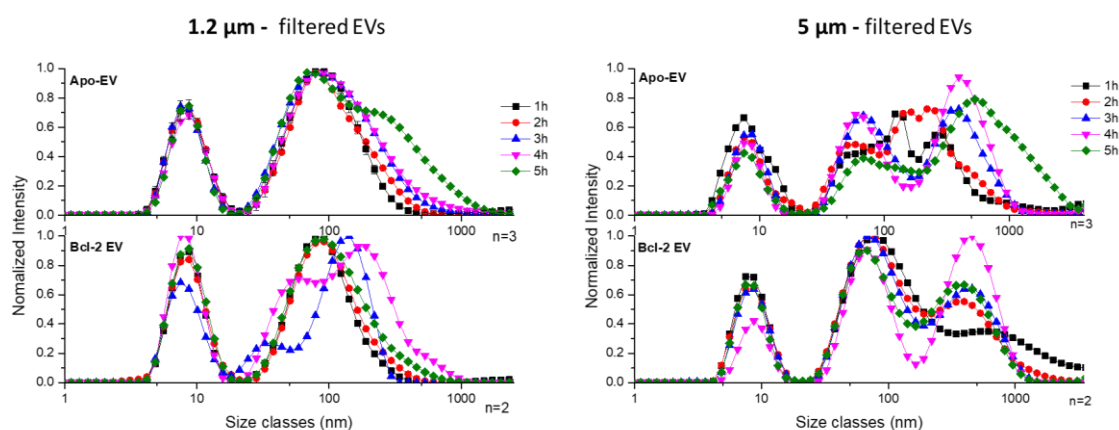
Figure 3-3. DLS size measurement for the cumulative BL2 cell-derived Apo-EVs in hourly intervals after UV treatment and with filtering through 1.2μm or 5μm filter.

The EVs collected every hour after the UV treatment of cells showed in this figure correspond to the cumulative EV amount of all vesicles produced from the beginning of the incubation up to the collection time. This means that for example, the 4h post UV vesicles measurement contain all EVs produced in 1h plus 2h and 3h since time zero. As a comparison, and in order to dissect the EV hourly production in more detail, the measurement was repeated for EVs harvested only during the period of one hour, for all time points. For instance, in order to collect the 4h time point, the cell media was replaced with fresh EV-free media after the 3rd

hour of incubation, so that the EVs collected within the 4th hour only correspond to this time window and do not contain EVs from the previous times.
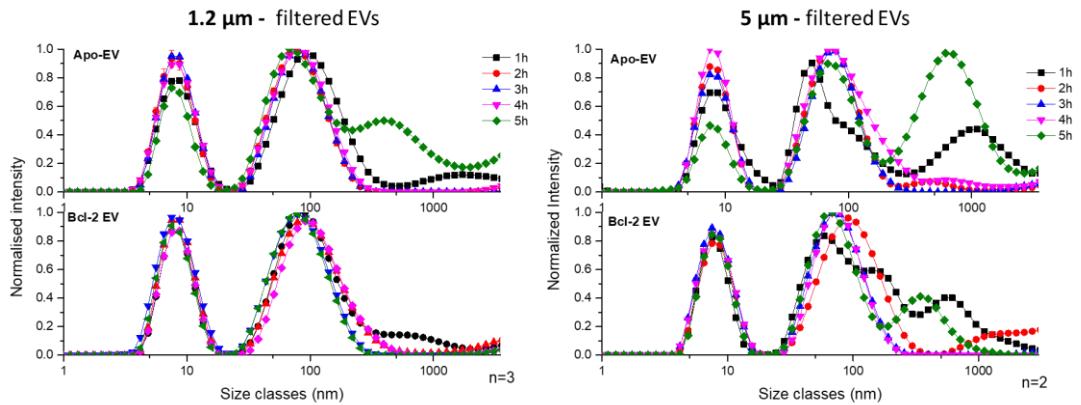
Figure 3-4. DLS size measurement for BL2 cell-derived Apo-EVs in hourly intervals after UV treatment with removal of EVs from previous time points and with filtering through 1.2μm or 5μm filter.

The trend of Apo-EVs towards larger diameters is maintained especially for 5h post UV, and it is also seen that especially for the 5μm filtered vesicles, there is an increased size of particles secreted from the cells after the first hour of incubation, which can indicate an initial 'burst' of particle release from the cells, which is followed by a more linear pattern.

The above measurements were quantitatively analyzed as per the peak center and the amount of EVs per time point which is expressed by the area under the curve (AUC). The results for Apo- and Bcl-2 EVs are presented in Figure 3-5, where is shown that both the peak of the size distribution, as well as the quantity of Apo-EVs are higher than the control vesicles, and also that this increase is more apparent for times after 3h, as discussed earlier.
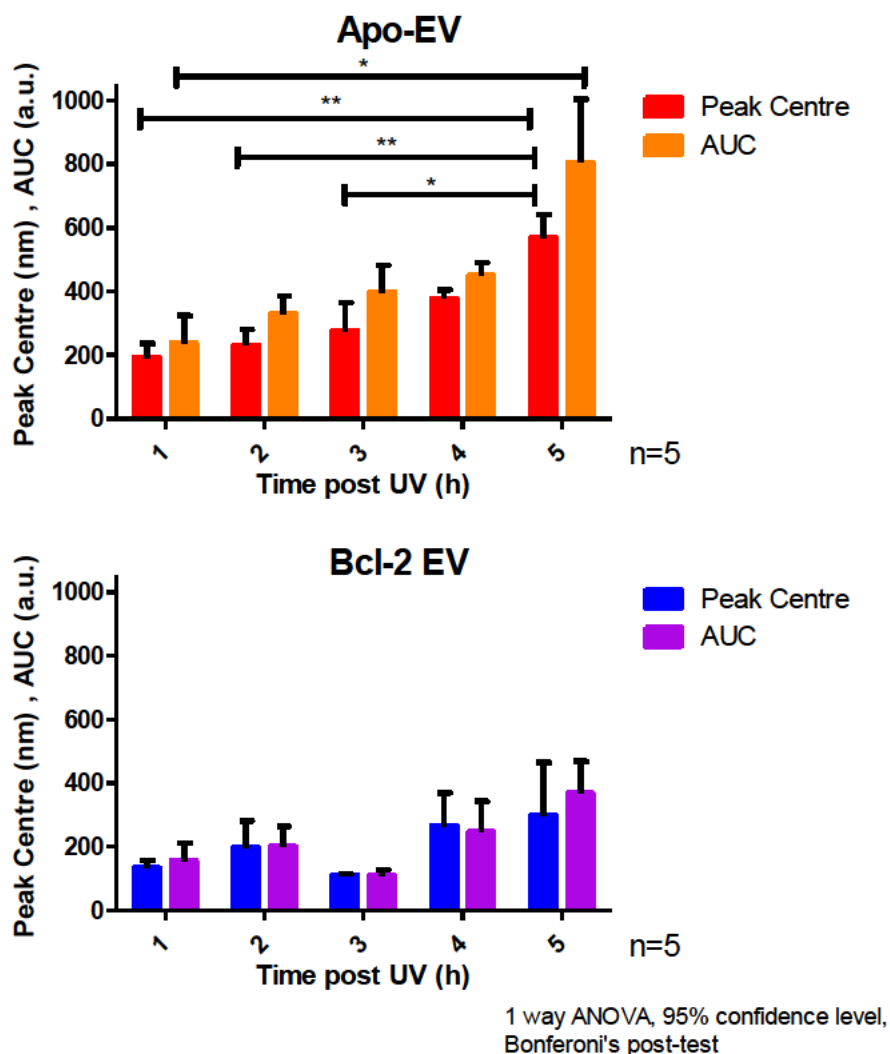
*Figure 3-5. Quantification of DLS size distribution curves for EVs measured every hour post UV irradiation of BL2 cells. Peak centre and AUC were calculated by Origin Pro8 software and the statistics from 5 individual experiments were processed with GraphPad Prism (for non-significant P > 0.05, * P ≤ 0.05 ** P ≤ 0.01, *** P ≤ 0.001, **** P ≤ 0.0001).*

In summary, the above results indicate that the apoptotic B cell lymphoma cells are releasing EVs in a manner which reveals the potential presence of a distinct population related to apoptosis. Taking into consideration the fact that non-apoptotic UV treated cells are also releasing vesicles but to a significantly lower amount and with smaller mean diameter than the apoptotic cells, it can be hypothesized that the sum of collected Apo-EVs contains vesicles which are physiologically generated plus a population specifically derived from the process of apoptosis. Dissecting the individual peaks in the size curves recorded for 1.2 µm filtered EVs in Figure 3-2, some Apo-EV populations are detected in the area of 30-50 nm,

while for the Bcl-2 EVs these peaks are less apparent. This is another piece of evidence that the production mechanism of Apo-EVs contains more complex pathways which result in a broader spectrum of particles compared to the control vesicles. In the next sections, other characteristics of the Apo-EVs are being discussed, focusing on the structural, phenotypic and functional properties, as well.

3.3. Structural study of Apo-EVs with CryoEM imaging and tomography

In order to examine the structure of the individual EVs in further detail, cryoEM imaging was performed in two and three dimensions (tomography). As mentioned in the Introduction and the Methods sections, the EVs were rapidly frozen in their suspension media and imaged in a layer of amorphous ice, in order to maintain their spherical properties and to avoid distortion due to dehydration which is a necessary preparation step in dry TEM.

The following images have been recorded with a 62,000x or 50,000x magnification and the EVs are defined by the lipid bilayer which appears as a dark circle. Dark spots, either spherical or irregular, stand for crystalline ice contamination from the freezing procedure and for both apoptotic and non-apoptotic cell-derived EVs, the population includes unilamellar and multilamellar vesicles.

Figure 3-6 and Figure 3-7 show a collection of representative Apo-EVs and Bcl-2 EVs respectively.
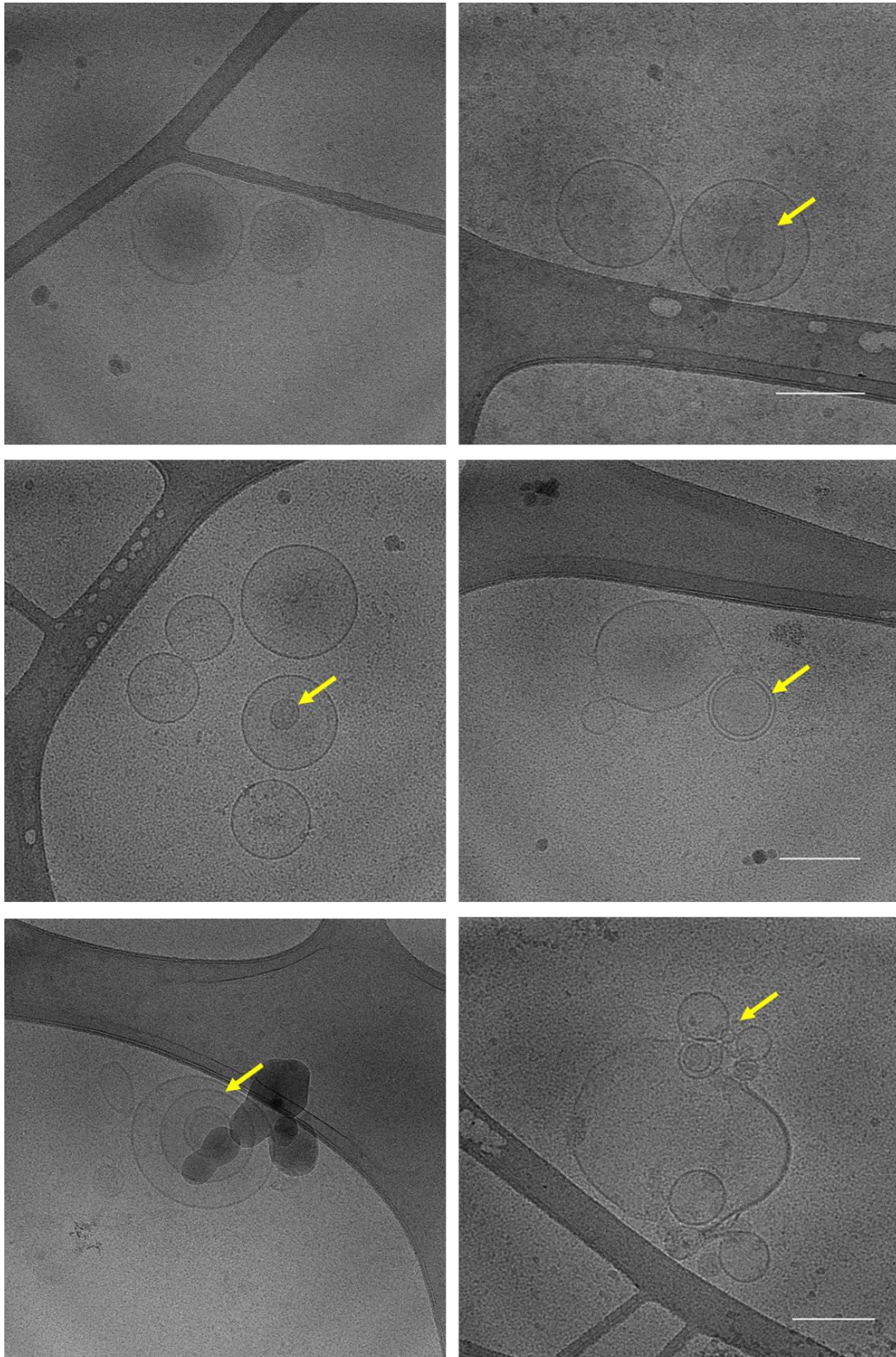
Figure 3-6. CryoEM 2-dimensional images of Apo-EVs. Vesicles with a single or multiple membranes (indicated by arrows) are observed. Scale bar 200nm.
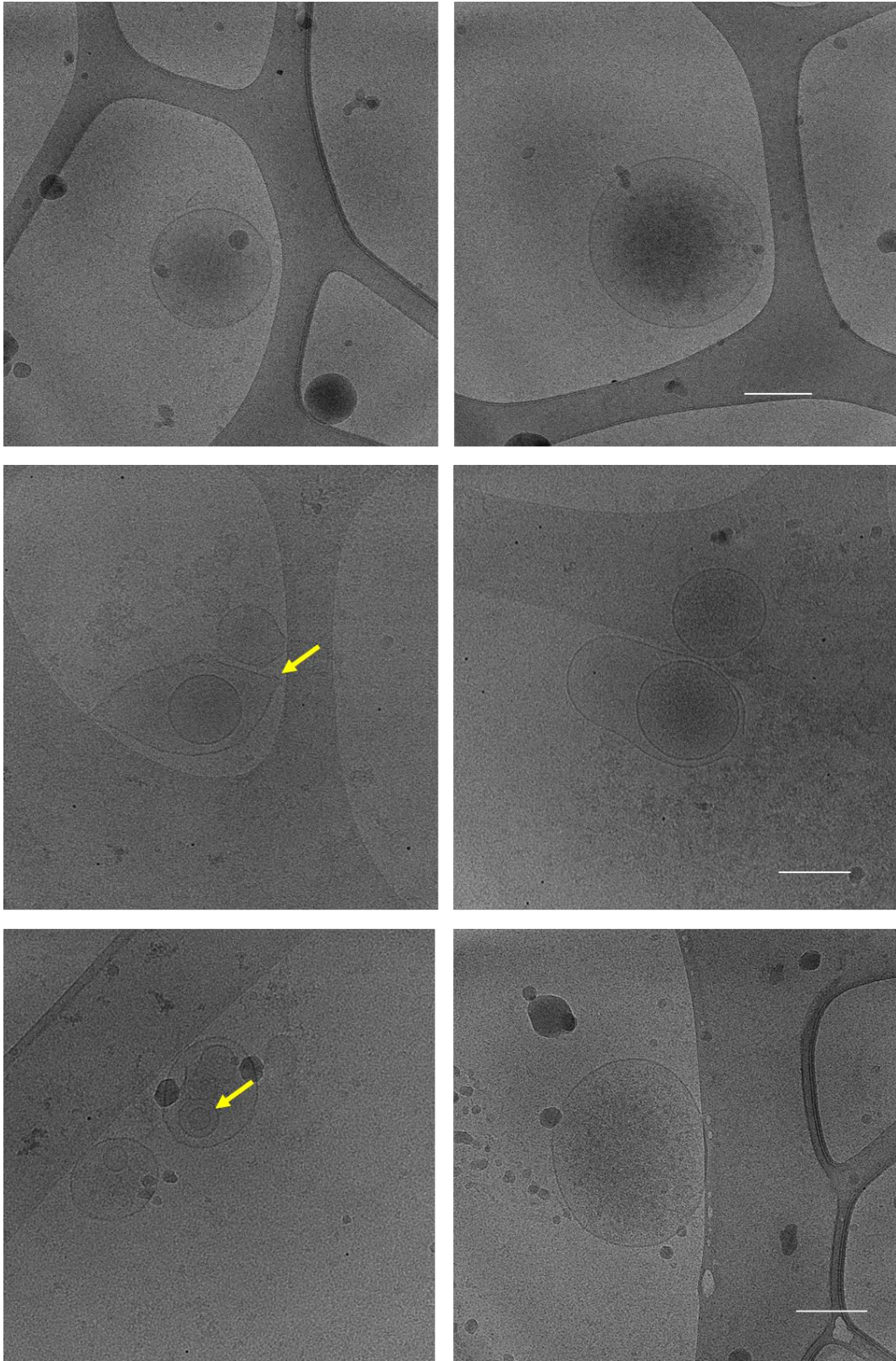
Figure 3-7. CryoEM 2-dimensional images of Bcl-2 EVs. Arrows indicate non-spherical EVs with multiple membranes; scale bar 200nm.

The next figure (Figure 3-8) shows a collection of *in vitro* prepared EVs, both Apo- and Bcl-2 vesicles which were observed as rare and unusual events in cryoEM imaging, showing the potential heterogeneity in the samples. In the top and second row of the images, vesicles either appear as 'empty', as there are no other characteristics apart from the vesicle membrane, or they appear to enclose fibrous-like entities inside the main membrane and also other structures on the surface which result in a 'hairy' appearance. The identity of these structures cannot be confirmed unless biochemical assays are performed, however the literature suggests that membrane and intravesicular proteins have been detected on several types of EVs, with similar electron microscopic appearance (see Introduction for references). Moreover, a vesicle with a double external membrane is depicted in the right image of the middle row, and the presence of this second membrane is evident by the increased thickness and also by the area where the two layers are locally separated for unknown reason.

Finally, the bottom row shows some special cases of EVs with more elongated shape and/or attached to each other similarly to 'beads on a string'. This effect has been also observed by I. Poon and group, in a study where these structures were suggested to be protrusions of the apoptotic cells, named apoptopodia (Atkin-Smith *et al.*, 2015).
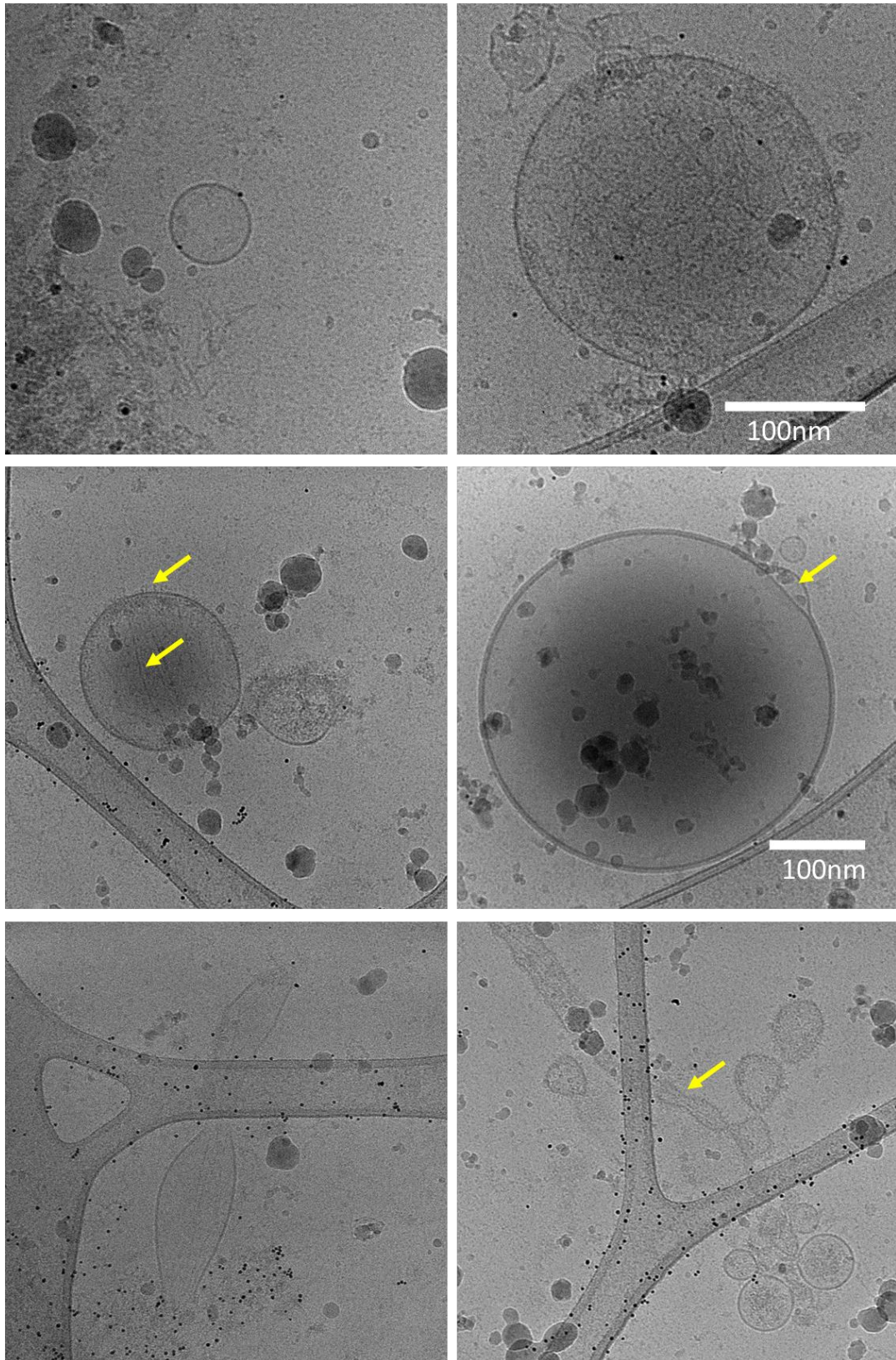
Figure 3-8. CryoEM 2-dimensional images of selected Apo-EVs and Bcl-2 EVs, to illustrate rare cases of vesicles with unusual shape and structure (indicated by arrows)

Following the visual observations on structure, some quantitative parameters were measured from the images. Firstly, the thickness of the vesicles' membrane was found at an average value of 7nm for both EV populations under examination, which is in agreement with the findings of another study on sperm-derived EVs where the double membrane was found to be around 15nm thick (Yuana *et al.*, 2013).

Image analysis for diameter measurement of all recorded bodies has been used to generate a density histogram (Figure 3-9). The differences observed in size using NTA or DLS cannot be examined in these histograms, as both populations appear very similar, with the main body of the sample located around 100-200nm. Because the layer of ice is only 200-300nm thick, some soft specimens such as the EVs are flattened, and therefore the diameter measured for some of the larger particles might not precisely reflect the size, as it has possibly been distorted (Yuana *et al.*, 2013). However, what this technique revealed, not detectable with either NTA or DLS is a population of vesicles as small as 25nm, for both samples.

Another quantifiable parameter from the 2-D images is the lamellarity of the individual EVs, which stands for the percentage of particles that have a simple structure with a single membrane in contrast to EVs with multiple other membranous vesicles enclosed in the main particle, as seen in the images earlier. The occurrence of multilamellar particles over single membrane vesicles for Apo- and Bcl-2 EVs is graphically shown in Figure 3-9. The Apo-EVs appear to be more simple than the Bcl-2 EVs, as their tendency to enclose multiple structures is 10% lower than the latter.
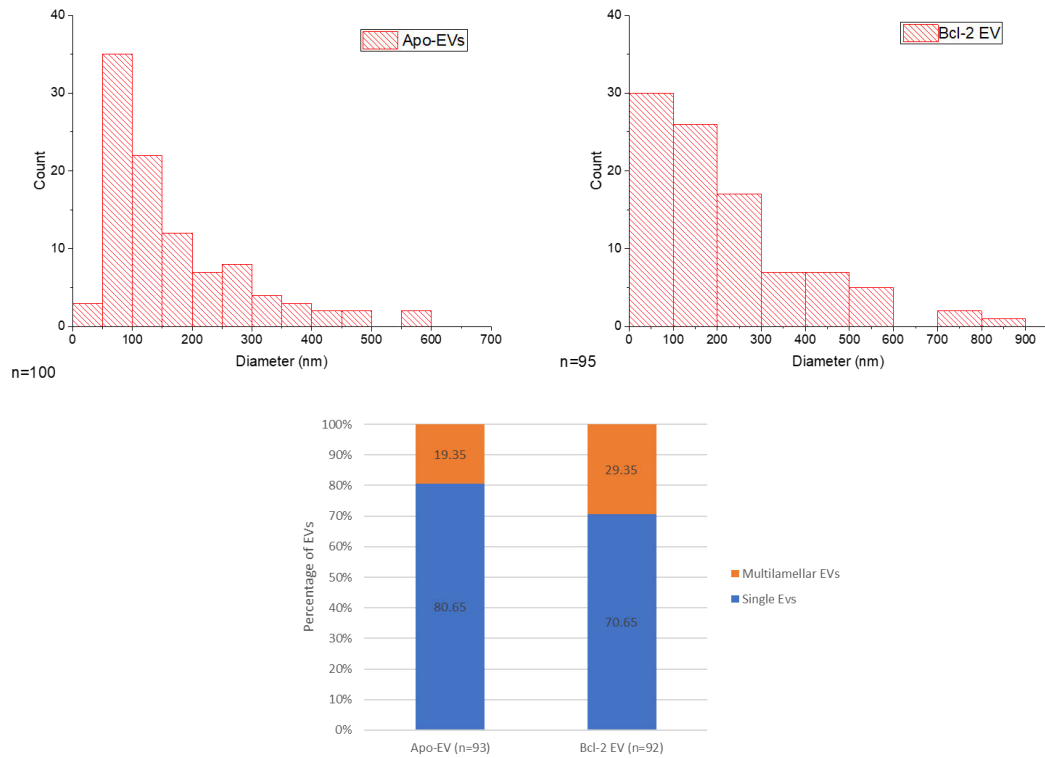
Figure 3-9. Size histograms for EVs as measured by cryoEM images (top row) and percentages of single and multilamellar EVs (bottom graph). The graphs have been generated by single EV analysis for n=100 or n=95 for ApoEV and Bcl-2 EV respectively, which derive from a summary of n=4 independent EV preparations.

Moving to a more advanced variation of two-dimensional imaging, cryoEM was used to record 3-D tomograms of the EVs. As shown in Figure 3-10, the smaller vesicles observed in the raw data are located inside the larger ones and are not compressed on the outside, something which would result in similar images as the electron beam penetrates the specimen. A second finding from these images is the presence of amorphous structures inside the vesicles, which is suggested to be proteins. Similarly to the previous 2-D images, a large variability is observed between the individual particles regarding the presence of other vesicles or proteins inside the main vesicle.
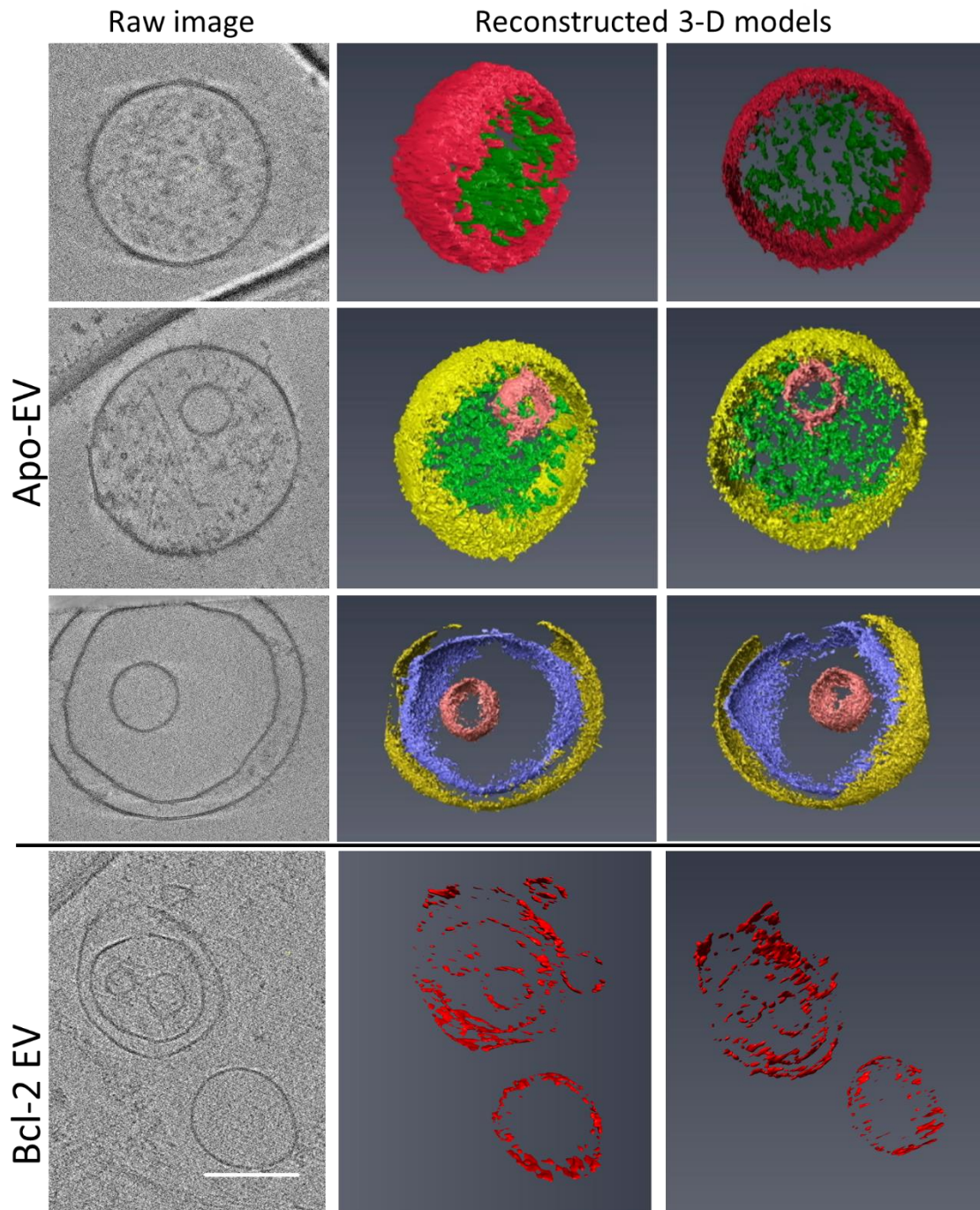
Figure 3-10. Raw images of a representative plane and 3-D reconstructed models of vesicles recorded with cryoEM; scale bar 200nm.

As a summary on cryoEM imaging, there were no major structural differences between the apoptotic and non-apoptotic cell-derived EVs, with the exception of the number of enclosed membranes which appears higher for the Bcl-2 EVs by 10%. Measuring the size for particles

larger than 200-300nm is not reliable with this method, as there are physical limitations attributed to preparation technicalities. This is due to the limited thickness of amorphous ice in which the particles are frozen, which also results in loss of the majority of EVs larger than 300nm during preparation. What can also be concluded, however, is that since the membrane thickness is around 7nm, and the smallest particle recorded in this study was around 25nm, it can be suggested that the formation of a spherical lipid bilayer - delimited vesicle with a diameter smaller than 15-20nm would be geometrically and thermodynamically unstable. This is a relieving finding, as it indicates that only a small part of the population is undetectable by NTA (minimum particle size 30nm). Finally, some EVs have a structure more complex than expected, and it can be speculated that these structures reflect the various biogenetic pathways through which those vesicles have been produced, albeit this hypothesis would need to be investigated with other methods, as well.

3.4. EV membrane study by fluorescence depolarization (anisotropy)

Fluorescence anisotropy is a spectroscopic method in which fluorescent dyes with specific affinity to the lipid bilayer can give information about the membrane fluidity and order. For the purpose of this work, the information expected to be obtained from this technique is the extracellular vesicles' membrane integrity and viscosity, which can reveal potential differences among the vesicles derived from different cellular paths (apoptotic and non-apoptotic cell-derived vesicles). The incorporation of an appropriate fluorescent molecule in the vesicles' membrane such as DPH and its derivative, TMA-DPH allows the measurement of depolarization of these molecules under different conditions. The experiments are focused on comparing Apo- and Bcl-2 EVs as to the membrane fluidity at different temperatures. In a more general frame, membrane integrity measurements can be applied to EVs from clinical samples in order to determine the effect of various storage conditions on the EV stability (for example temperature, freeze-thawing, addition of cryoprotectant). In this section, human plasma-derived EVs will be measured alongside the BL2 cell-derived EVs, setting the baseline for further clinical sample analyses.

3.4.1. Fluorescence depolarization measurements on liposomes

Acknowledging that the vesicles' membranes are complex systems that not only consist of a wide variety of lipids, but also macromolecules such as proteins, nucleic acids and even saccharides, simpler liposomal model vesicles were first prepared and analysed in order to obtain a set of data which can be used for comparison to the EV measurements.

Liposomes are spherical colloidal particles which form lipid bilayers, often one inside another, alternating with aqueous parts. The building blocks of those structures are lipids, phospholipids, and cholesterol. Because of the amphiphilic nature of the lipids, the presence of aqueous solution leads to a thermodynamic formation of a self-assembled lipid bilayer, which finally forms a spherical membrane, encapsulating the aqueous solution. The literature shows an extended interest in the anisotropic properties of the liposomal lipid bilayers from the past few decades until recently, and these systems have been studied as to the behaviour of the membranes under different conditions, usually altering the temperature, pH and lipid composition of the membrane (Birch, Holmes and Imhof, 1988). The results prove that depolarization measurements are sensitive to minor changes in the system under the impact of physical conditions and even the presence of chemical substances (Bisby and Birch, 1989), (Holmes *et al.*, 1991), (Holmes *et al.*, 1997).

Different liposomal preparations involved combinations of phospholipids and mixtures with cholesterol, as seen in Figure 3-11. The liposomal suspensions were characterized as to size distribution and colloid stability by zeta potential. Figure 3-11 shows the values of the size distribution peak along with the poly-dispersity index (PDI) for all preparations with different lipid compositions.
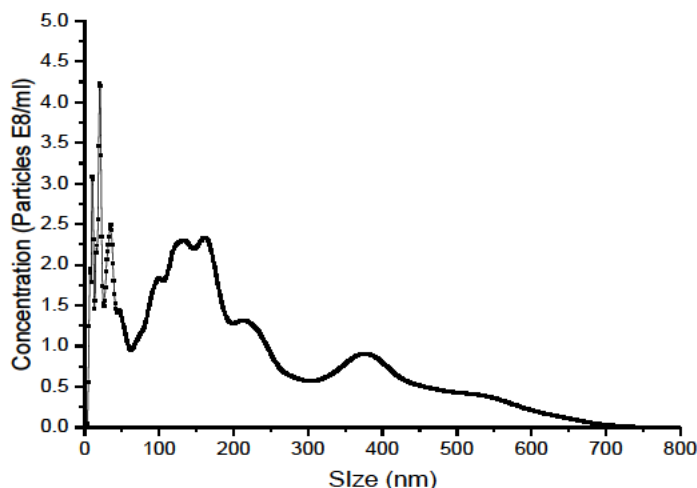
Liposomes	z-average size (nm)	PDI	Zeta potential (mV)
DPPC	213.1	0.77	-0.101±0.50
DPPC:Chol 2:1	200.7	0.131	-1.445±1.13
DMPC:Chol 2:1	311.8	1	-0.588±2.12
DPPC:Chol 1:1	596	1	0.061±0.82

Figure 3-11. Size distribution of DPPC liposomes as measured by NTA (top) and zeta potential and size distribution values for all liposomal samples as measured by DLS for one preparation (bottom table).

With the exception of DPPC:Chol 1:1 liposomes which appear at a higher peak around 600nm, the majority of the different lipid composition preparations have a size between 200 and 300nm, however the PDI values indicate a wide distribution for all samples except for the DPPC:Chol 2:1 liposomes (PDI 0.13) (Figure 3-11). The size distribution of DPPC liposomes as measured by the Nanoparticle Tracking Analysis microscope (Nanosight) is also shown as an indication of the large dispersity in diameter. The main population of particles is distributed around 150nm and not above 700nm in diameter. This dissimilarity between the different preparations can be attributed to the preparation method and the simplicity of the equipment used. The injection of lipids in the aquatic solution is subject to errors due to manual operation, and the lack of extrusion devices which would ensure a more uniform size is also a factor contributing to this variability.

The spectroscopic properties of the liposomal preparations rely on measuring dye incorporation in the lipid bilayer. To determine the maximum absorption and emission wavelength for DPH, the spectra were obtained for the free fluorophore dissolved in DMF

and for DPH stained liposomes suspended in PBS. The next graphs in Figure 3-12 show the absorption and emission spectra (374nm excitation beam) for DPH in solution and for liposomal DPH.
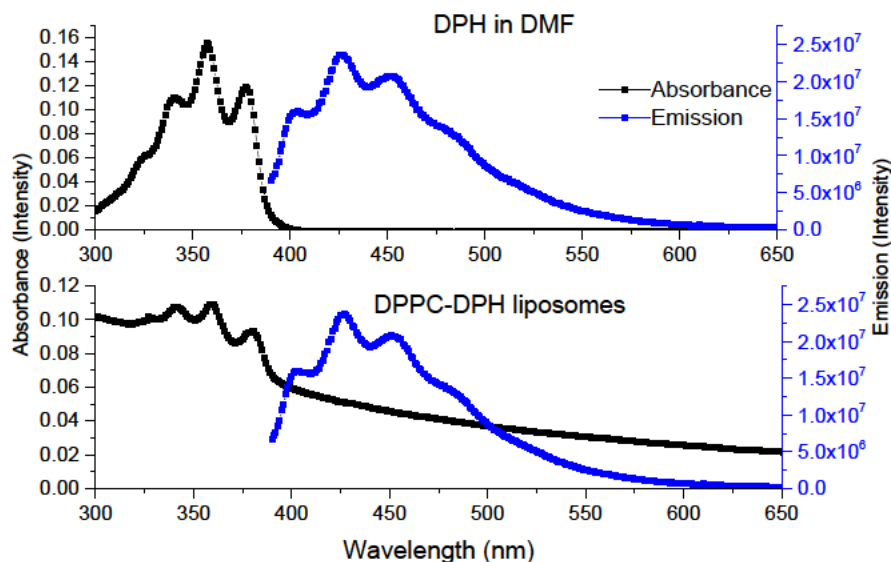
Figure 3-12. DPH (1.3μM in DMF) and DPPC liposomes stained with DPH (in PBS) absorbance and emission spectra at 374nm excitation.

As expected, both free and liposomal DPH show the same peaks in absorption and emission spectra. Absorption peaks appear at 339, 356 and 375nm and the maximum emission is recorded at 403, 427 and 451nm. In the liposomal absorption spectrum, there is increased absorption for wavelengths lower than 300nm and this effect is often attributed to the particles scattering light away from the detector due to their size and shape, decreasing the signal intensity, thus being recorded as higher absorption. From these spectra, the optimal parameters for anisotropy decay measurement indicate excitation at 374nm and emission collection at 450nm. DPH has been known to aggregate in water by forming dimers, trimers or larger structures and this adds another level of complexity in the spectral measurements, as free DPH molecules are also expected to be present in the liposomal suspensions (Gracetto *et al.*, 2010).

To ensure the TCSPC instrumentation beam path and the position of the polarizers are aligned, the anisotropy decay curves of DPH were recorded in a viscous non-polar solvent, ethylene glycol and also in a non-viscous solvent, DMF. The results are shown in Figure 3-13.
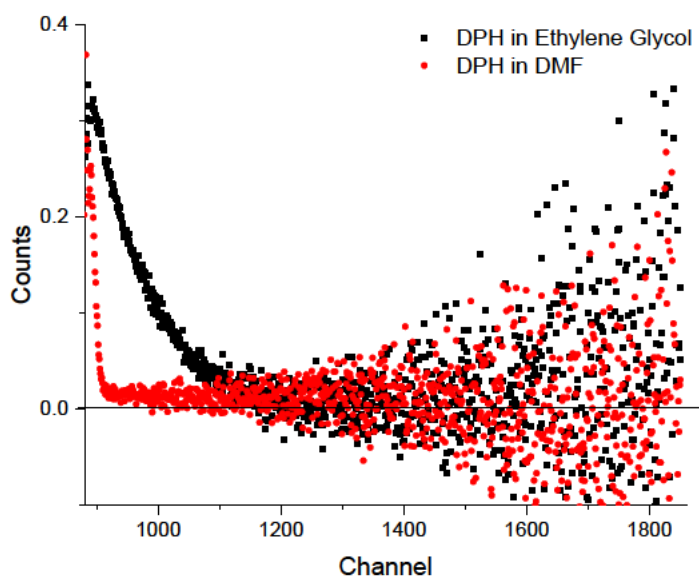
Figure 3-13. Anisotropy decay curves for DPH in Ethylene Glycol and DMF (1.3μM) at room temperature.

It is shown that the anisotropy of the DPH in DMF rapidly decays to 0.0, in contrast to a more viscous solvent (ethylene glycol), in which is the fluorophore exhibits slower rotation but again the final anisotropy is 0.0. This is a confirmation of an aligned system, as in case of misaligned polarizers, the final anisotropy would be different to 0.0, due to the light detected on a plane different than the standard Vertical and Horizontal configuration (see Introduction).

The anisotropy results for liposomal samples are presented in Figure 3-14 where the initial anisotropy A values are plotted over temperature for two of the liposomal preparations. The samples omitted from this graph (preparations containing cholesterol) have a high standard error value and are not presented. Anisotropy for DPH in DMF was calculated at 0.24 at room temperature and R_{inf} is manually fixed to 0 for all sets of data during analysis, to facilitate the fitting of the curve to an equation.
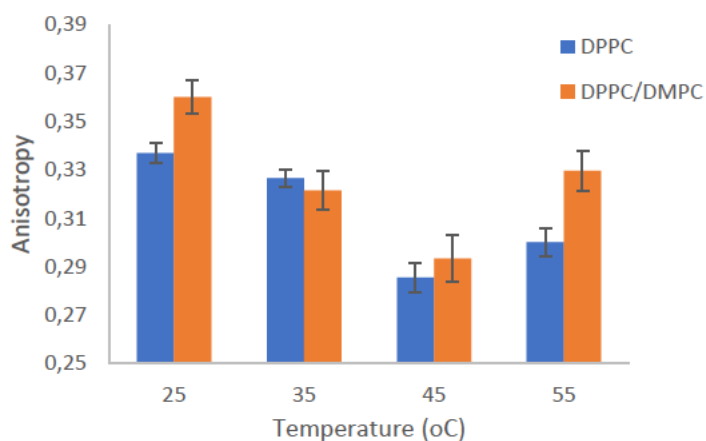
Figure 3-14. Anisotropy (A) for DPH in DPPC and DPPC/DMPC liposomes in increasing temperature points (average values from 3 runs plotted with SD).

It is overall observed that the maximum A is below 0.4 and the increase of temperature results in increased membrane fluidity, expressed as lower anisotropy. This trend changes for temperatures higher than 50^0C and this can be an indication of particle coalescence, with subsequent alteration of the rotational behaviour of the fluorophore.

Rotational correlation time values are extracted from the anisotropy decays and the cumulative graphs for T_1 and T_2 are shown in Figure 3-15. All data are fitted with a two-exponential equation.
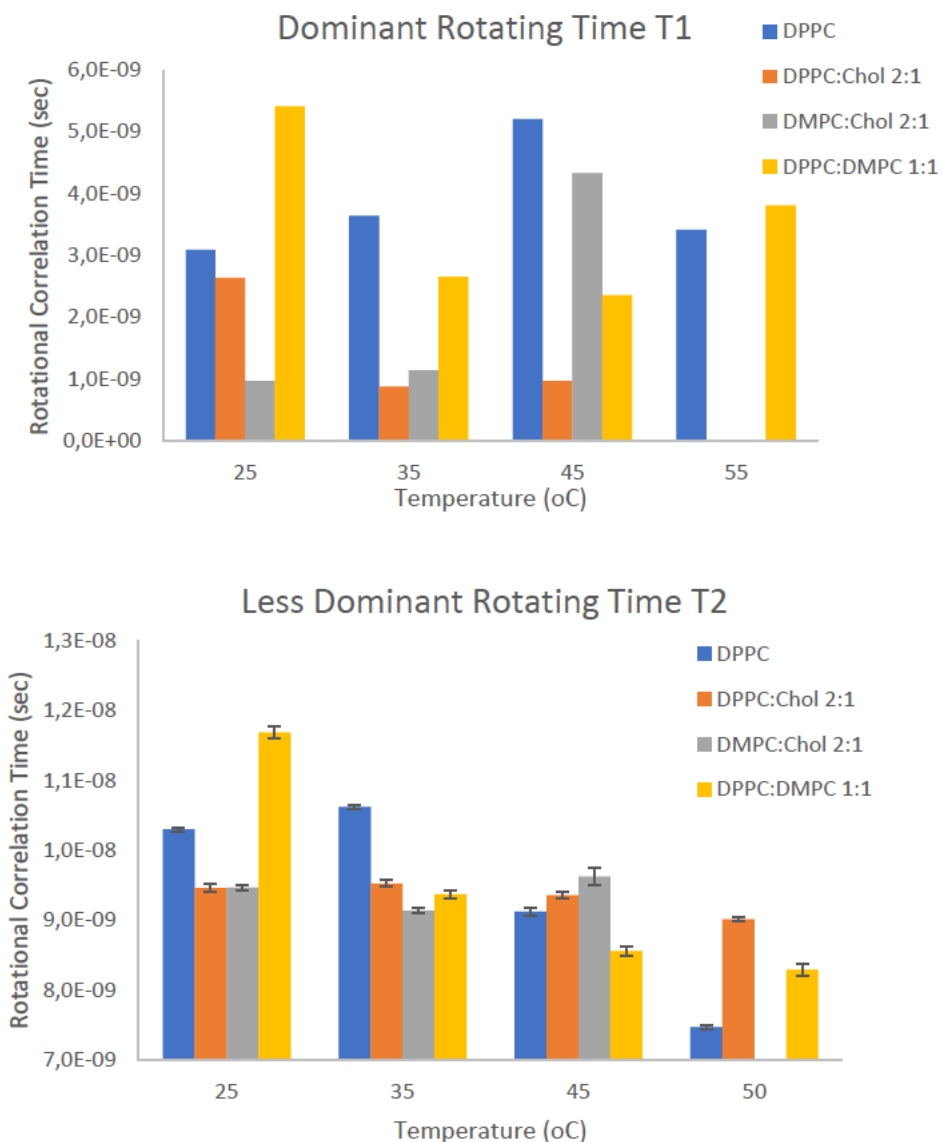
Figure 3-15. Rotational correlation time (T) for all liposomal preparations for increasing temperature points (dominant and less dominant rotating times). Values presented from a single representative experiment.

From the above data it is shown that the rotational correlation time of the less dominant time (T2) of the samples decreases with the increase of the temperature and the lowest values are generally observed for the preparations which do not contain cholesterol. In contrast, the liposomal formulations with cholesterol have a lower T in low temperatures and they are less sensitive to the temperature increase, indicating that these membranes have higher rigidity. For the T1, the values over temperature are more irregular, as most

liposomal types seem to have increased fluidity up to 37°C, albeit the pattern is altered for higher temperatures. However, there is a general trend indicating that the fluorophores in the non-cholesterol liposomes rotate faster than the cholesterol-containing samples, confirming the increased membrane rigidity caused by cholesterol.

The results obtained by liposomes stained with DPH have overall showed the dependence of the anisotropy and the rotational correlation time on the membrane microviscosity, and in addition have revealed a potential structural deformation of the particles for temperatures higher than 45°C, which becomes evident by the decrease in membrane fluidity and the possible re-arrangement of the lipids or particle fusion.

3.4.2. Fluorescence depolarization measurements on *in vitro* prepared Apo-EVs and blood plasma-derived EVs stained with DPH

In this section, the anisotropy measurements were applied for DPH-stained EVs, for which the staining protocol is different from the liposome staining. Because EV staining with DPH requires the initial stock dye solution in THF, the spectra of absorption and emission for DPH in THF are presented Figure 3-16.
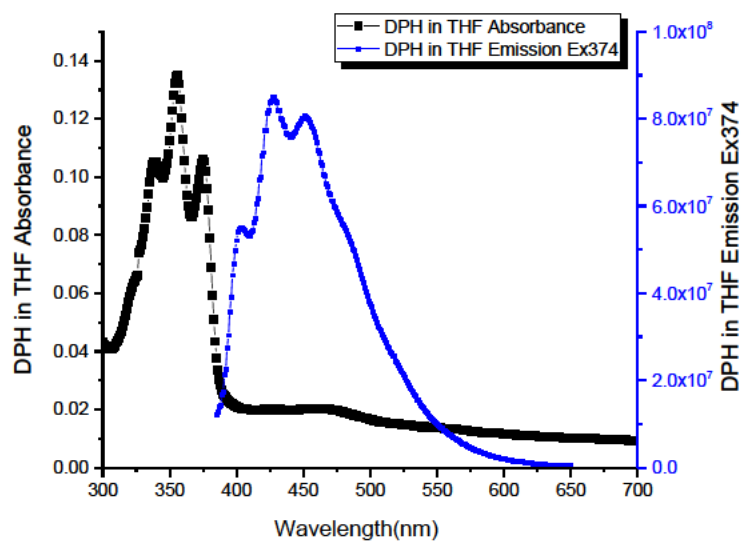
Figure 3-16. Absorption and Emission (Ex374nm) spectra for DPH in THF (1nM).

It is confirmed that the difference in solvent (DMF in Figure 3-12, instead of THF) does not affect the position of the spectral peaks for DPH and therefore, the excitation and emission parameters during the depolarization measurements are similar to the liposomal samples, i.e. excitation with 374nm Delta Diode and emission collection at 450nm.

The Apo- and Bcl-2 EVs are stained with DPH and time resolved anisotropy is measured at room temperature (22°C), 37°C and at 45°C. As indicated by the studies on liposomal membrane anisotropy, physical distortion of particles is suspected for temperatures higher than 45°C and therefore all anisotropy measurements for EVs will be performed for temperatures not higher than 45°C.

The fluorescence decay curves as recorded by TCSPC instrumentation with the mathematical fit and residuals are presented for the free DPH in THF and the DPH-stained EVs for all temperatures in Figure 3-17.
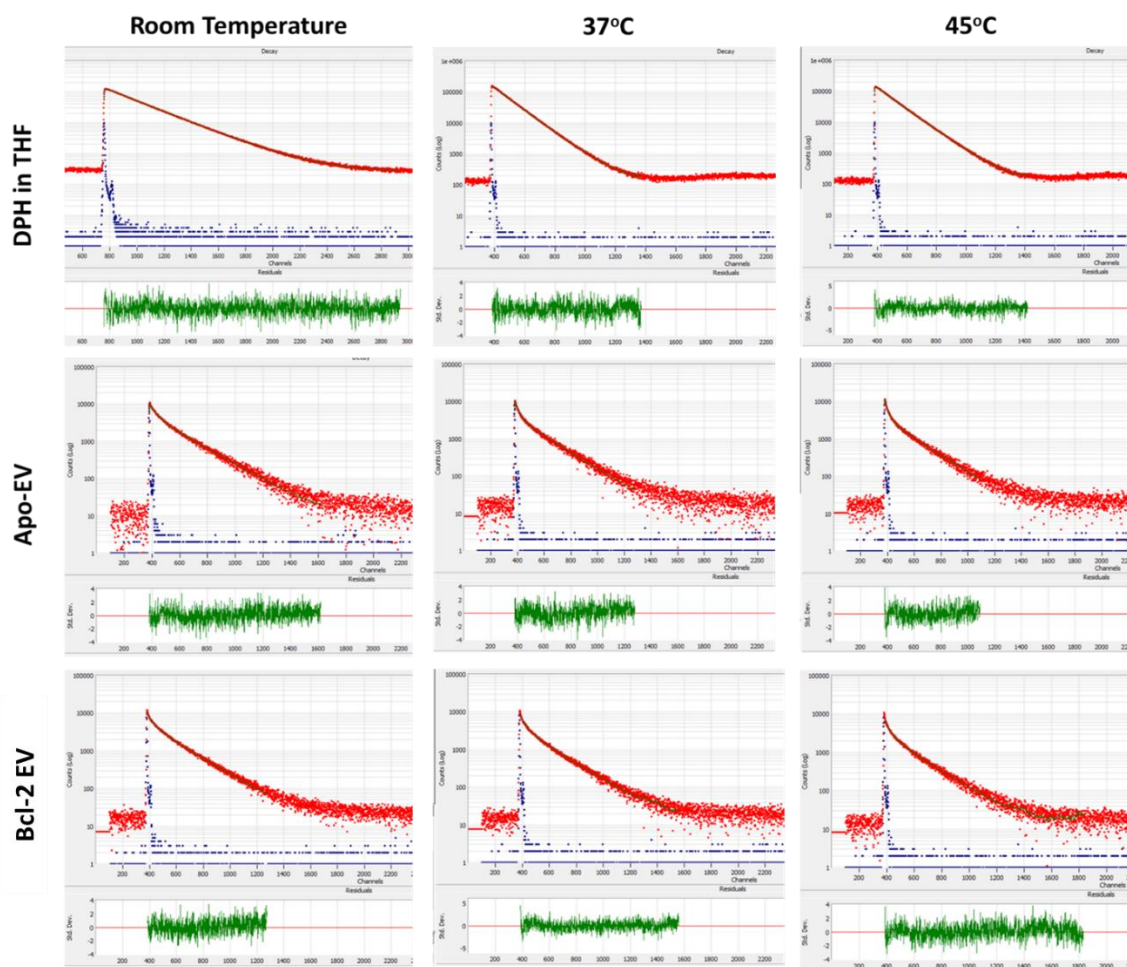
Figure 3-17. Anisotropy decays (red) and fitting curve residuals (green) for DPH in THF, Apo-EVs (at 46.4*108 particles/ml) and Bcl-2 EVs (at 17.7 *108 particles/ml) (Ex374nm Delta Diode, Em450nm). The curves have been extracted from one measurement, and are representative for all experiments.

The presence of the 'spike' on the beginning of the decay curve for all EV samples is due to detection of scattered excitation light due to the refractive index difference between the solvent and vesicle. However, by applying fitting equations to the lifetime and anisotropy decays for all samples and temperature points, cumulative data were extracted and the parameters which appear to be the most significant and statistically reliable have been plotted in the following graphs.

Figure 3-18 shows the anisotropy values and the membrane order parameter as calculated by the initial and the residual anisotropy (Equation 4 in Introduction).

Anisotropy
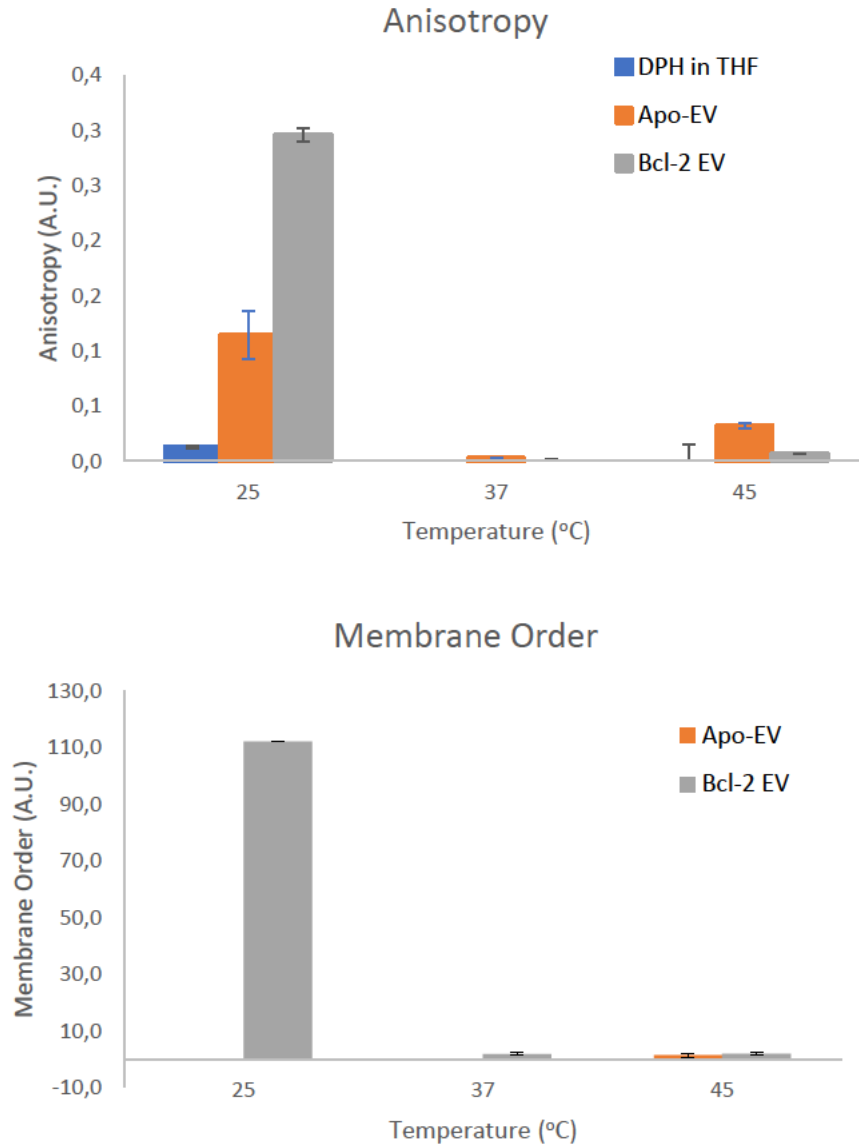
Membrane Order

Figure 3-18. Anisotropy (top) and membrane order graphs (bottom) for DPH in THF and DPH-stained EVs over temperature (average values from 3 runs plotted with SD).

It is evident that the Bcl-2 EVs show significantly higher rigidity at room temperature than the Apo-EVs, however this decreases and becomes almost equal for both types of EVs over the increase of temperature. For the DPH in solvent, the freedom of rotation of the molecules is very high, therefore the anisotropy values are close to 0.0 for all temperatures.

To explore the rotating pattern of the fluorophore in the membranes in more detail, the rotational correlation times of the most dominant and second most dominant rotating times are presented in Figure 3-19.

Dominant Rotating Time T1

Less dominant Rotating Time T2
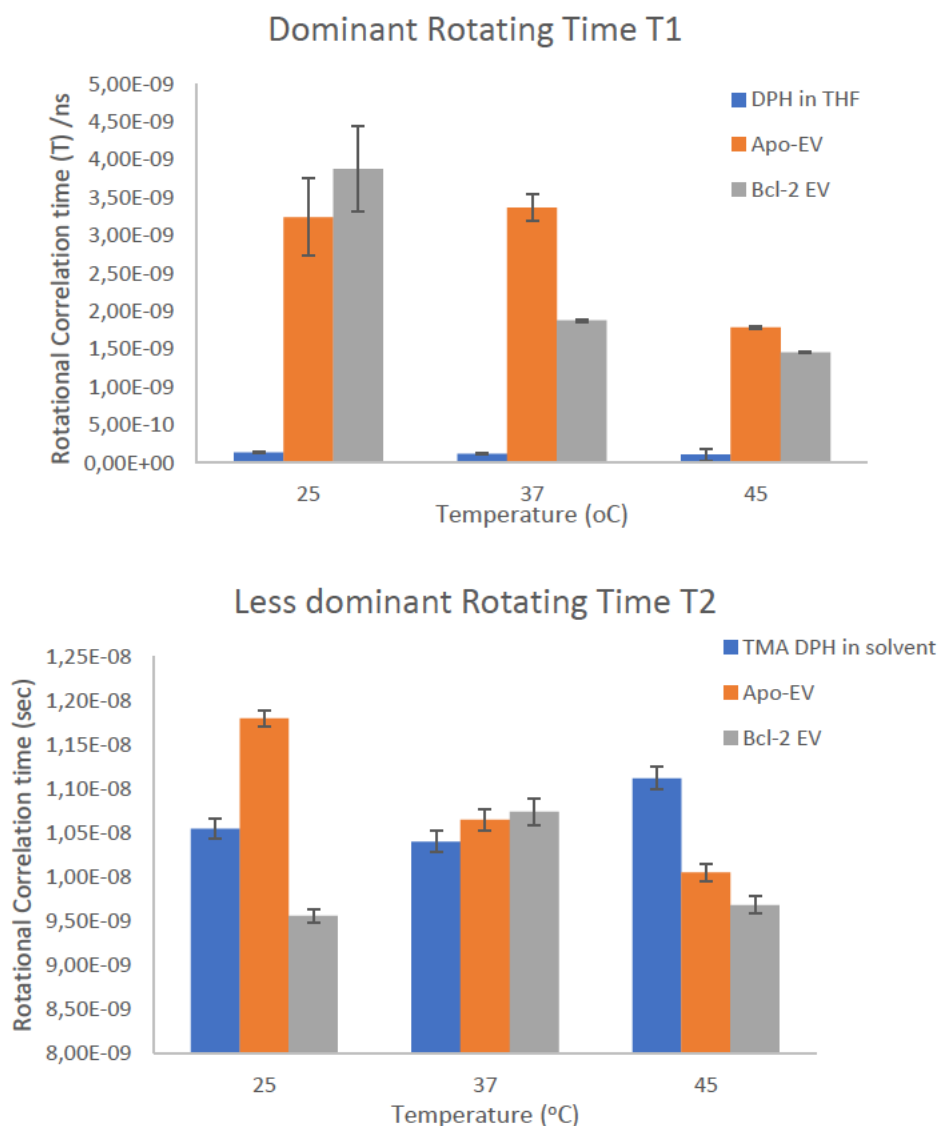
Figure 3-19. DPH Rotational Correlation time (T) for the two most dominant rotating times T1 and T2 for DPH in THF and EV samples at room temperature, 37°C and 45°C (average values from 3 runs plotted with SD).

A decreasing trend in the T values reflects the increase in freedom of the dye to rotate as the viscosity of the lipid bilayer decreases. It is shown that the most dominant rotating moiety has a large degree of freedom without a noticeable trend with the increase in temperature

for the free DPH, while for the EVs, it begins at 3-4 ns at room temperature, and although the two EV samples exhibit differences at 37°C, those values are almost equalized at 45°C. For the less dominant rotating pattern, the changes in correlation time are more irregular, possibly due to aggregates of free dye and more rigid microdomains in the membranes of EVs, as observed for the liposomal samples in the previous section.

In parallel to *in vitro* prepared EVs, which are characterised by a relatively wide size distribution, EVs with a more narrow size profile were also chosen for DPH staining, in order to compare the findings and assess the suitability of the technique on the Apo-EVs. Human blood plasma-derived EVs were isolated and stained with DPH under two different conditions: freshly prepared from plasma and after freezing and thawing, which corresponds to the clinically standard storing procedure at -80°C. The most significant parameters extracted from these measurements are presented in Figure 3-20.
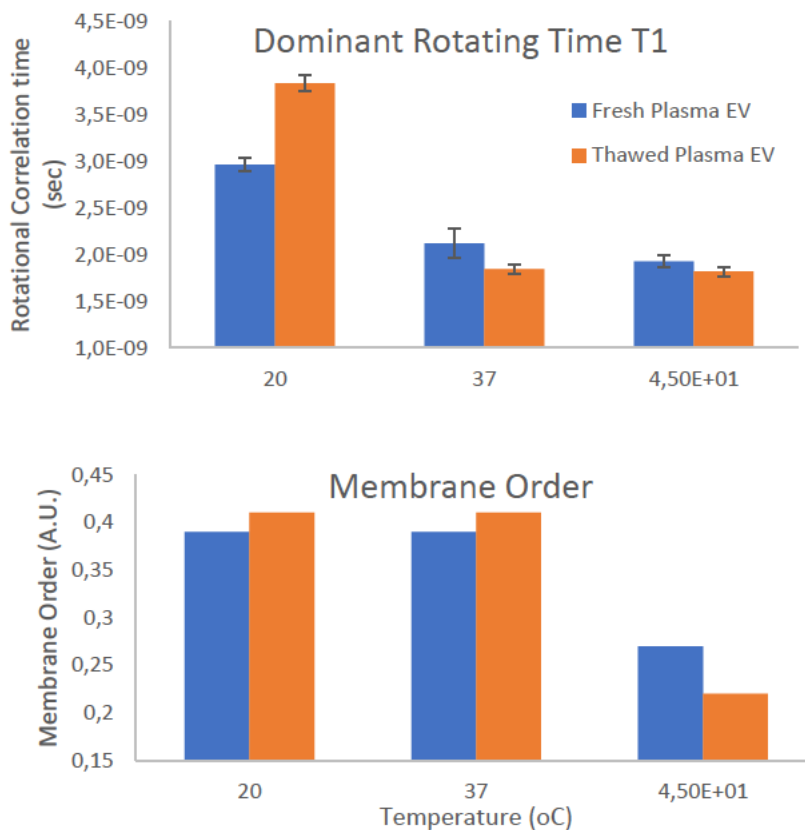
Figure 3-20. Rotational correlation time for the most dominant time and membrane order values for EVs from blood of healthy volunteers stained with DPH over temperature increase (average values from 3 runs plotted

with SD for rotational correlation time; for membrane order, the value was calculated using the average values from e experiments)

.

As seen in the graphs above, the rotational time drops rapidly from room temperature to 37°C and the difference is smoother for up to 45°C. Interestingly, the membrane order seems to be stable for both types of EVs up to 37°C, but there is a significant decrease between 37 and 45°C, indicating that the phase transition temperature of the membrane (the temperature point where the membrane loses its rigidity and becomes more fluid) is found between those temperature points.

3.4.3. Anisotropy measurements for EVs stained with TMA-DPH

In order to compare the findings of the DPH anisotropy on EVs, and in an attempt to examine the fluidic behaviour of the vesicle membranes in more detail, the measurements were performed with a second fluorophore, as an alternative to DPH. TMA DPH (trimethylamine DPH) is a derivative of the parental molecule with a polar head, which is localized only on the polar groups of the lipids and is therefore internalized to a lower extent compared to the parental molecule, remaining selectively on the membrane (Montaudon *et al.*, 1986).

The fluorescence lifetime decays for the free dye in solvent and for Apo- and Bcl-2 EVs are shown below.
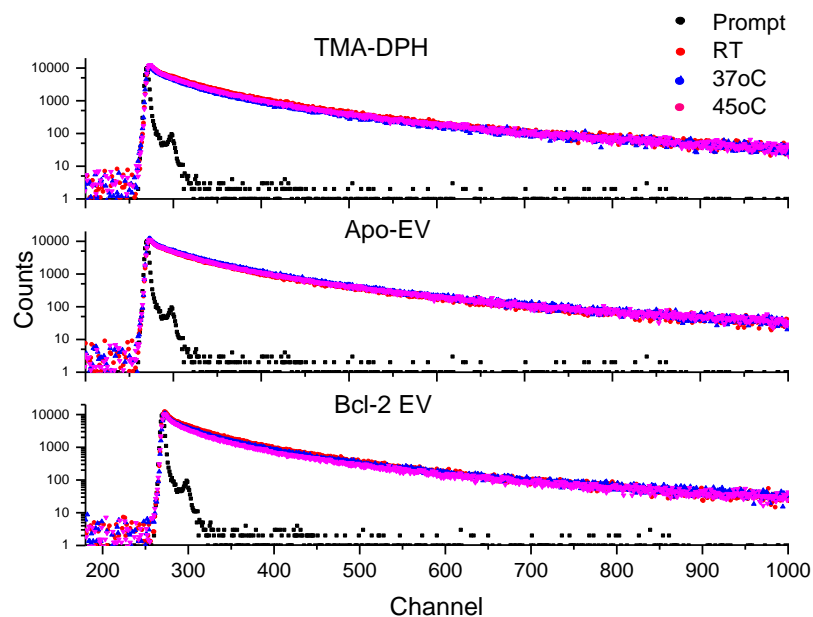
Sample	Temperature (°C)	Anisotropy	Average Lifetime (sec)	Rotational Correlation Time T1	Rotational Correlation Time T2
TMA-DPH in DMSO	22	4.40 ± 1.44	3.38E-06	4.51E-09 ± 6.25E-10	1.64E-09 ± 1.00E-10
	37	0.08 ± 0.01	1.32E-08	4.41E-09 ± 6.09E-10	1.40E-09 ± 1.10E-10
	45	0.12 ± 0.03	1.16E-08	5.29E-09 ± 9.84E-10	1.75E-09 ± 9.90E-11
Apo-EV	22	20.58 ± 4.24	9.81E-06	1.57E-09 ± 1.46E-10	4.95E-09 ± 1.60E-10
	37	10.89 ± 1.40	3.17E-06	3.49E-09 ± 1.47E-10	1.23E-08 ± 4.32E-10
	45	3.66 ± 2.24	1.18E-06	5.71E-09 ± 2.93E-09	2.52E-09 ± 3.45E-10
Bcl-2 EV	22	9.92 ± 1.59	3.34E-06	3.02E-09 ± 1.56E-10	1.03E-08 ± 3.43E-10
	37	0.56 ± 0.08	1.40E-07	3.89E-09 ± 6.29E-10	1.32E-08 ± 9.99E-10
	45	0.3 2± 0.04	7.80E-08	3.31E-09 ± 1.77E-10	1.13E-08 ± 5.70E-10

Figure 3-21. TMA-DPH fluorescence decay curves for free dye in DMSO at 2μM (top), Apo-EVs (middle) and Bcl-2 EVs (bottom) in a range of temperatures. The table following the graph presents all values extracted from fitting analysis.

In the decay curves in Figure 3-21, it would be expected that the increasing temperature would result in shorter decays, however this is only observed for the Bcl-2 EVs and not for free dye and Apo-EVs, which show an irregular decay pattern for the different temperatures. The values extracted from the mathematical fitting of the decays are presented in the next figures. For comparison, EVs from the blood plasma of healthy individuals is also analysed

here. These EVs have a smaller diameter than the Apo- and Bcl-2 EVs and would be therefore expected to give more reliable results.

The next figure illustrates the decay components of the two most dominant rotating moieties, as measured from the decay curves shown earlier.
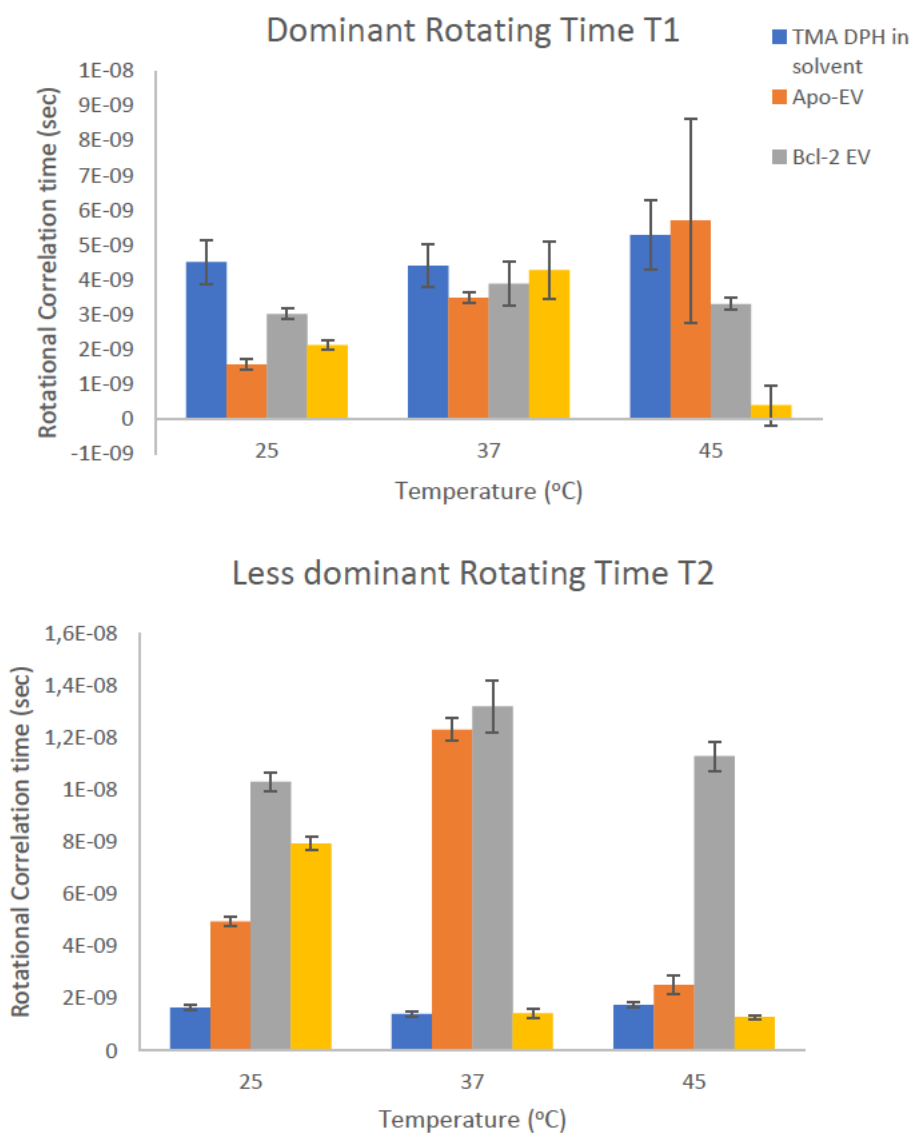

Figure 3-22. Rotational correlation time (T) for all EV preparations stained with TMA-DPH for increasing temperature points (dominant and less dominant rotating times T1 and T2), (average values from 3 runs plotted with SD).

From the values extracted for rotational correlation times in Figure 3-22, it is observed that TMA-DPH in DMSO is practically insensitive to the increase of the temperature, while irregular trends are seen for Apo-EVs and Bcl-2 EVs. Plasma-derived EVs seem to maintain a trend for decreasing T as the temperature rises, especially for T2.

Anisotropy and membrane order values are not presented, due to unacceptable values of the standard deviations.

From the graphs above, it is observed that TMA-DPH exhibits a rotational behaviour different to the parental molecule DPH, as some values change irregularly over the effect of temperature. The rotational correlation times of the two most dominant moieties decrease as the temperature increases for free dye in DMSO and for plasma-derived EVs, however the data for Apo-EVs and Bcl-2 EVs do not show a specific pattern and would be considered rather unreliable. This behaviour can be attributed to the fact that the TMA-DPH is bound more preferably on the outer surface of the EV membrane, thus its rotational behaviour can be more susceptible to EV coalescence, which would significantly alter the dye's microenvironment. In addition, TMA-DPH is considered to be less temperature dependent on the anisotropy of more rigid membranes, as shown on a study where plasma membranes of cells were compared to intercellular compartments (Montaudon *et al.*, 1986).

In this case, DPH would be considered a more suitable dye for anisotropy studies on time-resolved anisotropy studies, as it is located deeper in the lipid bilayer and therefore the impact of other particles interacting with the surface of the vesicles. The literature shows examples of EVs and similar particles studied with DPH and TMA-DPH, however only using steady state anisotropy and not time-resolved instrumentation (Laulagnier *et al.*, 2004), (Rejraji *et al.*, 2006), (Shenoy *et al.*, 2018).

3.5. Discussion

To summarize the findings of this chapter, DLS is commonly used for particle suspensions, although there are some clear limitations for samples with broad size distributions, such as the EV suspensions. Polydispersity index values suggest that the sample is possibly more heterogenous than the technique ideally analyzes, and the software gives information for a

limited number of peaks (up to 3). From the data acquired, there is an agreement with the NTA method, but with fewer details on the shape of the histogram. What distinguishes DLS from NTA is the practically unlimited range of sizes (with biological interest) the instrument can detect and interestingly, both for Apo- and Bcl-2 EVs, a peak around 8nm was detected, which may, though, be an artefact of the data fitting analysis, as the presence of vesicles of such small size have not been confirmed by cryoEM. DLS also offers zeta potential data with the values suggesting poor to moderate stability for the suspension.

Translating these results in a biological dimension, both techniques showed that the Apo-EVs include a population of larger vesicles and that the cells release a higher amount of Apo-EVs as they go into apoptosis, compared to the non-apoptotic cells. This trend suggests that the Apo-EVs can be potentially released via alternative routes or by taking advantage of the existing machinery, affecting the type of cargo and the messages they can deliver. Phenotypic characterization promises to give more information on the possible mechanisms of secretion and functions.

Next, imaging EVs under cryoEM offers the high resolution of TEM alongside the benefit of maintaining the sample closer to its native state, minimizing distortion from fixation. As shown in the results, the size distribution is generally similar to the size measured by NTA and DLS, although this method is less reliable for particles larger than 300nm. It is also shown that among other techniques, cryoEM is possibly the only tool that can provide detailed data on the shape, number of enclosed structures, tendency to aggregate or coalesce, presence of subcellular organelles and membrane thickness. CryoEM and tomography have so far provided high quality images of the structure, dimensions and the spatial arrangement of multilamellar particles, in which smaller vesicles are included in a main membranous structure. Another observation from the EM images is the high degree of heterogeneity among the vesicles of both populations, as they can range from single to double membrane, with or without membrane and intraluminal proteins.

Finally, fluorescence anisotropy decay curves can reveal details of the membrane structure and its viscosity, undetectable with other techniques. However, because of the high sensitivity in those measurements, the recording of meaningful sets of data can be a challenge for systems such as extracellular vesicles, where the variety of different components (membrane proteins with fluorescent amino acids) and the broad size

distribution increase the level of complexity. The results suggest that there are differences in the membrane rigidity of the two EV populations, as the DPH measurements revealed. In more detail, the Apo-EVs appear less rigid than the Bcl-2 EVs, which is an evidence that these vesicles are generated from different cellular compartments. This observation can be a starting point for further considerations about the potential biogenetic routes of these vesicles, as it can be correlated with other studies in which the plasma membrane was found more rigid than subcellular compartments (Montaudon *et al.*, 1986). In addition, looking at the effect of temperature on the fluidity of the membranes, it is evident that there are significant alterations in the rotational correlation times and anisotropy of samples as the temperature rises from ambient to 37°C, which reflects the proportion of cholesterol in the membranes. Comparing the EV data with the results from the anisotropy measurements on liposomes, it has been overall shown that the less rigid Apo-EVs resemble the formulations without cholesterol, while the Bcl-2 EVs follow a pattern similar to the cholesterol-containing liposomes, which is an additional indication that the two EV populations have differences in the lipid composition. Finally, regarding the technical aspect, DPH proved more suitable than TMA-DPH for this system and the vesicles derived from blood plasma seemed to be more suitable for this method than the *in vitro* prepared Apo-EVs, as they have a narrower size distribution, therefore lower degree of variability. Therefore, it was shown that fluorescence anisotropy is suitable for EVs from clinical samples and can be a useful method for the assessment of the vesicle stability under routinely used storage and isolation methods of the relevant biological fluids.

4. Study of EV cargo

4.1. Aims of the chapter

This chapter describes how the EVs can be analysed as to their surface receptors as well as internal proteins and nucleic acids. Some of the methods discussed here are mostly applied for basic research purposes, however, as it will be shown, there are techniques with potential applications on the clinical diagnostic practice, offering rapid results using clinically available equipment.

To begin with, one of the most commonly used methods for the analysis of disease-related markers is flow cytometry. In the case of EVs and due to their small size, this technique is being pushed beyond its resolution limits since conventional instruments are mainly designed for larger particles >200-500nm, depending on the cytometer (Lacroix *et al.*, 2010), (Nolan, 2015). As discussed in the Introduction, an adaptation of flow cytometry which can overcome the size limitations is the capturing of EVs on larger magnetic beads. In this work, the most effective bead capture probes for EVs were investigated, as the availability of surface molecules on the vesicle membrane affects the efficiency of binding. Starting from surface markers which would be expected to be highly expressed on EVs, the beads were coated with antibodies against those molecules and the binding efficiency was determined by flow cytometry with fluorescently stained EVs. The surface receptors of choice are: CD19 and CD20, as these are two classical B cell lymphoma markers (Kelemen *et al.*, 2010), MHC class I, as indicated by proteomics analysis on EVs (study performed by Gregory group members, results not shown here), PS which is generally expected to be exposed on EV membranes (Shih *et al.*, 2016) and the well-established 'exosome' markers CD9, CD63 and CD81 (Exocarta.org).

Phenotypic analysis was also performed with confocal fluorescence microscopy in order to visualize the EVs attached on a surface without using magnetic beads and finally, a number of surface molecules were examined by immunogold labelling and TEM imaging, providing high resolution visualization of individual particles.

All techniques discussed above concern the study of proteins and surface receptors as potential Apo-EV specific markers. However, nucleic acids and especially micro RNAs are biomarkers which are often used to identify EVs arising from a specific condition. RNA

sequencing of Apo-EVs has been performed by colleagues and the most significant results of this study will be verified *in vitro* in this thesis. The upregulation of a non-coding RNA species, the human Y4 RNA (hY4 RNA), was taken as a starting point from the RNA sequencing data, and reverse transcription quantitative PCR was performed on EVs and also on EV-conditioned endothelial cells in order to confirm the potential of this marker as an Apo-EV-specific molecule.

Finally, the findings from the techniques applied for phenotyping are critically discussed, highlighting the power of each method regarding the sensitivity and the potential use in a clinical setting.

4.2. Immunomagnetic bead-based EV capture and flow cytometry

Magnetic beads can be a powerful tool to isolate a targeted biological component of interest, while the magnetic properties of these particles enable purification of the material simply by using a magnet. Chemical modification of the bead surface with antibodies allows for high selectivity and makes this platform the method of choice for a number of applications (Ruffert, 2016).

As part of the process of identifying the most efficient capture probe for EVs, a variety of magnetic beads were coated with several antibodies against EV surface molecules. As some types of beads were coated in-house and using different chemistry platforms (Protein A-antibody affinity, or Streptavidin-Biotin interaction), the saturation of the beads' surface with each capture antibody was assessed by flow cytometry. In every case, a fluorescent secondary antibody against the capture antibody was added to the beads and the fluorescence readout from the flow cytometer was used to confirm the effective coating. The following figures (Figure 4-1 and Figure 4-2) show the coating validation results using a fluorescent secondary antibody against the coating antibody.
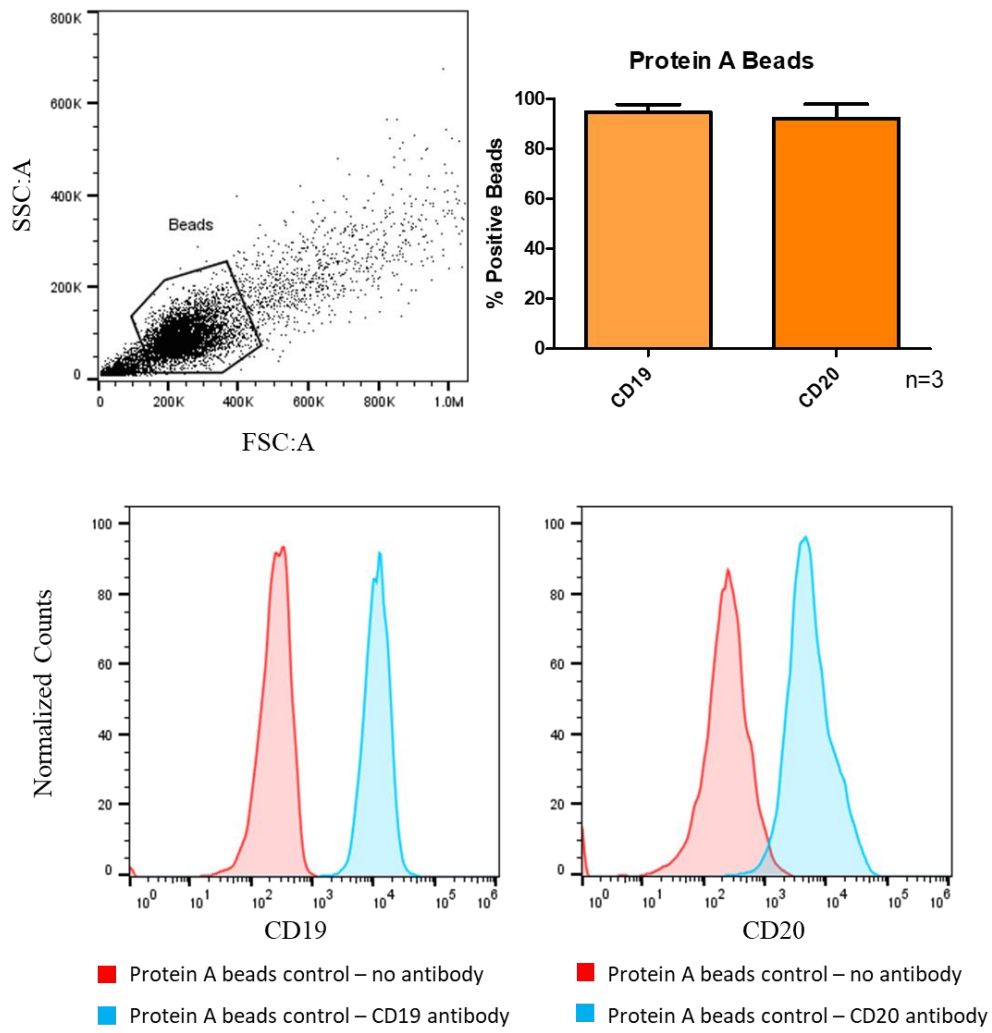
Figure 4-1. Validation of antibody coating efficiency on Protein A beads. Measurement was performed by flow cytometry for beads coated with antibody and stained with secondary antibody (error bars indicate standard deviation from n=3 independent experiments).
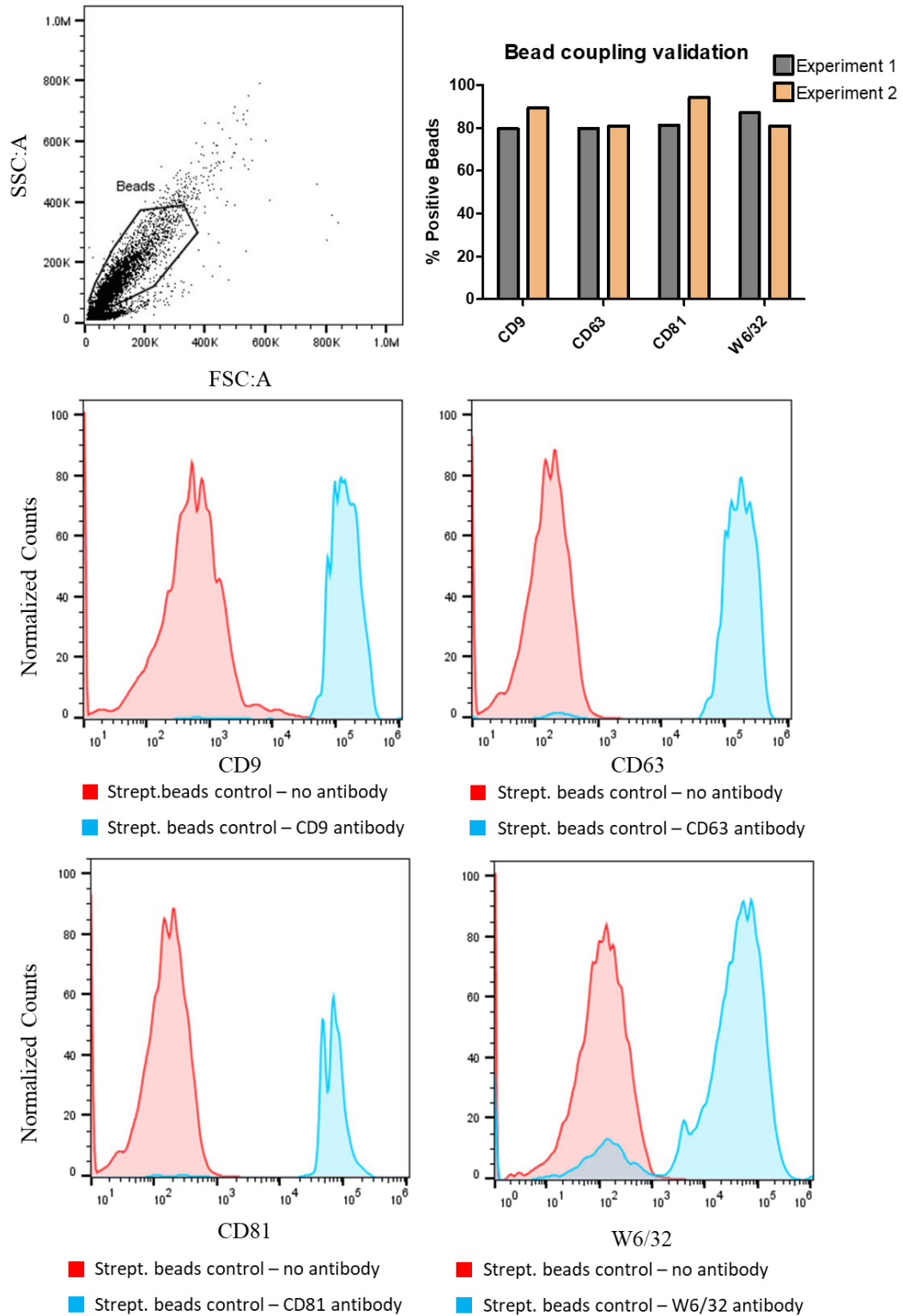
Figure 4-2. Validation of antibody coating efficiency for streptavidin magnetic beads from Exocap kit. Measurement performed by flow cytometry and staining with secondary antibody (bar chart shows the values from n=2 independent experiments).

Comparing the fluorescence intensity of the beads in the graphs above, it can be seen that the majority of the particles have been successfully coated with the capture probe, both the Protein A and Streptavidin beads from the Exocap commercial kit.

Besides the in-house coated beads against CD9, CD19, CD20, CD63, CD81 and MHC class I (W6/32 antibody), beads capturing PS and beads with surface -COOH groups which capture -NH$_2$ protein groups were used from commercially available sources (validation of protein binding capacity of -COOH beads is presented in supplementary Figure 4-22). Figure 4-3 shows the EV binding performance for every type of bead collectively, with large quantities of EVs and incubation of EV/beads at 4°C for 24h. The amount of EVs used to investigate the maximum binding capacity of the beads was the technically maximum possible quantity (due to limitations related to low EV concentration and EV:bead incubation volume).
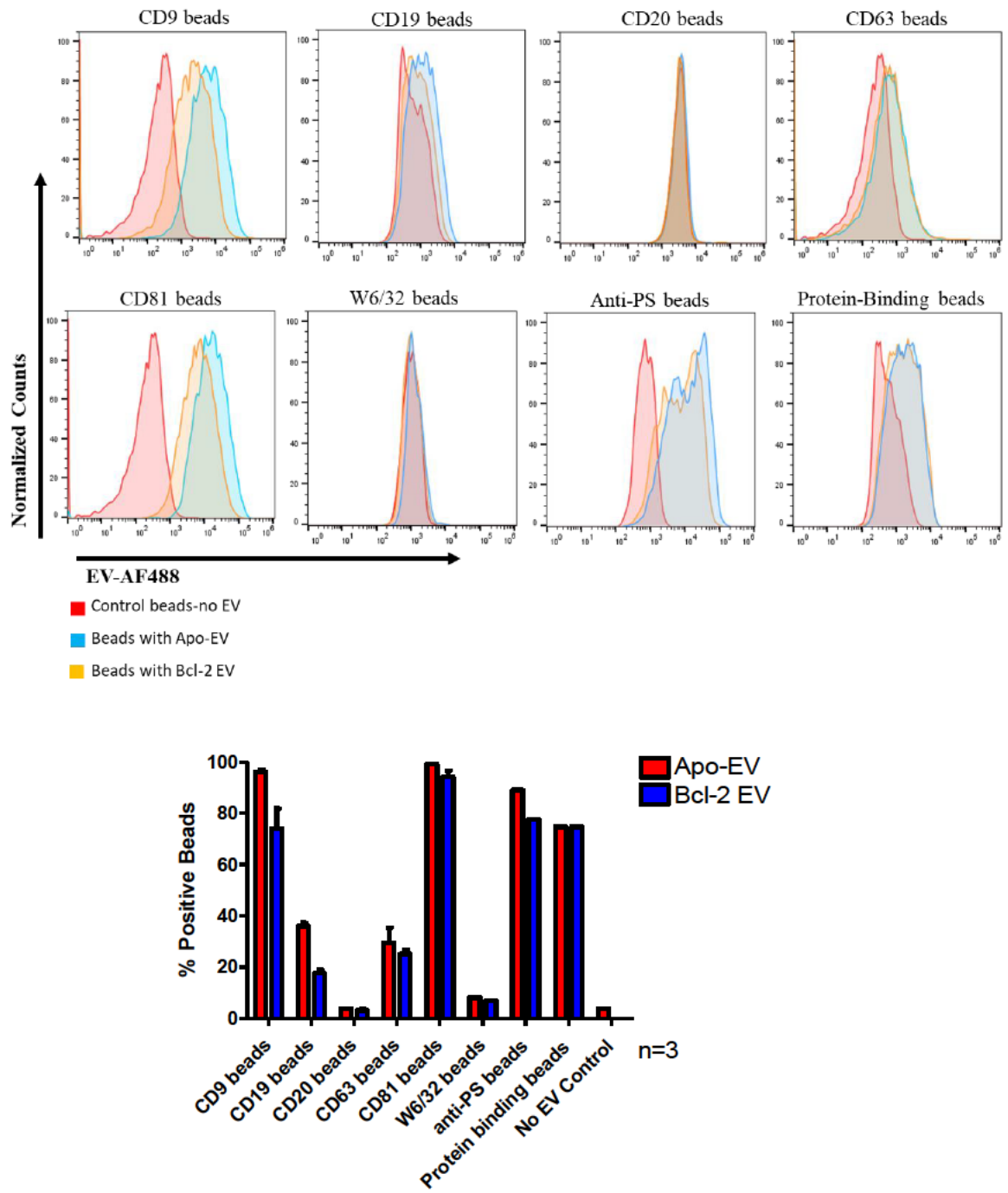
Figure 4-3. Maximum EV binding on magnetic beads coated with antibodies against EV surface molecules. Intensity histograms for all types of beads (top) and collective graphic representation of the results (bottom). The measurement of EV binding was performed by flow cytometry and EV staining with Annexin V-AlexaFluor 488 (error bars indicate standard deviation from n=3 independent experiments).

From the above results, it is interesting to find that antibodies against surface markers which are expected to be abundant on the EV surface, such as the CD19 and CD20 (B cell antigens),

the MHC class I (W6/32 antibody) and also the EV marker CD63 fail to capture the EVs effectively. On the other hand, the EV markers CD9 and CD81, as well as anti-PS and protein-binding -COOH beads are the most efficient capture probes for the EVs of this study.

Apart from the type of capture antibody which shows the most efficient EV binding, there are other parameters to be considered in order to establish the capturing protocol, whic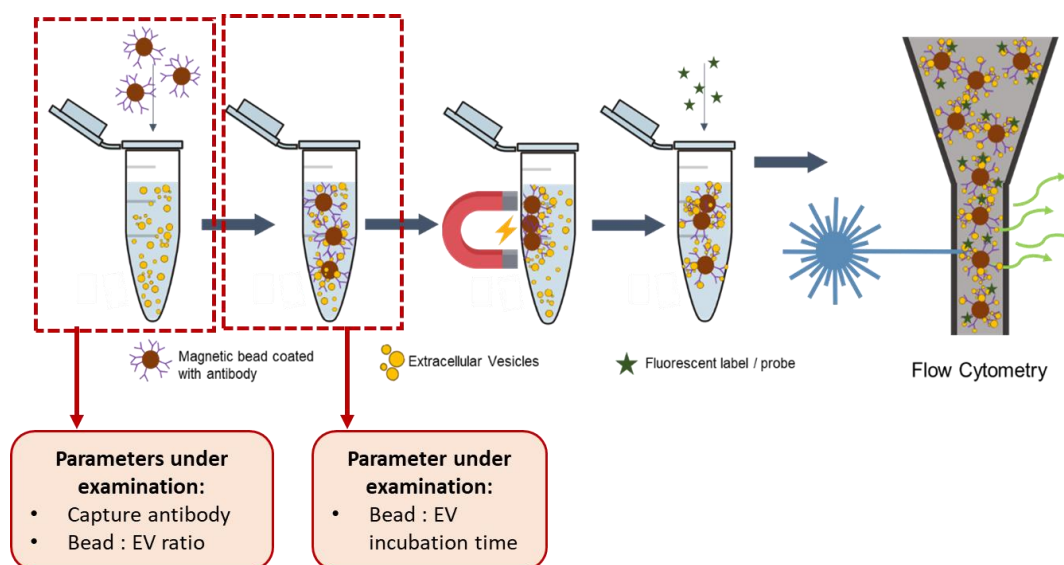h are schematically presented below in Figure 4-4. Strategy of EV-bead binding for flow cytometry analysis. The variable parameters under examination are the type of capture antibody, the ratio of beads:EVs and the time required for sufficient interaction between the beads and the vesicles.Figure 4-4 (EV: bead ratio and time required for incubation before washing). For the analyses to follow, the two most efficient bead types were selected in order to study the kinetics of the binding over time and also the range of bead:EV ratio which ensure maximum binding saturation. Figure 4-5 and Figure 4-6 include a summary of how EVs bind to anti-CD81 and anti-PS beads over a range of time and ratios.

Figure 4-4. Strategy of EV-bead binding for flow cytometry analysis. The variable parameters under examination are the type of capture antibody, the ratio of beads:EVs and the time required for sufficient interaction between the beads and the vesicles.
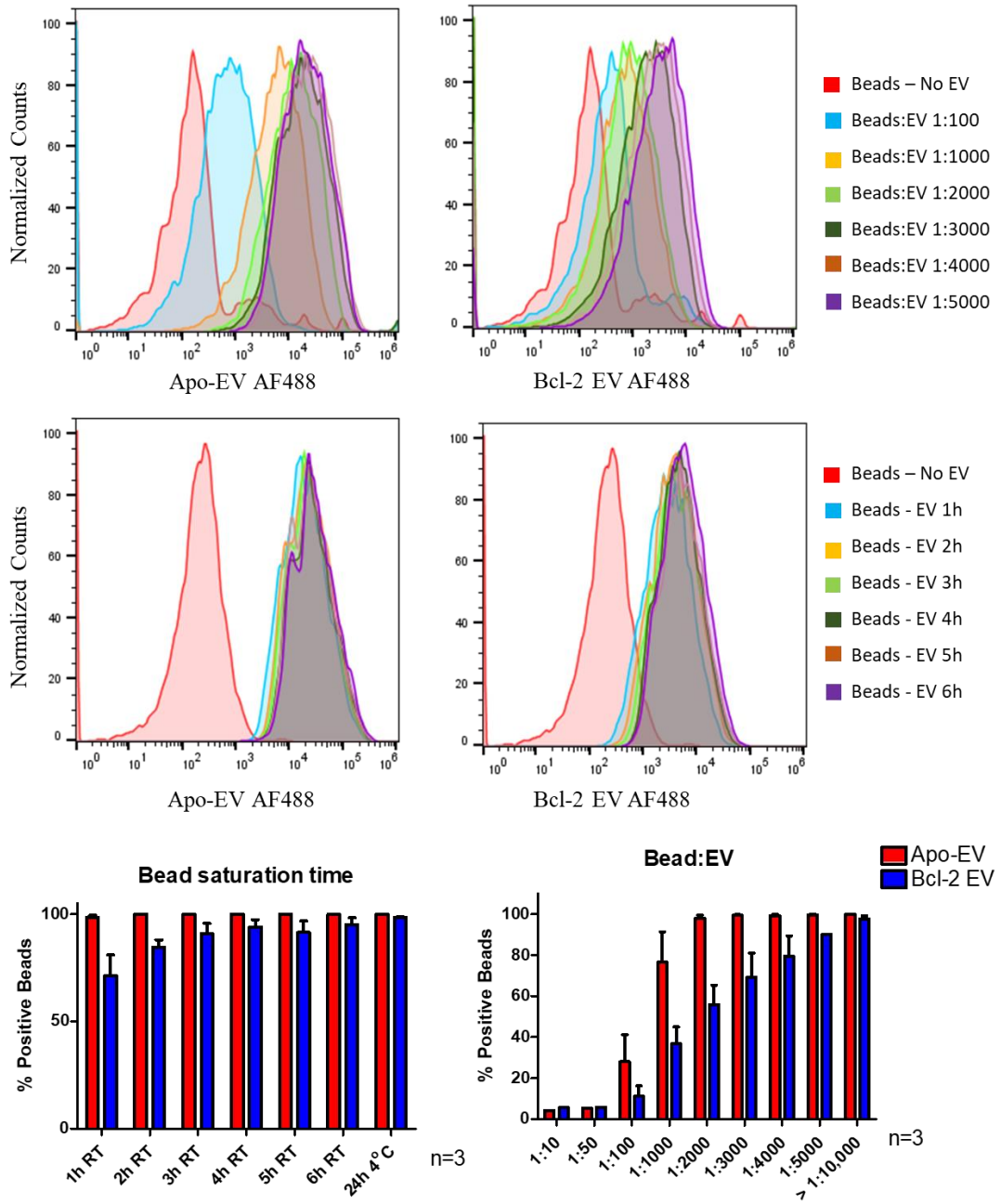
Figure 4-5. EV binding kinetics for anti-CD81 beads from Exocap kit. The EVs were added to the beads at a range of concentrations or for a range of time points for Bead:EV 1:5000. Measurement performed by flow cytometry with EV staining with Annexin V-AlexaFluor488 (error bars indicate standard deviation from n=3 independent experiments).
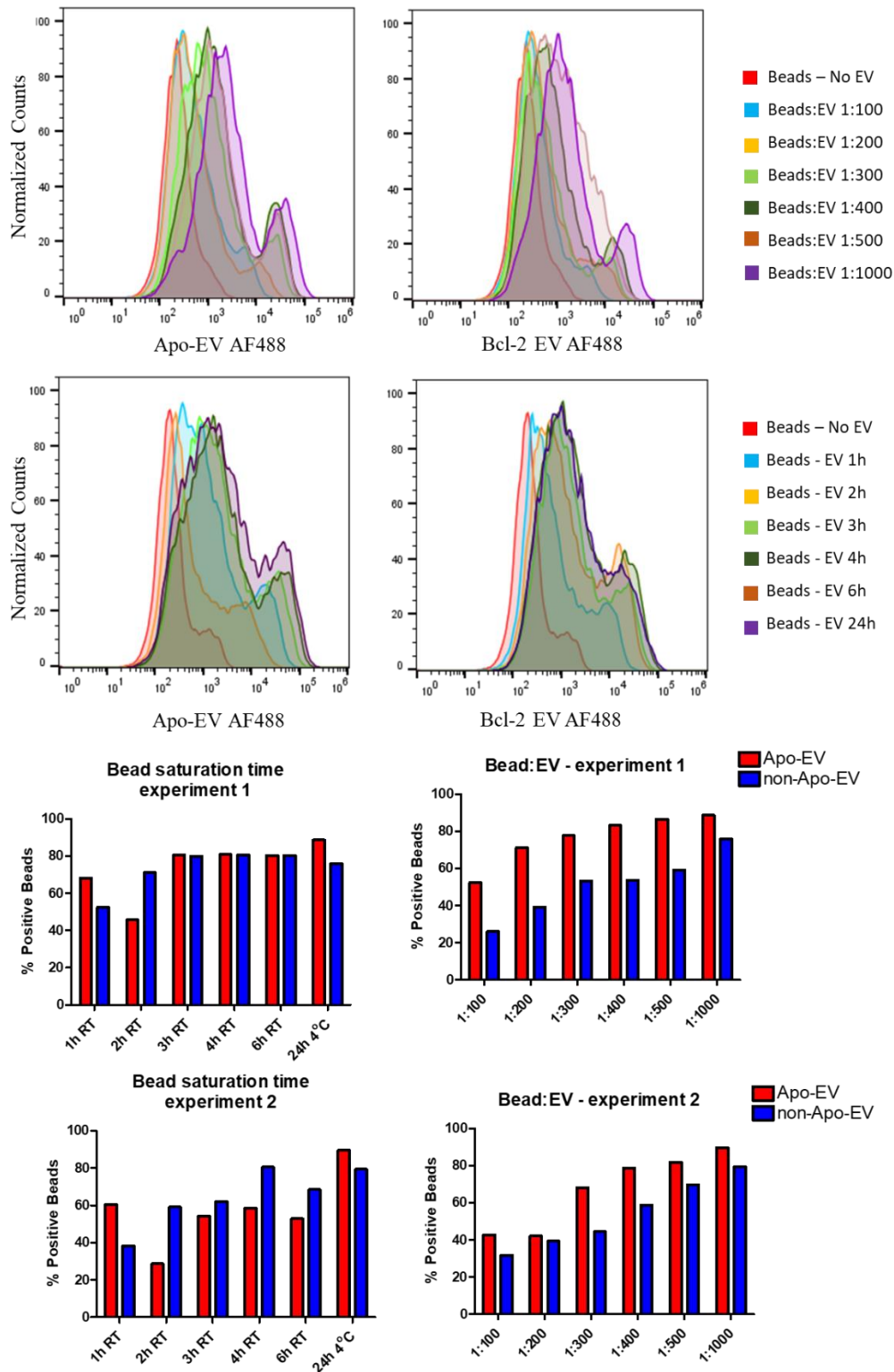
Figure 4-6. EV binding kinetics for anti-PS beads from MagCap kit. The EVs were added to the beads at a range of concentrations or for a range of time points for Bead:EV 1:1000. Measurement performed by flow cytometry with EV staining with Annexin V-AlexaFluor488 ((bar chart shows the values from n=2 independent experiments).

The kinetics of EV binding on anti-CD81 and anti-PS beads indicate that there is rapid interaction from the first hour of incubation which increases up to 3 hours and remains relatively stable for longer incubation times up to 24h. From these figures it is concluded that >3h incubation at room temperature provides sufficient binding for both types of beads. In addition, it is shown that anti-CD81 beads require a ratio of 5000 EV/bead, while the anti-PS bead can be sufficiently saturated with approximately 1000 EV/bead. This study was essential in order to ensure that the binding conditions used for the experiments to follow provide the desired binding. It is, however, important to mention here that an additional factor which might affect the EV binding efficiency is the volume in which the EV:bead interaction takes place. This means that in order for an EV to encounter a bead which can lead to a binding event, the volume of incubation can facilitate or hinder this interaction. It is logically expected that when a small volume of beads is diluted in a very large volume of dilute EVs, the binding might be less efficient. The volume factor has not been examined in detail in this work, as this would require the adjustment of the concentration of EVs (usually by increasing their concentration), which has been a technical challenge faced throughout this thesis. However, empirical ratios of volumes have been used, avoiding extremely small or large volumes of both components.

In order to visualize the EVs bound on beads and understand whether this is a 1:1 binding, anti-PS beads were saturated with EVs and were imaged by TEM (Figure 4-7).
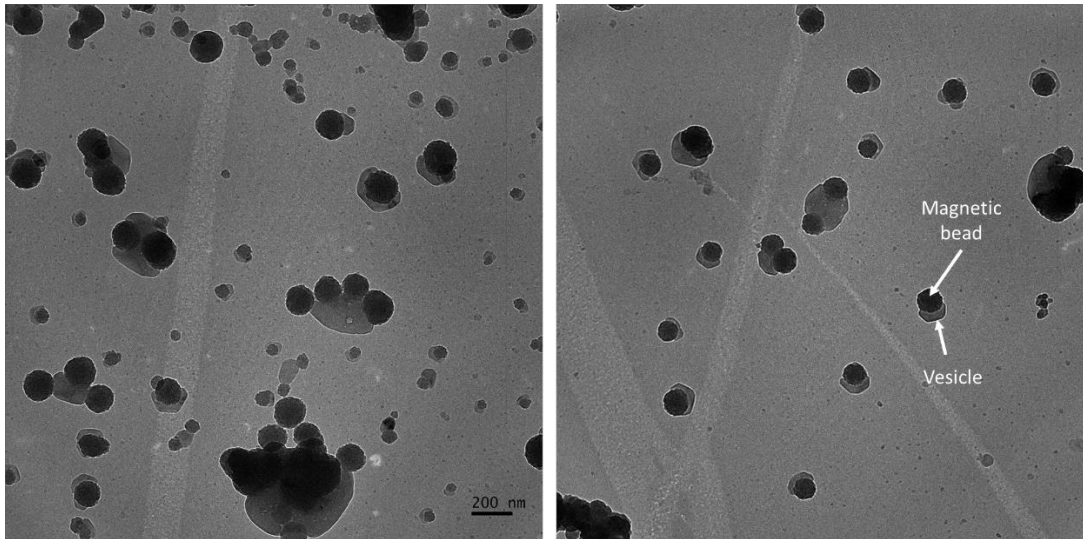
Figure 4-7. TEM images of EV bound on anti-PS magnetic beads from MagCap kit (mean bead diameter ~200nm). A representative bead and a bound EV are indicated by arrows. A variety of EV and bead sizes are shown, with larger and smaller EVs binding to larger or smaller beads respectively.

It is shown that the beads have a broad size distribution [in contrast to the manufacturer's product specifications (200nm monodisperse bead suspension)] and that the interaction with the surface of EVs is strong, indicated by the fact that EVs are not bound on a bead by a single-point interaction, but there is a rather extended surface of EV membrane coming in contact with the bead. An interesting observation is that the majority of EVs are bound on a bead on one side and some larger EVs attract multiple beads which seem to be binding on one domain of the membrane, indicating potential spatial selectivity in PS exposure. If PS would be exposed homogeneously on the surface of the membrane, then EVs would have multiple beads binding all around their perimeter, which is not seen here. Another EV characteristic highlighted by these images is the large size heterogeneity of EVs, however showing that binding on the anti-PS beads is independent of size, as both large and small EVs are attracted to one or more beads. At this point it is important to stress that in the above images, only the bead-bound EVs are present on the TEM grid, as the non-bound EVs had been washed off in the previous processing steps. This is a reminder that it is possible that there are EVs which are not expressing PS, but have been excluded from this imaging due to the preparation procedures.

The above imaging was performed on TEM, as the bead size was suitable for this type of microscopy, however, other beads such as the anti-CD81 or anti-CD19 have a larger diameter and therefore the EV binding has been visualized by fluorescence microscopy (Figure 4-8).
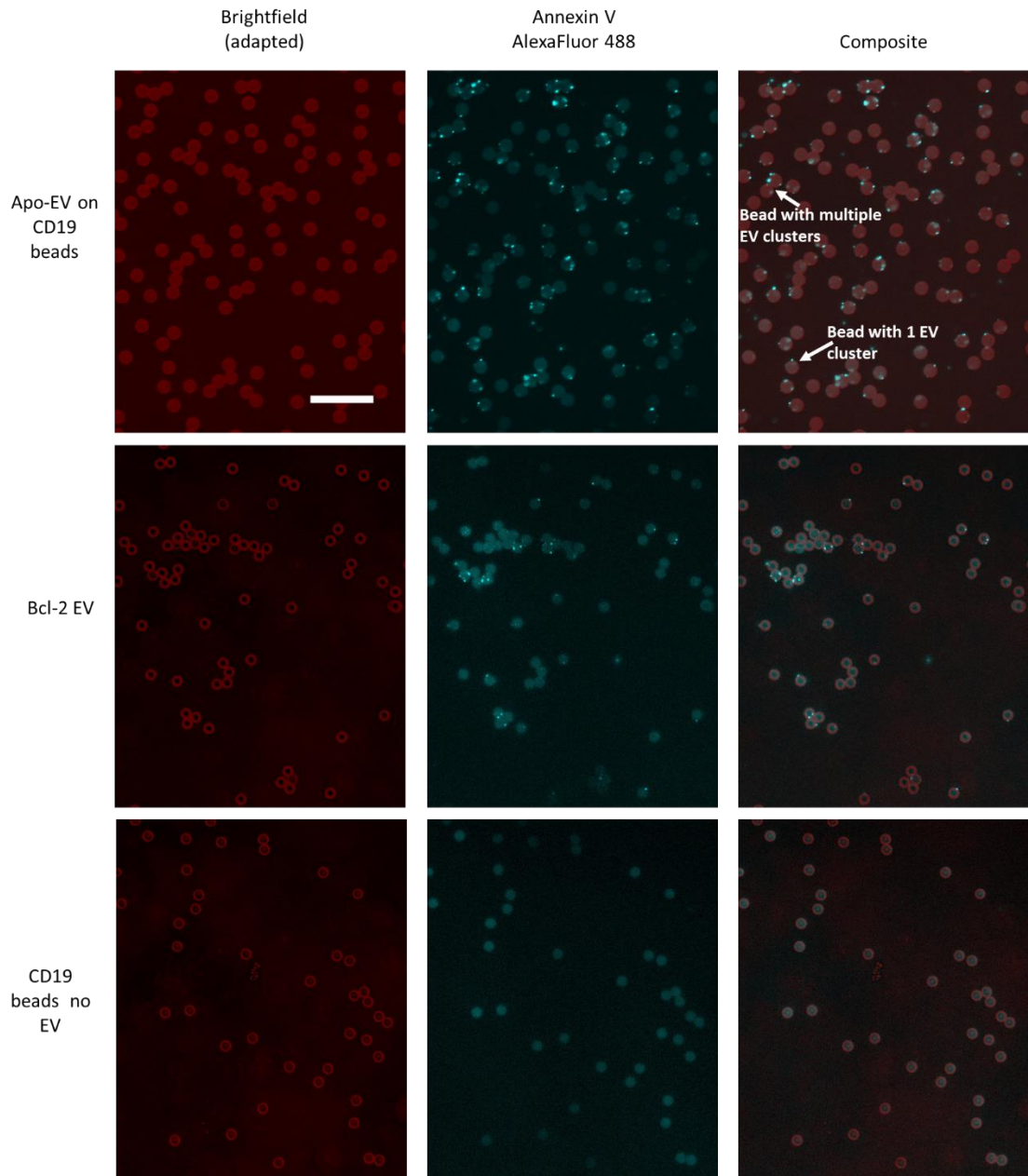

Figure 4-8. Fluorescence microscopy images of EVs bound on and-CD19 magnetic beads. EVs are stained with Annexin V-AlexaFluor488 (bead diameter 4.5μm, scale bar 20 μm). Arrows indicate beads with multiple EVs or with only one EV or EV cluster.

The EVs bound on the anti-CD19 beads appear as small fluorescent dots on the surface of the beads and because of the large bead diameter, there can be more than one vesicle bound on each bead, as well as there are complexes of EVs and beads which indicate that one vesicle (or vesicle cluster) can attract several beads on different sides of the membrane. As this type of microscopy imaging cannot give a resolution suitable for the visualisation of individual small vesicles, the EVs observed in these micrographs can be either single larger EVs or aggregates of smaller particles.

After selecting the most effective capture molecule (CD81) and having established the binding conditions, flow cytometry was performed on the Apo-EVs in order to investigate the levels of expression for a range of surface markers and also intravesicular markers upon EV permeabilization (Figure 4-9). The markers investigated in this experiment are either abundant EV molecules or have been associated with apoptosis, and have been selected for reasons described in more detail later in this chapter, in the discussion.
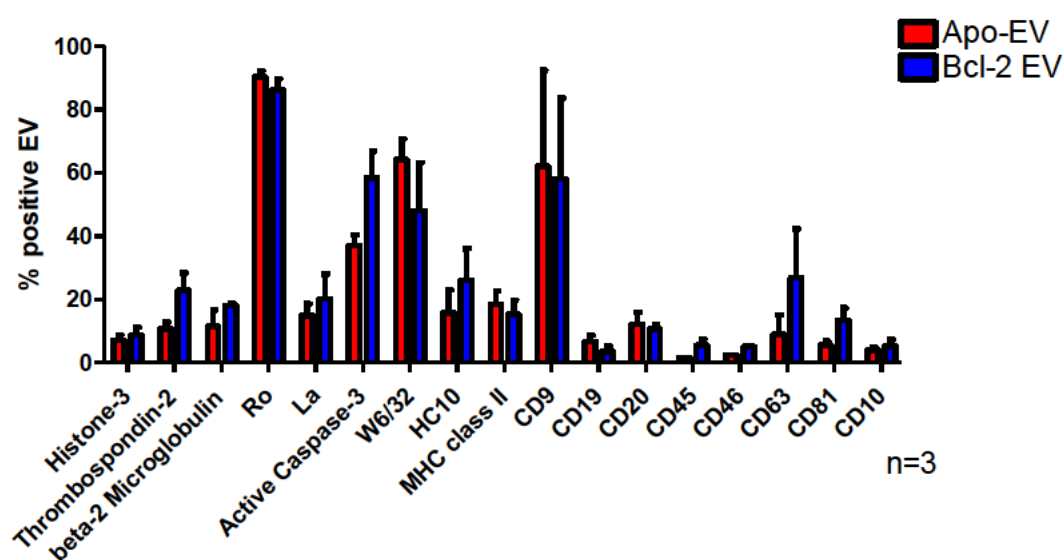

Figure 4-9. EV phenotyping for protein markers. Analysis performed by flow cytometry on EVs bound on anti-CD81 magnetic beads. For the measurement of histone-3, thrombospondin-2, beta-2 microglobulin and active caspase-3, the EVs were fixed and permeabilized while bound on beads prior to staining. All EVs were stained with Annexin V-Pacific Blue in order to gate the EV positive beads and exclude the beads without EVs. All antibody levels were measured by the use of isotype controls (for histone-3, active caspase-3, MHC class II, CD19, CD20, CD45, CD46, CD10) or secondary antibody controls (for thrombospondin-2, beta-2 microglobulin, Ro, La, W6/32, HC10, CD9, CD63 and CD81). The error bars correspond to standard deviation values from the measurements of 3 different EV preparations.

The findings of this phenotypic study are in general suggesting that there are no significant differences in the levels of expression of proteins in Apo-EVs compared to the control vesicles. In more detail, the highest expression (over 40%) is marked for the proteins Ro, active caspase-3, MHC class I (clone W6/32) and CD9. Lower levels are observed for the rest of the markers studied.

Interestingly, comparing the protein levels found for CD81 bead-bound EVs in Figure 4-9 with the efficiency of EV binding for beads in Figure 4-3, there are contradictory results for W6/32 and CD81, as in the first case the W6/32 is detected on the EV surface but fails to capture the EVs, and in the second case the CD81 is the best capture probe but is not detected in high levels by flow cytometry. These differences can be attributed to poor antibody-antigen affinity which does not permit effective capturing, or in the case of CD81, a potential explanation involves the spatial arrangement of the CD81 antigen in such a way that all molecules are grouped together at the binding site of the anti-CD81 bead, therefore there are no available molecules for a second anti-CD81 antibody used for phenotypic measurement. In addition, for some markers it is observed that the Bcl-2 EV have higher levels of expression, as for example in active caspase-3 and CD63. While the levels of CD63 have not been validated by other methods, for active caspase-3 the flow cytometry results contradict other methods (see microscopy below), which poses the question of reliability of this method on smaller EVs.

4.3. Fluorescence microscopy on EV

Another phenotyping method for EVs is labelling with a fluorescent antibody and performing direct imaging on a confocal microscope. As discussed in the Introduction, it is acknowledged that the resolution for this type of microscopy is physically limited to approximately 250nm, therefore the smaller EVs are not possible to be visualized as individual particles. However, the larger EVs and/or clusters of particles are can be imaged. Since EVs are not detectable by brightfield illumination, the imaging has been performed by staining the EVs with a general protein stain (AF568), to ensure the total population is 'lit up', followed by the addition of a primary fluorescent antibody. The following images show representative examples of imaging for a ubiquitous marker, PS, and for CD10 which is expressed to small percentages, for comparison. Images for other markers are presented in the Appendix of this chapter.
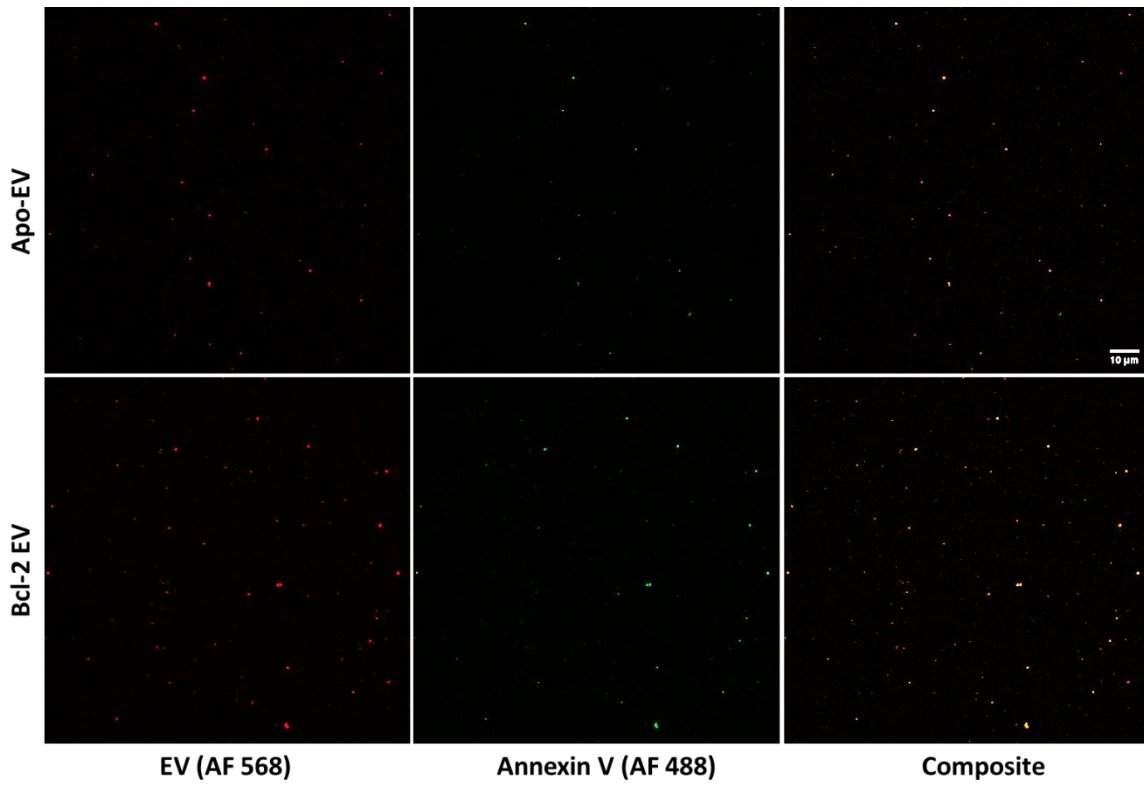
Figure 4-10. Confocal microscopy for EVs stained with Annexin V-AlexaFluor488. Images acquired on Leica SP8 system, 63x magnification.The total population of EVs is pre-stained with a protein dye, AF568.
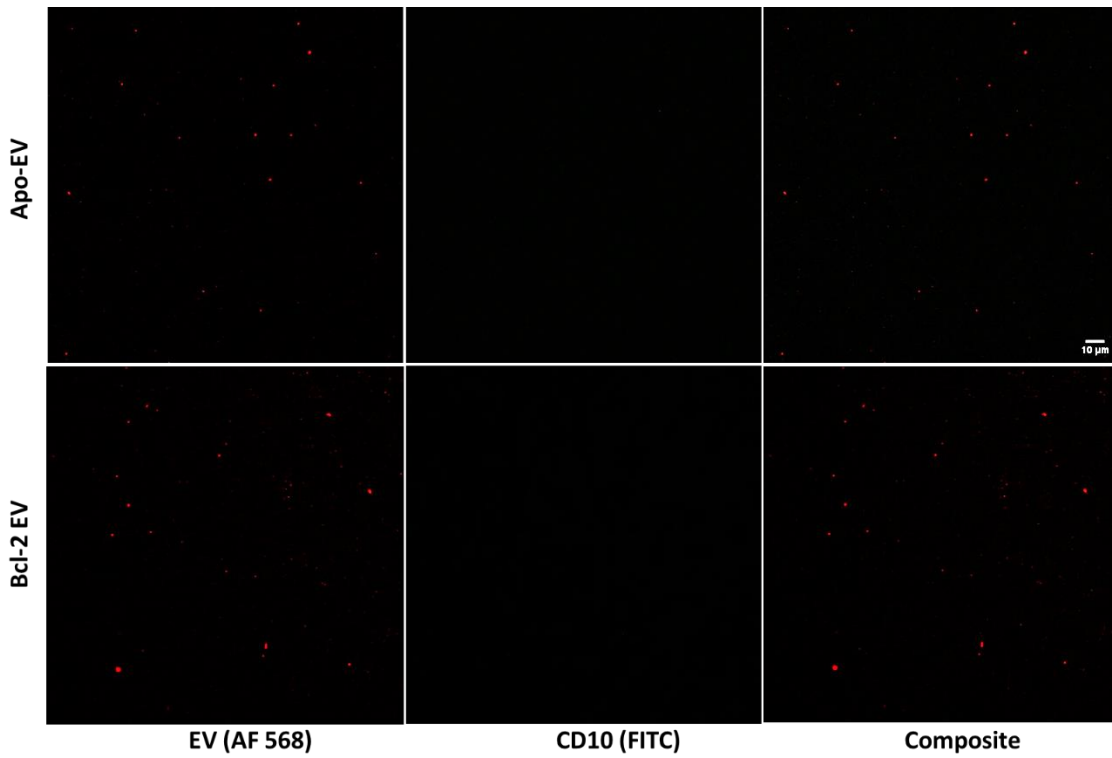
Figure 4-11.Confocal microscopy for EVs stained with CD10-FITC. Images acquired on Leica SP8 system, 63x magnification. The total population of EVs is pre-stained with a protein dye, AF568.

The following image (Figure 4-12) shows the staining for active caspase-3 in more detail, as this marker exhibited significantly higher expression on Apo-EVs compared to Bcl-2 EVs. The results on active caspase-3 contradict the flow cytometry figures which suggest that the levels of expression for Apo-EVs are lower than the control vesicles, however, as discussed at the end of this chapter, fluorescence microscopy is considered more reliable, as these observations have been cross-examined with other methods, as well.

Figure 4-11.Confocal microscopy for EVs stained with CD10-FITC. Images acquired on Leica SP8 system, 63x magnification. The total population of EVs is pre-stained with a protein dye, AF568.
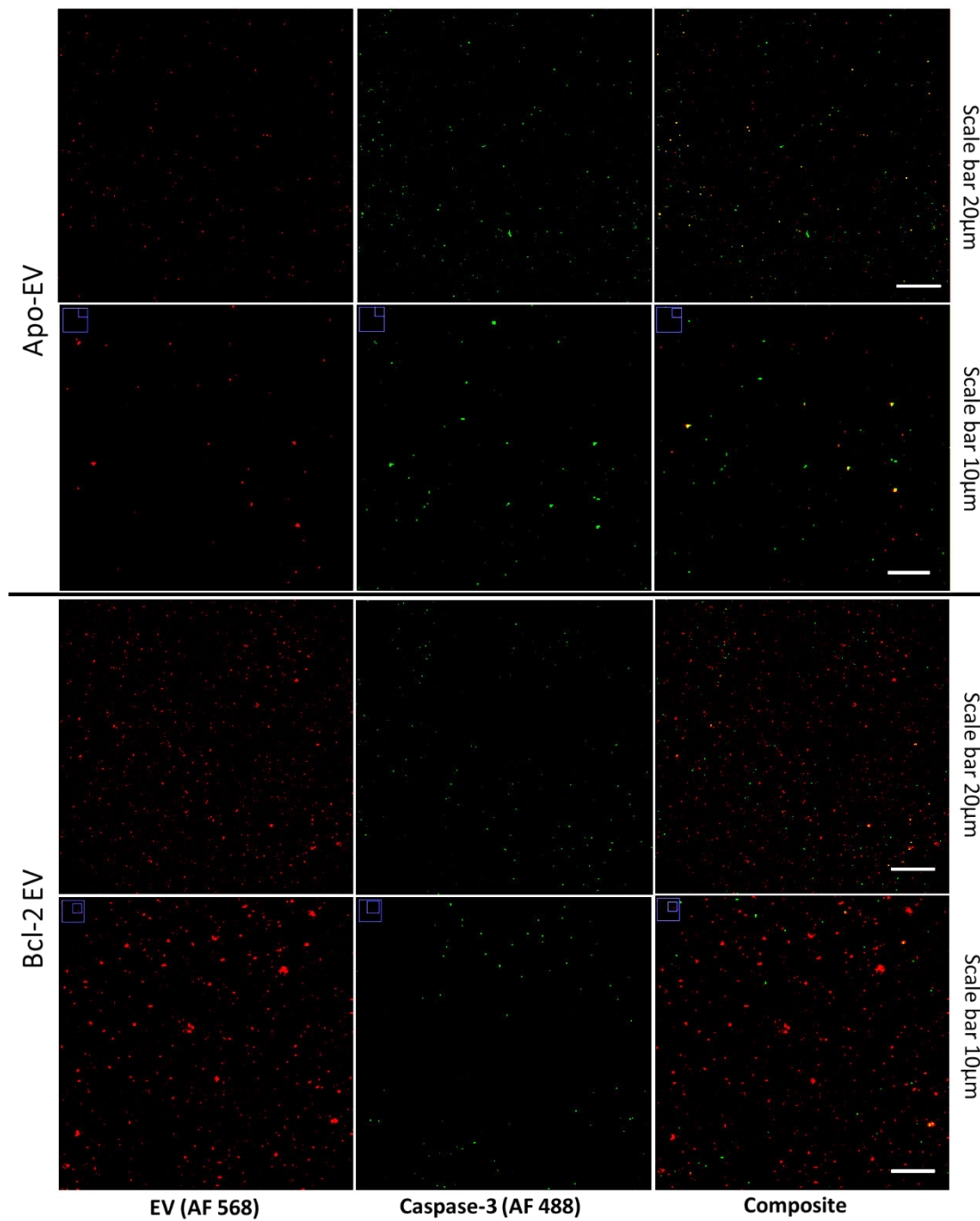
Figure 4-12. Confocal microscopy for EVs stained with active caspase-3 – AlexaFluor 488. The total population of EVs is pre-stained with a protein dye, AF568. Images without and with zoom (top and bottom row of each EV type respectively) are shown for better presentation of the labelling. Images acquired on Leica SP8 system, 63x magnification.

Quantitative analysis on the confocal microscopy images for all molecules studied is presented in Figure 4-13.
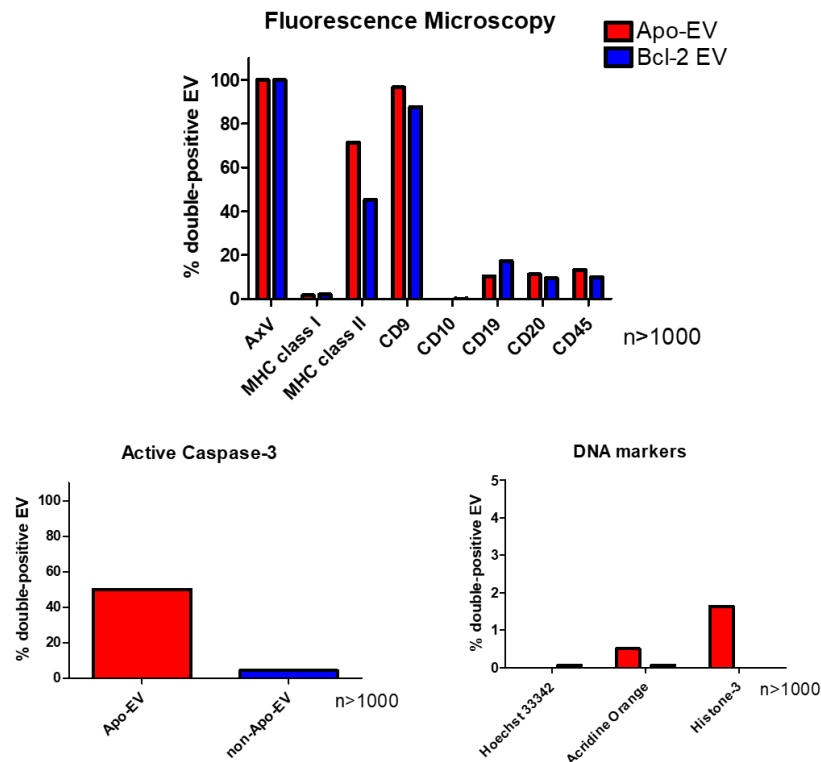
Figure 4-13. Expression levels of selected EV markers as measured by fluorescence microscopy. The values represent the % positive EVs double positive for both fluorophores in absolute counts from the analysis of multiple images deriving from n=2 EV preparations.

Two markers which appear exclusively on Apo-EVs are the active caspase-3 and the histone-3 which indicates the presence of DNA. For the rest of the markers expected to be generally expressed on EVs, no significant differences in the levels are observed.

4.4. EV surface markers studied by Immunogold on TEM

A method of phenotyping, alternative to fluorescent imaging, is the labelling of EVs with antibodies conjugated with gold nanoparticles followed by TEM imaging. Besides super resolution microscopy, this is perhaps the only method which allows single vesicle imaging and studying of the spatial arrangement of the target molecules on the membrane surface. However, it needs to be acknowledged that the spherical 3D morphology of EVs cannot be maintained intact by dry TEM (in contrast to cryoEM where the vesicles are frozen in their natural shape). In this measurement, the EVs have been attached on TEM grids and have

been labelled with in-house conjugated immunogold complexes against several surface markers and some of the most representative examples are shown in the following figures (Figure 4-14 and Figure 4-15).
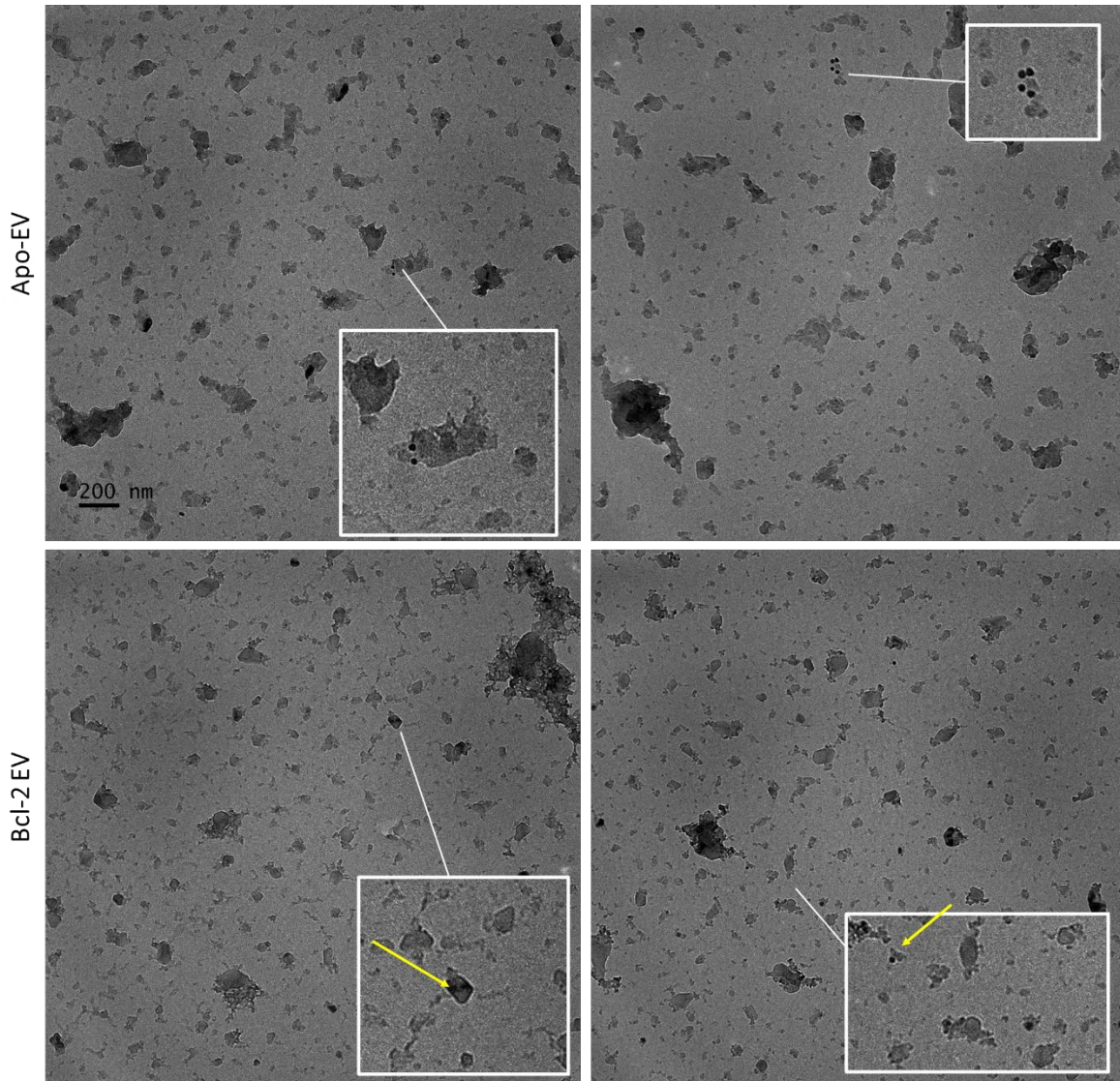

Figure 4-14. Immunogold TEM imaging of EVs labelled with 15nm anti-CD19 immunocomplex.
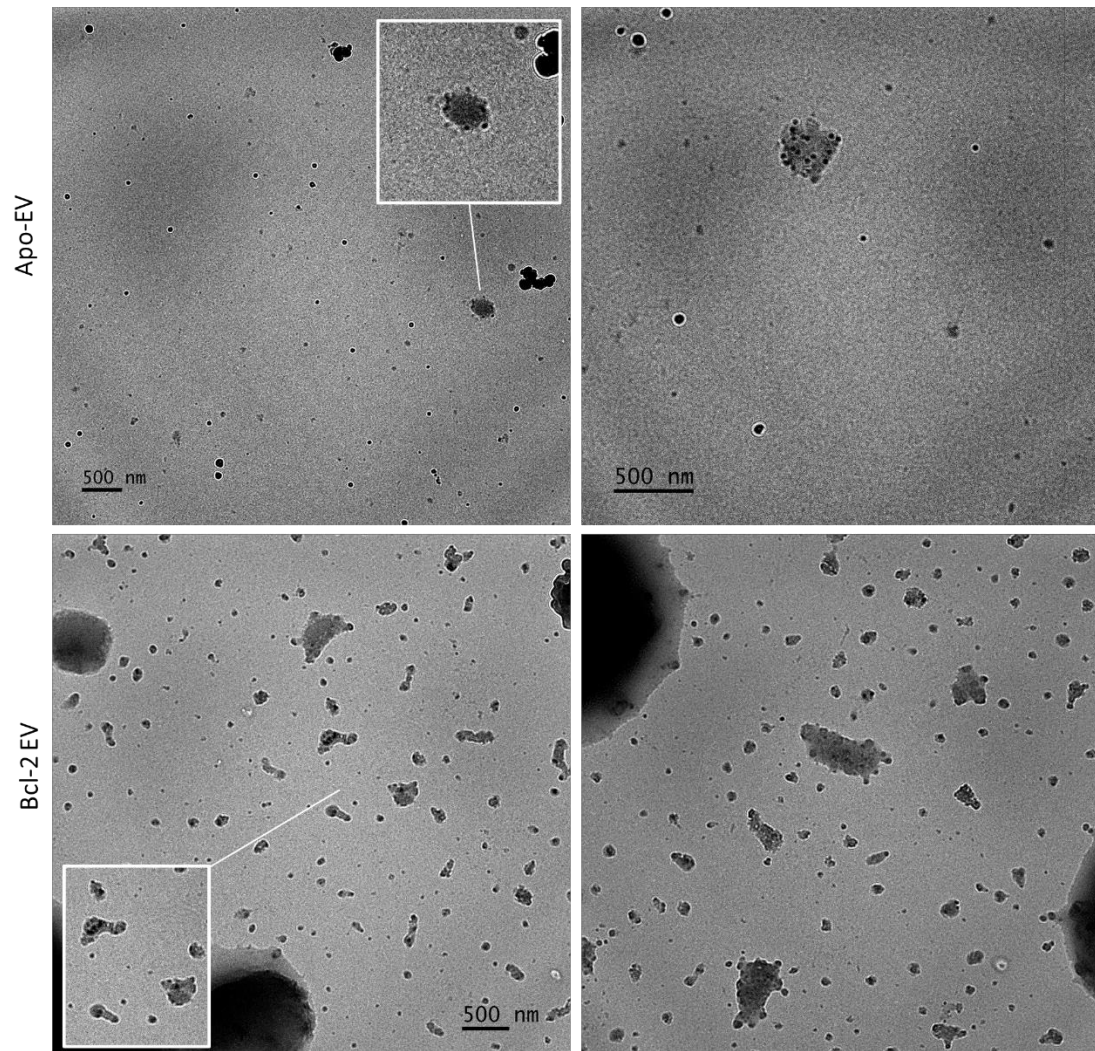
Figure 4-15. Immunogold TEM imaging of EVs labelled with 15nm anti-Ro immunocomplex.

The figures show indicative results for EV labelling with a marker with low and high expression (CD19 and Ro respectively), and more images of all markers can be found in the Appendix of this chapter. The next graph shows the quantification of TEM immunogold imaging for all markers. The quantification has been performed using the following exclusion criteria for the particles appearing in the images: as determined by cryoEM in Chapter 3, the minimum vesicle diameter has been found at 25nm, therefore all particles smaller than 25nm in the immunogold images have been excluded from the analysis.
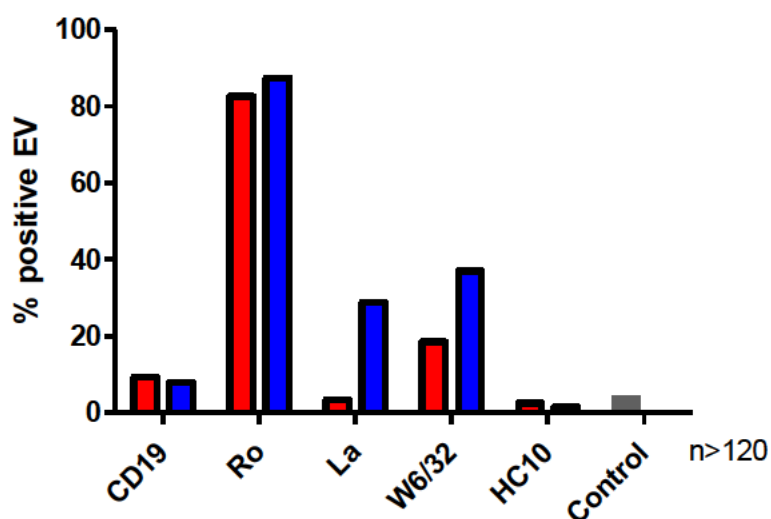
Figure 4-16. Expression levels of EV surface molecules as analysed by immunogold TEM imaging (left). The values represent the % positive EVs in absolute counts from the analysis of multiple images of n=1 EV preparation.

The values have been extracted from the count of individual vesicles applying the exclusion criteria described earlier using more than 120 particles for each marker. At this point, it is important to highlight the throughput capacity of this technique, which in comparison to other methods such as flow cytometry, the acquisition of a very large number of images is technically challenging, therefore limits the maximum possible n number. The above graph shows an overall trend of expression similar to the values presented earlier by flow cytometry, with the difference that the MHC class I antibodies W6/32 and HC10 seem to be better detected by flow cytometry rather than immunogold. There are no differences between the levels of expression in Apo-EVs and Bcl-2 EVs for any of the markers studied above, although Ro and La would be expected to appear in higher percentages in the Apo-EVs due to their correlation with apoptosis (see later in this chapter).

Regarding the spatial arrangement of the surface receptors on the vesicle membrane which can be visualized by TEM, it was overall observed that some EVs can have different numbers of surface molecules/receptors, ranging from zero, one or multiple, also depending on the available surface and the diameter of each particle. There was no strong evidence of clustering of markers on one side of the membrane, but in case of high expression molecules such as the Ro protein, the immunogold is distributed evenly on the surface.

4.5. Quantitative Reverse Transcription PCR for Apo-EV specific hY4 RNA detection

Small RNA species are often abundant in EVs and as mentioned in the introductory chapter, they are often selectively expressed in certain conditions, serving as highly reliable disease markers. In an effort to identify RNA-based characteristics of the Apo-EVs, RNA sequencing was performed on EVs and EV-producing BL2 cells upon UV irradiation and apoptosis triggering. This study was performed by Dr Margaret Paterson in our laboratory in collaboration with Dr Amy Buck at Ashworth laboratories, University of Edinburgh. For the purposes of this study, the following samples were prepared for RNA sequencing: BL2 and BL2-bcl-2 cells isolated 5h after UV irradiation (therefore the BL2 cells were apoptotic), Apo-EVs and Bcl-2 EVs purified from *in vitro* preparations, and finally HUVEC (human umbilical vein endothelial cells) cells after an 18h treatment with or without the two types of EVs. The HUVEC study was performed in order to examine the angiogenic effects of Apo-EVs, which concerns a different project of our laboratory. The isolated RNA from the above samples was sequenced and analyzed by Dr Amy Buck, and an initial screening of miRNAs indicated increased levels of human Y RNA for the Apo-EVs. Some more specific bioinformatics analysis was performed on all species of hY RNA (see next figure), comparing two samples at a time, for example BL2 cells versus BL2-bcl-2 cells, or Apo-EVs versus Bcl-2 EVs etc.

The most significant outcome of this analysis was the identification of a small non-coding RNA, the RNA-Y4 or hY4 RNA which is upregulated in Apo-EVs when these are compared with Bcl-2 EVs, however the apoptotic versus the non-apoptotic cells do not seem to follow the same trend. hY4 RNA is one of the four hY RNAs which were first discovered by their association with the autoimmune disease lupus erythematosus (Lerner *et al.*, 1981). The hY RNAs are parts of the Ro protein complex and have physiologically been linked with the initiation of DNA chromosomal replication (Christov *et al.*, 2006), while in disease they have been associated with apoptosis (Rutjes *et al.*, 1999; Hizir *et al.*, 2017) and tumour (Christov, Trivier and Krude, 2008), among others.

Figure 4-17 presents a summary of the RNA sequencing results which shows that hY4 RNA is overexpressed in Apo-EVs (please note the scale numbers).
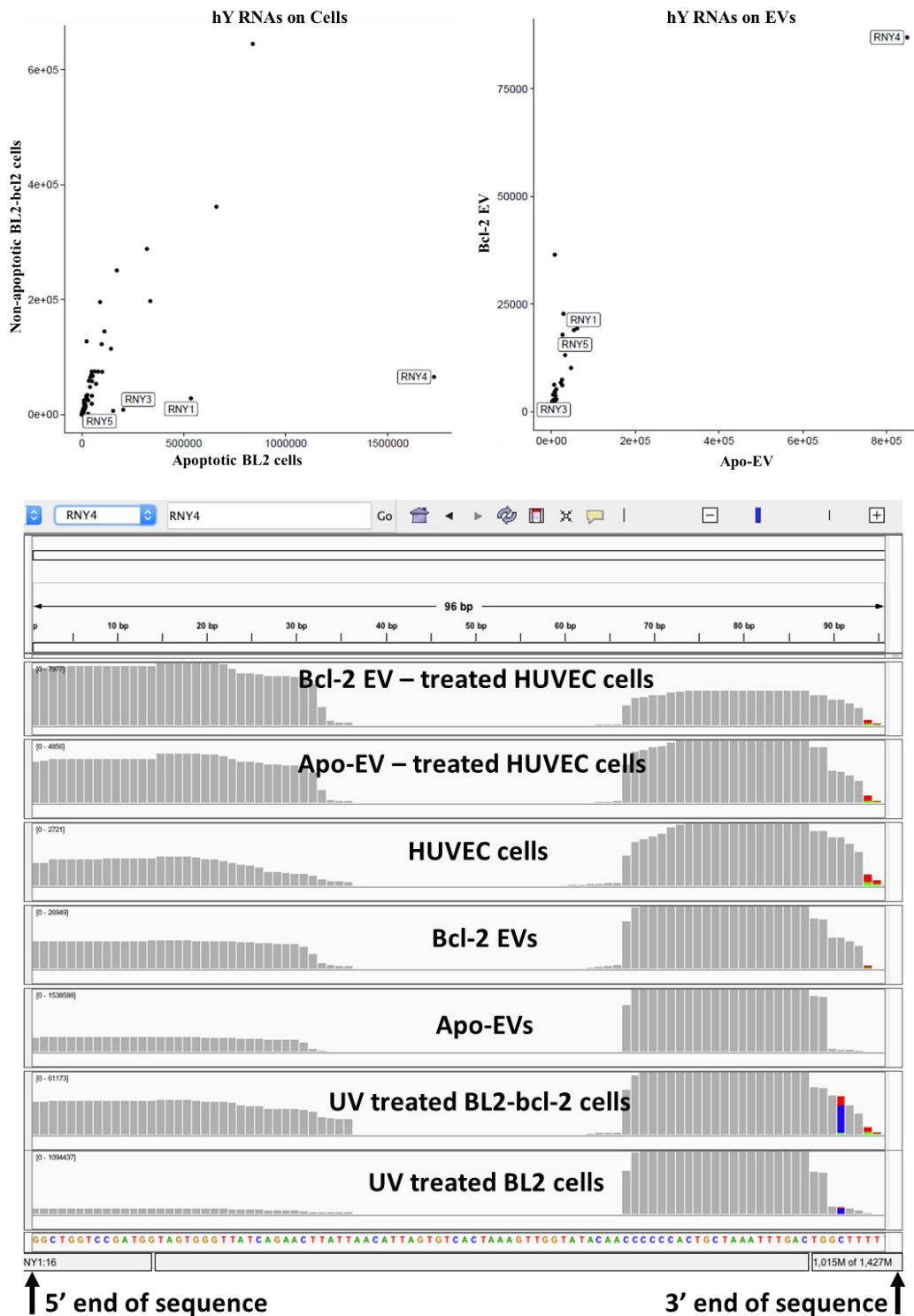

Figure 4-17. RNA sequencing data indicating RNA-Y4 levels for cells and EVs upon stimulation of apoptosis (top row) and hY4 RNA sequence counts in all samples (bottom graph). Data provided by Amy Buck, Ashworth laboratories, University of Edinburgh (the scales are not the same for all axes; therefore for the cells graph, hY4

RNA is more than 15fold higher in apoptotic cells, while in EVs, hY4 RNA is expressed 100 times more in the Apo-EVs!). The bottom image shows the hY4 RNA sequence in the bottom line (the 5' and 3' ends of the 96 nucleotide sequence are highlighted by arrows) and the number of 'hits' of the two ends of the sequence on all individual samples.

In order to confirm the above results *in vitro*, traverse transcription quantitative PCR (RT qPCR) was performed, targeting hY4 RNA. The total sequence of the molecule consists of 96 nucleotides:

5'-

GGCTG**GTCCGATGGTAGTGGGTTAT**CAGAACTTATTAACATTAGTGTCACTAAAGTTGGTATACAA CCCCCCACTGCTAAATTTGACTGGCTTTTT-3'

The two ends of this sequence were shown to match the majority of reads in the RNA sequencing data (results shown above) and were therefore examined for the potential selection of primers. The primer sequence was extracted from the underlined part of the sequence shown above and therefore the forward primer was:

Forward primer: 5' -GTCCGATGGTAGTGGGTTAT- 3'

The following paragraphs describe the various parameters which the qPCR measurement of the RNA levels is dependent on and need to be optimized as a preparation before the experiment.

Selection of normalization genes

For the performance of RT qPCR, some normalization controls are required for the reaction. The normalization genes are usually housekeeping genes of the biological system, the expression of which remains stable under the conditions of the experiment. The expression levels of these genes are used in the data analysis procedure for setting the baseline for the relative measurement of expression of the genes of interest. It is therefore crucial to select housekeeping genes for which the expression has been shown stable for Apo-EVs and Bcl-2 EVs. A helpful tool for this decision is the data obtained by RNA sequencing of the EVs, performed and analysed by Amy Buck and lab group, Ashworth laboratories, University of Edinburgh (unpublished data). From this analysis, the miRNAs and the -fold change between the EV populations were listed, and the miRNA-21 was identified as a species with 0.0074-fold change of expression between the Apo- and the Bcl-2 EVs. An additional gene, the RNA-

U6 was selected based on literature referenced (Choong, Yang and McNiece, 2007; Corney *et al.*, 2007).

Efficiency slopes

According to the minimum information for publication of qPCR data (Bustin *et al.*, 2009), the efficiency of the reaction is required to be determined for each gene used in the experiment, using dilutions of template cDNA. The efficiency is determined by the slope of the linear fitting of the data points and the results are shown in Figure 4-18.
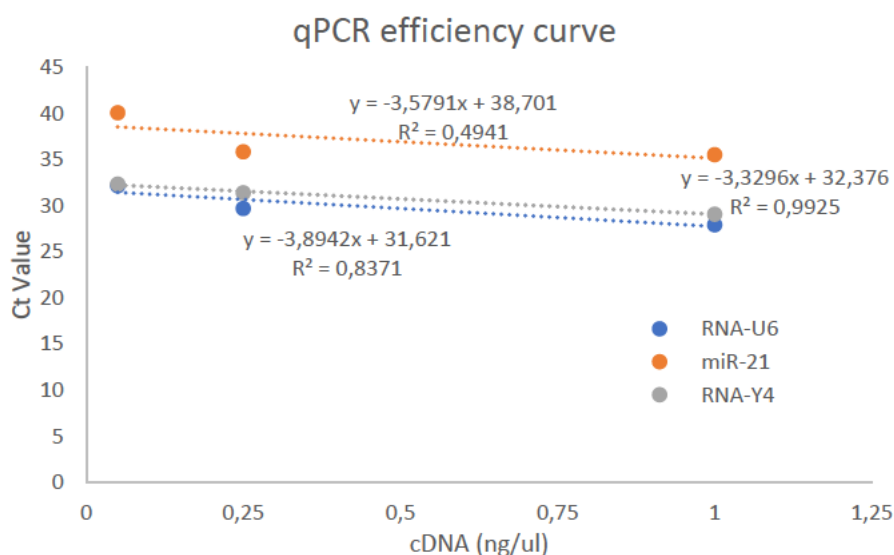
Primer	Slope, a (y=ax+b)	Efficiency =10^(-1/slope)-1 (Bustin *et al.*, 2009)
RNA-Y4	-3.33	99.6 %
RNA-U6	-3.89	80.6 %
miRNA-21	-3.58	90.2 %

Figure 4-18. qPCR efficiency curves for all primers and efficiency calculation.

The primers amplifying the hY4 RNA and miRNA-21 are efficient in the acceptable range (90-110%), however the RNA-U6 shows lower efficiency. Another point of qualitative control of the qPCR performance is the behavior of the primers in increasing temperature, as some sequences can fold and form primer-dimers, reducing the quality of the reaction. Figure 4-19 represents the primer melting curves and shows that there is one main peak for every primer, indicative of only one primer configuration (in case of dimer formation, a second peak would appear).
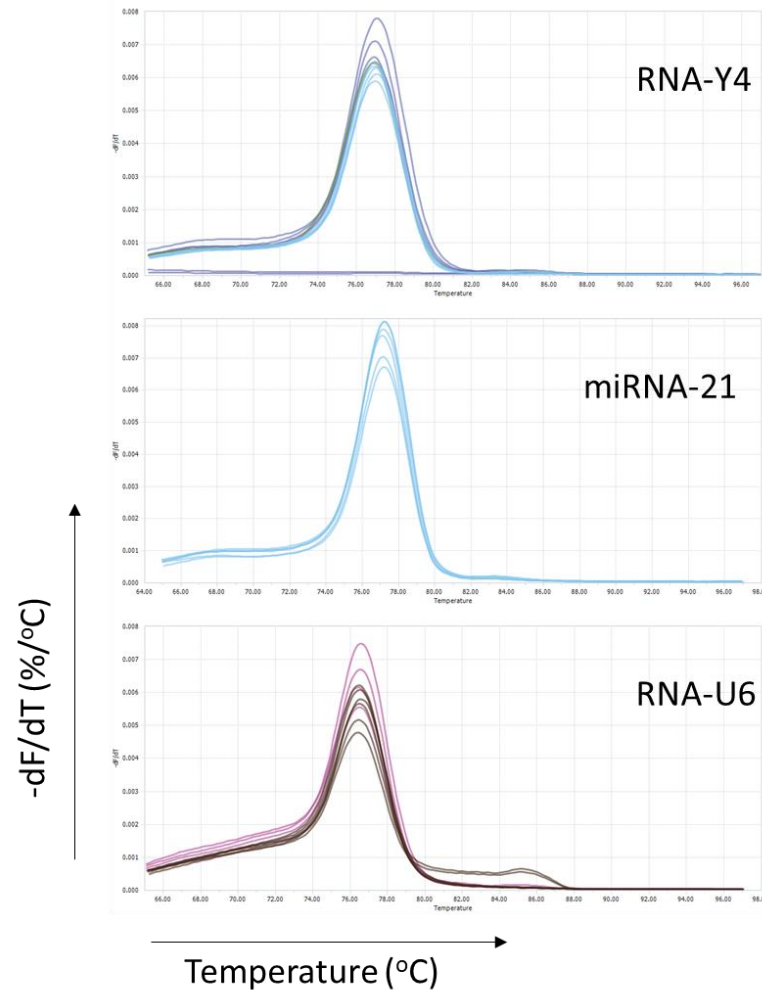

Figure 4-19. Primer melting curves after a qPCR cycle with the same conditions used in the qPCR amplification of hY4 RNA.

Taking into account the melting curves and the previous efficiency results from the cDNA dilution slopes, RNA-Y4, miRNA-21 were both shown to be sufficiently reliable genes, and

the RNA-U6 was also included in the measurement, although its efficiency was found lower by 10% from the desired.

Data analysis

The main sample under measurement was Apo-EVs, using Bcl-2 EVs as the control condition of the system. Because qPCR is a method of quantifying the relative expression level and not the absolute values, some internal controls of the measurement need to be applied in every experiment. The measurement outcome of each experiment is the Ct value, which stands for the number of reaction cycles needed in order for the fluorescence intensity to exceed a threshold limit after the initiation of the reactions. This value is an indication of production of the sequence under examination, and the lower this value is, the larger the quantity of the RNA template, therefore the higher the expression level. However, in order to normalize the Ct values of each reaction and minimize the effects of variations in RNA quantity added for each sample, the normalization controls are 'housekeeping' genes of the biological system, meaning that these genes have been found to have a stable expression for both the sample under measurement (Apo-EVs in this case) and the control condition (Bcl-2 EVs). The Ct values of those genes are used to set a common baseline for both conditions and ensure that only the relative differences due to expression levels can be revealed, eliminating factors related to differences in the absolute Ct value of each reaction. The data analysis procedure is summarized here:

For each gene, either the gene of interest (RNA-Y4) or a housekeeping gene (RNA-U6, miRNA-21), there are two sets of reactions, one for the condition of interest (Apo-EVs) and one for the control Bcl-2 EVs, in duplicates. The Ct Values of the duplicates of each sample were averaged, followed by the calculation of the difference between the conditions (RQ), setting the control Bcl-2 EVs as the baseline expression, at 1.0. The normalization factor of the experiment is calculated by extracting the geometric mean value of the RQ of all the housekeeping genes for the control conditions (normalization factor =1) and for the Apo-EVs. Finally, applying the normalization factors of the control and Apo-EV condition to the respective RNA-Y4 RQ values, the level of expression of the Apo-EVs in comparison to a baseline expression of 1 for the Bcl-2 EVs is extracted (J. Vandesompele *et al.*, 2002; De Spiegelaere *et al.*, 2015).

The Ct values for all reactions are presented in the table below.

Table 4.1. Raw Ct values for all repeats of RT qPCR for Apo-EVs and Bcl-2 EVs.

Gene Name	Sample Name	Repeat 1	Repeat 2	Repeat 3
hY4 RNA	Apo-EV	20.03	19.71	18.75
		19.88	19.91	18.78
	Bcl-2 EV	23.33	22.73	23.74
		22.43	22.83	23.69
RNA-U6	Apo-EV	19.11	19.25	17.73
		19.21	19.36	17.72
	Bcl-2 EV	20.86	21.38	22.89
		20.4	21.45	23
miR-21	Apo-EV	34.04	34.73	34.68
		32.88	34.17	33.99
	Bcl-2 EV	34.32	32.99	35.82
		33.07	32.84	35.07

Applying the analysis procedure mentioned earlier to the Ct values finally yields the -fold expression levels for all samples, as these are compared with their control.

Besides the extraction of RNA from isolated Apo-EVs, RNA was also extracted from Apo-EV treated HUVEC cells in an effort to detect hY RNA transfer from the EVs to the cells. In the case of EVs, the Bcl-2 EVs are the control, while in the case of EV-conditioned endothelial cells, the control can be either the Bcl-2 EV cells or the cells alone (comparisons for each case are described on the graph, Figure 4-20).
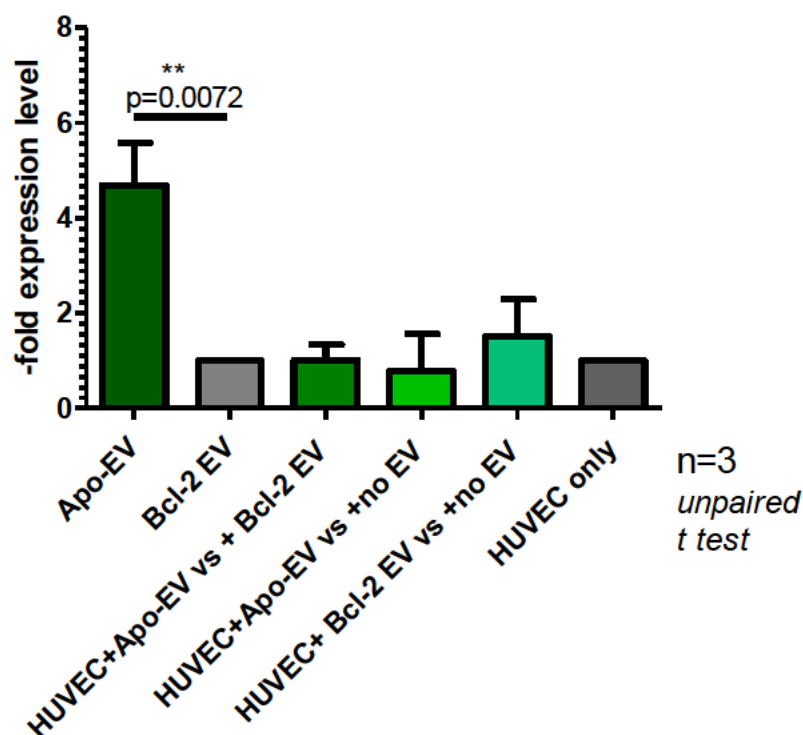
Figure 4-20. RT-qPCR results for hY4 RNA for EVs and HUVECs incubated with EVs. The error bars represent standard deviation from 3 individual experiments and the statistics were processed with GraphPad Prism (for non-significant P > 0.05, * P ≤ 0.05 ** P ≤ 0.01, *** P ≤ 0.001, **** P ≤ 0.0001).

A statistically significant difference in the level of hY4 RNA expression is confirmed for Apo-EVs when these are compared to the Bcl-2 EVs, although no differences are noted for endothelial cells upon their interaction with EVs.

4.6. Discussion

In an attempt to find the most efficient capture antibody against EVs in order to couple vesicles to magnetic beads for flow cytometry, unexpected and interesting data emerged, suggesting that the levels of expression of certain surface molecules can be different than estimated. In more detail, it was shown that CD19, CD20 and MHC class I (clones W6/32 and HC10) which would be expected to be abundant on B cell-derived vesicles were ineffective as capture probes. A partial explanation for the inability of MHC I to serve as a capture probe, although the analyses performed later showed that it is present on the EV membrane (flow

cytometry, microscopy and proteomics data collected by other studies on the Gregory group, results not shown here) comes from the mechanistic and spatial interactions between protein molecules. This can be because MHC class I is a comparatively "shorter" molecule and could be spatially 'blocked' or 'hidden' by neighbouring larger surface molecules, thus providing with a poor capture receptor (Barclay *et al.*, 1997). Another reason which was hypothesised as a potential factor contributing to poor MHC class I - mediated capture was the absence of beta-2 microglobulin, a molecule involved in the formation of MHC class I molecules (*Entrez Gene: Beta-2-microglobulin*, 2014). In other words, if the EVs lack beta-2 microglobulin, this could lead to malfunction of the MHC class I. However, the expression levels of this molecule were studied by flow cytometry (Figure 4-9) and as it was found that both Apo- and control EVs express it, this hypothesis has been rejected.

Capturing the total population of EVs with a single probe remains a question, since there is evidence that a large number of EVs might not express this marker -or any marker-, leading to the conclusion that immunomagnetic capture would require the use of multiple capture targets and even in this case, there can be vesicles which would not present any of those surface molecules, rendering immunomagnetic isolation unsuitable for total vesicle isolation. The heterogeneity of the population is strongly evident from this work, but also other groups have highlighted the need for multiple probes to successfully recover the majority of vesicles (Koliha *et al.*, 2016). For CD81 and CD63 particularly, it has been suggested that some EVs associated with early endocytic membranes or plasma membranes might lack those two markers (Kowal *et al.*, 2016).

Applying flow cytometry on EV-bead complexes yielded results which showed no statistically significant difference between Apo-EVs and Bcl-2 EVs, however it became evident that cell lineage markers such CD19 and CD20 were expressed in lower levels in comparison to the classical 'exosome markers' CD9, CD63 and CD81 (Figure 4-9). Looking into the individual markers measured, Ro/SSA and La/SSB are autoantigens which are exposed on the surface of apoptotic blebs playing significant roles in autoimmune diseases and especially lupus erythematosus (Lerner *et al.*, 1981) and have also been found on EVs isolated from neoplastic cells (Kapsogeorgou *et al.*, 2005). Although the literature suggested the potential over-expression of these markers on the Apo-EVs, this was not confirmed by flow cytometry. Next, previous studies of BL2 derived Apo-EVs on the total proteome have shown significant expression levels of CD10, CD45, CD46 and thrombospondin-2 in Apo-EVs compared to the

control EVs (unpublished data, Gregory group), therefore flow cytometry was used to investigate this result *in vitro*. However, the immunomagnetic method has not indicated differences in the level of expression. Active caspase-3 and histone-3 have been highlighted as proteins specifically expressed on Apo-EVs by previous studies by western blotting (unpublished data, Gregory group) and from the literature (Böing *et al.*, 2013), (Schiller *et al.*, 2008), however no differences between the two EV populations were found by flow cytometry. Methods used as a comparison to flow cytometry phenotyping are discussed in the following paragraphs.

Next, confocal fluorescence microscopy was applied on Apo-EVs and the findings on active caspase-3 and histone-3 indicated that those markers can be selectively expressed on Apo-EVs, although flow cytometric analysis results did not support this finding. This indicates that flow cytometry is potentially less sensitive and selective compared to the counting of individual vesicles from microscopy images. Taking a step beyond conventional confocal microscopy, super resolution imaging can be an effective tool for investigating the presence of fluorescent markers on the EV surface and an example proving the degree of resolution achieved by STORM is shown below (Figure 4-21).
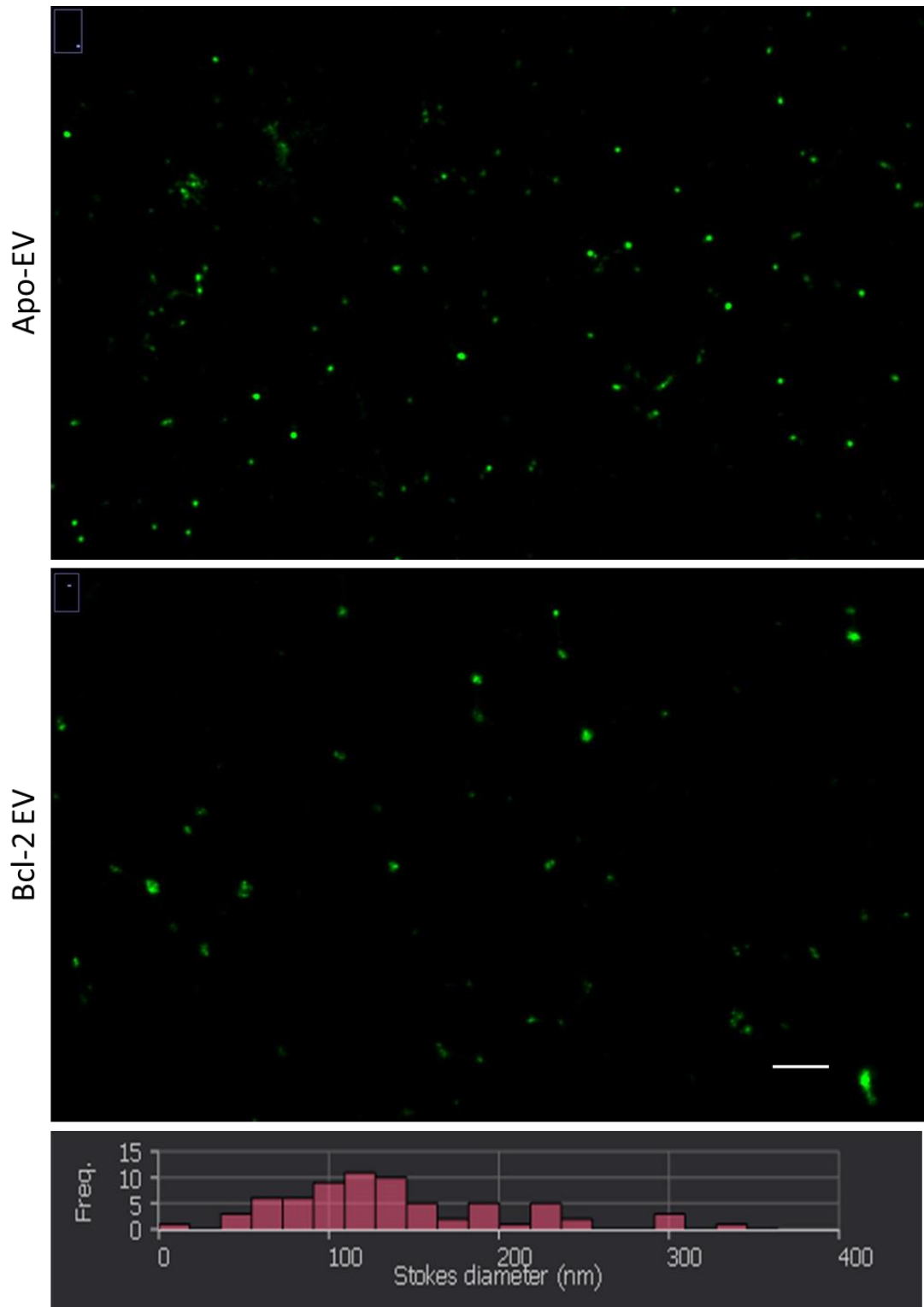
Figure 4-21. Super resolution microscopy imaging by STORM for EVs labelled with covalent protein staining AlexaFluor568, scale Bar 500nm. A quantification of the EV diameter for Apo-EV is shown in the bottom graph. Images were recorded on Nanoimager and processed by ONI scientists during instrument demonstration (Oxford Nanoimaging, Oxford UK).

STORM is a mode of imaging which can visualize single fluorescent molecules, therefore, as also proved in the figure above, can result in highly reliable and robust data. For the purposes of this work, proof-of-concept imaging on EVs was performed on the Nanoimager system during demonstration, indicating the suitability of the method for further analyses in the future (ONI, Oxford, UK).

Finally, immunogold labelling on TEM is a very efficient method when details on the arrangement and the number of target molecules are needed, however it is a low throughput technique which would be unsuitable for clinical applications. In this work, it was used as a comparison to flow cytometry, in order to validate the quality of flow cytometric measurements where the EVs are bound on magnetic bead complexes. It is generally observed that immunogold particles label a smaller number of EVs compared to the expression levels recorded by flow cytometry, which is unknown whether it can be due to the sample preparation method or due to over-estimation of levels by flow cytometry. In addition, accepting the fact that flow cytometry only enables the phenotyping of larger vesicles, the differences in measured levels could be a reflection of the actual levels in the larger versus the smaller EVs measured by each technique. In other words, a direct comparison of the phenotypic results might not be fully relevant, because each method looks at a slightly different target group of EVs.

Moving away from protein targets, the qPCR study for hY4 RNA on Apo-EVs confirmed the significant over-expression of the sequence in the Apo-EVs, as those have been isolated from EV suspensions. However, when EVs were added in endothelial cells, the increase in the levels of this RNA was not detectable, possibly due to the already existing copies of this sequence in the cells (Appendix Figure 4-31 shows the EV uptake by HUVEC cells, as performed by Dr Margaret Paterson, confirming the interaction of EVs with the cells). Overall, the hY4 RNA was proven to be the first non-coding RNA marker which was identified for the BL2-cell derived EVs. However, the potential use of this small RNA as a diagnostic marker is a matter which requires further investigation with *in vivo* studies, as it has been shown that EVs from several cell types and body fluids contain all types of RNA Y, including the hY4 RNA (Driedonks and Nolte-T'Hoen, 2019).

In conclusion, a range of methods for EV phenotyping have been presented, each of which has provided with interesting findings such as the identification of active caspase-3 and the

hY4-RNA as unique Apo-EV markers. Comparing the results obtained with each method is also another aspect worth considering, as the strengths and limitations of each of them are revealed. For example, in the case of active caspase-3, flow cytometry failed to highlight the importance of this protein for Apo-EVs, due to non-specific binding of the fluorescent antibody on the immunomagnetic bead/EV complexes. When choosing a method of phenotypic analysis, the time and equipment required for the measurement need to be also considered, as for example in the case of immunogold labelling and TEM imaging, for which the speed of measurement for each sample is significantly lower than flow cytometry or fluorescent NTA.
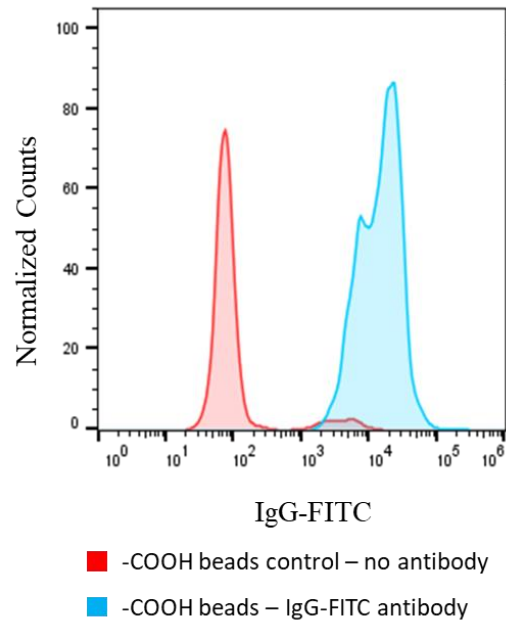
Appendix for Chapter 4

Figure 4-22. Validation of antibody coating efficiency for -COOH surface magnetic beads. Measurement performed by flow cytometry and staining with IgG-FITC (results from 1 experiment).
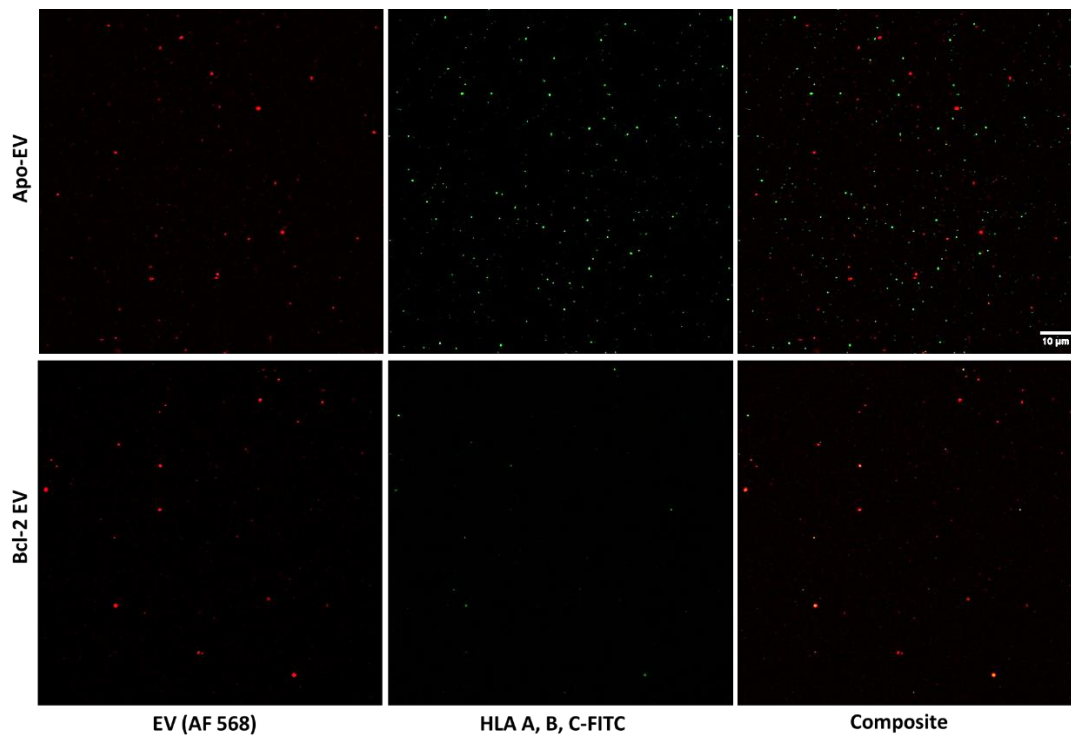

Figure 4-23. Confocal imaging of EVs attached on glass coverslips stained with general protein dye AlexaFluor 568 and with anti-MHC class I-FITC antibody.
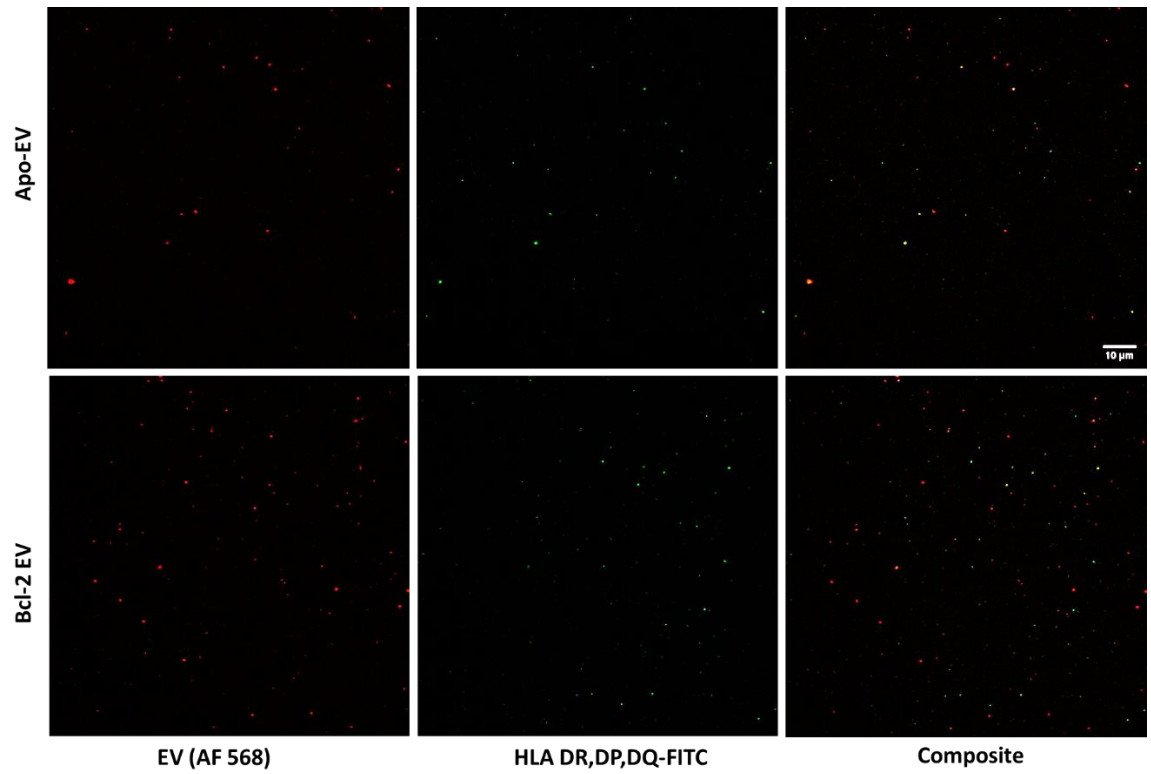
Figure 4-24. Confocal imaging of EVs attached on glass coverslips stained with general protein dye AlexaFluor 568 and with anti-MHC class II-FITC antibody.

Figure 4-25. Confocal imaging of EVs attached on glass coverslips stained with general protein dye AlexaFluor 568 and with anti-CD45-AlexaFluor 488 antibody.

Figure 4-26. Confocal imaging of EVs attached on glass coverslips stained with general protein dye AlexaFluor 568 and with anti-CD20-AlexaFluor 488 antibody.

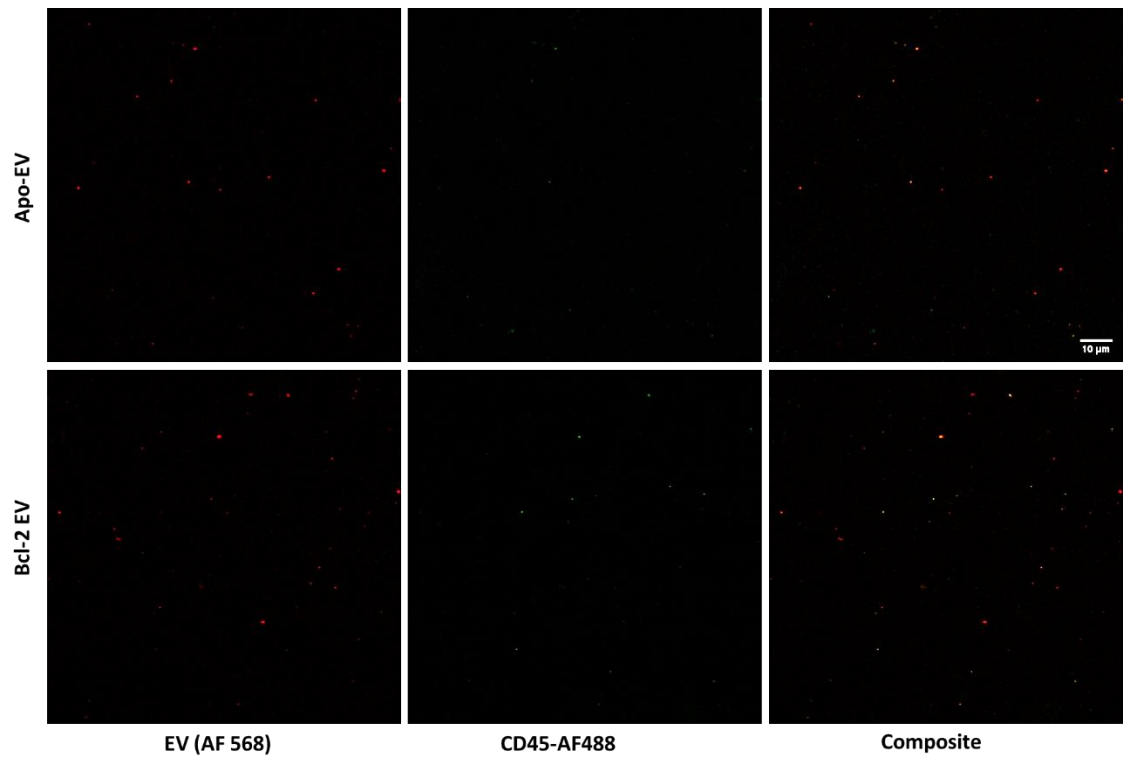*Figure 4-27. Confocal imaging of EVs attached on glass coverslips stained with general protein dye AlexaFluor 568 and with anti-CD19-AlexaFluor 488 antibody.*
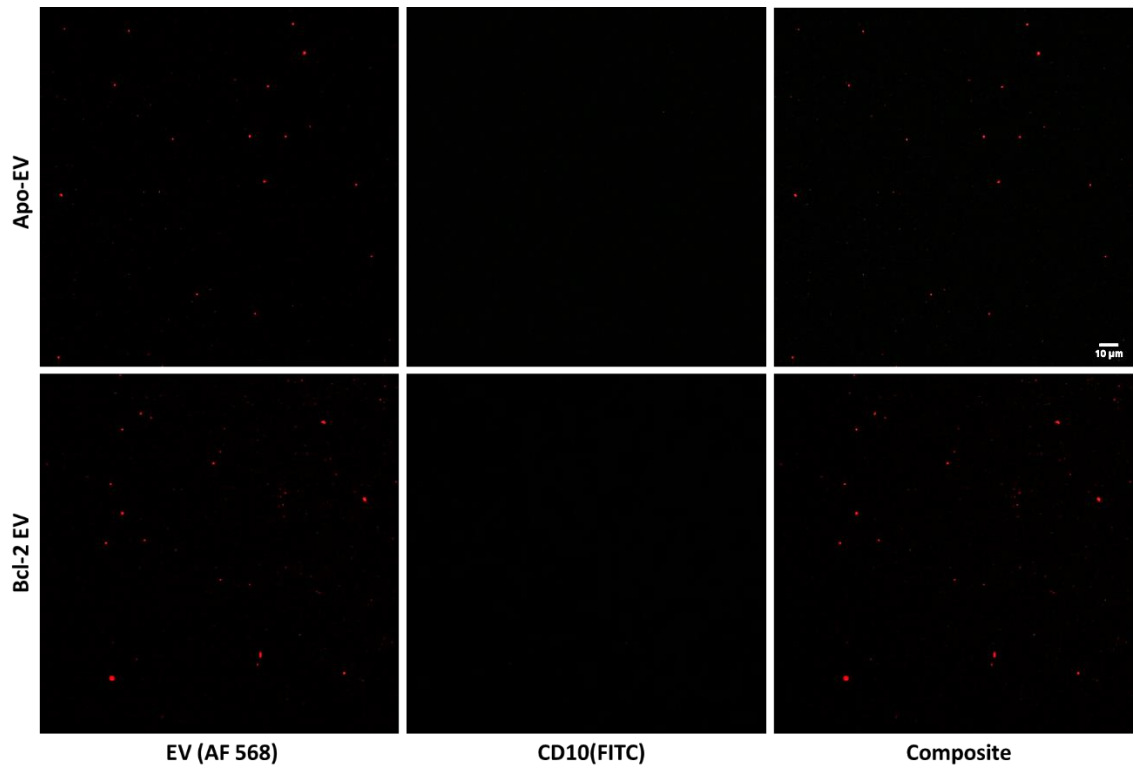
Figure 4-28. Confocal imaging of EVs attached on glass coverslips stained with general protein dye AlexaFluor 568 and with anti-CD10-FITC antibody.
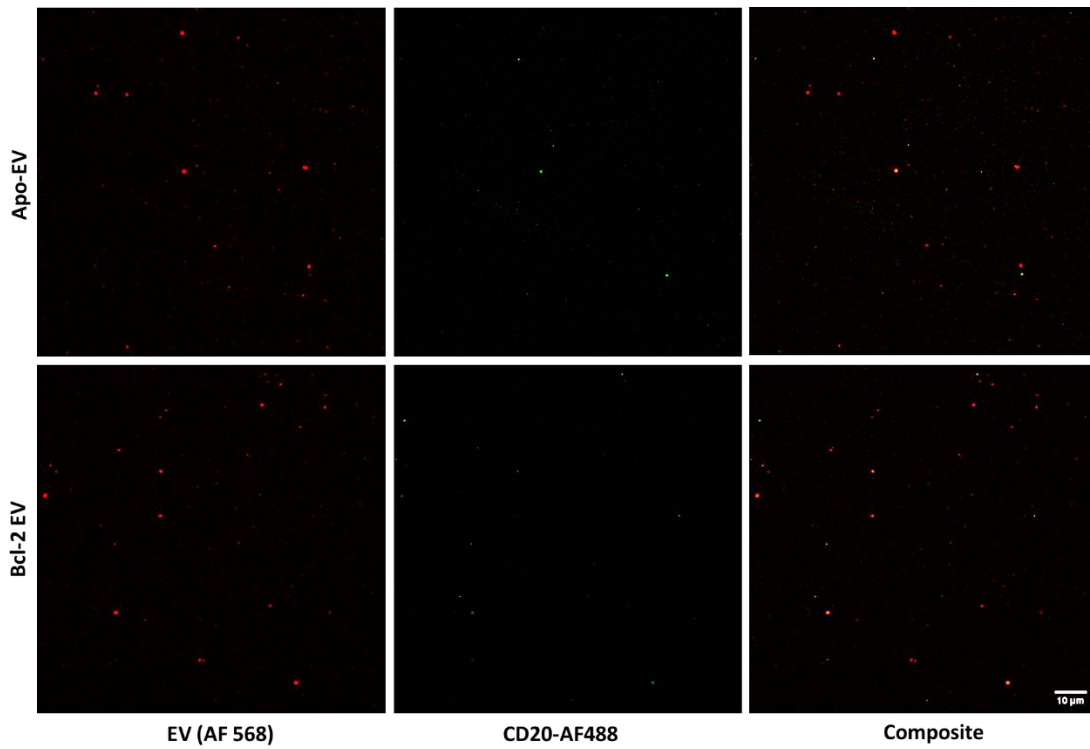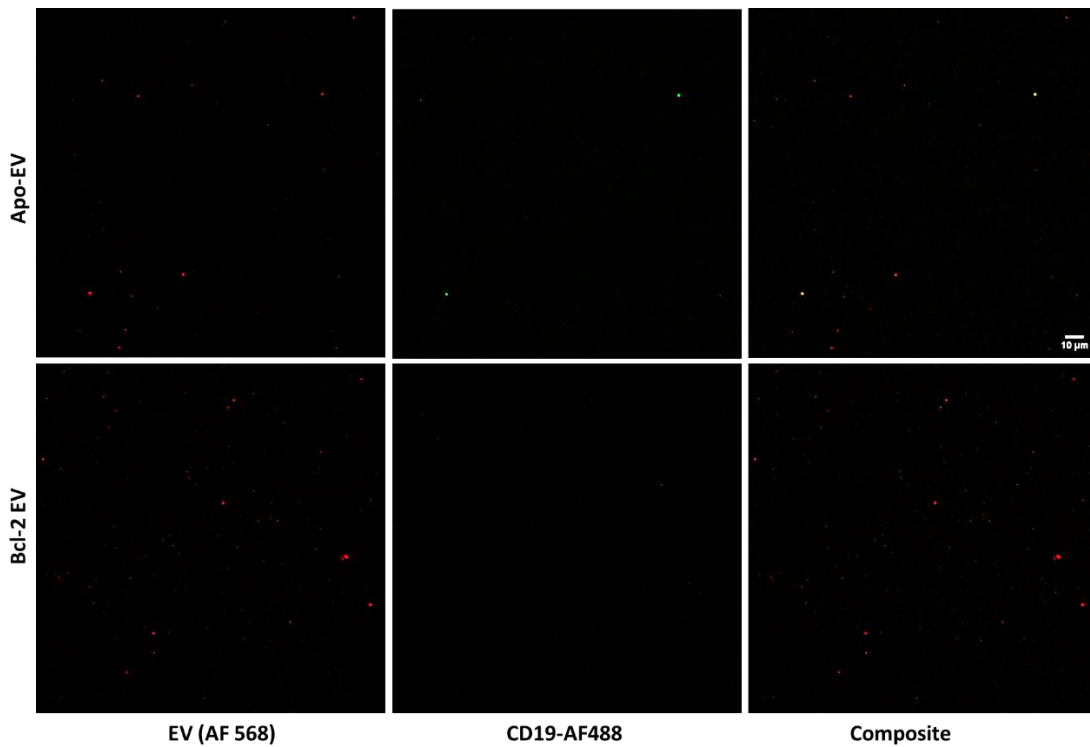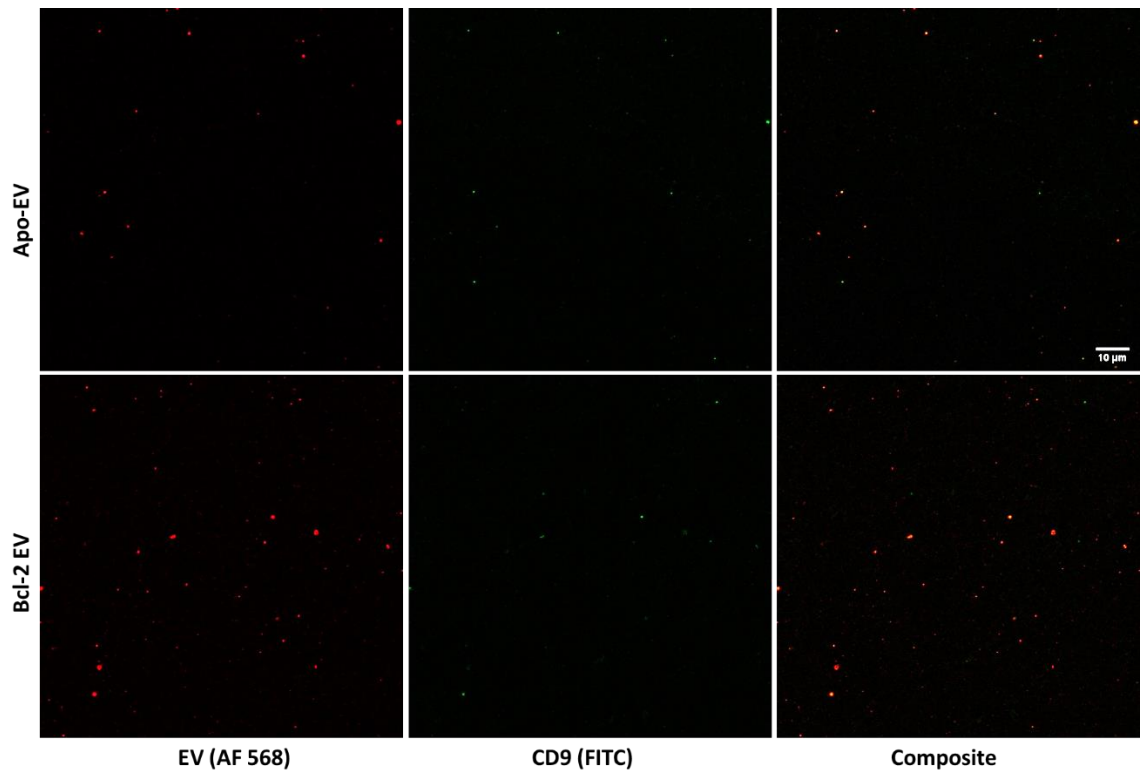

Figure 4-29. Confocal imaging of EVs attached on glass coverslips stained with general protein dye AlexaFluor 568 and with anti-CD9-FITC antibody.
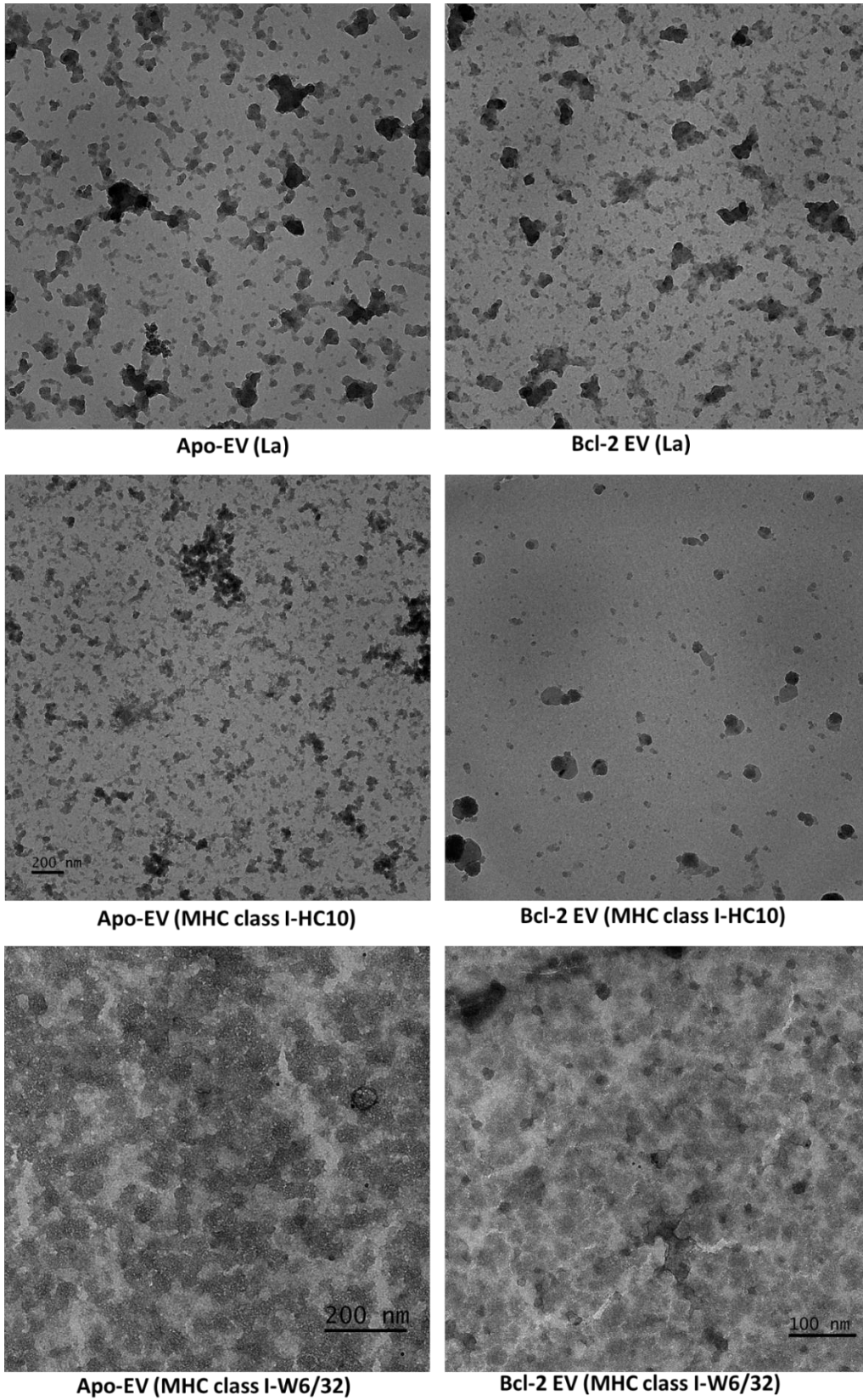
Figure 4-30. Immunogold labelling of EVs on TEM.

EV per HUVEC cell	250	500	750	1000
■ Geometric mean	13900	18800	21900	25200
■ Conc EV x E8/ml	0,388	0,675	1,01	1,35

Figure 4-31. HUVEC cells uptake of Apo-EVs after 3h incubation at 37°C in a range of EV concentrations. The EVs were pre-stained with AlexaFluor488 and the readout was performed by flow cytometry after washing of excessive EVs. This experiment was performed by Dr Margaret Paterson who kindly provided this graph.

5. Study of Apo-EVs in blood – the role of platelets and blood cells

5.1. Aims of the chapter

In the final chapter of this work, the analysis of EVs is moving from the characterisation of the particles alone to the environment of the blood circulation, aiming to examine the potential recipients of the Apo-EV cargo. The conceptual basis of this project is to use Apo-EVs as diagnostic and prognostic indicators of cancer progress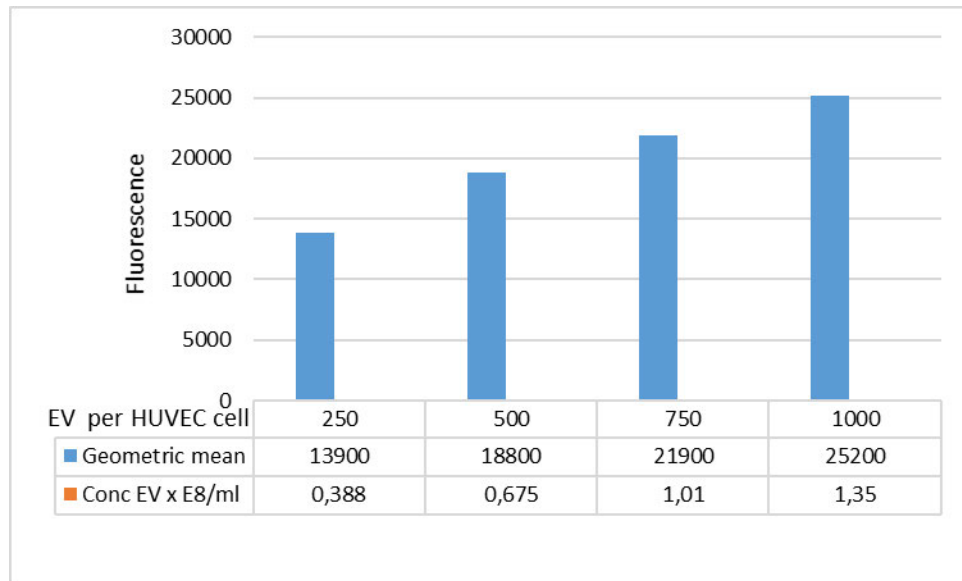ion, therefore their behaviour in the blood is a crucial factor which can affect their availability for analysis from e.g. blood samples. As blood is an organ rich in cells and cellular fragments, the platelets, their interactions with the tumour-derived Apo-EVs are examined quantitatively by the degree of uptake, as well as biochemically, by the cargo they deliver.

Red and white blood cells will be examined mainly for their ability to take up EVs, however, the delivery of Apo-EV molecules will be primarily studied in platelets. As platelets are the most abundant cellular entity in the circulation after erythrocytes, the signal transduction from the EVs to the platelets can potentially reveal alternative sources for EV cargo detection in blood, which can affect the Apo-EV analysis procedures in the clinical practice. In other words, as EVs encounter and interact with platelets or leukocytes in blood, EV material could be transferred to the second. From this point, the cells or platelets can bear Apo-EV signals themselves, or can release other EVs, which will act as secondary Apo-EV signal mediators. This phenomenon (also described in Figure 5-1) can have clinical significance, as for example, hypothesizing that the endpoint of Apo-EV signal expression in blood is via platelets after the interaction, the isolation and analysis of platelets may prove sufficient as a diagnostic tool avoiding all the EV isolation steps which can be impractical for conventional clinical laboratories.

A schematic summary of the rationale of this chapter is presented in Figure 5-1.
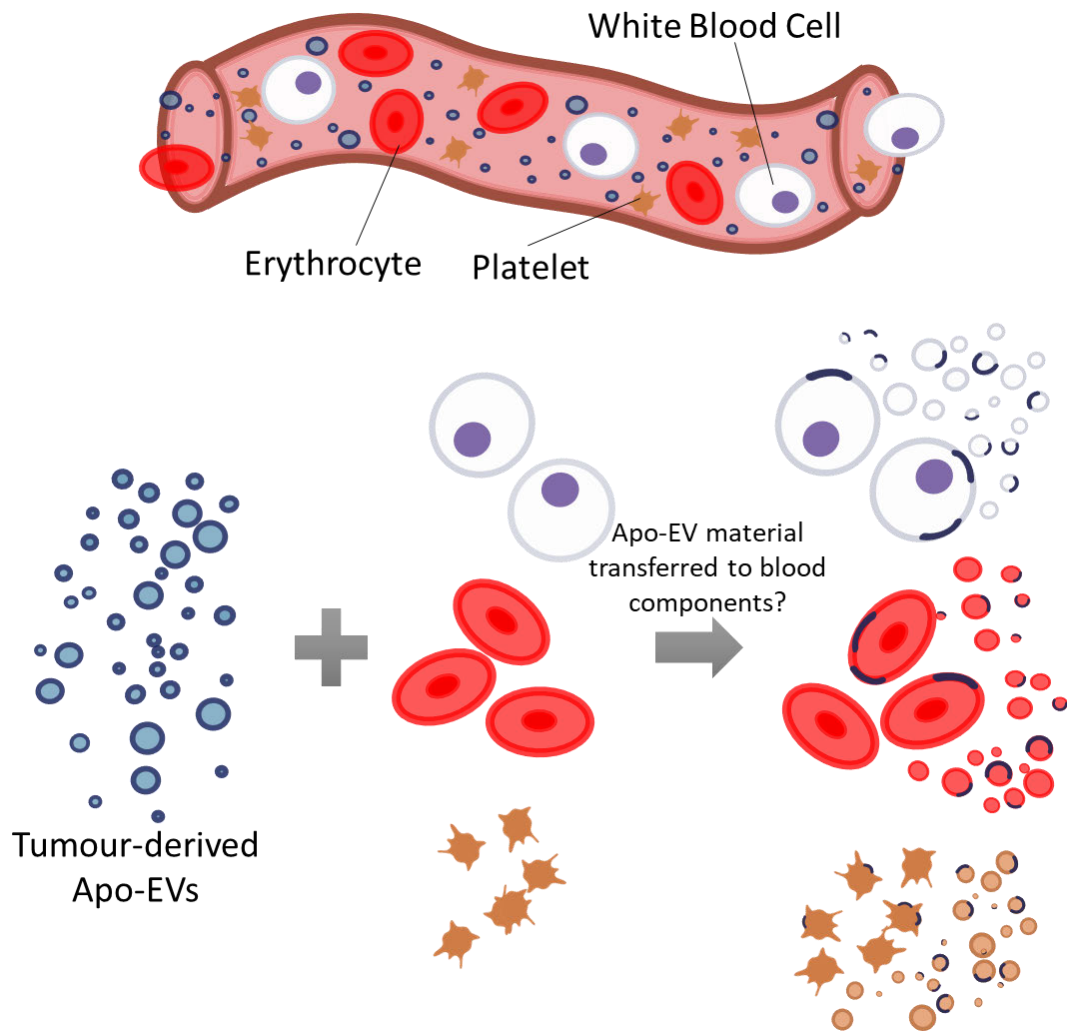
Figure 5-1. Hypothesis of Apo-EV signal transduction to blood cells and platelets. Tumour-derived EVs can potentially interact with blood cells and platelets and deliver their cargo to the second. The result of this interaction could lead to a secondary expression of EV material by the recipient cells and platelets.

In more detail, this chapter mainly presents flow cytometric studies of EV uptake by blood cells and platelets, followed by confocal fluorescence microscopy for the direct visualization of the internalization of EVs and finally biochemical analysis for the transfer of Apo-EV cargo on platelets or study of the internalization mechanism of EVs in blood cells.

5.2. Platelets and Apo-EVs

In this section, the interactions of *in vitro* prepared Apo-EV with platelets derived from the blood of healthy volunteers are discussed. The first part of the study involves the platelet

isolation and confirmation of their presence on the flow cytometry dot plots. Blood from healthy volunteers was used to isolate plasma from which the platelets were extracted and suspended in Tyrode's buffer supplemented with PGE1 to inhibit activation. The following graph shows the gating of platelets as dictated by CD42 staining, a platelet surface marker (Blair, Michelson and Frelinger, 2018) and Cell Tracker Violet stain, which fluoresces once being trapped inside living cells/platelets (Invitrogen) (Figure 5-2). In this figure, the Cell Tracker staining appears to form a biphasic curve, which shows that a part of the platelets are negative to this dye, although they are positive for CD42. This is an indication of the fragility of the platelets, as they tend to collapse and release large vesicles, therefore the dye leaks out of their interior, resulting in them appearing as unstained.
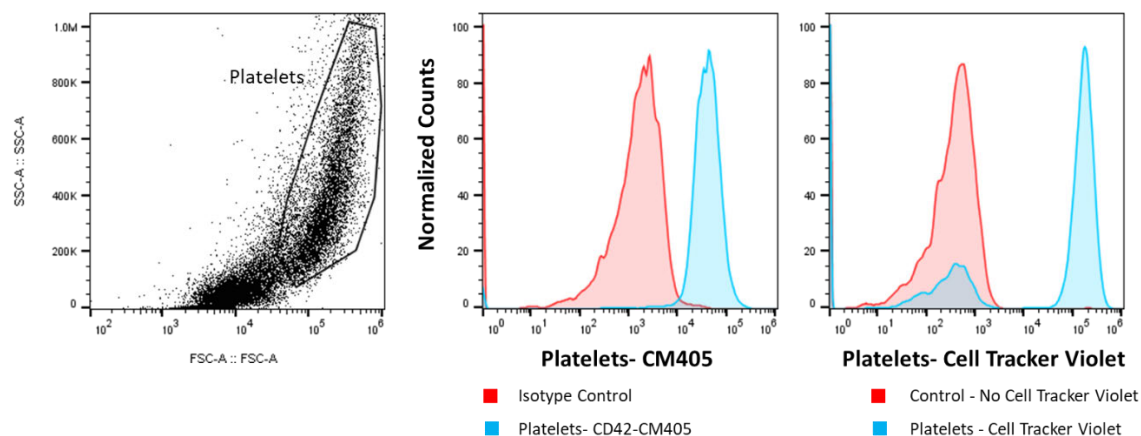
Figure 5-2. Flow cytometry dot lot and fluorescence histograms for freshly prepared platelets stained with anti-CD42 antibody or Cell Tracker Violet.

Following the establishment of the platelets gate on flow cytometry, pre-stained AF488 EVs are added to the platelet suspension and are allowed to interact at 37°C for 0, 1, 2 or 3h with and without the addition of PGE1 during incubation. The results of the measured uptake are presented in Figure 5-3.
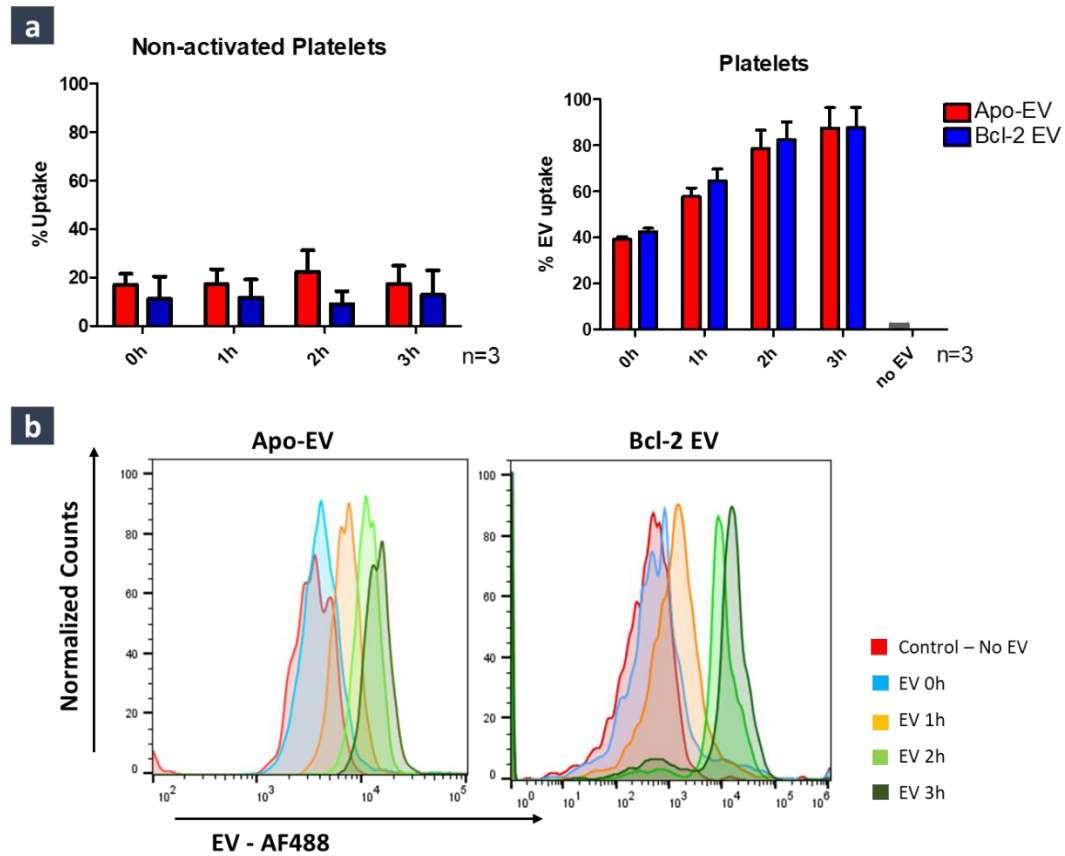
Figure 5-3. a) levels of EV uptake by non-activated platelets with the addition of PGE1 (left) and platelets without PGE1 (right), b) fluorescence intensity histograms for EV uptake in platelets without PGE1. Study performed by flow cytometry for AF-488 stained EVs using 5,000 EVs/platelet (error bars indicate standard deviation from n=3 independent experiments).

From the above figures, no significant differences in the level of uptake between the Apo-EV and the Bcl-2 EV are observed, however, the non-activated platelets in which PGE1 was present at all times, during storage, incubation with EVs and measurement, show significantly lower percentages of uptake which remains steady up to 3 hours of incubation. In contrast, the platelets which were exposed to EVs without the addition of PGE1 were almost saturated with EVs by 3 hours of incubation. Interestingly, a strong interaction between the platelets and EVs is observed instantly (time 0h, which in reality reflects a time period of 15-20min), as 40% of platelets are positive for EVs.

The observations from flow cytometry will next be confirmed by confocal fluorescence microscopy on platelets stained with Cell Tracker Violet and AF488 EVs after an incubation

of 3h at 37°C followed by quantification of the AF488 intensity levels as an alternative method to measure the uptake (Figure 5-4).
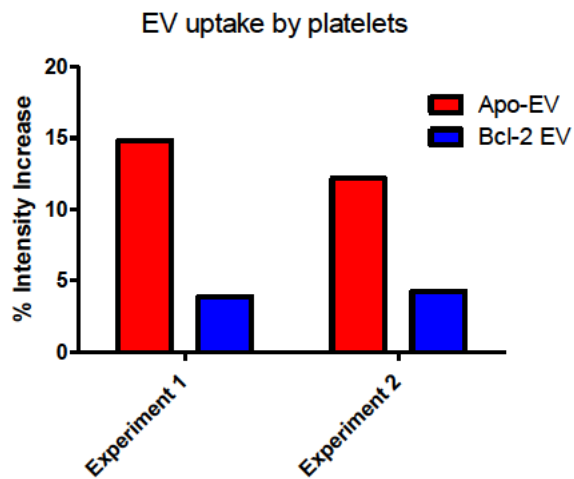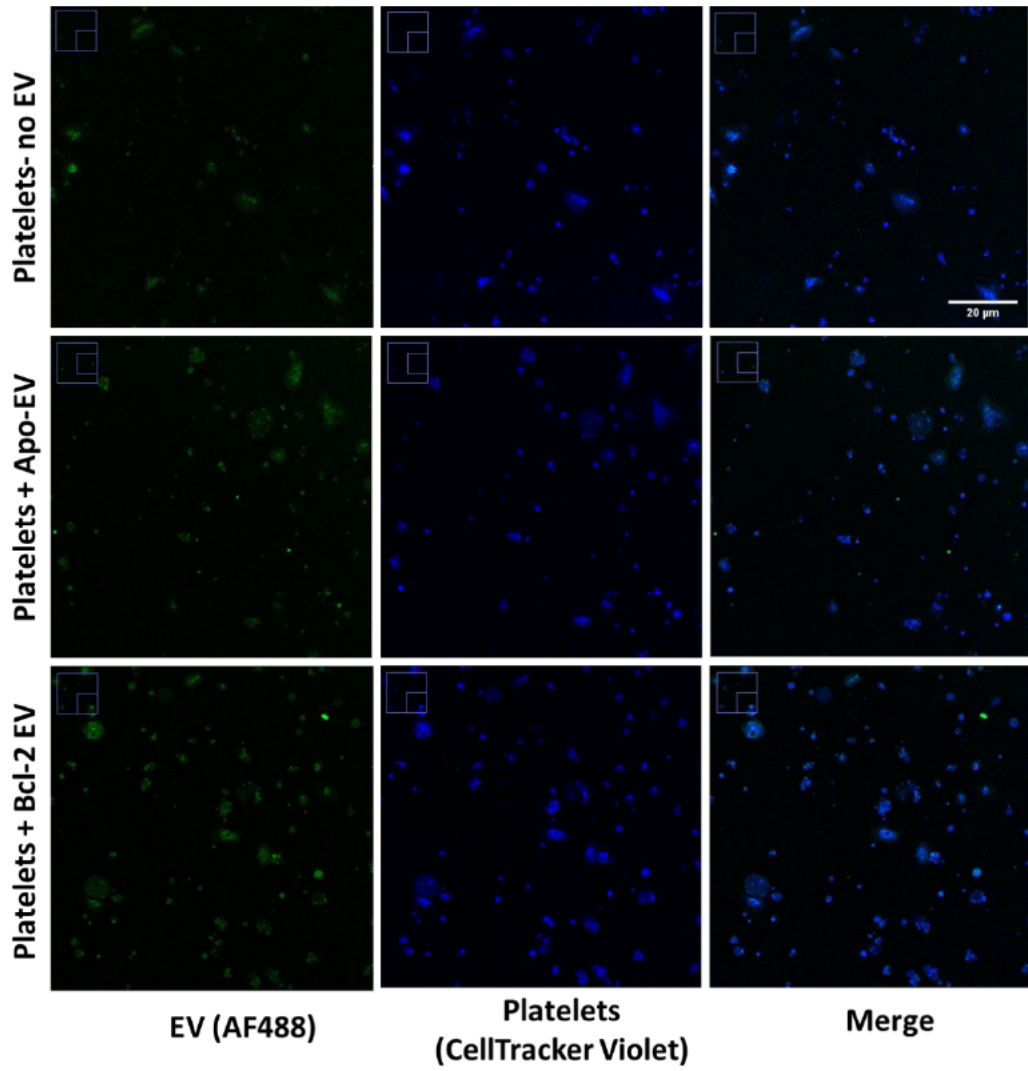
Figure 5-4. Confocal microscopy on platelets stained with Cell Tracker Violet (blue) interacting with AF-488 EVs (green) after 3h incubation at 37°C and quantification of the fluorescence intensity of EV signal (green) (bottom bar chart shows the values from n=2 independent experiments).

As platelets are significantly smaller than cells, it is challenging to visualize them by brightfield illumination, therefore the staining with a general fluorescent dye (Cell Tracker Violet) is essential in order to study the EV interactions in detail. However, the violet fluorophore appears in the emission channel of the AF488 dye, causing a background signal in the non-EV treated platelets, which is presented in the quantification graph in Figure 5-4.

To further examine the localization of the EVs on the surface or inside the platelets, three-dimensional images were reconstructed and vertical sections of the 3-D models show the presence of EVs in the inside of platelets Figure 5-5.
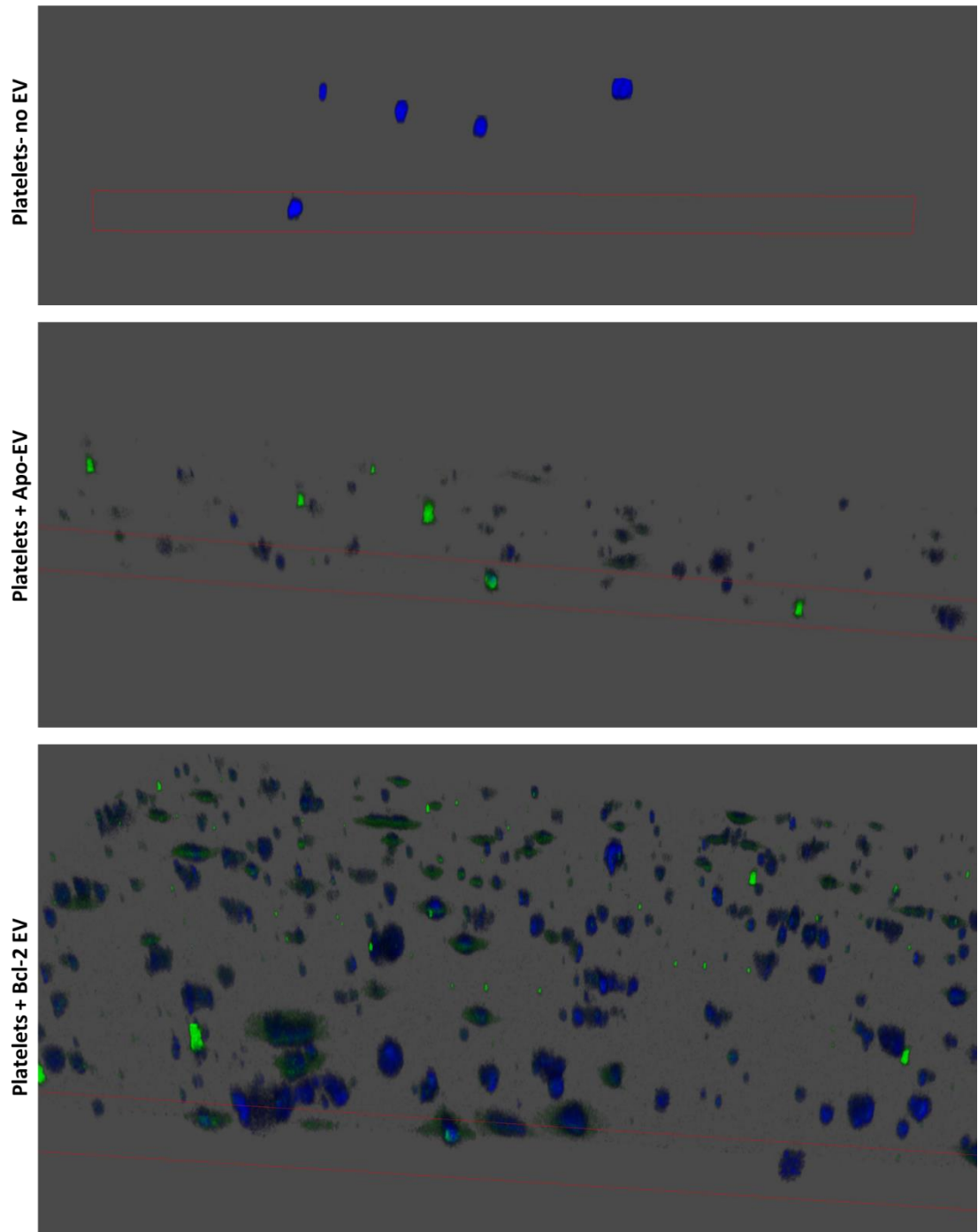
Figure 5-5. Three-Dimensional representation of platelets (blue) with EVs (green) after 3h incubation at 37oC with section on the vertical plane (red lines indicate the plane of sectioning).

Figure 5-5 shows a large number of EVs interacting with the surface of platelets, however, the vertical sections highlight the cases where EVs are found inside the main body of a platelet.

In brief, it has been shown that both Apo-EVs and Bcl-2 EVs interact strongly with platelets to which activation inhibitors have not been added, and as flow cytometry measurements revealed, this interaction is rapid regarding the time of incubation. The microscopy images confirm that the uptake is happening with EVs attached on the outer or inner side of the platelet membrane.

The confirmation of this interaction leads to the next question which is whether the Apo-EVs selectively transfer their molecular signatures to platelets, rendering the second a potential source of Apo-EV signal in blood. To investigate this hypothesis, some of the known EV markers for the *in vitro* derived BL2 EVs (expression levels shown in Chapter 4) were measured on platelets, in order to find candidates with low platelet expression, but abundant on EVs. The following graph presents the % positive platelets for BL2 EV markers such as CD19, CD20, CD77 (Mangeney *et al.*, 1991) as well as universal EV markers, the CD9 and CD63. In addition, DNA is a recognized Apo-EV component (Chapter 4 and other unpublished data from Gregory lab), therefore the platelets were stained with Hoechst for DNA and also with Annexin V for PS (Figure 5-6).
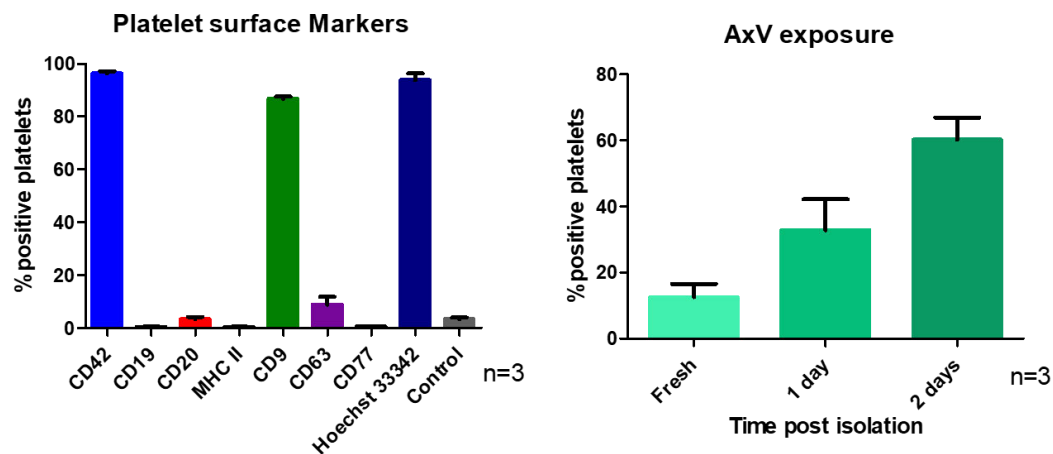
Figure 5-6. Study of surface markers expressed on platelets by flow cytometry on freshly isolated platelets in suspension. Isotype controls were used for every antibody staining (CD42, CD19, CD20, CD9, CD62, CD77 and MHC class II), while unstained platelets were used as a control for Hoechst and Annexin V staining. For Annexin V, measurements were taken at different days post isolation, as it was observed that the levels of PS exposure increase over storage (error bars indicate standard deviation from n=3 independent experiments).

156

As expected, platelets have low levels of B cell related markers such as CD19, CD20 and CD77, as well as MHC class II, however the EV marker CD9 is detected in the majority of platelets, followed by CD63 which shows a smaller percentage. Surprisingly, all platelets were positive for DNA as indicated by the Hoechst staining, and this is a finding that was further investigated by microscopy, which suggested that this is free circulating DNA attached on the outside of platelets, although platelets do not contain DNA themselves (figures in Appendix) (Dorsch, 1981). Another characteristic of the platelets was the exposure of PS, especially as this increases over storage of non-activated platelets at room temperature. The above measurement indicated the selection of three EV markers with low platelet expression which can potentially show elevated levels in platelets after their interaction with EVs. Figure 5-7 shows the collective results of three studies on EV marker expression on platelets after increasing time of interaction with the EVs.
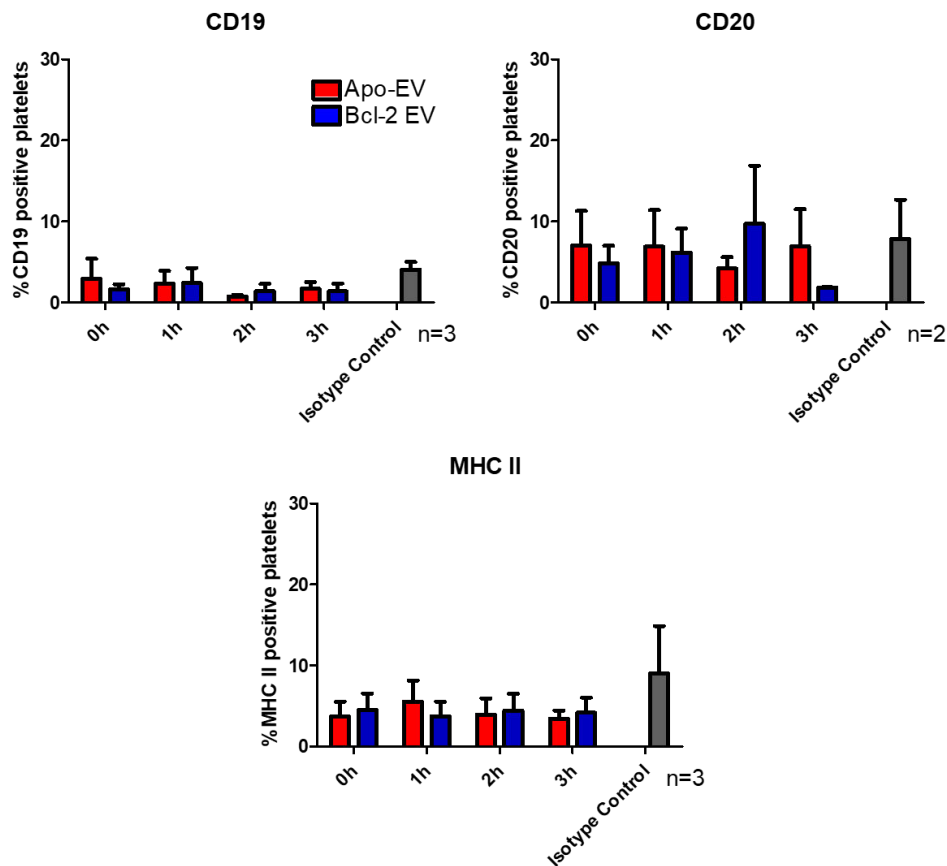
Figure 5-7. Levels of expression of EV markers on platelets after interaction of EV-platelets for 3h at 37ºC. Study conducted by flow cytometry using isotype controls for each antibody (the error bars indicate standard deviation from n=3 independent experiments).

It is observed that for all three markers examined here, the number of positive platelets is not higher than the isotype control, and overall not higher than 10%. Since no EV cargo transfer has been shown by flow cytometry on platelets, a more sensitive method will be next used to investigate the presence of the B cell-EV specific marker CD19 and Apo-EV marker Histone-3, the western blotting (histone-3 present in Apo-EVs as shown in Chapter 4 and from previous data from western blots performed by Catriona Ford, Gregory group). Platelets were saturated with EVs for 3h at 37ºC and after the excessive EVs were washed off, the platelets were used for total protein extraction, blotted and probed for CD19 and histone-3 (Figure 5-8).
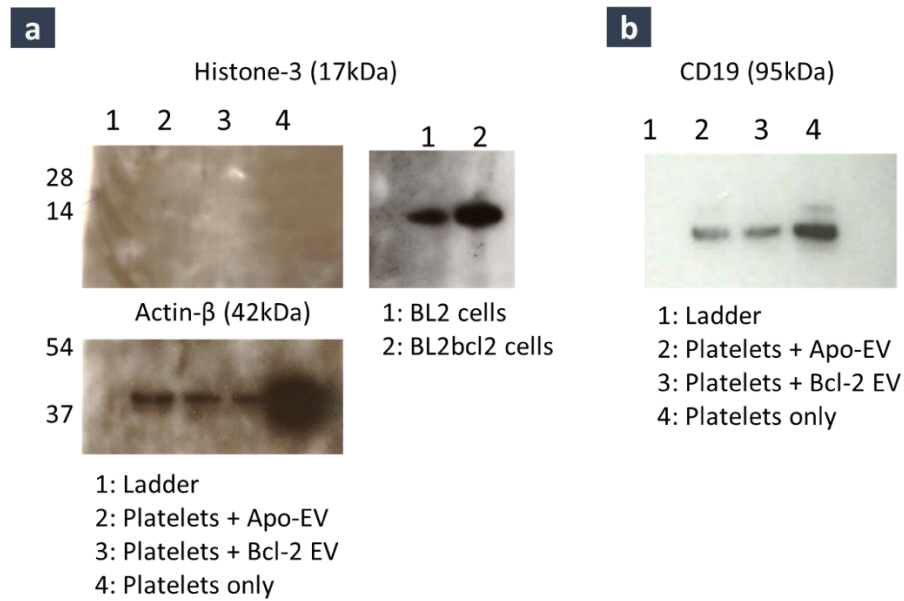
Figure 5-8. Western blotting of platelets after incubation with EVs. a) histone-3 blot for platelets with EVs, using BL2 cells as positive control and confirmation of platelets sample protein concentration by probing for actin-β. b) probing for CD19 on platelets and EV-treated platelets.

The above blots show that there are no detectable levels of histone-3 transferred to platelets from the Apo-EVs, and also there is some reaction of the anti-CD19 antibody with the platelets alone, therefore the band of a potential transferred signal is undetectable.

As a summary, there is a strong interaction of platelets with Apo-EVs and Bcl-2 EVs as measured by flow cytometry, however, the quantification of uptake measured by microscopy appears lower and this can be partially due to the high background noise from the platelet violet staining, masking the signal from small EVs. Three-dimensional microscopy showed that the EVs approach the external surface of the platelets but also get internalized. Those observations lead to the hypothesis that EV cargo is transferred to the platelets, therefore flow cytometry and western blotting were used to examine the presence of EV signature molecules such as proteins and DNA on EV-treated platelets, showing no significant indication of EV molecule up-regulation, which could also be attributed to low sensitivity of the selected techniques.

5.3. Blood cells and Apo-EVs

Apart from platelets, blood contains a large number of erythrocytes and leukocytes, which appear in high numbers and their interactions with EVs are also important to examine. The white blood cells are generally categorised in granulocytes, monocytes and lymphocytes, each of which contain other sub-sets of immune cells, however, for the purpose of this work, data on the general populations are sought without details on the exact subtype, as this is a preliminary study. The erythrocytes, on the other hand, are a homogenous population and can be isolated as a pure set of cells. The flow cytometry dot plots of the blood cells are presented in Figure 5-9 and the gating for the leukocytes has been done according to the side and forward light scattering properties of the cells (Silva *et al.*, 2013).
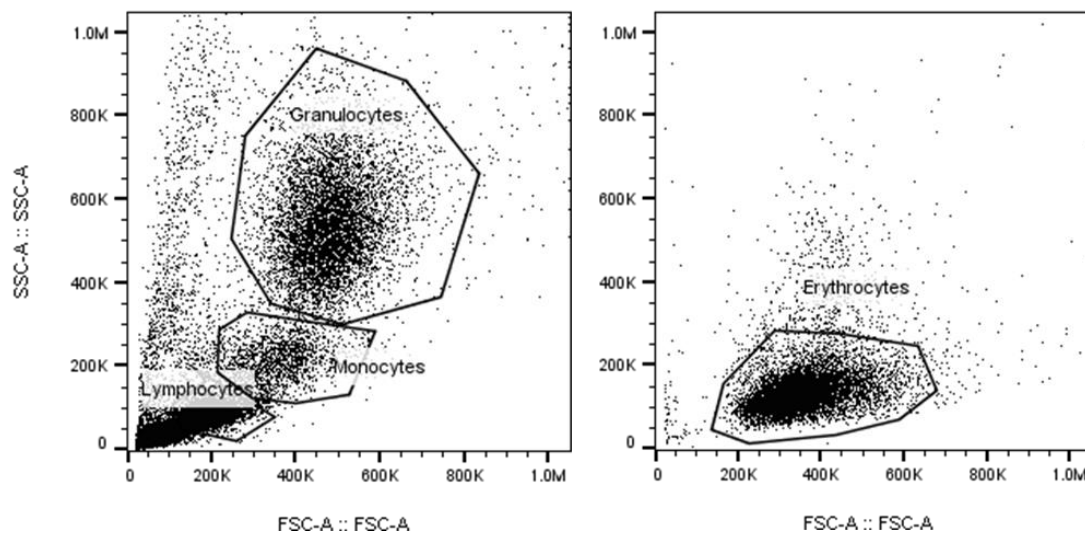
Figure 5-9. Flow cytometry dot plots for preparations of white blood cells (left) and erythrocytes (right).

Apo-EVs and Bcl-2 EVs were co-incubated with erythrocytes or leukocytes (as a mixture of granulocytes, monocytes and lymphocytes) and the levels of interaction are measured by flow cytometry, as the EVs are pre-stained with AF488 (Figure 5-10).
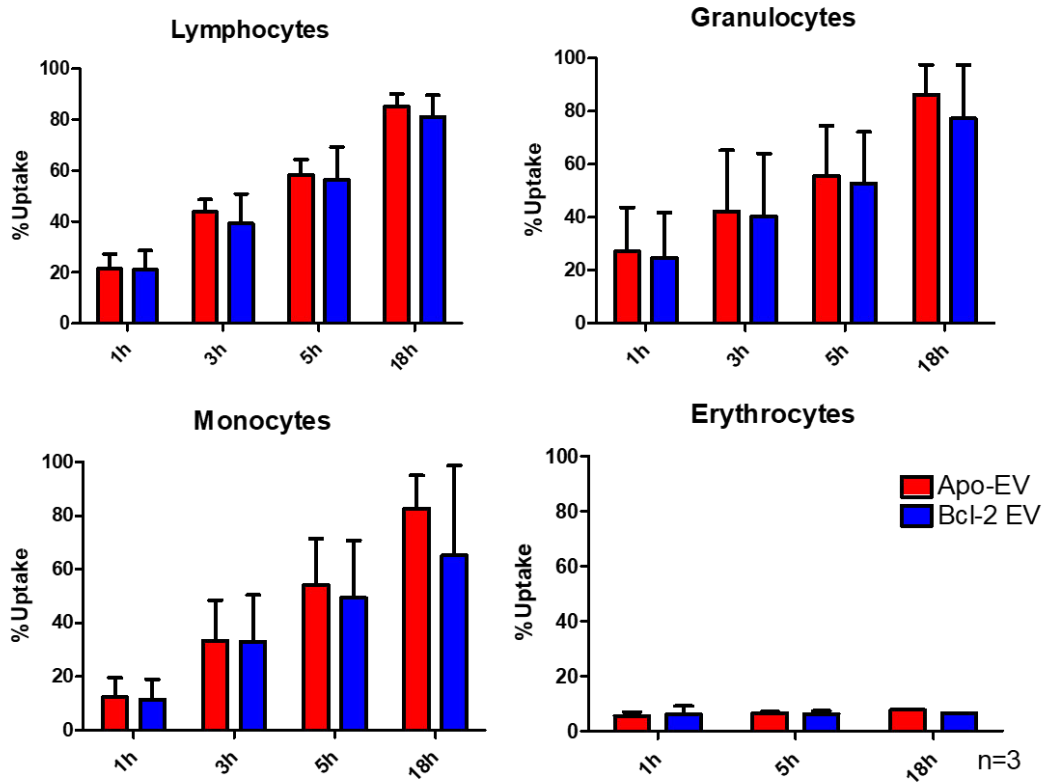
Figure 5-10. EV uptake levels for freshly isolated blood cells when incubated at 10,000 EV/cell for lymphocytes, granulocytes, monocytes and 5,000 EV/cell for erythrocytes at 37oC. Study performed by flow cytometry for AF-488 stained EVs (the error bars indicate standard deviation from n=3 independent experiments).

As a first observation from the uptake levels on EV, erythrocytes are the only type of cells which are not interacting with EVs, even after overnight incubation. Figure 5-11 also shows the fluorescence intensity histograms for the different categories of leukocytes over time of incubation with EVs.
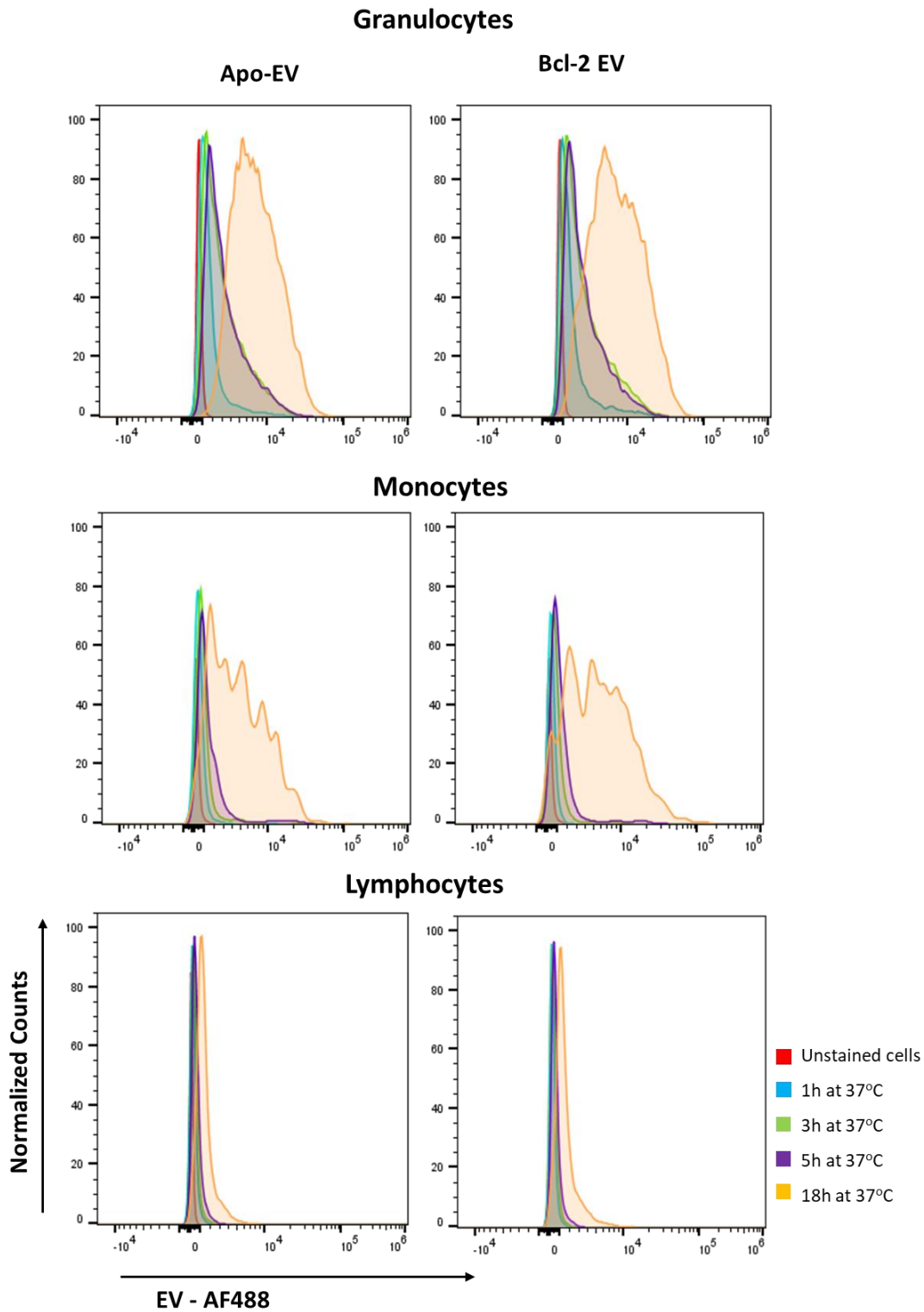
Figure 5-11. Flow cytometry fluorescence intensity histograms for blood cells interacting with EVs stained with AF488 with 10,000 EV/cell at 37oC. The histogram show data from one experiment, which is representative of the total number of independent experimental repeats (n=3).

As shown in the histograms, the biggest increase in intensity is recorded for overnight incubation of EVs with cells, and this change is evident for all cell types (erythrocytes are not presented, as there is no apparent interaction with EVs). Although the percentages of uptake shown in Figure 5-10 indicate some increase from 5h to 18h incubation, the degree to which the intensity of the signal increases is not proportional to this change in the percentage value, suggesting that the cells take EVs up continuously, therefore the EVs are accumulated in cells over time. A common feature for all the trends above is that there are no significant differences in the uptake level of Apo-EVs compared to the Bcl-2 EVs.

In order to examine the nature of interaction between the cells and EVs, and determine whether EVs are internalized or adhered on the outer surface of the plasma membrane, a series of studies has been conducted, where the co-incubation conditions are altered. As erythrocytes showed no uptake of EVs, the following measurements are made on leukocytes only. Lowering the temperature of the co-incubation to ambient (22°C) or even 4°C is used to examine the level of passive adherence and internalization, while treating the cells with trypsin/EDTA after incubation at 37°C gives the percentage of EV which are adhered on the plasma membrane via receptors or non-specific protein binding. The detailed uptake values for every condition over time are presented in the Appendix. Figure 5-12 is a summary of the calculated percent reduction of uptake of EVs for all conditions, using the uptake values at 37°C as reference (from Figure 5-10).
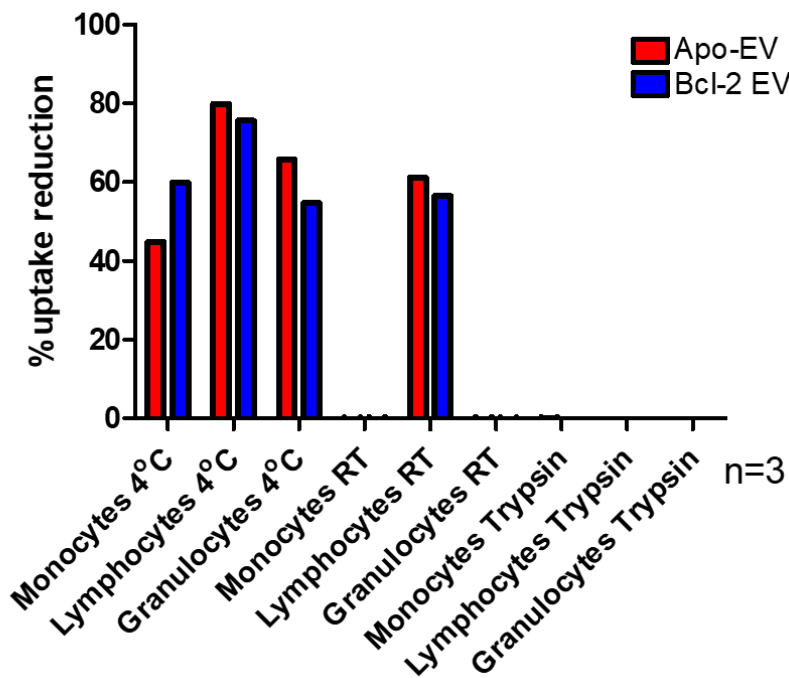
Figure 5-12. Percentage of reduction in EV uptake by white blood cells when EVs were incubated with cells for 5h at 4ºC and room temperature, or at 37ºC with trypsin treatment after uptake. The average of the % reduction of three experiments was calculated using the 37ºC at 5h uptake values obtained from Figure 5-10 (standard deviation bars not shown because the calculation was performed on the average values of the 3 experiments which were not paired in the with and without trypsin conditions).

The most significant reduction of uptake is noted for 4ºC incubation, as all types of cells see a reduction of around 50% of their uptake, with lymphocytes being affected the most. For room temperature, only lymphocyte uptake is dropping to about 60%, while granulocytes and monocytes are still interacting with EVs without a difference from 37ºC. What is also obvious is that trypsin/EDTA treatment after uptake has had no impact on the final quantity of EVs measured in cells. A positive control of trypsin/EDTA digestion, confirming the biological activity of the enzymatic reaction is shown in Figure 5-17 in the Appendix.

To confirm the localization of EVs and assess whether the vesicles are internalized, fluorescence confocal microscopy is used on the mixture of leukocytes incubated with AF488 EVs for 1h, 2h or 5h. The images from the respective time points are shown in Figure 5-13, Figure 5-14 and Figure 5-15, where the different categories of cells can be identified by the appearance of the nucleus (Dan, 2012).
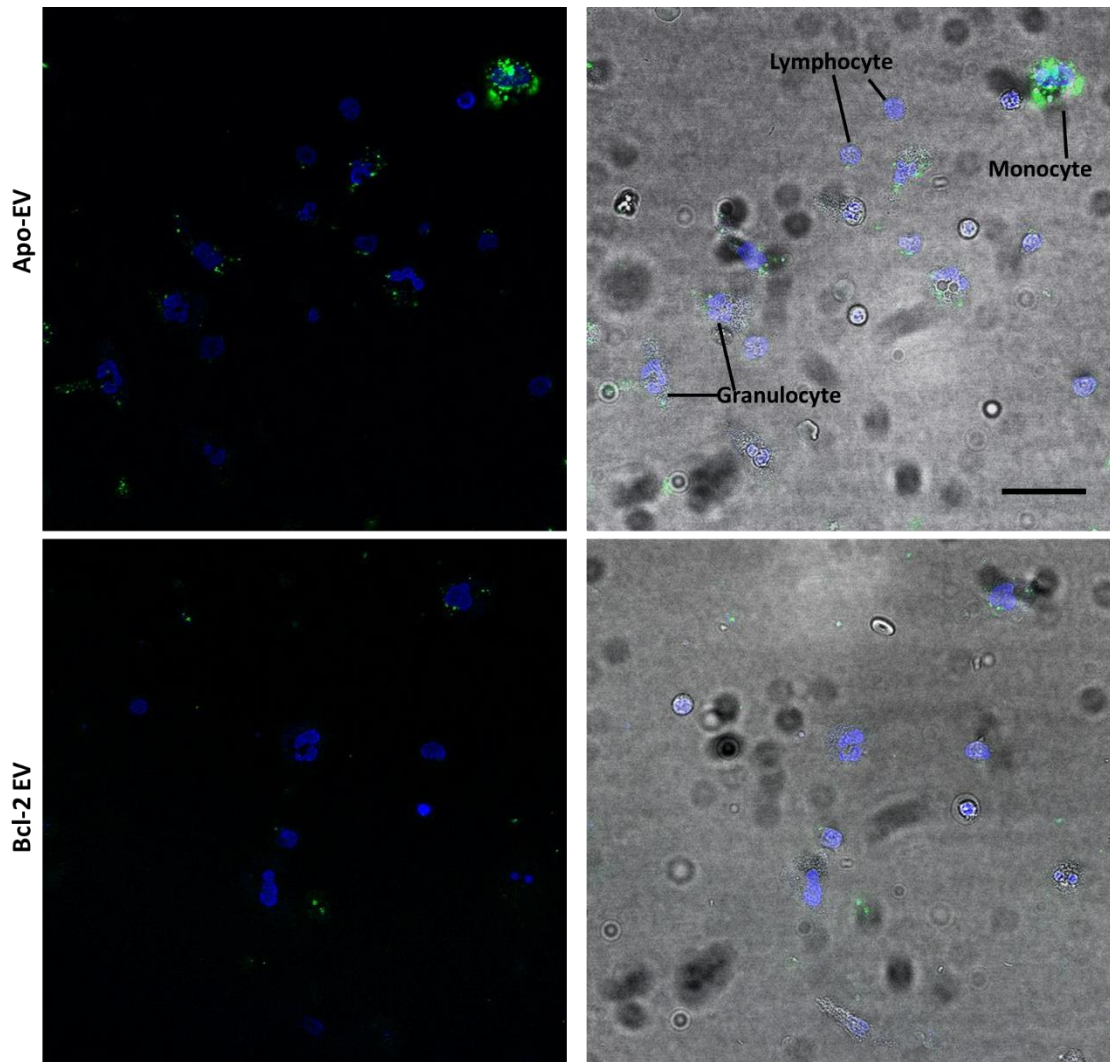
Figure 5-13. Confocal microscopy on white blood cells from 1 donor stained with nuclear stain Hoechst (blue) interacting with AF488 EVs (green) after 5h incubation at 37°C. Scale bar 30μm.
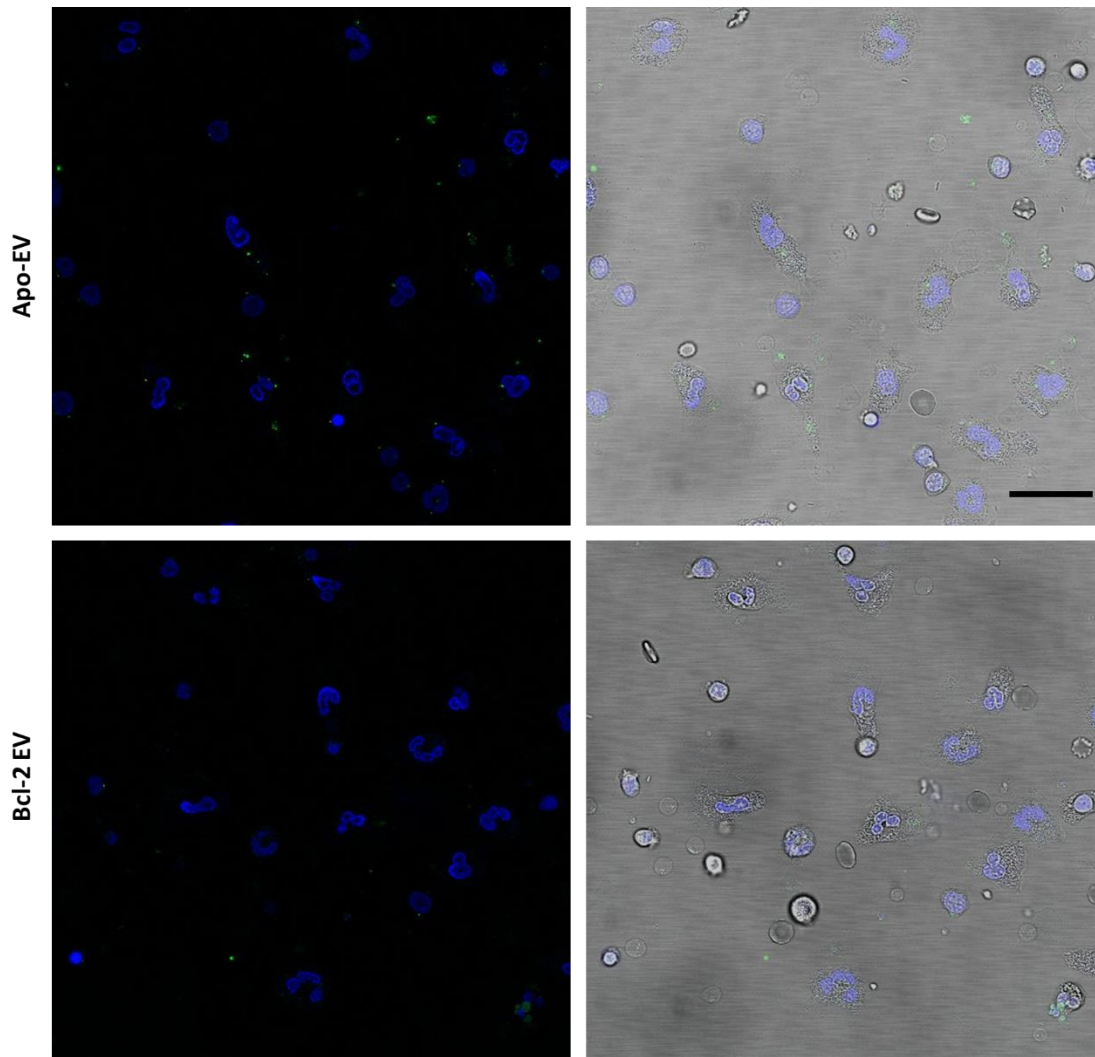
Figure 5-14. Confocal microscopy on white blood cells from 1 donor stained with nuclear stain Hoechst (blue) interacting with AF488 EVs (green) after 2h incubation at 37ºC. Scale bar 30μm.
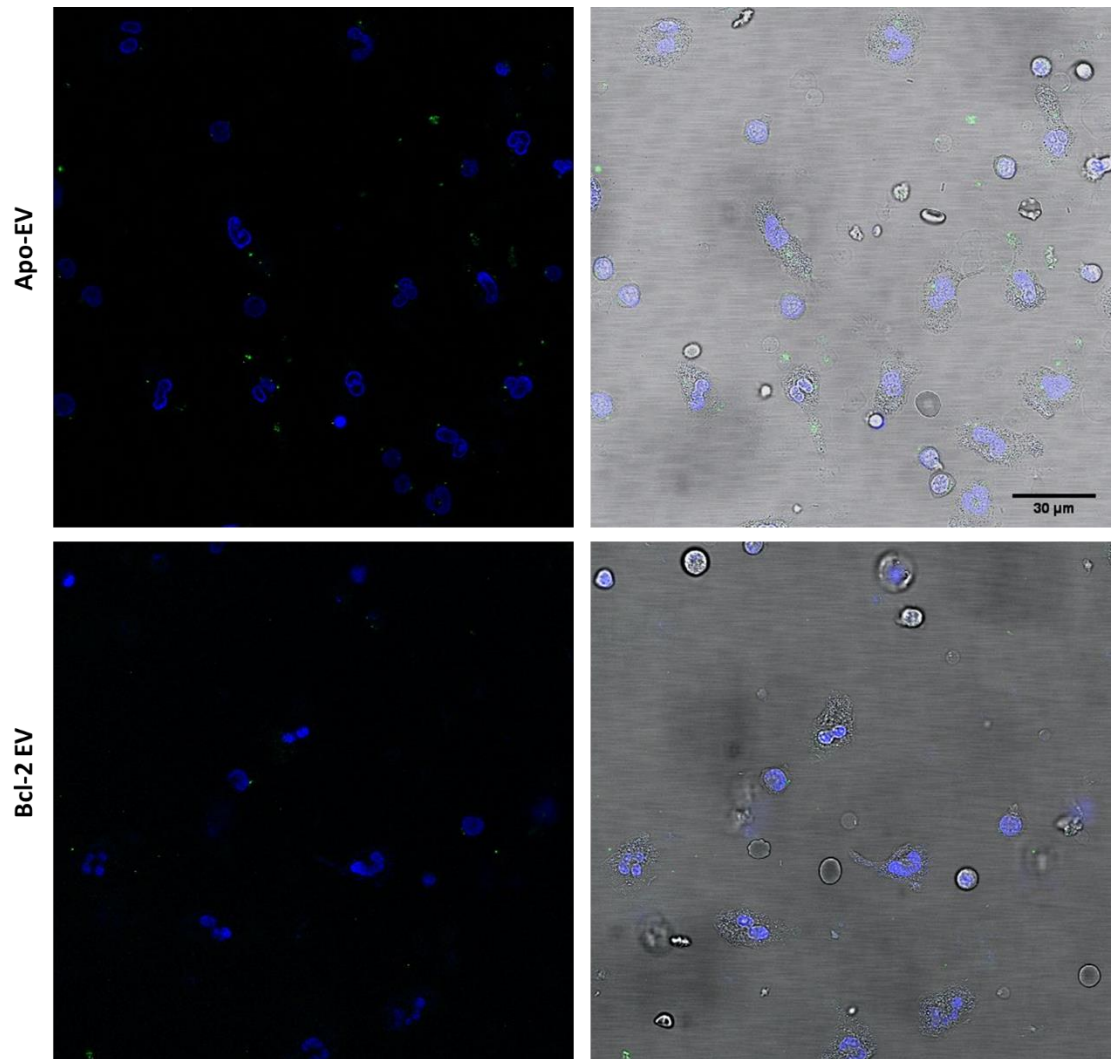
Figure 5-15. Confocal microscopy on white blood cells from 1 donor stained with nuclear stain Hoechst (blue) interacting with AF-488 EVs (green) after 1h incubation at 37ºC.

The microscopy images show that there are fewer EVs in the cells for incubation periods shorter than 5h, while for 5h the EVs are located inside the cells and closer to the nucleus. These results agree with the previous data on the trypsin-treated cells which imply that EVs are rather fused with the plasma membrane or internalized, than bound on the exterior via protein interactions.

5.4. Discussion

As a conclusion to the platelet studies, the data support that the EVs interact rapidly with the platelets and this interaction is surface binding and also internalization of the EVs, as microscopy showed. With this evidence, the secondary expression of markers delivered to platelets by EVs was examined, however, neither flow cytometry nor western blotting yielded positive results. This observation leads to the hypothesis that the transfer of protein markers might be a method not sensitive enough for analysis, therefore other molecules such as RNA can be studied, as has been shown for the case of tumour-derived RNA which has been found in platelets (Nilsson *et al.*, 2016), (Nilsson *et al.*, 2011), (Del Conde *et al.*, 2005). As shown in Chapter 4, Apo-EVs express high levels of hY4 RNA which could be potentially measured on EV-saturated platelets as a secondary signal. However, the literature suggests that the platelets also express high levels of hY4 RNA, thus, the detection of the EV contribution to this signal would not be feasible (Itoh and Reichlin, 1991). At this point, future work will need to be focused on alternative detection methods and also on potential micro RNA sequences which can be detected on platelets upon their interaction with EVs. Another result which shows contradictory data is the presence of DNA on the surface of the platelets. Flow cytometry and confocal microscopy (Figure 5-16 in the Appendix) for platelets stained with a DNA dye (Hoechst) have indicated the presence of large quantities of DNA, while the western blot with histone-3 appears negative, even for non-treated fresh platelets (control). This phenomenon can be possibly explained by the fact that circulating single-stranded DNA has been found on platelets before, therefore it is histone-3 (Dorsch, 1981). Although it is known that platelets do not carry any DNA of their own, this unexpected result proved to be of importance because it indicated this potential source of DNA contamination in other studies within our laboratory. For example, in cases where EV-derived DNA transfer to platelets is examined, it is essential to remove the surface DNA in order to avoid false positive results.

To sum this chapter up, the study of EV uptake from all blood cells has not been previously described in the literature as a whole, apart from a small number of examples where only a subset of leukocytes have been co-incubated with EVs ((Danesh *et al.*, 2014) have found that monocytes internalize red blood cell-derived EVs). Here, it has been shown that both Apo-EVs and their control vesicles, Bcl-2 EVs are taken up by platelets, granulocytes, monocytes and lymphocytes but not by erythrocytes. This observation can be starting point for further

considerations about the possible uptake mechanisms which erythrocytes lack. Moreover, the reduction in the levels of uptake as the temperature decreases indicates higher probability for an active mechanism rather than passive binding of EVs on the cell surface. It has also been confirmed that these interactions are not surface binding or non-specific attachment of EVs on the surface of a membrane, but the vesicles are transferred in the cells or platelets with a mechanism still to be examined. Those early data suggest that the cells are receiving the vesicles in an active manner, as the decrease of temperature hinders the uptake and the microscopy images show their migration towards the nucleus over time. Finally, microscopy revealed that the EVs are internalized in cells, suggesting that the Apo-EV cargo can be transferred and possibly replicated via leukocytes, providing evidence that there can be secondary Apo-EV signals in leukocytes as well as platelets. The biochemical analysis on the specific EV cargo transfer to platelets has not highlighted protein markers which can be detected as a secondary signal, however, these markers can also be RNAs, opening a new area of future studies. Acknowledging these challenges from the platelet study, and given the higher level of complexity for cells, the biochemical analyses on EV-conditioned leukocytes were not performed, as more robust markers need to be established before this step.

Appendix for chapter 5
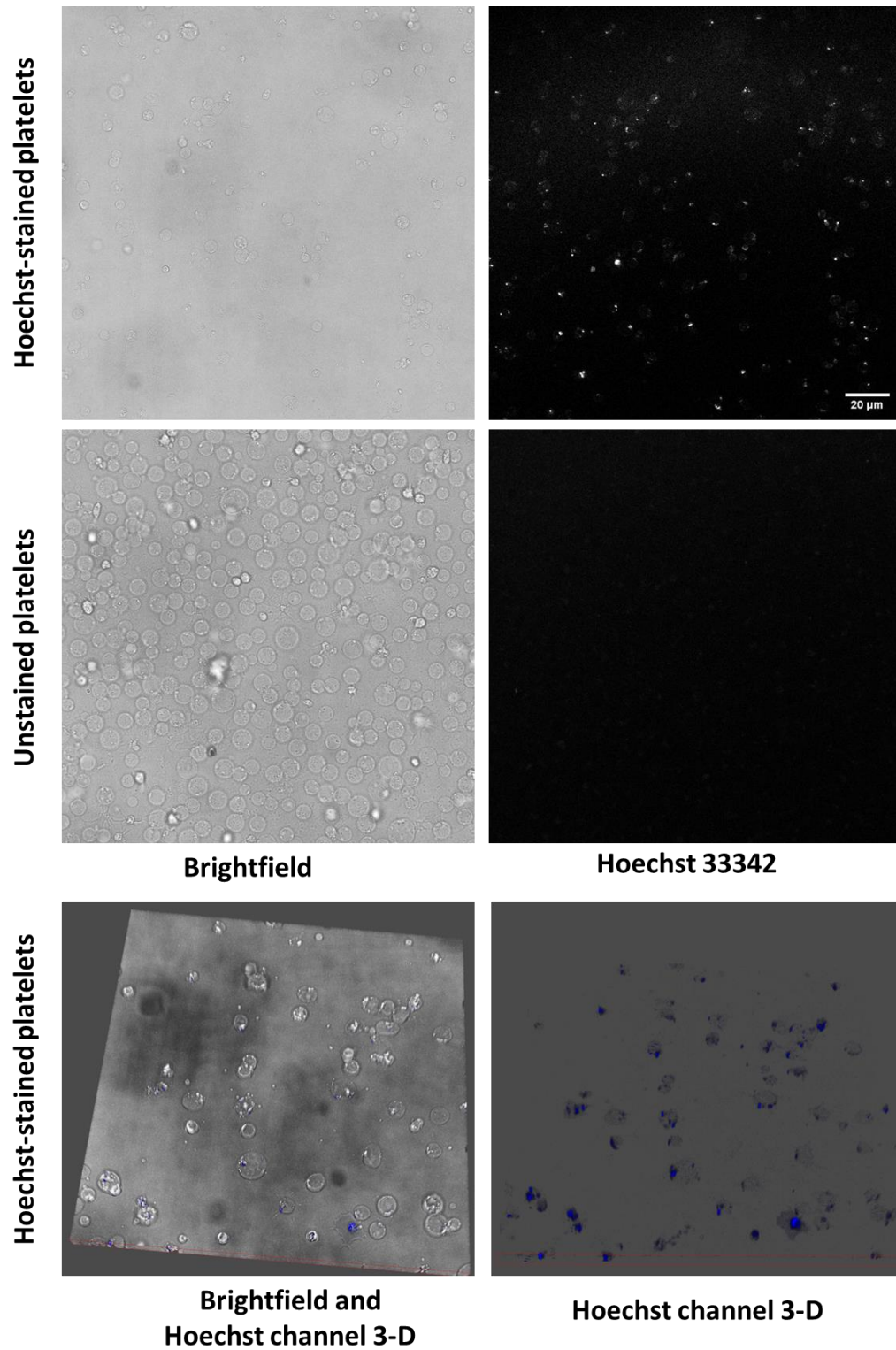
Figure 5-16. Hoechst 33342 staining on fresh platelets from 1 donor in 2-D and 3-D confocal imaging.
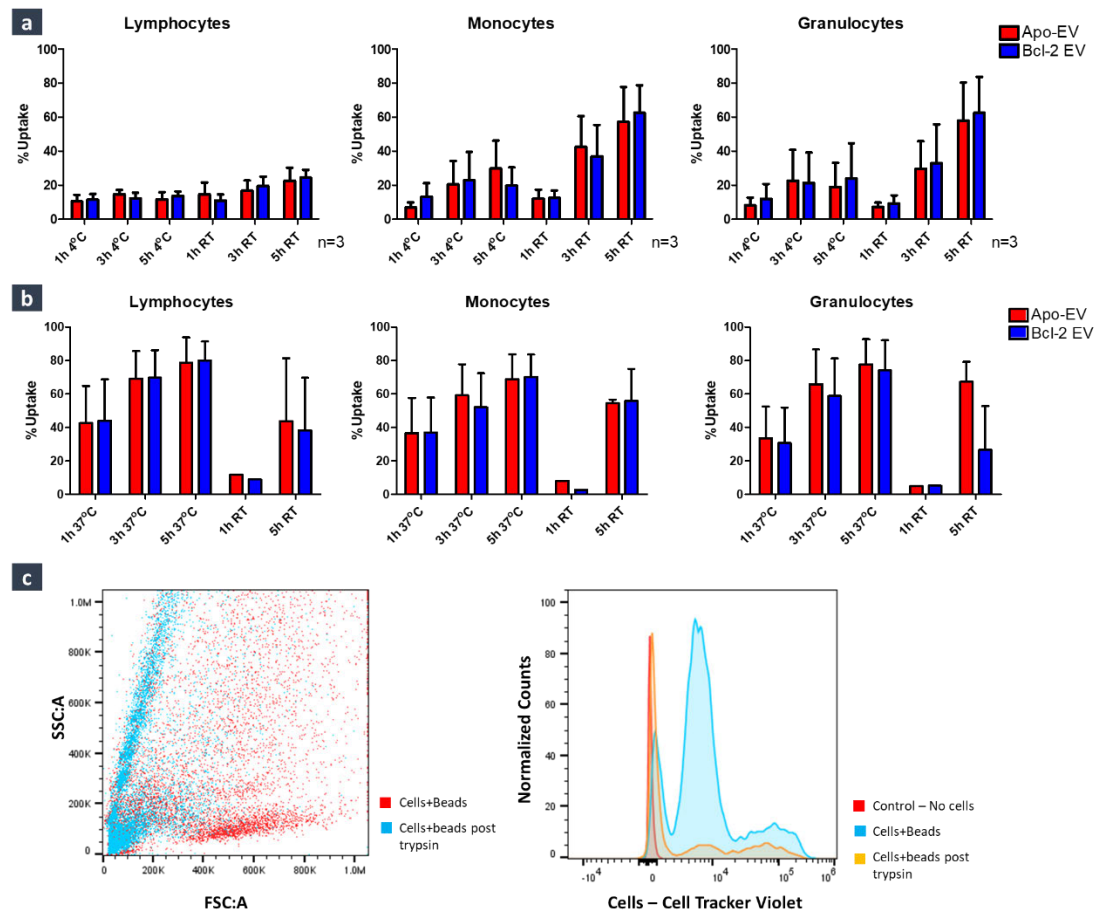
Figure 5-17. EV uptake levels for blood cells when incubated at 10,000 EV/cell for lymphocytes, granulocytes, monocytes at 4°C or toom temperature (row a) and at 37°C with trypsin treatment after uptake. Study performed by flow cytometry for AF-488 stained EVs. c) positive control for trypsin/EDTA efficiency: BL2 cells were attached on anti-CD19 magnetic beads followed by trypsin digestion of the bead-cell bonds to remove the cells from the beads. Error bars show standard deviation values from n=3 independent experiments.

6. General discussion

6.1. Thesis Objectives and Summary of Findings

The purpose of this study was to examine the distinct features of Apo-EVs derived from tumour cells as to their physical and biochemical properties and also regarding their interactions with the components of the blood (cells and platelets). Comparing those results with the non-apoptotic cell derived vesicles has highlighted some differences which can be potentially used in order to distinguish and selectively analyse Apo-EVs in the context of diagnosis and therapy. In this section, a summary of the most significant findings is presented, followed by a discussion on the future studies needed in order to bring the use of Apo-EVs to the clinic.

To begin with, the mechanism of biogenesis for Apo-EVs remains largely unknown. From the findings of this work, it is proved that the secretion pattern of Apo-EVs from cells in culture upon stimulation of apoptosis is different from the physiologically released EVs, however, the intracellular processes leading to this pattern have not been studied in this project and the literature also shows that they generally remain unexplored. One of the few examples which show the variety of Apo-EVs and highlight their different nature is the 'beads on a string' structure of apoptotic monocyte-derived bodies, described by I. Poon's group (Atkin-Smith *et al.*, 2015). In this study, the authors came across an unusual apoptotic body configuration in monocytes, which was further examined to reveal that the apoptotic bodies were connected in a linear structure generated by actomyocin contractions and the formation of apoptopodia. Another more recent example is a study on apoptotic bone marrow-derived macrophages showing that the Apo-EV formation was dependent on S1P/S1PRs signalling in the initial stages of apoptosis, followed by EV maturation in multivesicular endosomes where F-actin and CD63 were involved, among others (Park *et al.*, 2018). These mechanisms can be specifically apoptosis-related and completely different from the classical pathways such as ESCRT machinery and the EV formation from the plasma membrane, or the Apo-EVs might be formed through those mechanisms, but with different purpose and cargo, or can be a combination of all the above. This third option appears to be the most credible, as the data have suggested that a part of the Apo-EV population is very similar to the non-Apo-EVs, therefore indicating that an apoptotic cell can secrete both the

apoptosis-independent EVs (with unknown presence/levels of apoptosis-related cargo) and the Apo-EVs (loaded with Apo-related material). More specifically, the structural studies by cryoEM as well as the phenotypic investigation of a variety of protein markers (MHC class I and II, CD19, CD20 etc.) have shown very few differences between the two types of particles, which leads to the above assumption.

Considering the data acquired for size distribution and kinetics of EV release together with the cryoEM imaging and tomography and fluorescence anisotropy, it is shown that once the EV have been produced, the physical characteristics of the individual particles are not significantly different for Apo-EVs. In more detail, both EV populations under examination show similar structure under EM and a similar membrane thickness, however the quantification of the bodies with single versus multiple lamellae indicated a 10% difference between the two. Apo-EVs seem to be more single-membraned compared to the Bcl-2 EVs and this can be a potential indication about their different biogenetic origin. Also, regarding the fluorescence depolarization results, it has been observed that the membrane of the Bcl-2 EVs is less fluid than the Apo-EVs, which is another potential evidence about their different biogenesis mechanism. Similarly to the cryoEM studies, the literature shows that there is very poor reference to time-resolved fluorescence anisotropy measurements on EVs and especially on Apo-EVs, therefore comparison of the results obtained here with other groups cannot be made at this stage. Moreover, the heterogeneity of the EVs is a fundamental issue which has been faced throughout this study, but also in the general EV field (Sork, H., Corso, G., Krjutskov, 2018). It is therefore, expected that although the individual Apo-EVs might have a few unique phenotypic signatures, the sum of all EVs which are released from an apoptotic cell are probably a mixture of Apo- and non-Apo- related EV types (Figure 1-1). The persistent question is whether the Apo-EVs can be clearly discriminated from the non-Apo-related vesicles in terms of phenotype, but also whether there is a possibility for selectively sorting and purifying the Apo-EVs from a mixture of other types of EVs. Looking at the findings of this study, and keeping in mind that the differences between the two types are mainly evident by intracellular molecules such as active caspase-3 and hY4 RA, some classic sorting approaches which would involve binding on a substrate using surface markers do not seem to be possible in the near future. For instance, it has been demonstrated that tumour-derived EVs can be selectively isolated and quantified using a surface receptor the EVs

express and its binding to gold nanoparticles (Liang *et al.*, 2017). However, this might not be applicable to the Apo-EVs at this stage and with the current knowledge.

In an effort to identify EV surface targets which could be effectively used for capturing on immunomagnetic beads, the results were in some cases unexpected, as it was seen that markers abundant on EVs such as the MHC class I are not suitable for the capturing of the majority of EVs. This can be potentially explained by the steric conformation of the molecules on the EV membrane or the affinity strength of the target with the capture antibody. In contrast, although the classic exosome markers CD9, CD63 and CD81 would be expected to only capture a smaller fraction of EVs, they appear to be effective for a broader spectrum of vesicles, including the Apo-EVs. Regarding those results, as mentioned earlier, one of the general conclusions of the present work is the high degree of EV heterogeneity, even from the EV preparations which have been released by a single type of cells. The discovery of exomeres in EV preparations from B16 melanoma cells has added another level of complexity in the analysis of the EVs. Exomeres have been described as non-membranous particles which can be seperated from large or smaller EVs and show a distinct biochemical profile. Assymetric-flow field-flow fractionation isolation of the exomeres followed by proteome, lipidome and nucleic acid analysis identified unique exomere markers compared to the EVs derived from the same cell line. These results suggest that the exomeres can play a role in diseases such as cancer, therefore, understanding their biology can help the EV field to understand the effects of all types of cell-derived particles respectively (Zhang *et al.*, 2018).

However, flow cytometry using immunomagnetic complexes of EVs showed no difference in the expression levels of all markers studied on Apo-EV, although other techniques such as fluorescence microscopy (and western blotting from previous studies in the Gregory group) could highlight selective expression of markers on Apo-EV. These comparisons suggest that flow cytometry does not offer the required level of sensitivity for EV phenotyping when the differences in the expression level are small, such as in the case of histone-3. Interestingly, confocal fluorescence microscopy has proven the most sensitive method based on immunophenotyping by fluorescence, as it has revealed the selective histone-3 and active caspase-3 expression on Apo-EVs, as well as the presence of double stranded DNA.

Within the immunophenotypic studies of EV markers, an approach which does not involve fluorescence as a readout is immunogold labelling and imaging by TEM. This method offers

the highest resolution when it comes to visualising each target molecule, however the quantification of the surface marker levels did not show differences for the two populations of interest.

Finally, small RNAs are often used as EV biomarkers for several conditions and indeed, hY4 RNA was shown to be expressed in significantly higher numbers in the Apo-EVs than the Bcl-2 EVs in an RNA sequencing experiment which was also confirmed by RT-qPCR. One of the challenges of qPCR is to identify and use the appropriate genes as housekeeping controls, and these should be specific for the tissue of the sample. In addition, in the case of small RNA sequences such as the hY4 RNA, some of the classic controls such as GAPDH and other genes often used for larger RNA sequences might not be suitable, therefore it is important to seek for potential small RNAs the expression of which remains constant for all samples. Comparative results available from Dr Amy Buck's lab contributed to the selection of these controls and it was shown that upon establishing a standard protocol for the technique, a large number of samples can be analysed with the same template, therefore RT-qPCR is considered a method of great value to the clinics, especially for EVs.

The functional studies of Apo-EVs in blood cells and platelets have shown that both types of vesicles studied here interact strongly with platelets and white blood cells (monocytes, lymphocytes and granulocytes), although their uptake by red blood cells has not been confirmed. Interestingly, looking at the mechanisms EVs use to interact with these components, fluorescence microscopy showed that both for platelets and white cells, pre-stained EVs are found internalized and also bound on the surface, which appears to be a time-dependent process. In addition, measuring the uptake under the effect of several conditions such as reduced incubation temperature and trypsinization of the EVs from the surface of cells after uptake have indicated a rather active mode of uptake, therefore passive and non-specific binding are considered less likely to occur. Those observations increase the probability for transfer of Apo-related material in those cells and opens the field of Apo-EV biomarker detection in blood cells and platelets besides circulating EVs alone. Preliminary studies on the transfer of Apo-EV markers in platelets have not indicated a clear increase of the tested Apo-EV markers in the EV-treated platelets, however this is an area which requires additional studies, as the references from the literature mainly focus on non-apoptotic cell derived EVs. For example, it has been shown that neutrophil-derived EVs can cross-interact with platelets, orchestrating anti-bacterial immune response (Rossaint *et al.*, 2016), while

vesicles released from monocytes or macrophages contain tissue factor which upon fusion with activated platelets, enables coagulation (Del Conde *et al.*, 2005).

A variety of analytical techniques has been used for the analysis of EVs, and by comparing the data and the general characteristics of these methods, some conclusions can be drawn on the suitability of each approach depending on the desired outcome. A distinction which can be immediately made on these methods is their application in the clinical or research laboratories. TEM and especially cryoEM, fluorescence anisotropy, western blotting and confocal microscopy are methods which are rarely found in the majority of the clinical laboratories, while the time of measurement and data analysis is relatively long. In contrast, the most rapid measurements can be conducted by flow cytometry, NTA, DLS and qPCR, and especially flow cytometry and qPCR are methods which are used more often in clinics.

A second point for consideration for the selection of the method is whether single vesicle is required, or whether bulk analysis is sufficient. Only a small number of methods can provide with structural or phenotypic information on individual particles, which are super resolution microscopy, electron microscopy and potentially NTA for unstained particles - or as a variation of the technique, NTA where EVs are stained with a fluorescent reporter and dual imaging determines the levels of the marker on each vesicle. The majority of the methods discussed in this work such as qPCR and DLS for example, are applied on a sample consisting of a mixture of EVs, therefore the resolution is lower, but they can provide with robust data on the general characteristics of an EV population such as the Apo-EVs.

Moreover, as shown in in the Introduction (Figure 1-9), not all of these methods are applicable to the full size spectrum of the EVs, therefore the selection of the mode of analysis needs to be studied carefully, considering the subset of EVs of interest.

In general, it was found that Apo-EVs differ from the non-Apo-EVs in a number of features. Their structure reveals a clear difference in diameter, as Apo-EVs are larger than the vesicles not related to apoptosis, as well as a tendency for the formation of multiple lamellas in Bcl-2 EVs. Qualitatively, however, the structure of the vesicles in the two populations appears very similar, as shown by cryo electron tomography. The kinetics of secretion from cells is another point where Apo-EVs differ from control EVs, as cells rapidly increase the number of released vesicles as apoptosis progresses, which can be used as a potential apoptosis indicator in the number of EVs isolated from patients' blood.

Biochemical analysis of Apo-EVs has highlighted the presence of active caspase-3, histone-3 and hY4 RNA in higher levels than Bcl-2 EVs, which can be the first biomarkers to be potentially used as a starting point for further studies.

Functionally, and looking at how EVs interact with the circulating blood cells and platelets, there are no apparent indications of effects occurring specifically due to Apo-EV, but there is evidence that this area can provide with interesting results, as it has been confirmed that EVs are internalized in leukocytes and platelets.

6.2. Future work

A common point arising from all the analyses conducted in this work is the fact that the vesicles used throughout the experiments are prepared from BL2 cells, therefore all the results correspond to this particular cell line and it is unknown whether the same trends are maintained among vesicles from other tissues. Comparing the findings from several cell lines could provide with interesting conclusions about the structural and biochemical characteristics of the Apo-EVs. Especially in the case of malignant versus physiological EVs and Apo-EVs, the markers or signature nucleic acids can differ, therefore detection for diagnostic procedures needs to be tailored to the specific tissue (Kosaka, N., Kogure, A., Yamamoto, 2019). Those EVs differ not only on the level of biochemical characteristics, but also regarding functional properties, as it is generally believed that physiological EVs can have roles within metabolic pathways and signalling crosstalk among cells, while cancer-derived vesicles mainly facilitate tumour growth by supporting angiogenesis or the formation of metastatic niches, for example (Nieuwland and Sturk, 2010; Minciacchi, Freeman and Di Vizio, 2015).

Moreover, this thesis can serve two basic purposes: the first is the use by researchers for the continuation of Apo-EV related studies and the second and more translationally important is the contribution to the development of a platform which can be applied in the clinic. The *in vitro* findings of this study provide with a variety of information about the nature and the behaviour of Apo-EVs regarding their physicochemical, biochemical characteristics as well as the degree to which they interact with components of the blood once they are in circulation. This knowledge can be used as a starting point for further investigations and assist with the process of understanding their function in cancer. In addition, a number of methods and

protocols have been adjusted or created *de novo* for the purpose of EV analysis, such as the fluorescence anisotropy measurements, the flow cytometry on immunomagnetic beads, fluorescence microscopy and immunogold staining protocols. These methods can be re-used on the basis of EV analysis, accelerating the pace of EV studies in the future.

On the other hand, applying the key results of this study on a healthcare solution which could be used for patients would add tremendous value to this research, as it could help tackling cancer. For this purpose, future work would include the introduction of patient samples and samples from *in vivo* studies which would provide with information about how the Apo-EVs can be eventually detected from body fluids as diagnostic or prognostic markers or how they are related to the different stages of the disease. Therefore, it would be relevant to repeat some of the analytical procedures presented in the previous chapters, using *in vivo* produced EVs and observe the trends and characteristics of these populations.

As discussed in the Introduction, for some tumours the levels of apoptosis can suggest the staging of the disease and therefore assist clinicians shape the next steps of the therapeutic procedures. However, the direct measurement of apoptosis in the tumour tissue cannot yet be achieved in a non-invasive procedure, therefore this assessment is currently impossible. Measuring the Apo-EVs in blood is a non-invasive method of assessing the levels of apoptosis in the tissue, as those would be reflected by the Apo-EV levels throughout the various stages of the disease. In order to achieve an analytical platform sensitive and selective for the particular tumour Apo-EVs, it is essential to establish robust Apo-EV markers which can give reliable results and exclude all other physiological Apo-EVs related to non-cancerous tissue. The present *in vitro* studies have highlighted a small number of potential Apo-specific markers, however it is important to acknowledge that these measurements were conducted on pure populations prepared by a single cell line, without interference from EV of other tissues. Although little is known about how the vesicles and specifically Apo-EVs released by solid cancerous tissues enter the bloodstream, given the indications on the rapid clearance of smaller EVs by the liver and the lungs, one would expect that the larger the particle, the faster it will be removed from the circulation (Matsumoto *et al.*, 2020). With this in mind, the significance of Apo-EV study in patients or tumour-bearing animals' blood is highlighted.

In vivo, it is likely that the co-isolation of EVs from other cells could alter the degree of sensitivity needed, or might highlight other markers besides the ones identified in this study,

thus it is important to assess those parameters and evaluate the potential of the Apo-EV markers in biological samples. For example, it is possible that active caspase-3 and hY4-RNA are loaded on EVs from multiple tissues, rendering the selective detection of the tumour-derived Apo-EVs more challenging, and the results would depend on the sensitivity of the analysis. In such cases, more than one marker would be necessary for the sorting and measurement of tumour Apo-EVs (multiplexed platform) in order to exclude interference from non-cancer EV.

Another potential issue could arise from the clearance of EVs from the circulation, which could result in significant losses of EV numbers, and depending on the kinetics of this process, this could mean that the time of sampling would have an impact on the number of EVs available for measurement. In contrast, other markers could be highlighted, or the analysis could be even more simple, supposing that the stages of the tumour could be assessed only by the quantification of the total EV number. In addition, looking at the uptake tendency of EVs by the leukocytes, the question of EV numbers versus cell numbers arises, as if one assumes that all circulating EVs get fused with cells, the amount of remaining available EVs for diagnostic detection will be insufficient. As mentioned in the Introduction, and although the numbers of circulating EVs varies hugely not only between donors but also between healthy versus diseased individuals, a very rough estimation of the range of EVs would yield around 10^{10} particles/ml (Johnsen $et\ al.$, 2019). With the number of leukocytes being around $5*10^6$/ml and platelets around $300*10^6$/ml in healthy donors (Dean L., 2005), it can be seen that there is a 10^4-fold excess of EVs, which can mean that there is high probability that there will be available EVs for measurement, even after interaction with the above components. All the above points can only be addressed by the performance of i$n\ vivo$ studies initially on animal models and subsequently in the clinics, and those findings will be crucial for the design and development of a final diagnostic procedure or device.

As mentioned in the Introduction, one of the main reasons why cancer management and prevention still remain unresolved issues to date is late diagnosis. Such is the case for Burkitt's lymphoma, which is a highly curable cancer when it is diagnosed at early stages (Fayad $et\ al.$, 2011). It is also a fact that there are high rates of this particular type of cancer in regions of Africa and a large percentage of the patients are children, as well as elderly patients (Orem $et\ al.$, 2007). With these data in mind, the need for a diagnostic tool with low

invasiveness and of low cost, designed to be transported and used in places with minimum infrastructure is emerging.

Microfluidics-based technologies are being continuously evolved over biological and analytical applications, and especially in the field of EV detection. In most cases, these involve the capturing and separation of EVs on a solid substrate surface localized within a microfluidic compartment. The analytes can be detected by a variety of different methods depending on the desired readout signal. For instance, nucleic acids can be amplified on-chip with PCR-based methods (Chiriacò *et al.*, 2018), (Ko, Carpenter and Issadore, 2016).

EV enrichment for mRNA recovery and subsequent analysis has been achieved specifically for tumour-derived EVs using a mixture of capture antibodies. The device was applied on blood-derived EVs from glioblastoma patients and the RNA analysis confirmed the detection of EGFRvIII mutation, a glioblastoma biomarker (Reátegui *et al.*, 2018) (Chen *et al.*, 2010).

The miniaturization of EV capture and detection processes on microfluidic chips has promoted research towards the development of hand-held analysis devices, and the literature provides examples of the potential utility of these platforms for the analysis of (Apo)-EVs (Ko *et al.*, 2016). Below is presented a hypothetical 'prototype' of the key mechanical parts of a point-of-care blood test device for the diagnosis of non-Hodgkin lymphoma (Figure 6-1). Based on the results of the present work, the first compartment can be dedicated to the selective capture of EVs of the tumour tissue of interest using the relevant cocktail of capture probes (CD19) and the RNA extraction, followed by the second compartment where RNA amplification can take place (hY4 RNA) (more details in the figure legend).
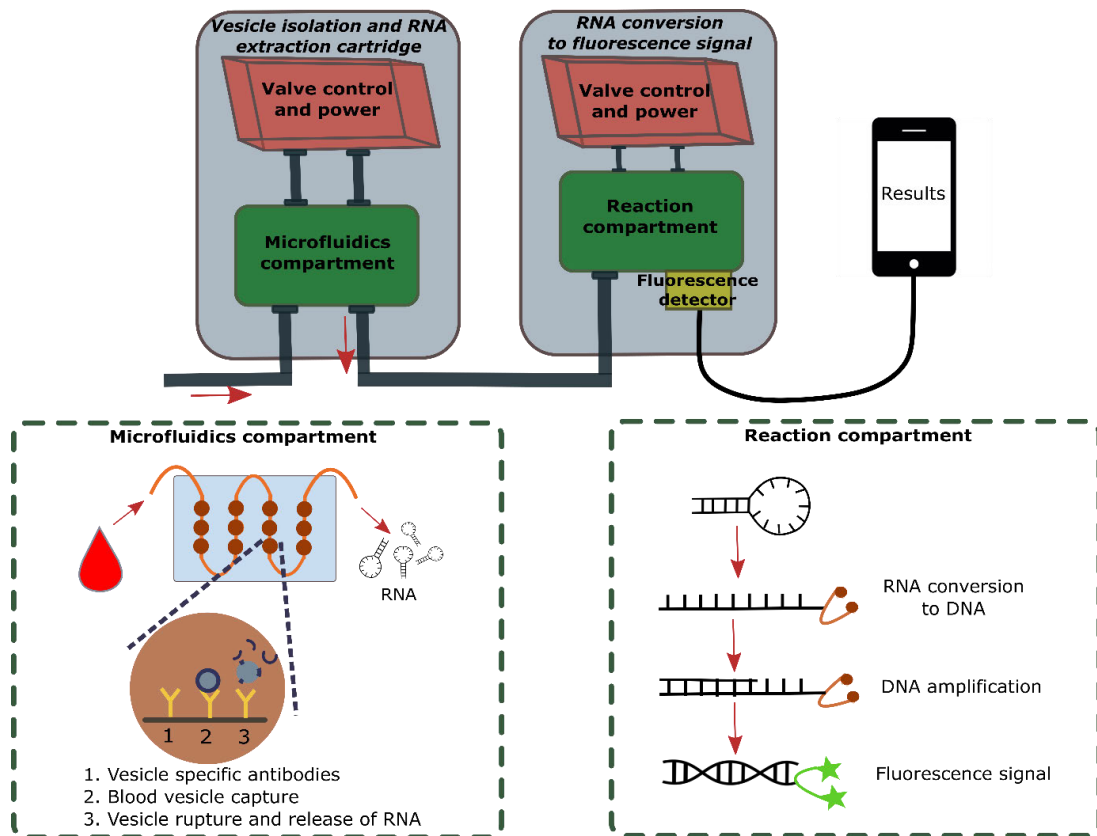
Figure 6-1. Simplified schematic representation of an EV analysis point-of-care device. The device consists of two main compartments: a) the vesicle isolation and RNA extraction cartridge (top left) where the blood sample is inserted and processed in order to extract RNA from EVs and b) the RNA to fluorescence conversion compartment (top right), where the purified RNA is amplified and measured. The readout from the fluorescence detector is transferred to another portable electronic device for further evaluation by the operator. Details on the procedure are shown in the perforated boxes at the bottom: the microfluidics compartment (bottom left) and the RNA conversion compartment (bottom right).

Besides the direct EV analysis from biological samples, another stream which can be potentially followed in order to assess the presence of Apo-EVs in the blood is by utilizing their ability to interact with blood cells and platelets. To achieve this, a set of analyses which can improve our understanding of the specific molecular patterns occurring on/in cells due to their interaction with Apo-EVs includes -omics sequencing for several biomolecule categories such as RNA, proteins etc. In this work, data from previous protein and RNA sequencing on EVs have been used as a guide to the evaluation of Apo-related markers, however, this analysis could be expanded to EV-treated platelets and blood cells. With data proving that Apo-EVs strongly interact with all components of the blood except for erythrocytes, performing total RNA sequencing on those cells upon EV treatment could reveal potential sequences which are altered under the effect of Apo-EV uptake. An example

of this transfer of material to components of the blood is the case of tumour-educated platelets which receive tumour RNA which can be then be detected in them (Best, Wesseling and Wurdinger, 2018). Regarding the Apo-EVs, the respective markers could be subsequently used as secondary markers of Apo-related activity in the blood, moving the analysis from individual EVs to cells or platelets. In other words, the existence of secondary markers on cells can simplify the analytical workflow, as the isolation of cells is a standard procedure most clinical laboratories already perform, avoiding the additional step of vesicle isolation.

Finally, the above platforms for EV analysis in patient samples have been described here in the context of apoptosis and its diagnostic/prognostic use in Burkitt's lymphoma. However, similar approaches could possibly apply to other types of cancer with high levels of apoptosis or even other diseases which release vesicles related or unrelated to cell death. EVs have proved to be versatile carriers of information and with the use of appropriate markers, vesicle detection can be useful for a number of purposes. For example, by adapting the reaction parts of the microfluidics platform presented earlier to the particular EV reagents, the analysis can be expanded beyond lymphoma, ensuring low invasiveness and flexibility.

6.3. Philosophical considerations

As this thesis has been dedicated to cancer management, it is important to consider that there is currently a wide variety of therapeutic approaches for several types of cancer, and looking at the lists of available medicinal agents used globally, it could be assumed that those solutions would suffice. However, it is observed that cancer continues to be one of the leading causes of death and this contradicts the number of the approved medicinal treatments. One of the reasons why most medicines are unsuccessful for a large percentage of patients is the high degree of heterogeneity of the disease in among individuals. The scientific community are increasingly stressing out the importance of precision medicine, which highlights the need for individualized assessment of the disease in order to deliver personalized therapy supporting that general treatment schemes applied to all patients are ineffective or cause adverse responses due to this heterogeneity. The administration of therapeutics at an individualized pattern with the appropriate doses and timings could improve response and finally overall survival (Whitcomb, 2012). Of course, bringing personalized tests to all patients requires the establishment of robust biomarkers, and this

is where Apo-EVs can appear useful in order to evaluate the levels of apoptosis and subsequently the stage and progression of the tumour. In addition, early detection by non-invasive means is key to improved outcomes in the community, both with respect to the patient's survival and quality of life, but also financially for the healthcare systems.

As a final comment on this work, if one focuses on what remains unknown about the Apo-EVs and EVs in general, those questions lead to the fundamental principles of the physical world, to which science has no answers yet. Quantum physicists have long debated about how a phenomenon evolves in reality, versus how it appears when it is measured. With initial observations that some events cannot be precisely measured, but one can only look at the probability that the event will happen in a certain way, Everett - based on Schrödinger's initial work - was one of the first to describe that the physical world is oscillating in 'many worlds' states, indicating that what the observer measures is only one of the probable states of the system. In other words, the famous Schrödinger wave function (fundamental for quantum physics) suggests a continuous oscillation for the states of a system which are independent from external parameters. However, when the observer decides to measure a variable of this system, the system becomes entangled with the observer and the wave function collapses to a single point, therefore the observer is only measuring this single point, ignoring the rest of the probable states (Everett *et al.*, 1957). Having those theories in mind, it is unavoidable to wonder how the quantum effects can exist beyond the sub-atomic world and affect the nano-world of vesicles and the measurements of several parameters. If there is no single state for a system and it is rather split in 'many worlds', then how can science ever make safe conclusions about any hypothesis, and if what is measured is only one probable outcome, then will we ever able to understand why some systems 'decide' to evolve in a certain direction, where the probabilities increase for this state and not for others? These considerations also bring another issue to the surface, which is the extent to which human senses can understand the world.

Technology has helped overcoming limitations related to measuring nano-sized entities which are not noticed by the human sensory organs such as the eyes, but all measuring devices, as well as their outcomes have been created for the human standards. Therefore, how can one be certain that measuring all these parameters can still give a safe representation of what actually exists in the nano-world (not to mention the sub-atomic

world)? These thoughts can be summarized in the Greek philosopher Socrates' saying: 'I know that I know nothing', or 'εν οίδα ότι ουδέν οίδα', as spelled in the original language.

The answer to these questions is not known yet, but until an explanation is found (if ever), the only option for medical scientists is to continue researching with the available means. As it has been proven in several occasions, achievements in medical sciences have led to significant improvement in the lives of millions of people, and it is one of the scientists' duties to ensure that these advances can be enjoyed by all, equally.

References

Admyre, C. *et al.* (2003) 'Exosomes with major histocompatibility complex class II and co-stimulatory molecules are present in human BAL fluid', *European Respiratory Journal*, 22(4).

Admyre, C. *et al.* (2007) 'Exosomes with immune modulatory features are present in human breast milk.', *Journal of immunology (Baltimore, Md. : 1950)*. American Association of Immunologists, 179(3), pp. 1969–78. doi: 10.4049/JIMMUNOL.179.3.1969.

Akers, J. C. *et al.* (2013) 'Biogenesis of extracellular vesicles (EV): exosomes, microvesicles, retrovirus-like vesicles, and apoptotic bodies', *Journal of Neuro-Oncology*. Springer US, 113(1), pp. 1–11. doi: 10.1007/s11060-013-1084-8.

Akers, J. C. *et al.* (2016) 'Comparative Analysis of Technologies for Quantifying Extracellular Vesicles (EVs) in Clinical Cerebrospinal Fluids (CSF).', *PloS one*. Public Library of Science, 11(2), p. e0149866. doi: 10.1371/journal.pone.0149866.

Almizraq, R. J., Holovati, J. L. and Acker, J. P. (2018) 'Characteristics of Extracellular Vesicles in Red Blood Concentrates Change with Storage Time and Blood Manufacturing Method', *Transfusion Medicine and Hemotherapy*, 45(3), pp. 185–193. doi: 10.1159/000486137.

Antounians, L. *et al.* (2019) 'The Regenerative Potential of Amniotic Fluid Stem Cell Extracellular Vesicles: Lessons Learned by Comparing Different Isolation Techniques', *Scientific Reports*. Nature Publishing Group, 9(1). doi: 10.1038/s41598-018-38320-w.

Arraud, N. *et al.* (2014) 'Extracellular vesicles from blood plasma: Determination of their morphology, size, phenotype and concentration', *Journal of Thrombosis and Haemostasis*, 12(5), pp. 614–627. doi: 10.1111/jth.12554.

Atkin-Smith, G. K. *et al.* (2015) 'A novel mechanism of generating extracellular vesicles during apoptosis via a beads-on-a-string membrane structure', *Nature Communications*. Nature Publishing Group, 6(1), pp. 1–10. doi: 10.1038/ncomms8439.

Atkin-Smith, G. K. *et al.* (2017) 'Isolation of cell type-specific apoptotic bodies by fluorescence-activated cell sorting', *Scientific Reports, 7, art. no. 39846*.

Atkin-Smith, Georgia K. *et al.* (2016) 'Disassembly of the Dying: Mechanisms and Functions', *Trends in Cell Biology*. Elsevier, 0(0), pp. 7439–11. doi: 10.1016/j.tcb.2016.08.011.

Aubertin, K. *et al.* (2016) 'Massive release of extracellular vesicles from cancer cells after photodynamic treatment or chemotherapy', *Scientific Reports*. Nature Publishing Group, 6(1), p. 35376. doi: 10.1038/srep35376.

Bachurski, D. *et al.* (2019) 'Extracellular vesicle measurements with nanoparticle tracking analysis–An accuracy and repeatability comparison between NanoSight NS300 and ZetaView', *Journal of Extracellular Vesicles*. Taylor and Francis Ltd., 8(1). doi: 10.1080/20013078.2019.1596016.

Baranyai, T. *et al.* (2015) 'Isolation of exosomes from blood plasma: Qualitative and quantitative comparison of ultracentrifugation and size exclusion chromatography methods', *PLoS ONE*, 10(12), pp. 1–13. doi: 10.1371/journal.pone.0145686.

Barclay, A. *et al.* (1997) *The Leucocyte Antigen Factsbook*. London: Academic Press.

Barok, M. *et al.* (2018) 'Cancer-derived exosomes from HER2-positive cancer cells carry trastuzumab-emtansine into cancer cells leading to growth inhibition and caspase activation.', *BMC cancer*, 18(1), p. 504. doi: 10.1186/s12885-018-4418-2.

Ben-Dov, N. and Korenstein, R. (2013) 'Proton-induced endocytosis is dependent on cell membrane fluidity, lipid-phase order and the membrane resting potential', *Biochimica et Biophysica Acta - Biomembranes*, 1828(11), pp. 2672–2681. doi: 10.1016/j.bbamem.2013.07.027.

Berard, C., G. T. O'Conor, L. B. Thomas, H. T. (1969) 'Histopathological definition of Burkitt's tumour.', *Bulletin of the World Health Organization*, 40(4), pp. 601–7. Available at: http://www.ncbi.nlm.nih.gov/pubmed/5306724 (Accessed: 25 November 2019).

Bergsmedh, A. *et al.* (2001) 'Horizontal transfer of oncogenes by uptake of apoptotic bodies.', *Proceedings of the National Academy of Sciences of the United States of America*. National Academy of Sciences, 98(11), pp. 6407–11. doi: 10.1073/pnas.101129998.

Best, M. G., Wesseling, P. and Wurdinger, T. (2018) 'Tumor-Educated Platelets as a Noninvasive Biomarker Source for Cancer Detection and Progression Monitoring', *Cancer Research*. American Association for Cancer Research, 78(13), pp. 3407–3412. doi: 10.1158/0008-5472.CAN-18-0887.

Bhattacharjee, S. (2016) 'DLS and zeta potential - What they are and what they are not?', *Journal of Controlled Release*. Elsevier B.V., 235, pp. 337–351. doi: 10.1016/j.jconrel.2016.06.017.

Birch, D. J. S., Chen, Y. and Rolinski, O. J. (2015) 'Biological and Medical Photonics, Spectroscopy and Microscopy Vol 4. Photonics', *Biological and Medical Photonics, Spectroscopy and Microscopy Vol 4. Photonics*, IV(Chapter 1 Fluorescence), pp. 1–56.

Birch, D. J. S., Holmes, A. S. and Imhof, R. E. (1988) 'PPO excimers in lipid bilayers studied using single-photon timing array detection', *Chemical Physics Letters*, 148(5), pp. 435–444.

Bisby, R. H. and Birch, D. J. S. (1989) 'A time-resolved fluorescence anisotropy study of bilayer membranes containing alpha-tocopherol.', *Biochem Biophys Res Commun.*, 158(2), pp. 386–391.

Blair, T. A., Michelson, A. D. and Frelinger, A. L. (2018) 'Mass Cytometry Reveals Distinct Platelet Subtypes in Healthy Subjects and Novel Alterations in Surface Glycoproteins in Glanzmann Thrombasthenia', *Scientific Reports*. Nature Publishing Group, 8(1), pp. 1–13. doi: 10.1038/s41598-018-28211-5.

Bobrie, A. *et al.* (2011) 'Exosome Secretion: Molecular Mechanisms and Roles in Immune Responses', *Traffic*. Blackwell Publishing Ltd, 12(12), pp. 1659–1668. doi: 10.1111/j.1600-0854.2011.01225.x.

Böing, A. N. *et al.* (2013) 'Active caspase-3 is removed from cells by release of caspase-3-enriched vesicles', *Biochimica et Biophysica Acta - Molecular Cell Research*. Elsevier, 1833(8), pp. 1844–1852. doi: 10.1016/j.bbamcr.2013.03.013.

Böing, A. N. *et al.* (2014) 'Single-step isolation of extracellular vesicles by size-exclusion chromatography', *Journal of Extracellular Vesicles*. Co-Action Publishing, 3(1). doi: 10.3402/jev.v3.23430.

Boukouris, S. and Mathivanan, S. (2015) 'Exosomes in bodily fluids are a highly stable resource of disease biomarkers', *Proteomics - Clinical Applications*, 9(3–4), pp. 358–367. doi: 10.1002/prca.201400114.

Bradford, M. M. (1976) 'A rapid and sensitive method for the quantitation of microgram quantities of protein utilizing the principle of protein-dye binding', *Analytical Biochemistry*. Academic Press, 72(1–2), pp. 248–254. doi: 10.1016/0003-2697(76)90527-3.

Bu, H. *et al.* (2019) 'Exosomes: Isolation, Analysis, and Applications in Cancer Detection and Therapy', *ChemBioChem*, 20(4), pp. 451–461. doi: 10.1002/cbic.201800470.

Bustin, S. A. *et al.* (2009) 'The MIQE guidelines: Minimum information for publication of quantitative real-time PCR experiments', *Clinical Chemistry*, 55(4), pp. 611–622. doi: 10.1373/clinchem.2008.112797.

Cai, J. *et al.* (2015) 'SRY gene transferred by extracellular vesicles accelerates atherosclerosis by promotion of leucocyte adherence to endothelial cells', *Clinical science (London, England : 1979)*. Portland Press Limited, 129(3), pp. 259–69. doi: 10.1042/CS20140826.

Campoy, I. *et al.* (2016) 'Exosome-like vesicles in uterine aspirates: a comparison of ultracentrifugation-based isolation protocols', *Journal of Translational Medicine*, 14(1), p. 180. doi: 10.1186/s12967-016-0935-4.

Canella, A. *et al.* (2016) 'The potential diagnostic power of extracellular vesicle analysis for multiple myeloma', *Expert Review of Molecular Diagnostics*, 16(3), pp. 277–284. doi: 10.1586/14737159.2016.1132627.

do Canto, A. M. T. M. *et al.* (2016) 'Diphenylhexatriene membrane probes DPH and TMA-DPH: A comparative molecular dynamics simulation study', *Biochimica et Biophysica Acta - Biomembranes*. Elsevier B.V., 1858(11), pp. 2647–2661. doi: 10.1016/j.bbamem.2016.07.013.

Carnell-Morris, P. *et al.* (2017) 'Analysis of Extracellular Vesicles Using Fluorescence Nanoparticle Tracking Analysis', in. Humana Press, New York, NY, pp. 153–173. doi: 10.1007/978-1-4939-7253-1_13.

Chargaff, E. and West, R. (1946) 'The biological significance of the thromboplastic protein of blood.', *The Journal of biological chemistry*, 166(1), pp. 189–197.

Chen, C. *et al.* (2010) 'Microfluidic isolation and transcriptome analysis of serum microvesicles', *Lab Chip*. Royal Society of Chemistry, 10(4), pp. 505–511. doi: 10.1039/B916199F.

Chen, C. *et al.* (2016) 'Imaging and Intracellular Tracking of Cancer-Derived Exosomes Using Single-Molecule Localization-Based Super-Resolution Microscope', *ACS Applied Materials & Interfaces*, 8(39), pp. 25825–25833. doi: 10.1021/acsami.6b09442.

Cheruvanky, A. *et al.* (2007) 'Rapid isolation of urinary exosomal biomarkers using a nanomembrane ultrafiltration concentrator', *American Journal of Physiology-Renal Physiology*, 292(5), pp. F1657–F1661. doi: 10.1152/ajprenal.00434.2006.

Chiriacò, M. *et al.* (2018) 'Lab-on-Chip for Exosomes and Microvesicles Detection and Characterization', *Sensors*. Multidisciplinary Digital Publishing Institute, 18(10), p. 3175. doi:

10.3390/s18103175.

Choong, M. L., Yang, H. H. and McNiece, I. (2007) 'MicroRNA expression profiling during human cord blood-derived CD34 cell erythropoiesis', *Experimental Hematology*. Elsevier, 35(4), pp. 551–564. doi: 10.1016/j.exphem.2006.12.002.

Christov, C. P. *et al.* (2006) 'Functional Requirement of Noncoding Y RNAs for Human Chromosomal DNA Replication', *Molecular and Cellular Biology*, 26(18), pp. 6993–7004. doi: 10.1128/MCB.01060-06.

Christov, C. P., Trivier, E. and Krude, T. (2008) 'Noncoding human Y RNAs are overexpressed in tumours and required for cell proliferation', *British Journal of Cancer*, 98(5), pp. 981–988. doi: 10.1038/sj.bjc.6604254.

Clayton, A. *et al.* (2001) 'Analysis of antigen presenting cell derived exosomes, based on immuno-magnetic isolation and flow cytometry', *Journal of Immunological Methods*, 247(1–2), pp. 163–174. doi: 10.1016/S0022-1759(00)00321-5.

Clayton, A. *et al.* (2019) 'Considerations towards a roadmap for collection, handling and storage of blood extracellular vesicles', *Journal of Extracellular Vesicles*, 8(1), p. 1647027. doi: 10.1080/20013078.2019.1647027.

Colombo, M., Raposo, G. and Théry, C. (2014) 'Biogenesis, Secretion, and Intercellular Interactions of Exosomes and Other Extracellular Vesicles', *Annu. Rev. Cell Dev. Biol*, 30(1), pp. 255–89. doi: 10.1146/annurev-cellbio-101512-122326.

Conde-Vancells, J. *et al.* (2010) 'Candidate biomarkers in exosome-like vesicles purified from rat and mouse urine samples', *Proteomics - Clinical Applications*. WILEY-VCH Verlag, 4(4), pp. 416–425. doi: 10.1002/prca.200900103.

Del Conde, I. *et al.* (2005) 'Tissue-factor-bearing microvesicles arise from lipid rafts and fuse with activated platelets to initiate coagulation', *Blood*, 106(5), pp. 1604–1611. doi: 10.1182/blood-2004-03-1095.

Corney, D. C. *et al.* (2007) 'MicroRNA-34b and MicroRNA-34c are targets of p53 and cooperate in control of cell proliferation and adhesion-independent growth', *Cancer Research*. American Association for Cancer Research, 67(18), pp. 8433–8438. doi: 10.1158/0008-5472.CAN-07-1585.

Costa, J. (2017) 'Glycoconjugates from extracellular vesicles: Structures, functions and emerging potential as cancer biomarkers', *Biochimica et Biophysica Acta (BBA) - Reviews on Cancer*, 1868(1), pp. 157–166. doi: 10.1016/j.bbcan.2017.03.007.

Cvjetkovic, A., Lötvall, J. and Lässer, C. (2014) 'The influence of rotor type and centrifugation time on the yield and purity of extracellular vesicles', *Journal of Extracellular Vesicles*, 3(1), p. 23111. doi: 10.3402/jev.v3.23111.

Dabrowska, S. *et al.* (2018) 'Imaging of extracellular vesicles derived from human bone marrow mesenchymal stem cells using fluorescent and magnetic labels.', *International journal of nanomedicine*. Dove Press, 13, pp. 1653–1664. doi: 10.2147/IJN.S159404.

Dachary-Prigent, J. *et al.* (1993) 'Annexin V as a probe of aminophospholipid exposure and platelet membrane vesiculation: a flow cytometry study showing a role for free sulfhydryl groups.', *Blood*, 81(10), pp. 2554–65. Available at:

http://www.ncbi.nlm.nih.gov/pubmed/8490169 (Accessed: 26 March 2018).

Dai, S. *et al.* (2005) 'More efficient induction of HLA-A*0201-restricted and carcinoembryonic antigen (CEA) - Specific CTL response by immunization with exosomes prepared from heat-stressed CEA-positive tumor cells', *Clinical Cancer Research*, 11(20), pp. 7554–7563. doi: 10.1158/1078-0432.CCR-05-0810.

Dan, L. (2012) *Atlas of hematology and analysis of peripheral blood smears*, *McGraw-Hill*.

Danesh, A. *et al.* (2014) 'Exosomes from red blood cell units bind to monocytes and induce proinflammatory cytokines, boosting T-cell responses in vitro', *Blood*. American Society of Hematology, 123(5), pp. 687–696. doi: 10.1182/blood-2013-10-530469.

Davidson, J. D. (2015) 'Percoll Isolation of PMN and PBMC', in *The University of Edinburgh*. Edinburgh: The University of Edinburgh, pp. 1–9.

Dean L. (2005) 'Blood and the cells it contains', in *Blood Groups and Red Cell Antigens*. Bethesda (MD): National Center for Biotechnology Information (US). Available at: https://www.ncbi.nlm.nih.gov/books/NBK2263/.

Dejan Arzenšek (2010) 'Dynamic light scattering and application to proteins in solutions', *Ljubljana Uni press*.

Denzer, K. *et al.* (2000) 'Exosome: from internal vesicle of the multivesicular body to intercellular signaling device.', *Journal of cell science*, 113 Pt 19, pp. 3365–74. Available at: http://www.ncbi.nlm.nih.gov/pubmed/10984428 (Accessed: 24 November 2016).

Dooley, D., Simpson, J. and Meryman, H. (1982) 'Isolation of large numbers of fully viable human neutrophils: a preparative technique using percoll density gradient centrifugation', *Exp Hematol.*, 10(7), pp. 591–9.

Dorsch, C. A. (1981) 'Binding of single-strand DNA to human platelets', *Thrombosis Research*. Pergamon, 24(1–2), pp. 119–129. doi: 10.1016/0049-3848(81)90037-2.

Dragovic, R. A. *et al.* (2011) 'Sizing and phenotyping of cellular vesicles using Nanoparticle Tracking Analysis', *Nanomedicine: Nanotechnology, Biology, and Medicine*. Elsevier Inc., 7(6), pp. 780–788. doi: 10.1016/j.nano.2011.04.003.

Driedonks, T. A. P. and Nolte-T'Hoen, E. N. M. (2019) 'Circulating Y-RNAs in extracellular vesicles and ribonucleoprotein complexes; Implications for the immune system', *Frontiers in Immunology*. Frontiers Media S.A. doi: 10.3389/fimmu.2018.03164.

Dubochet, J. *et al.* (2016) 'Cryo-electron microscopy of vitrified specimens', *Q Rev Biophys.* Edinburgh College of Art, 2(1988), pp. 129–228.

Ehnfors, J. *et al.* (2009) 'Horizontal transfer of tumor DNA to endothelial cells in vivo', *Cell Death and Differentiation*. Nature Publishing Group, 16(5), pp. 749–757. doi: 10.1038/cdd.2009.7.

Elfeky, O. *et al.* (2017) 'Influence of maternal BMI on the exosomal profile during gestation and their role on maternal systemic inflammation', *Placenta*. W.B. Saunders, 50, pp. 60–69. doi: 10.1016/J.PLACENTA.2016.12.020.

van Engeland, M., Nieland, L. J. W., Ramaekers, F. C. S., Schutte, B. and Reutelingsperger, C.

P. M. (1998) 'Annexin V-Affinity assay: A review on an apoptosis detection system based on phosphatidylserine exposure.', Cytometry,.

Entrez Gene: Beta-2-microglobulin (2014) *NCBI.nih.gov*. Available at: https://www.ncbi.nlm.nih.gov/gene?cmd=Retrieve&dopt=full_report&list_uids=567.

Erdbrügger, U. *et al.* (2014) 'Imaging flow cytometry elucidates limitations of microparticle analysis by conventional flow cytometry', *Cytometry Part A*. Wiley-Blackwell, 85(9), pp. 756–770. doi: 10.1002/cyto.a.22494.

Erdbrügger, U. and Lannigan, J. (2016) 'Analytical challenges of extracellular vesicle detection: A comparison of different techniques', *Cytometry Part A*, 89(2), pp. 123–134. doi: 10.1002/cyto.a.22795.

Everett, H. *et al.* (1957) *The Many-Worlds Interpretation of Quantum Mechanics*. Princeton, NJ: Princeton University Press.

Fayad, L. E. *et al.* (2011) 'Chapter 8. Aggressive and Highly Aggressive B-Cell Lymphomas', in Kantarjian, H. M., Wolff, R. A., and Koller, C. A. (eds) *The MD Anderson Manual of Medical Oncology, 2e*. New York, NY: The McGraw-Hill Companies. Available at: http://accessmedicine.mhmedical.com/content.aspx?aid=8301790.

Fendl, B. *et al.* (2016) 'Characterization of extracellular vesicles in whole blood: Influence of pre-analytical parameters and visualization of vesicle-cell interactions using imaging flow cytometry', *Biochemical and Biophysical Research Communications*, 478(1), pp. 168–173. doi: 10.1016/j.bbrc.2016.07.073.

Filipe, V., Hawe, A. and Jiskoot, W. (2010) 'Critical evaluation of nanoparticle tracking analysis (NTA) by NanoSight for the measurement of nanoparticles and protein aggregates', *Pharmaceutical Research*, 27(5), pp. 796–810. doi: 10.1007/s11095-010-0073-2.

Ford, C. A. *et al.* (2015) 'Oncogenic properties of apoptotic tumor cells in aggressive B cell lymphoma', *Current Biology*. The Authors, 25(5), pp. 577–588. doi: 10.1016/j.cub.2014.12.059.

Gámez-Valero, A. *et al.* (2016) 'Size-Exclusion Chromatography-based isolation minimally alters Extracellular Vesicles' characteristics compared to precipitating agents', *Scientific Reports*. Nature Publishing Group, 6, p. 33641. doi: 10.1038/srep33641.

Gardiner, C. *et al.* (2016) 'Techniques used for the isolation and characterization of extracellular vesicles: Results of a worldwide survey', *Journal of Extracellular Vesicles*. Taylor and Francis Ltd., 5(1). doi: 10.3402/jev.v5.32945.

Gercel-Taylor, C. *et al.* (2012) 'Nanoparticle analysis of circulating cell-derived vesicles in ovarian cancer patients', *Analytical Biochemistry*. Elsevier Inc., 428(1), pp. 44–53. doi: 10.1016/j.ab.2012.06.004.

Gerritsen, H. C. *et al.* (2009) *Time domain FLIM: Theory, instrumentation, and data analysis*. 1st edn, *Fret and Flim Techniques*. 1st edn. Elsevier B.V. doi: 10.1016/S0075-7535(08)00003-X.

Godin, A. G., Lounis, B. and Cognet, L. (2014) 'Super-resolution microscopy approaches for live cell imaging', *Biophysical Journal*. Biophysical Society, pp. 1777–1784. doi: 10.1016/j.bpj.2014.08.028.

Gould, S. J. and Raposo, G. (2013) 'As we wait: coping with an imperfect nomenclature for extracellular vesicles.', *Journal of extracellular vesicles*. Taylor & Francis, 2. doi: 10.3402/jev.v2i0.20389.

Gracetto, A. C. *et al.* (2010) 'Unusual 1,6-diphenyl-1,3,5-hexatriene (DPH) spectrophotometric behavior in water/ethanol and water/DMSO mixtures', *Journal of the Brazilian Chemical Society*, 21(8), pp. 1497–1502.

Gray, W. D., Mitchell, A. J. and Searles, C. D. (2015) 'An accurate, precise method for general labeling of extracellular vesicles', *MethodsX*. Elsevier, 2, pp. 360–367. doi: 10.1016/J.MEX.2015.08.002.

Gregory, C. D., Ford, C. A. and Voss, J. J. L. P. (2016) 'Microenvironmental Effects of Cell Death in Malignant Disease.', *Advances in experimental medicine and biology*, 930, pp. 51–88. doi: 10.1007/978-3-319-39406-0_3.

Gregory, C. D. and Pound, J. D. (2010) 'Microenvironmental influences of apoptosis in vivo and in vitro', *Apoptosis*, 15(9), pp. 1029–1049. doi: 10.1007/s10495-010-0485-9.

Gregory, C. D. and Pound, J. D. (2011) 'Cell death in the neighbourhood: Direct microenvironmental effects of apoptosis in normal and neoplastic tissues', *Journal of Pathology*, 223(2), pp. 177–194. doi: 10.1002/path.2792.

Grizzle, W. E. and Zhang, H.-G. (2013) 'The Effects of Exosomes and Related Vesicles on Cancer Development, Progression, and Dissemination', in *Emerging Concepts of Tumor Exosome–Mediated Cell-Cell Communication*. New York, NY: Springer New York, pp. 107–129. doi: 10.1007/978-1-4614-3697-3_5.

György, B. *et al.* (2015) 'Therapeutic Applications of Extracellular Vesicles: Clinical Promise and Open Questions', *Annual Review of Pharmacology and Toxicology*. Annual Reviews, 55(1), pp. 439–464. doi: 10.1146/annurev-pharmtox-010814-124630.

Hannafon, B. N. and Ding, W. Q. (2013) 'Intercellular communication by exosome-derived microRNAs in cancer', *International Journal of Molecular Sciences*, 14(7), pp. 14240–14269. doi: 10.3390/ijms140714240.

Hisada, Y. *et al.* (2017) 'Detection of tissue factor-positive extracellular vesicles by laser scanning confocal microscopy', *Thrombosis Research*, 150, pp. 65–72. doi: 10.1016/j.thromres.2016.12.021.

Hizir, Z. *et al.* (2017) 'RNY (YRNA)-derived small RNAs regulate cell death and inflammation in monocytes/macrophages', *Cell Death and Disease*. Nature Publishing Group, 8(1), pp. e2530-8. doi: 10.1038/cddis.2016.429.

Ho, J. L. and Lo, J. (2015) 'Diversity of extracellular vesicles in human ejaculates revealed by cryo-electron microscopy', *J Extracell Vesicles*, 1, pp. 1–11.

Holmes, A. S. *et al.* (1991) 'Evidence for donor-donor energy transfer in lipid bilayers: perylene fluorescence quenching by CO2+ ions', *Chemical Physics Letters*, 186(2–3), pp. 189–194. doi: 10.1016/S0009-2614(91)85127-I.

Holmes, A. S. *et al.* (1997) 'Time-resolved fluorescence photophysics of trans-stilbene in a DPPC lipid bilayer: evidence for a free rotation, location within two sites and a pre-liquid crystalline phase transition', *Chemical Physics Letters*, 266(3–4), pp. 309–316. doi:

10.1016/S0009-2614(97)00016-X.

Hu, J. *et al.* (2017) 'A signal-amplifiable biochip quantifies extracellular vesicle-associated RNAs for early cancer detection', *Nature Communications*. Nature Publishing Group, 8(1), p. 1683. doi: 10.1038/s41467-017-01942-1.

Hugel, B. *et al.* (2005) 'Membrane Microparticles: Two Sides of the Coin', *Physiology*, 20(1), pp. 22–27. doi: 10.1152/physiol.00029.2004.

Huyan, T. *et al.* (2018) 'Uptake characterization of tumor cell-derived exosomes by natural killer cells', *Iranian Journal of Public Health*. Iranian Journal of Public Health, 47(6), pp. 803–813.

Imai, T. *et al.* (2015) 'Macrophage-dependent clearance of systemically administered B16BL6-derived exosomes from the blood circulation in mice', *Journal of Extracellular Vesicles*. Co-Action Publishing, 4(2015), pp. 1–8. doi: 10.3402/jev.v4.26238.

IRIC (2017) 'Understanding qPCR results', *Institute of research in immunology and cancer (University of Montreal)*, pp. 1–3. Available at: https://genomique.iric.ca/resources/files/Understanding_qPCR_results.pdf.

Issman, L. *et al.* (2013) 'Cryogenic transmission electron microscopy nanostructural study of shed microparticles', *PLoS ONE*, 8(12). doi: 10.1371/journal.pone.0083680.

Itoh, Y. and Reichlin, M. (1991) 'Ro / SS-A Antigen in Human Platelets', *Arthritis and Rheumatism*, 34(7).

Jalalinadoushan, M., Peivareh, H., Azizzadeh Delshad, A. (2004) 'Correlation between apoptosis and histological grade of transitional cell carcinoma of urinary bladder', *Urol. J*, 1(3), pp. 177–179.

Jeyaram, A. and Jay, S. M. (2018) 'Preservation and Storage Stability of Extracellular Vesicles for Therapeutic Applications', *AAPS Journal*. Springer New York LLC. doi: 10.1208/s12248-017-0160-y.

Jin, L. *et al.* (2006) 'Characterization and application of a new optical probe for membrane lipid domains.', *Biophysical journal*. Elsevier, 90(7), pp. 2563–75. doi: 10.1529/biophysj.105.072884.

Jin, Y. *et al.* (2016) 'DNA in serum extracellular vesicles is stable under different storage conditions', *BMC Cancer*. BioMed Central Ltd., 16(1). doi: 10.1186/s12885-016-2783-2.

Johnsen, K. B. *et al.* (2019) 'What is the blood concentration of extracellular vesicles? Implications for the use of extracellular vesicles as blood-borne biomarkers of cancer', *Biochimica et Biophysica Acta - Reviews on Cancer*. Elsevier B.V., pp. 109–116. doi: 10.1016/j.bbcan.2018.11.006.

Kalisz, K. *et al.* (2019) 'An update on Burkitt lymphoma: a review of pathogenesis and multimodality imaging assessment of disease presentation, treatment response, and recurrence', *Insights into Imaging*. Springer Verlag. doi: 10.1186/s13244-019-0733-7.

Kalra, H. *et al.* (2013) 'Comparative proteomics evaluation of plasma exosome isolation techniques and assessment of the stability of exosomes in normal human blood plasma', *Proteomics*, 13(22), pp. 3354–3364. doi: 10.1002/pmic.201300282.

Kanwar, S. S. *et al.* (2014) 'Microfluidic device (ExoChip) for on-chip isolation, quantification and characterization of circulating exosomes', *Lab on a Chip*, 14(11), pp. 1891–1900. doi: 10.1039/c4lc00136b.

Kapsogeorgou, E. K. *et al.* (2005) 'Salivary gland epithelial cell exosomes: A source of autoantigenic ribonucleoproteins', *Arthritis and Rheumatism*. John Wiley & Sons, Ltd, 52(5), pp. 1517–1521. doi: 10.1002/art.21005.

Kastelowitz, N. and Yin, H. (2014) 'Exosomes and microvesicles: Identification and targeting by particle size and lipid chemical probes', *ChemBioChem*. Wiley-VCH Verlag, pp. 923–928. doi: 10.1002/cbic.201400043.

Kawauchi, S. *et al.* (2000) 'Prognostic significance of apoptosis in synovial sarcoma: Correlation with clinicopathologic parameters, cell proliferative activity, and expression of apoptosis-related', *Modern Pathology*. Lippincott Williams and Wilkins, 13(7), pp. 755–765. doi: 10.1038/modpathol.3880131.

Kelemen, K. *et al.* (2010) 'Immunophenotypic Variations of Burkitt Lymphoma', *American Journal of Clinical Pathology*. Oxford Academic, 134(1), pp. 127–138. doi: 10.1309/AJCP93LJPTRQPDKR.

Kesimer, M. and Gupta, R. (2015) 'Physical characterization and profiling of airway epithelial derived exosomes using light scattering', *Methods*. Elsevier Inc., 87, pp. 59–63. doi: 10.1016/j.ymeth.2015.03.013.

Kim, J. W. *et al.* (2005) 'Fas Ligand – Positive Membranous Vesicles Isolated from Sera of Patients with Oral Cancer Induce Apoptosis of Activated T Lymphocytes Fas Ligand – Positive Membranous Vesicles Isolated from Sera of Patients with Oral Cancer Induce Apoptosis of Activated T', *Clinical Cancer Research*, 11, pp. 1010–1020.

Ko, J. *et al.* (2016) 'Smartphone-enabled optofluidic exosome diagnostic for concussion recovery.', *Scientific reports*. Nature Publishing Group, 6, p. 31215. doi: 10.1038/srep31215.

Ko, J., Carpenter, E. and Issadore, D. (2016) 'Detection and isolation of circulating exosomes and microvesicles for cancer monitoring and diagnostics using micro-/nano-based devices', *Analyst*. Royal Society of Chemistry, 141(2), pp. 450–460. doi: 10.1039/c5an01610j.

Koga, K. *et al.* (2005) 'Purification, characterization and biological significance of tumor-derived exosomes', *Anticancer Research*, 25(6 A), pp. 3703–3707.

Koliha, N. *et al.* (2016) 'A novel multiplex bead-based platform highlights the diversity of extracellular vesicles', *Journal of Extracellular Vesicles*, 5(17), pp. 1–15. doi: 10.3402/jev.v5.29975.

Konoshenko, M. Y. *et al.* (2018) 'Isolation of Extracellular Vesicles: General Methodologies and Latest Trends', *BioMed Research International*. Hindawi, 2018, pp. 1–27. doi: 10.1155/2018/8545347.

Kormelink, T. G. *et al.* (2016) 'Prerequisites for the analysis and sorting of extracellular vesicle subpopulations by high-resolution flow cytometry', *Cytometry Part A*, 89(2), pp. 135–147. doi: 10.1002/cyto.a.22644.

Kosaka, N., Kogure, A., Yamamoto, T. et al. (2019) 'Exploiting the message from cancer: the diagnostic value of extracellular vesicles for clinical applications', *Exp Mol Med*, 51, pp. 1–9.

Available at: https://doi.org/10.1038/s12276-019-0219-1.

Kowal, J. *et al.* (2016) 'Proteomic comparison defines novel markers to characterize heterogeneous populations of extracellular vesicle subtypes', *Proceedings of the National Academy of Sciences of the United States of America*. National Academy of Sciences, 113(8), pp. E968–E977. doi: 10.1073/pnas.1521230113.

Kriebardis, A. G. *et al.* (2016) 'Microparticles variability in fresh frozen plasma: Preparation protocol and storage time effects', *Blood Transfusion*, 14(3), pp. 228–237. doi: 10.2450/2016.0179-15.

Kroemer, G. *et al.* (2009) 'Classification of Cell Death 2009', *Cell death and differentiation*, 16(1), pp. 3–11. doi: 10.1038/cdd.2008.150.Classification.

Kumar, A. and Dixit, C. K. (2017) 'Methods for characterization of nanoparticles', in *Advances in Nanomedicine for the Delivery of Therapeutic Nucleic Acids*. Elsevier Inc., pp. 44–58. doi: 10.1016/B978-0-08-100557-6.00003-1.

Kwiatek, J. M. *et al.* (2013) 'Characterization of a New Series of Fluorescent Probes for Imaging Membrane Order', *PLoS ONE*, 8(2), pp. 1–7. doi: 10.1371/journal.pone.0052960.

Labi, V. *et al.* (2010) 'Apoptosis of leukocytes triggered by acute DNA damage promotes lymphoma formation', *Genes and Development*, 24(15), pp. 1602–1607. doi: 10.1101/gad.1940210.

Lacroix, R. *et al.* (2010) 'Overcoming Limitations of Microparticle Measurement by Flow Cytometry', *Seminars in Thrombosis and Hemostasis*, 36(08), pp. 807–818. doi: 10.1055/s-0030-1267034.

Lai, C. P. *et al.* (2015) 'Visualization and tracking of tumour extracellular vesicle delivery and RNA translation using multiplexed reporters', *Nature Communications*. Nature Publishing Group, 6(1), p. 7029. doi: 10.1038/ncomms8029.

Lakowicz, J. R. and Knutson, J. R. (1980) 'Hindered depolarizing rotations of perylene in lipid bilayers. Detection by lifetime-resolved fluorescence anisotropy measurements', *Biochemistry*, 19(0006–2960), pp. 905–911. doi: 10.1021/bi00546a013.

Lane, R. E. *et al.* (2018) 'Extracellular vesicles as circulating cancer biomarkers: opportunities and challenges', *Clinical and translational medicine*. Springer, 7(1), p. 14. doi: 10.1186/s40169-018-0192-7.

Lane, R. E. *et al.* (2019) 'Optimizing Size Exclusion Chromatography for Extracellular Vesicle Enrichment and Proteomic Analysis from Clinically Relevant Samples', *PROTEOMICS*, 19(8), p. 1800156. doi: 10.1002/pmic.201800156.

Lannigan, J. and Erdbruegger, U. (2017) 'Imaging flow cytometry for the characterization of extracellular vesicles', *Methods*. Academic Press, 112, pp. 55–67. doi: 10.1016/J.YMETH.2016.09.018.

Lara, P. C. *et al.* (1999) 'Apoptosis in carcinoma of the bladder: Relation with radiation treatment results', *International Journal of Radiation Oncology Biology Physics*. Int J Radiat Oncol Biol Phys, 43(5), pp. 1015–1019. doi: 10.1016/S0360-3016(98)00472-6.

Laulagnier, K. *et al.* (2004) 'Mast cell- and dendritic cell-derived exosomes display a specific

lipid composition and an unusual membrane organization', *Biochemical Journal*, 380(1), pp. 161–171. doi: 10.1042/bj20031594.

Lawrie, A. S. *et al.* (2009) 'Microparticle sizing by dynamic light scattering in fresh-frozen plasma', *Vox Sanguinis*, 96(3), pp. 206–212. doi: 10.1111/j.1423-0410.2008.01151.x.

Lee, K. *et al.* (2018) 'Multiplexed Profiling of Single Extracellular Vesicles', *ACS Nano*. American Chemical Society, 12(1), pp. 494–503. doi: 10.1021/acsnano.7b07060.

Leoncini, L. *et al.* (1993) 'Correlations between apoptotic and proliferative indices in malignant non- Hodgkin's lymphomas', *American Journal of Pathology*. American Society for Investigative Pathology, 142(3), pp. 755–763.

Lerner, M. R. *et al.* (1981) 'Two novel classes of small ribonucleoproteins detected by antibodies associated with lupus erythematosus', *Science*, 211(4480), pp. 400–402. doi: 10.1126/science.6164096.

Lerner, N., Avissar, S. and Beit-Yannai, E. (2017) 'Extracellular vesicles mediate signaling between the aqueous humor producing and draining cells in the ocular system.', *PloS one*. Public Library of Science, 12(2), p. e0171153. doi: 10.1371/journal.pone.0171153.

Liang, K. *et al.* (2017) 'Nanoplasmonic quantification of tumour-derived extracellular vesicles in plasma microsamples for diagnosis and treatment monitoring', *Nature Biomedical Engineering*. Nature Publishing Group, 1(4), p. 21. doi: 10.1038/s41551-016-0021.

Van De Linde, S. *et al.* (2011) 'Direct stochastic optical reconstruction microscopy with standard fluorescent probes', *Nature Protocols*, 6(7), pp. 991–1009. doi: 10.1038/nprot.2011.336.

Lips, E. *et al.* (2018) 'PO-498 Spliced rna panels from tumor-educated platelets (tep) enable detection of early breast cancer', in. BMJ, p. A424.3-A425. doi: 10.1136/esmoopen-2018-eacr25.999.

Liu, Y. and Lu, Q. (2015) 'Extracellular vesicle microRNAs: biomarker discovery in various diseases based on RT-qPCR', *Biomarkers in Medicine*. Future Medicine Ltd., 9(8), pp. 791–805. doi: 10.2217/BMM.15.45.

Livshts, M. A. *et al.* (2015) 'Isolation of exosomes by differential centrifugation: Theoretical analysis of a commonly used protocol', *Scientific Reports*. Nature Publishing Group, 5. doi: 10.1038/srep17319.

Lobb, R. J. *et al.* (2015) 'Optimized exosome isolation protocol for cell culture supernatant and human plasma', *Journal of Extracellular Vesicles*, 4(1), p. 27031. doi: 10.3402/jev.v4.27031.

Lorincz, Á. M. *et al.* (2014) 'Effect of storage on physical and functional properties of extracellular vesicles derived from neutrophilic granulocytes', *Journal of Extracellular Vesicles*. Co-Action Publishing, 3(1). doi: 10.3402/jev.v3.25465.

Lynch, C., Panagopoulou, M. and Gregory, C. D. (2017) 'Extracellular Vesicles Arising from Apoptotic Cells in Tumors: Roles in Cancer Pathogenesis and Potential Clinical Applications', *Frontiers in Immunology*. Frontiers, 8, p. 1174. doi: 10.3389/fimmu.2017.01174.

Maas, S. L. N. *et al.* (2015) 'Possibilities and limitations of current technologies for quantification of biological extracellular vesicles and synthetic mimics', *Journal of Controlled Release*. Elsevier, 200, pp. 87–96. doi: 10.1016/J.JCONREL.2014.12.041.

Macey, M. G. (2007) 'Principles of Flow Cytometry', *Flow Cytometry - Principles and Applications*, pp. 12–27.

Macklin, R. *et al.* (2016) 'Extracellular vesicles secreted by highly metastatic clonal variants of osteosarcoma preferentially localize to the lungs and induce metastatic behaviour in poorly metastatic clones', *Oncotarget.*, 7(28), pp. 43570–43587. doi: 10.18632/oncotarget.9781.

Malvern (2011) 'Inform White Paper Dynamic Light Scattering', *Malvern Guides*, pp. 1–6.

Mangeney, M. *et al.* (1991) 'CD77: an antigen of germinal center B cells entering apoptosis', *European Journal of Immunology*, 21(5), pp. 1131–1140. doi: 10.1002/eji.1830210507.

Matsumoto, A. *et al.* (2020) 'Blood concentrations of small extracellular vesicles are determined by a balance between abundant secretion and rapid clearance', *Journal of Extracellular Vesicles*, 9(1), p. 1696517. doi: 10.1080/20013078.2019.1696517.

Menck, K. *et al.* (2017) 'Isolation and characterization of microvesicles from peripheral blood', *Journal of Visualized Experiments, 2017 (119), art. no. e55057*.

Michalak, E. M. *et al.* (2010) 'Apoptosis-promoted tumorigenesis: γ-irradiation-induced thymic lymphomagenesis requires Puma-driven leukocyte death', *Genes and Development*, 24(15), pp. 1608–1613. doi: 10.1101/gad.1940110.

Mielanczyk, L. *et al.* (2014) 'Closer to the native state. Critical evaluation of cryo-techniques for Transmission Electron Microscopy: preparation of biological samples', *Folia Histochemica et Cytobiologica*, 52(1), pp. 1–17. doi: 10.5603/FHC.2014.0001.

Minciacchi, V. R., Freeman, M. R. and Di Vizio, D. (2015) 'Extracellular vesicles in cancer: exosomes, microvesicles and the emerging role of large oncosomes.', *Seminars in cell & developmental biology*. NIH Public Access, 40, pp. 41–51. doi: 10.1016/j.semcdb.2015.02.010.

Miranda, J. *et al.* (2018) 'Placental exosomes profile in maternal and fetal circulation in intrauterine growth restriction - Liquid biopsies to monitoring fetal growth', *Placenta*, 64, pp. 34–43. doi: 10.1016/j.placenta.2018.02.006.

Mitchell, P. J. *et al.* (2009) 'Can urinary exosomes act as treatment response markers in prostate cancer?', *Journal of Translational Medicine*, 7(1), p. 4. doi: 10.1186/1479-5876-7-4.

Momen-Heravi, F., Getting, S. J. and Moschos, S. A. (2018) 'Extracellular vesicles and their nucleic acids for biomarker discovery', *Pharmacology & Therapeutics*. Pergamon, 192, pp. 170–187. doi: 10.1016/J.PHARMTHERA.2018.08.002.

Montaudon, D. *et al.* (1986) *Fluorescence Anisotropy of Cell Membranes of Doxorubicin-sensitive and-resistant Rodent Tumoral Cells*, *Cancer Research*.

Morales-Kastresana, A. and Jones, J. . (2017) 'Flow cytometric analysis of extracellular vesicles', *Methods in Molecular Biology,* 1545, pp. 215–225.

Mussack, V., Wittmann, G. and Pfaffl, M. W. (2019) 'Comparing small urinary extracellular vesicle purification methods with a view to RNA sequencing—Enabling robust and non-invasive biomarker research', *Biomolecular Detection and Quantification*. Elsevier GmbH, 17. doi: 10.1016/j.bdq.2019.100089.

Nagata, S. *et al.* (2016) 'Exposure of phosphatidylserine on the cell surface', *Cell Death & Differentiation*. Nature Publishing Group, 23(6), pp. 952–961. doi: 10.1038/cdd.2016.7.

Nakamura, K. *et al.* (2016) 'Clinical relevance of circulating cell-free microRNAs in ovarian cancer', *Molecular Cancer*, 15(1), p. 48. doi: 10.1186/s12943-016-0536-0.

Nakano, A. (2002) 'Spinning-disk confocal microscopy -- a cutting-edge tool for imaging of membrane traffic.', *Cell structure and function*, 27(5), pp. 349–355. doi: 10.1247/csf.27.349.

Nanou, A., Zeune, L. L. and Terstappen, L. W. M. M. (2019) 'Leukocyte-Derived Extracellular Vesicles in Blood with and without EpCAM Enrichment', *Cells*, 8(8), p. 937. doi: 10.3390/cells8080937.

Naresh, K. N. *et al.* (2001a) 'Apoptosis index is a predictor of metastatic phenotype in patients with early stage squamous carcinoma of the tongue', *Cancer*, 91(3), pp. 578–584. doi: 10.1002/1097-0142(20010201)91:3<578::AID-CNCR1037>3.0.CO;2-W.

Naresh, K. N. *et al.* (2001b) 'Apoptosis index is a predictor of metastatic phenotype in patients with early stage squamous carcinoma of the tongue', *Cancer*. John Wiley & Sons, Ltd, 91(3), pp. 578–584. doi: 10.1002/1097-0142(20010201)91:3<578::AID-CNCR1037>3.0.CO;2-W.

Nelson, S. C. *et al.* (2012) 'Fluorescence anisotropy of diphenylhexatriene and its cationic Trimethylamino derivative in liquid dipalmitoylphosphatidylcholine liposomes: opposing responses to isoflurane.', *BMC biophysics*. BioMed Central Ltd, 5(1), p. 5. doi: 10.1186/2046-1682-5-5.

Nicola, A. M., Frases, S. and Casadevall, A. (2009) 'Lipophilic dye staining of cryptococcus neoformans extracellular vesicles and capsule', *Eukaryotic Cell*, 8(9), pp. 1373–1380. doi: 10.1128/EC.00044-09.

Nieuwland, R. and Sturk, A. (2010) 'Why do cells release vesicles?', *Thrombosis Research*. Elsevier Ltd, 125(SUPPL. 1), pp. S49–S51. doi: 10.1016/j.thromres.2010.01.037.

Nilsson, R. J. A. *et al.* (2011) 'Blood platelets contain tumor-derived RNA biomarkers', *Blood*, 118(13), pp. 3680–3683. doi: 10.1182/blood-2011-03-344408.

Nilsson, R. J. A. *et al.* (2016) 'Rearranged EML4-ALK fusion transcripts sequester in circulating blood platelets and enable blood-based crizotinib response monitoring in non-small-cell lung cancer', *Oncotarget*. Impact Journals LLC, 7(1), pp. 1066–1075. doi: 10.18632/ONCOTARGET.6279.

Nolan, J. P. (2015) 'Flow cytometry of extracellular vesicles: Potential, pitfalls, and prospects', *Current Protocols in Cytometry*, 2015(July), pp. 13.14.1-13.14.16. doi: 10.1002/0471142956.cy1314s73.

Nudelman, F., de With, G. and Sommerdijk, N. a. J. M. (2011) 'Cryo-electron tomography: 3-dimensional imaging of soft matter', *Soft Matter*, 7, p. 17. doi: 10.1039/c0sm00441c.

O'Malley, D. P., Auerbach, A. and Weiss, L. M. (2015) 'Practical applications in immunohistochemistry: Evaluation of diffuse large B-cell lymphoma and related large B-cell lymphomas', *Archives of Pathology and Laboratory Medicine*. College of American Pathologists, pp. 1094–1107. doi: 10.5858/arpa.2014-0451-CP.

Ogden, C. A. *et al.* (2001) 'C1q and mannose binding lectin engagement of cell surface calreticulin and CD91 initiates macropinocytosis and uptake of apoptotic cells', *Journal of Experimental Medicine*, 194(6), pp. 781–795. doi: 10.1084/jem.194.6.781.

Ogden, C. A. *et al.* (2005) 'Enhanced Apoptotic Cell Clearance Capacity and B Cell Survival Factor Production by IL-10-Activated Macrophages: Implications for Burkitt's Lymphoma', *The Journal of Immunology*. The American Association of Immunologists, 174(5), pp. 3015–3023. doi: 10.4049/jimmunol.174.5.3015.

Oksvold, M. P., Neurauter, A. and Pedersen, K. W. (2015) 'Magnetic Bead-Based Isolation of Exosomes', in *Methods in Molecular Biology*, pp. 465–481. doi: 10.1007/978-1-4939-1538-5_27.

ONI (2019) *A guide to imaging Extracellular Vesicles with super-resolution microscopy*, *ONI Application note*.

Oosthuyzen, W. *et al.* (2013) 'Quantification of human urinary exosomes by nanoparticle tracking analysis', *J Physiol.*, 591(23), pp. 5833–5842. doi: 10.1113/jphysiol.2013.264069.

Orem, J. *et al.* (2007) 'Burkitt's lymphoma in Africa, a review of the epidemiology and etiology.', *African health sciences*. Makerere University Medical School, 7(3), pp. 166–75. doi: 10.5555/afhs.2007.7.3.166.

Palmieri, V. *et al.* (2014) 'Dynamic light scattering for the characterization and counting of extracellular vesicles: A powerful noninvasive tool', *Journal of Nanoparticle Research*, 16(9). doi: 10.1007/s11051-014-2583-z.

Panagopoulou, M. S. *et al.* (2020) 'Phenotypic analysis of extracellular vesicles: a review on the applications of fluorescence', *Journal of Extracellular Vesicles*, 9(1), p. 1710020. doi: 10.1080/20013078.2019.1710020.

Park, S. J. *et al.* (2018) 'Molecular mechanisms of biogenesis of apoptotic exosome-like vesicles and their roles as damage-associated molecular patterns', *Proceedings of the National Academy of Sciences of the United States of America*, 115(50), pp. E11721–E11730. doi: doi:10.1073/pnas.1811432115.

Pasalic, L. *et al.* (2016) 'Enumeration of extracellular vesicles by a new improved flow cytometric method is comparable to fluorescence mode nanoparticle tracking analysis', *Nanomedicine: Nanotechnology, Biology, and Medicine*. Elsevier B.V., 12(4), pp. 977–986. doi: 10.1016/j.nano.2015.12.370.

Patel, G. K. *et al.* (2019) 'Comparative analysis of exosome isolation methods using culture supernatant for optimum yield, purity and downstream applications', *Scientific Reports*. Nature Publishing Group, 9(1). doi: 10.1038/s41598-019-41800-2.

Peinado, H. *et al.* (2012) 'Melanoma exosomes educate bone marrow progenitor cells toward a pro-metastatic phenotype through MET', *Nature Medicine*. Nature Publishing Group, 18(6), pp. 883–891. doi: 10.1038/nm.2753.

van der Pol, E. *et al.* (2013a) 'Innovation in detection of microparticles and exosomes', *Journal of Thrombosis and Haemostasis*, 11(Suppl.1), pp. 36–45. doi: 10.1111/jth.12254.

van der Pol, E. *et al.* (2013b) 'Innovation in detection of microparticles and exosomes', *Journal of Thrombosis and Haemostasis*. John Wiley & Sons, Ltd (10.1111), 11, pp. 36–45. doi: 10.1111/jth.12254.

Polanco, J. C. *et al.* (2018) 'Exosomes taken up by neurons hijack the endosomal pathway to spread to interconnected neurons', *Acta Neuropathologica Communications*, 6(1), p. 10. doi: 10.1186/s40478-018-0514-4.

Pons, M., Foradada, M. and Estelrich, J. (1993) 'Liposomes obtained by the ethanol injection method', *International Journal of Pharmaceutics*, 95(1–3), pp. 51–56. doi: 10.1016/0378-5173(93)90389-W.

Pospichalova, V. *et al.* (2015) 'Simplified protocol for flow cytometry analysis of fluorescently labeled exosomes and microvesicles using dedicated flow cytometer.', *Journal of extracellular vesicles*. Taylor & Francis, 4, p. 25530. doi: 10.3402/JEV.V4.25530.

Rabesandratana, H. *et al.* (1998) 'Decay-accelerating factor (CD55) and membrane inhibitor of reactive lysis (CD59) are released within exosomes during In vitro maturation of reticulocytes', *Blood*, 91(7), pp. 2573–2580. doi: papers3://publication/uuid/4B0F1787-8145-48BC-930C-6B2DDCF1AC3E.

Ramirez, M. I. *et al.* (2018) 'Technical challenges of working with extracellular vesicles', *Nanoscale*. The Royal Society of Chemistry, 10(3), pp. 881–906. doi: 10.1039/C7NR08360B.

Reátegui, E. *et al.* (2018) 'Engineered nanointerfaces for microfluidic isolation and molecular profiling of tumor-specific extracellular vesicles', *Nature Communications*. Nature Publishing Group, 9(1), p. 175. doi: 10.1038/s41467-017-02261-1.

Rejraji, H. *et al.* (2006) 'Lipid Remodeling of Murine Epididymosomes and Spermatozoa During Epididymal Maturation1', *Biology of Reproduction*, 74(6), pp. 1104–1113. doi: 10.1095/biolreprod.105.049304.

Renelli, M. *et al.* (2004) 'DNA-containing membrane vesicles of Pseudomonas aeruginosa PAO1 and their genetic transformation potential', *Microbiology*, 150(7).

Ries, J. *et al.* (2012) 'A simple, versatile method for GFP-based super-resolution microscopy via nanobodies', *Nature Methods*. Nature Publishing Group, 9(6), pp. 582–584. doi: 10.1038/nmeth.1991.

Roca, E. *et al.* (2016) 'Detection of EpCAM-positive microparticles in pleural fluid: A new approach to mini-invasively identify patients with malignant pleural effusions.', *Oncotarget*. Impact Journals, LLC, 7(3), pp. 3357–66. doi: 10.18632/oncotarget.6581.

Rood, I. M. *et al.* (2010) 'Comparison of three methods for isolation of urinary microvesicles to identify biomarkers of nephrotic syndrome', *Kidney International*, 78(8), pp. 810–816. doi: 10.1038/ki.2010.262.

Rossaint, J. *et al.* (2016) 'Directed transport of neutrophil-derived extracellular vesicles enables platelet-mediated innate immune response', *Nature Communications*. Nature Publishing Group, 7. doi: 10.1038/ncomms13464.

Ruffert, C. (2016) 'Magnetic Bead—Magic Bullet', *Micromachines*, 7(2), p. 21. doi: 10.3390/mi7020021.

Rust, M. J., Bates, M. and Zhuang, X. (2006) 'Sub-diffraction-limit imaging by stochastic optical reconstruction microscopy (STORM)', *Nature Methods*, 3(10), pp. 793–795. doi: 10.1038/nmeth929.

Rutjes, S. A. *et al.* (1999) 'Rapid nucleolytic degradation of the small cytoplasmic Y RNAs during apoptosis', *Journal of Biological Chemistry*, 274(35), pp. 24799–24807. doi: 10.1074/jbc.274.35.24799.

Saeedi, S. *et al.* (2019) 'The emerging role of exosomes in mental disorders', *Translational Psychiatry*. Nature Publishing Group. doi: 10.1038/s41398-019-0459-9.

Salehi, M. and Sharifi, M. (2018) 'Exosomal miRNAs as novel cancer biomarkers: Challenges and opportunities', *Journal of Cellular Physiology*. doi: 10.1002/jcp.26481.

Sandlund, J. T. (2012) 'Burkitt lymphoma: Staging and response evaluation', *British Journal of Haematology*, pp. 761–765. doi: 10.1111/j.1365-2141.2012.09026.x.

Schachter, D. and Shinitzky, M. (1977) 'Fluorescence polarization studies of rat intestinal microvillus membranes', *Journal of Clinical Investigation*, 59(3), pp. 536–548. doi: 10.1172/JCI108669.

Schiller, M. *et al.* (2008) 'Autoantigens are translocated into small apoptotic bodies during early stages of apoptosis', *Cell Death and Differentiation*. Nature Publishing Group, 15(1), pp. 183–191. doi: 10.1038/sj.cdd.4402239.

Sesques, P. and Johnson, N. A. (2017) 'Approach to the diagnosis and treatment of high-grade B-cell lymphomas with MYC and BCL2 and/or BCL6 rearrangements', *Blood*. American Society of Hematology, pp. 280–288. doi: 10.1182/blood-2016-02-636316.

Seyoum, M., Enawgaw, B. and Melku, M. (2018) 'Human blood platelets and viruses: Defense mechanism and role in the removal of viral pathogens', *Thrombosis Journal*. BioMed Central Ltd. doi: 10.1186/s12959-018-0170-8.

Shao, H. *et al.* (2012) 'Protein typing of circulating microvesicles allows real-time monitoring of glioblastoma therapy', *Nature Medicine*, 18(12), pp. 1835–1840. doi: 10.1038/nm.2994.

Sharma, P. *et al.* (2018) 'Immunoaffinity-based isolation of melanoma cell-derived exosomes from plasma of patients with melanoma', *Journal of Extracellular Vesicles*. Taylor & Francis, 7(1), p. 1435138. doi: 10.1080/20013078.2018.1435138.

Shenoy, G. N. *et al.* (2018) 'Exosomes Associated with Human Ovarian Tumors Harbor a Reversible Checkpoint of T-cell Responses.', *Cancer immunology research*. American Association for Cancer Research, 6(2), pp. 236–247. doi: 10.1158/2326-6066.CIR-17-0113.

Shih, C. L. *et al.* (2016) 'Development of a magnetic bead-based method for the collection of circulating extracellular vesicles', *New Biotechnology*. Elsevier B.V., 33(1), pp. 116–122. doi: 10.1016/j.nbt.2015.09.003.

Shinitzky, M. and Inbar, M. (1976a) 'Microviscosity parameters and protein mobility in biological membranes', *BBA - Biomembranes*, 433(1), pp. 133–149. doi: 10.1016/0005-

2736(76)90183-8.

Shinitzky, M. and Inbar, M. (1976b) 'Microviscosity parameters and protein mobility in biological membranes', *BBA - Biomembranes*, 433(1), pp. 133–149. doi: 10.1016/0005-2736(76)90183-8.

Shlomovitz, I., Speir, M. and Gerlic, M. (2019) 'Flipping the dogma - Phosphatidylserine in non-apoptotic cell death', *Cell Communication and Signaling*. BioMed Central Ltd., pp. 1–12. doi: 10.1186/s12964-019-0437-0.

Silva, D. *et al.* (2013) 'A whole blood assay as a simple, broad assessment of cytokines and chemokines to evaluate human immune responses to Mycobacterium tuberculosis antigens', *Acta Tropica*. Elsevier, 127(2), pp. 75–81. doi: 10.1016/j.actatropica.2013.04.002.

Simonsen, J. B. (2017) 'What Are We Looking At? Extracellular Vesicles, Lipoproteins, or Both?', *Circulation Research*, 121, pp. 920–922. doi: 10.1161/CIRCRES.

Sódar, B. W. *et al.* (2016) 'Low-density lipoprotein mimics blood plasma-derived exosomes and microvesicles during isolation and detection', *Scientific Reports*. Nature Publishing Group, 6, pp. 1–12. doi: 10.1038/srep24316.

Son, S. H. *et al.* (2020) 'White blood cell labeling with Technetium-99m (99mTc) using red blood cell extracellular vesicles-mimetics', *Blood Cells, Molecules, and Diseases*. Elsevier, 80(October 2019), p. 102375. doi: 10.1016/j.bcmd.2019.102375.

Soo, C. Y. *et al.* (2012) 'Nanoparticle tracking analysis monitors microvesicle and exosome secretion from immune cells', *Immunology*, 136(2), pp. 192–197. doi: 10.1111/j.1365-2567.2012.03569.x.

Sorensen, T. *et al.* (2013) 'Azadioxatriangulenium: a long fluorescence lifetime fluorophore for large biomolecule binding assay', *Methods Appl. Fluoresc.*, 1:025001(2).

Sork, H., Corso, G., Krjutskov, K. et al. (2018) 'Heterogeneity and interplay of the extracellular vesicle small RNA transcriptome and proteome', *Sci Rep*, 8(10813). Available at: https://doi.org/10.1038/s41598-018-28485-9.

De Spiegelaere, W. *et al.* (2015) 'Reference gene validation for RT-qPCR, a note on different available software packages', *PLoS ONE*. Public Library of Science, 10(3). doi: 10.1371/journal.pone.0122515.

Sreenivasan, V. K. A., Zvyagin, A. V and Goldys, E. M. (2013) 'Luminescent nanoparticles and their applications in the life sciences', *Journal of Physics: Condensed Matter*. IOP Publishing, 25(19), p. 194101. doi: 10.1088/0953-8984/25/19/194101.

Stoner, S. A. *et al.* (2016) 'High sensitivity flow cytometry of membrane vesicles', *Cytometry Part A*, 89(2), pp. 196–206. doi: 10.1002/cyto.a.22787.

Sun, B. *et al.* (2006) 'Extent, relationship and prognostic significance of apoptosis and cell proliferation in synovial sarcoma', *European Journal of Cancer Prevention*, 15(3), pp. 258–265. doi: 10.1097/01.cej.0000198896.02185.68.

Sun, Z. *et al.* (2018) 'Effect of exosomal miRNA on cancer biology and clinical applications', *Molecular Cancer*, 17(1), p. 147. doi: 10.1186/s12943-018-0897-7.

Sutter, M., Fiechter, T. and Imanidis, G. (2004) 'Correlation of Membrane Order and Dynamics Derived from Time-Resolved Fluorescence Measurements with Solute Permeability', *Journal of Pharmaceutical Sciences*, 93(8). doi: 10.1002/jps.20114.

Swerdlow, S. H. *et al.* (2016) 'The 2016 revision of the World Health Organization classification of lymphoid neoplasms', *Blood*. American Society of Hematology, pp. 2375–2390. doi: 10.1182/blood-2016-01-643569.

Tataruch-Weinert, D. *et al.* (2016) 'Urinary extracellular vesicles for RNA extraction: optimization of a protocol devoid of prokaryote contamination', *Journal of Extracellular Vesicles*, 5(1), p. 30281. doi: 10.3402/jev.v5.30281.

Tauro, B. J. *et al.* (2012) 'Comparison of ultracentrifugation, density gradient separation, and immunoaffinity capture methods for isolating human colon cancer cell line LIM1863-derived exosomes', *Methods*, 56(2), pp. 293–304. doi: 10.1016/j.ymeth.2012.01.002.

Tauro, B. J. *et al.* (2013) 'Oncogenic H-ras reprograms Madin-Darby canine kidney (MDCK) cell-derived exosomal proteins following epithelial-mesenchymal transition.', *Molecular & cellular proteomics : MCP*. American Society for Biochemistry and Molecular Biology, 12(8), pp. 2148–59. doi: 10.1074/mcp.M112.027086.

Taylor, D. D. and Shah, S. (2015) 'Methods of isolating extracellular vesicles impact down-stream analyses of their cargoes', *Methods*. Academic Press Inc., pp. 3–10. doi: 10.1016/j.ymeth.2015.02.019.

Tegegn, T. Z. *et al.* (2016) 'Characterization of procoagulant extracellular vesicles and platelet membrane disintegration in DMSO-cryopreserved platelets', *Journal of Extracellular Vesicles*. Taylor and Francis Ltd., 5(1). doi: 10.3402/jev.v5.30422.

Théry, C. *et al.* (2006) 'Isolation and Characterization of Exosomes from Cell Culture Supernatants and Biological Fluids', *Current Protocols in Cell Biology*. Wiley, 30(1), pp. 3.22.1-3.22.29. doi: 10.1002/0471143030.cb0322s30.

Théry, C., Zitvogel, L. and Amigorena, S. (2002) 'Exosomes: composition, biogenesis and function', *Nature Reviews Immunology*. Nature Publishing Group, 2(8), p. 569. doi: 10.1038/nri855.

Tian, Q. *et al.* (2018) 'Nanoparticle Counting by Microscopic Digital Detection: Selective Quantitative Analysis of Exosomes via Surface-Anchored Nucleic Acid Amplification', *Analytical Chemistry*. American Chemical Society, 90(11), pp. 6556–6562. doi: 10.1021/acs.analchem.8b00189.

Troup, G. M. *et al.* (2006) 'A time-resolved fluorescence diphenylhexatriene (DPH) anisotropy characterization of a series of model lipid constructs for the sperm plasma membrane', *Industrial and Engineering Chemistry Research*, 45(21), pp. 6939–6945. doi: 10.1021/ie058084d.

Turpin, P., Kruglik, S. G. and Curie, M. (2012) 'Original research article', 1, pp. 1–11.

Upstone, S. L. (2006) 'Ultraviolet/Visible Light Absorption Spectrophotometry in Clinical Chemistry', *Encyclopedia of Analytical Chemistry*, pp. 1699–1714. doi: 10.1002/9780470027318.a0547.

Vagida, M. *et al.* (2017) 'Flow analysis of individual blood extracellular vesicles in acute

coronary syndrome', *Platelets*, 28(2), pp. 165–173.

Valentino, A. *et al.* (2017) 'Exosomal microRNAs in liquid biopsies: future biomarkers for prostate cancer', *Clinical and Translational Oncology*, 19(6), pp. 651–657. doi: 10.1007/s12094-016-1599-5.

Vallabhaneni, K. C. *et al.* (2016) 'Mesenchymal Stem/Stromal Cells under Stress Increase Osteosarcoma Migration and Apoptosis Resistance via Extracellular Vesicle Mediated Communication', *PLOS ONE*. Edited by G. Camussi. Public Library of Science, 11(11), p. e0166027. doi: 10.1371/journal.pone.0166027.

Vandesompele, J. *et al.* (2002) 'Accurate normalization of real-time quantitative RT-PCR data by geometric averaging of multiple internal control genes.', *Genome biology*. BioMed Central, 3(7), p. research0034.1. doi: 10.1186/gb-2002-3-7-research0034.

Vandesompele, Jo *et al.* (2002) 'Accurate normalization of real-time quantitative RT-PCR data by geometric averaging of multiple internal control genes', *Genome biology*, pp. 1–12. doi: 10.1186/gb-2002-3-7-research0034.

Verweij, F. J. *et al.* (2019) 'Live Tracking of Inter-organ Communication by Endogenous Exosomes In Vivo', *Developmental Cell*. Cell Press, 48(4), pp. 573-589.e4. doi: 10.1016/J.DEVCEL.2019.01.004.

van der Vlist, E. J. *et al.* (2012) 'Fluorescent labeling of nano-sized vesicles released by cells and subsequent quantitative and qualitative analysis by high-resolution flow cytometry', *Nature Protocols*. Nature Publishing Group, 7(7), pp. 1311–1326. doi: 10.1038/nprot.2012.065.

Wang, H. *et al.* (1996) 'Repression of apoptosis in human B-lymphoma cells by CD40-ligand and Bcl-2: Relationship to the cell-cycle and role of the retinoblastoma protein', *Oncogene*, 13(2), pp. 373–379. Available at: https://europepmc.org/article/med/8710376 (Accessed: 11 July 2020).

Wang, L. *et al.* (2018) 'Exosomal double-stranded DNA as a biomarker for the diagnosis and preoperative assessment of pheochromocytoma and paraganglioma', *Molecular Cancer*. BioMed Central, 17(1), p. 128. doi: 10.1186/s12943-018-0876-z.

Ward, M. *et al.* (2009) 'Fundamentals of acoustic cytometry', *Current Protocols in Cytometry*, (Suppl. 49), pp. 1–12. doi: 10.1002/0471142956.cy0122s49.

Webber, J. and Clayton, A. (2013) 'How pure are your vesicles?', *Journal of Extracellular Vesicles*, 2(1), p. 19861. doi: 10.3402/jev.v2i0.19861.

Welton, J. L. *et al.* (2015) 'Ready-made chromatography columns for extracellular vesicle isolation from plasma', *Journal of Extracellular Vesicles*, 4(1), p. 27269. doi: 10.3402/jev.v4.27269.

Westphal, M. and Lamszus, K. (2015) 'Circulating biomarkers for gliomas', *Nature Reviews Neurology*. Nature Publishing Group, 11(10), pp. 556–566. doi: 10.1038/nrneurol.2015.171.

Whitcomb, D. C. (2012) 'What is personalized medicine and what should it replace?', *Nature Reviews Gastroenterology and Hepatology*. NIH Public Access, pp. 418–424. doi: 10.1038/nrgastro.2012.100.

Wickman, G. R. *et al.* (2013) 'Blebs produced by actin-myosin contraction during apoptosis release damage-associated molecular pattern proteins before secondary necrosis occurs.', *Cell death and differentiation*. Nature Publishing Group, 20(10), pp. 1293–305. doi: 10.1038/cdd.2013.69.

Wiklander, O. P. B. *et al.* (2018) 'Systematic Methodological Evaluation of a Multiplex Bead-Based Flow Cytometry Assay for Detection of Extracellular Vesicle Surface Signatures', *Frontiers in Immunology*, 9. doi: 10.3389/fimmu.2018.01326.

Wilkerson, M. J. (2012) 'Principles and Applications of Flow Cytometry and Cell Sorting in Companion Animal Medicine', *Veterinary Clinics of North America - Small Animal Practice*. Elsevier Inc., 42(1), pp. 53–71. doi: 10.1016/j.cvsm.2011.09.012.

Williams, D. B. (David B. and Carter, C. B. (2009) *Transmission electron microscopy : a textbook for materials science*. Springer.

Willms, E. *et al.* (2018) 'Extracellular vesicle heterogeneity: Subpopulations, isolation techniques, and diverse functions in cancer progression', *Frontiers in Immunology*. Frontiers Media S.A. doi: 10.3389/fimmu.2018.00738.

Witwer, K. W. *et al.* (2013) 'Standardization of sample collection, isolation and analysis methods in extracellular vesicle research.', *Journal of extracellular vesicles*, 2, pp. 1–25. doi: 10.3402/jev.v2i0.20360.

Wolf, P. (1967) 'The Nature and Significance of Platelet Products in Human Plasma', *British Journal of Haematology*. Blackwell Publishing Ltd, 13(3), pp. 269–288. doi: 10.1111/j.1365-2141.1967.tb08741.x.

Wook Youn Kim, Matthew Pugh, Stefan Dojcinov, L. Q.-M. (2019) '"Grey zones" in the differential diagnosis of lymphoma pathology', *Diagnostic Histopathology*, 25(6), pp. 191–216. Available at: https://doi.org/10.1016/j.mpdhp.2019.04.006.

Xie, Y. *et al.* (2009) 'Tumor Apoptotic Bodies Inhibit CTL Responses and Antitumor Immunity via Membrane-Bound Transforming Growth Factor-β1 Inducing CD8+ T-Cell Anergy and CD4+ Tr1 Cell Responses', *Cancer Research*, 69(19). Available at: http://cancerres.aacrjournals.org/content/69/19/7756.long (Accessed: 22 April 2017).

Xu, R. *et al.* (2015) 'Highly-purified exosomes and shed microvesicles isolated from the human colon cancer cell line LIM1863 by sequential centrifugal ultrafiltration are biochemically and functionally distinct', *Methods*, 87, pp. 11–25. doi: 10.1016/j.ymeth.2015.04.008.

Yamamoto, K. R. *et al.* (1970) 'Rapid bacteriophage sedimentation in the presence of polyethylene glycol and its application to large-scale virus purification', *Virology*, 40(3), pp. 734–744. doi: 10.1016/0042-6822(70)90218-7.

Yuana, Y. *et al.* (2013) 'Cryo-electron microscopy of extracellular vesicles in fresh plasma', *J Extracell Vesicles*, 1, pp. 1–7.

Yuana, Y., Bertina, R. M. and Osanto, S. (2011) 'Pre-analytical and analytical issues in the analysis of blood microparticles', *Thrombosis and Haemostasis*, 105(3), pp. 396–408. doi: 10.1160/TH10-09-0595.

Zeev-Ben-Mordehai, T. *et al.* (2014) 'Extracellular Vesicles: A Platform for the Structure

Determination of Membrane Proteins by Cryo-EM', *Structure*, 22(11), pp. 1687–1692. doi: 10.1016/j.str.2014.09.005.

Zhang, H. *et al.* (2018) 'Identification of distinct nanoparticles and subsets of extracellular vesicles by asymmetric flow field-flow fractionation', *Nature Cell Biology*. Nature Publishing Group, 20(3), pp. 332–343. doi: 10.1038/s41556-018-0040-4.

Zhang, J. *et al.* (2015) 'Exosome and exosomal microRNA: Trafficking, sorting, and function', *Genomics, Proteomics and Bioinformatics*, 13(1), pp. 17–24. doi: 10.1016/j.gpb.2015.02.001.

Zhang, P., Yeo, J. C. and Lim, C. T. (2019) 'Advances in Technologies for Purification and Enrichment of Extracellular Vesicles.', *SLAS technology*, 24(5), pp. 477–488. doi: 10.1177/2472630319846877.